The Effect of Flourescent Tagging of 1,2-Propanediol Utilization Microcompartment Shell Proteins on the Shell Formation and Spatial Organization Within the Bacterial Cell

A thesis submitted to the University of Kent for the degree of PhD in the Faculty of Sciences.

2017

Sarah Packwood

Abstract

Bacterial microcompartments are isohedral structures composed entirely of protein and contain a 2-4 nm thick proteinaceous shell. This shell encases enzymes which act in a sequential manner to carry out a specific metabolic reaction. There are seven essential shell proteins encoded on the propanediol utilization microcompartment (Pdu) operon, Pdu −A −B −B' −J −K −N and − U, each having a critical role in the formation of the compartment. Other genes in the Pdu operon interact to form enzymes in the metabolic pathway with some having unknown functions such as PduV which has been shown to form filament-like structures. These filaments only appear in the presence of microcompartments and often co-localise with them and it is thought that PduV plays a role in the spatial distribution of microcompartments. This study has explored the interaction between PduV and the microcompartment shell. The shell protein involved in this interaction is thought to be PduK, and to characterise the mechanism of this interaction PduK truncations were generated and novel microcompartments containing these truncations were engineered. The ability of these microcompartments to form was examined, as well as the ineraction between PduV and these truncated forms of PduK. Filament formation of the small GTPase, PduV, was studied by site directed mutagenesis of the GTP binding site, which was then examined by microscopic and biochemical approaches. In addition, to further characterise how microcompartments form each individual shell protein was tagged with mCherry. Microscopy techniques such as live cell imaging and transfer electron microscopy were used in order to determine if these novel compartments were able to form correctly, if PduV filament formation was affected in any way and whether this subsequently had an effect on the distribution of microcompartments within the bacterial cell. The work presented has given insight into the formation of the microcompartment shell, higlighting the sensitivity of individual shell proteins to minor modifications such as fluorescent tagging and the effect this can have on the formation of the shell. It has also revealed possible previously undiscovered regulatory mechanisms of shell proteins on PduV filament formation and length, with the modification of shell proteins affecting PduV filaments. Finally, it has given greater evidence to previous suggestions that PduV may be a GTPase.

Declaration

No part of this thesis has been submitted in support of any other application for a degree or

qualification of the University of Kent or any other University or institution of learning.

All work is my own based on research conducted during my PhD.

Sarah Packwood 17-3-2017

Contents

Figures

Tables

Table 1.1 - The proteins associated with α and β-carboxysomes and the role they play in carboxysome formation and function.

Table 2.1. List of bacterial strains used in this study.

Table 2.2. List of plasmids used in this study.

Table 2.3. List of primers used in this study.

Table 2.4. Composition of SDS gels.

Table 2.5. Composition of typical PCR reactions**.**

Table 2.6. Typical PCR conditions.

Table 2.7. Composition of a typical restriction digest.

Table 2.8. Excitation and emission filters used to visualise Cerulean, GFP, Ypet and mCherry fusion proteins.

Table 2.9. The solvent gradient used for the dehydration of samples for electron microscopy.

Table 2.10. Low viscosity resin constituents used to produce a block of medium hardness

Table 2.11. The solvent gradient used for the dehydration of samples for immuno-labelled electron microscopy.

Table 3.1. Exploring the effect of truncating PduK on the length of PduV filaments.

Table 4.1. Engineered constructs that encode BMCs containing a mCherry-tagged shell protein.

Table 4.2. The molecular weights of untagged shell protein compared with mCherry-tagged shell proteins.

Abbreviations

1,2-PD	1,2-propanediol
3-HP	3-hydroxypropionic acid
3-HPA	3-hydroxypropionaldehyde
3-pga	3-Phosphoglycerate
α	alpha
β	beta
γ	gamma
Δ	delta, deletion of a gene
μL	Microlitre
μM	Micromolar
BMC	Bacterial microcompartment
CA	Carbonic anhydrase
co_2	Carbon dioxide
Da	Dalton
DDH	diol dehydratase
DNA	Deoxyribonucleic Acid
E. coli	Escherichia coli
Eut	Ethanolamine utilisation
FLIM	Fluorescence Lifetime Imaging Microscopy
GDP	Guanosine Diphosphate
GFP	Green Fluorescent Protein
GTP	Guanosine Triphosphate
hco3	Bicarbonate
IMAC	Immobilised Metal Affinity Chromatography
kb	Kilobase
kDa	Kilodalton

LB	Luria Bertani Broth
MCP	Microcompartment
MDa	Megadalton
mg	Milligrams
ml	Millilitre
mM	Millimolar
nm	nanometer
nM	Nanomolar
PCR	Polymerase Chain Reaction
Pdu	Propanediol utilisation
PEG-4000	Polyethylene glycol - 4000
Pi	Inorganic phosphate
PTAC	Phosphotransacylase
RuBisCO	D-Ribulose 1,5- bisphosphate carboxylase
RNA	Ribonucleic Acid
RPM	Revolutions Per Minute
TRIS	Tris(hydroxymethyl)aminomethane
YFP	Yellow Fluorescent Protein

Chapter 1- Introduction

1.1. An Introduction to Bacterial Microcompartments

Organelles are structures that can be used to segregate metabolic processes or compartmentalise genetic material. They are often used to define the difference between eukaryotes and prokaryotes as it is commonly thought that prokaryotic cells lack any membrane-bound structures. Although it is widely known that the interior of prokaryotic cells are far less organised than that of eukaryotic cells, emerging evidence has shown that the interior of prokaryotic cells are more organised than initially believed. The recognition of prokaryotic internal cell organisation stems from the discovery of cytoplasmic, subcellular inclusions, most of which remain uncharacterised. Some of these inclusions act as storage granules for compounds or polymers (Bazylinski & Frankel 2004; Steinbuchel et al. 1995) others are more complex and can generally be categorised into two groups. The first are the inclusions that are membrane-bound, including compartments such as magnetosomes (Murat et al. 2010). However some prokaryotes, specifically bacteria, are able to segregate specific processes from the cellular environment by encasing them in a proteinaceous shell; these protein bound inclusions constitute the second group that form a diverse family of organelles known as bacterial microcompartments, or BMCs.

BMCs are polyhedral inclusions, located within the cell cytoplasm and vary between 100 and 200 nm in cross section; a simplified model is shown in Figure 1.1 (Kerfeld et al. 2005; Cheng et al. 2008). They are composed entirely of protein, with no associated lipids and, based on sequence analysis are thought to be present in approximately 20% of all sequenced bacteria (Cheng et al. 2008). They are encoded by genes that are clustered into operons that group together genes required to form a thin, 3 – 4 nm protein shell, as well as the enzymes and auxiliary proteins necessary for the enclosed pathway (G C Cannon et al. 2001). BMCs primarily function to optimise metabolic pathways; the protein shell typically encases enzymes of a single metabolic pathway, which act in a sequential manner to carry out a specific metabolic reaction (Huseby & Roth 2013). Compartmentalisation of metabolic processes has allowed bacteria to occupy niches that other organisms cannot, as BMCs can be the main source of carbon, nitrogen and energy (Bobik 2006).

It is thought that BMCs may function in 23 or more different metabolic processes and are used by a wide variety of heterotrophic bacteria which express multiple compartments per cell (Bobik 2006). BMCs are capable of meeting the functional definition of an organelle, despite not being bound by a membrane through the complexity of their metabolic activities. (Shively et al. 1973).

BMCs have several distinctive features; they all contain a thin protein shell, which encapsulates functionally related enzymes while allowing the transport of substrates and products across the compartment, while the reaction contained within the BMS includes a toxic or volatile intermediate, shown in Figure 1.1. Therefore there are a number of advantages for the evolutionary emergence of BMCs. With the presence of BMCs, bacteria are able to concentrate and confine enzymes together with their substrates to enhance the efficiency of reactions. In addition the protein shell not only acts as a barrier to the loss of metabolites, but also acts as a barrier to prevent the leakage of any toxic intermediate into the cell cytoplasm, thus preventing DNA damage and cell death (Kerfeld, Heinhorst & Cannon 2010).
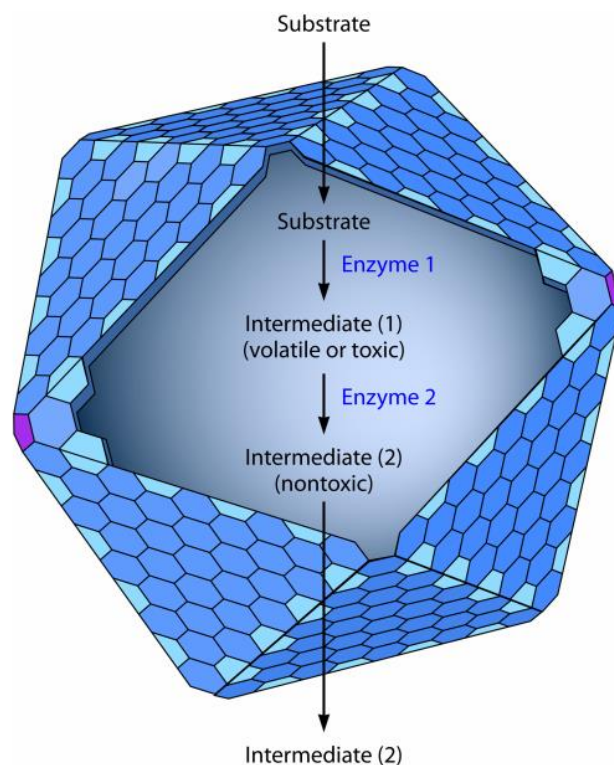
Figure 1.1 – Simplified model of the BMC structure and pathway. BMCs optimise pathways containing a volatile or toxic intermediate. The protein shell functions as a barrier to channel this intermediate to the

next reaction step and preventing its release into the cytoplasm where it can cause cellular toxicity or volatility. In addition the shell concentrates enzymes, substrates and cofactors together, improving the efficiency of reactions. Adapted from (Chowdhury et al. 2014)

1.1.1. An Overview of Studied Bacterial Microcompartments

To date, only a few BMCs have been characterised. Polyhedral organelles in bacteria were first described in 1956 and were isolated and visualised by electron microscopy in 1973 (Niklowitz & Drews 1956; Shiveley, Ball & Kline 1973). The inclusions were initially thought to be viruses, but after isolation, these structures were named carboxysomes due to the discovery of the carbon dioxide fixing enzyme D-ribulose 1,5- bisphosphate carboxylase, commonly known as RuBisCO, contained within the compartment lumen (Shiveley, Ball & Kline 1973). Carboxysomes are now recognised as the first of three main characterised microcompartments found within bacterial cells, followed by the discovery of propanediol utilization (Pdu) and ethanolamine utilisation (Eut) microcompartments in 1999 which function to catabolise 1,2 propanediol and degrade ethanolamine respectively (T. A. Bobik et al. 1999; Kofoid et al. 1999). Unlike carboxysomes, Pdu and Eut BMCs are involved with a specific metabolic activity, so are subdivided into a category of compartments known as metabalosomes. These metabolosomes both involve metabolic activities that require adenosylcobalamin, or vitamin B_{12}, as a cofactor (Brinsmade et al. 2005; T. A. Bobik et al. 1999) and were both identified in heterotrophic bacteria found in the mammalian gut (G C Cannon et al. 2001).

There are three main families of BMC that have been characterised to date; these include carboxysomes, 1,2-propanediol utilisation (Pdu) and ethanolamine utilisation (Eut) BMCs. These three BMCs have three main unifying features. The first is the presence of a compartment shell composed exclusively of protein, with no known associated lipids (Fan et al., 2010). This proteinaceous shell encases the second unifying feature - enzymes which act in a sequential manner to carry out a specific metabolic process; 1,2-propanediol, carbon dioxide or ethanolamine are fixed or broken down to generate energy. Lastly these metabolic processes always involve a

toxic or volatile intermediate, in the form of an aldehyde or in the case of carboxysomes, an oxygen sensitive enzyme (Kerfeld, Heinhorst & Cannon 2010; Yeates et al. 2008)

There are consequently two suggested primary functions of compartmentalising metabolic pathways; (I) to sequester toxic intermediates, preventing the cell from damage and (II) to increase the efficiency of metabolic reactions. By the compartmentalisation of pathways, enzymes and substrates are concentrated in the same locality, in addition the BMC shell acts as a barrier to prevent the loss of metabolites by diffusion (Kerfeld, Heinhorst & Cannon 2010). This phenomenon then creates a paradox, how is the compartment shell able to confine intermediates, enzymes and substrates, while allowing products and cofactors to pass through? (Cheng et al. 2008).

1.1.2. The Bacterial Microcompartment Shell

BMCs are organised into a polyhedral structure from the assembly of phylogenetically related shell proteins. Open reading frames (ORFs) of bacteria containing BMCs have been found to encode proteins that contain BMC domains, associated with the formation of the compartment shell. Genomic studies have identified two shell protein families, distinguished by the presence of two distinct BMC domains, PFAM 00936 and PFAM 03319 (Kerfeld, Heinhorst & Cannon 2010). These BMC domain-containing proteins form the building blocks of the BMC shell.

Typically, the conventional BMC domain consists of 90 amino acids and adopts an alpha/beta fold (Kerfeld et al. 2005). Currently there are approximately 1700 proteins that have been identified to contain BMC domains, throughout 10 different bacterial phyla (Yeates, Thompson & Bobik 2011). Each shell protein contains one or two copies of these highly conserved BMC domains and each domain determines the overall structure of the protein, comprising of either hexamers (upto 2 per protein: PFAM 00936) or pentamers (1 per protein: PFAM 03319) (Frank et al. 2013). Structural studies have shown that BMC shells usually consist of single layers of protein hexamers; these hexamers can also be arranged into pseudo hexameric trimers, and function to form the planar facets of the compartment shell (Kerfeld et al. 2005; Sargent, F. a Davidson, et al. 2013; Yeates, Thompson & Bobik 2011). Studies have also suggested that pentameric proteins form the vertices

of the shell, linking the hexameric facets together and it's thought that this gives the BMC it's unique structure, allowing for the curvature and helping it to fold, as shown in Figure 1.2 (Tanaka et al. 2008; Wheatley et al. 2013).
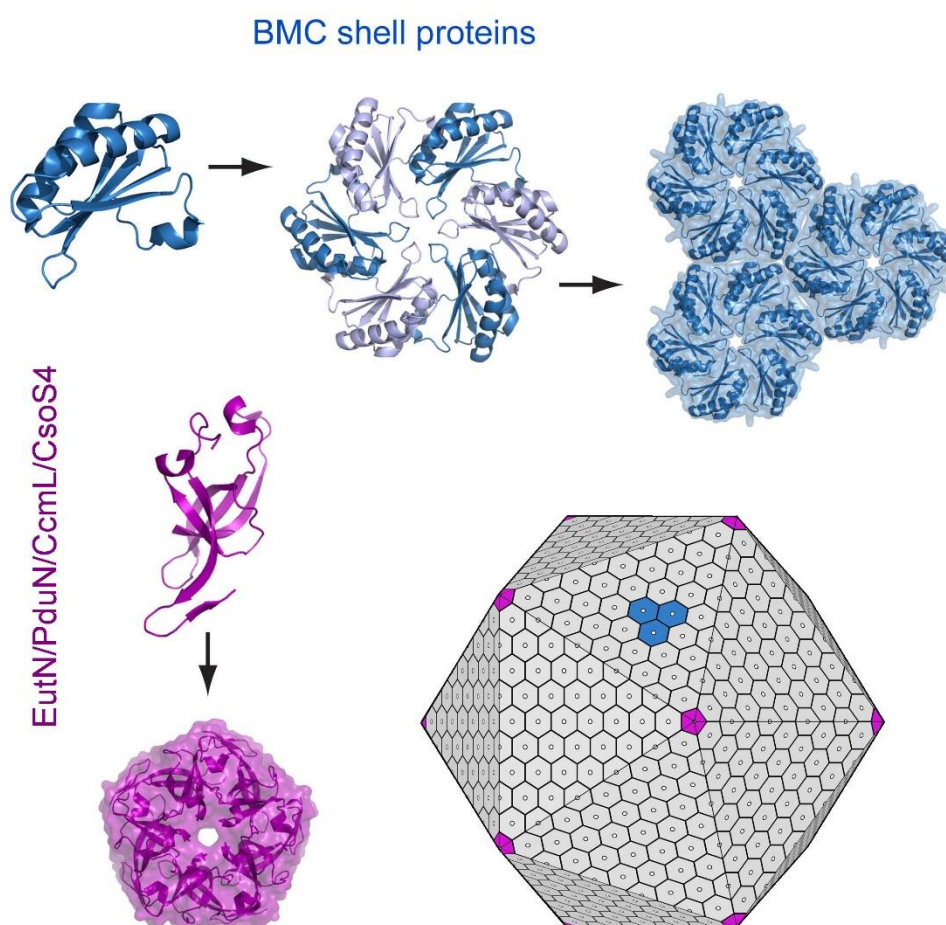
Figure 1.2 – Simplified model of BMC shell assembly. Main shell proteins assemble as hexamers which further assemble into molecular sheets that form the facets of the BMC shell structure, shown in blue. Specialised pentameric proteins, shown in pink, are thought to form the vertices of the BMC and help to close the structure. Adapted from (Yeates, Thompson & Bobik 2011)

1.1.3. Protein Pores, Molecular Transport and Selective Permeability; Properties of the Protein Shell

Interestingly, each shell protein hexamer contains a pore through the centre, along the axis of symmetry. This pore is thought to facilitate the movement of substrates, products and cofactors through the shell, although the mechanism for this is unclear (Kerfeld et al. 2005; Yeates, Thompson

& Bobik 2011). Several features of the pores have been identified as potentially important in allowing only certain small molecules to be transported; this includes size, electrostatic forces and hydrogen bonding (Yeates, Thompson & Bobik 2011). In some cases, these pores are thought to have an overall positive charge, allowing opposite charged cofactors to pass, whilst restricting the transport of other molecules through the shell (Yeates et al. 2007). In this way the shell can be thought of as a semi-permeable barrier.

Similarly, metabolosomes are able to sequester intermediates containing a toxic aldehyde group, preventing the cell from damage. To achieve this, the properties of the protein shell would have to allow the diffusion of cofactors into the compartment whilst restricting the transport of these toxic intermediates into the cellular environment. Therefore the BMC shell would need to be selectively permeable. Previous studies have supported this hypothesis; a *Salmonella enterica* mutant, lacking the BMC shell but retaining the Pdu pathway, was found to have an increased build-up of the toxic intermediate propionaldehyde. This led to an increased frequency of DNA mutations and the inhibition of respiratory processes (Sampson & Bobik 2008). This suggests that the primary function of the Pdu BMC is the mitigation of toxicity and consequent DNA damage by propionaldehyde.

Although the mechanism for selective permeability of the BMC shell remains largely elusive, there have been several suggestions to explain how molecules are both sequestered and transported across the shell. The first is the association of lumen enzymes with the shell protein pores which could cause molecules that move into the BMC from the cytoplasm to be channelled to active sites, in a process referred to as 'molecular routing' (Cheng et al. 2008). Another possibility is that these substrate-specific pores somehow mediate the transportation of small molecules across the shell (Cheng et al. 2008). It has also been shown that one of the Pdu shell proteins, PduB consists of three pores within a trimeric structure that function to channel glycerol, and potentially 1,2-propanediol, into the metabolosome. In addition to glycerol channelling, glycerol was also found to occupy a central binding pocket, with flexible loops above and below it. When glycerol was bound, the loops were locked closed. This suggests a role in closing the central pore and providing the possibility of

a ligand-gated channel, preventing aldehyde efflux while allowing glycerol, and possibly other substrates, to enter the shell (Pang et al. 2012). Similarly the Eut microcompartment shell protein, EutL has also been shown to contain a central channel that can adopt an open or closed state (Takenoya, Nikolakakis & Sagermann 2010).

The ability to understand the mechanism of transport across the BMC shell is key for the use of microcompartments in synthetic biology. To be able to utilise efficiently BMCs as nanobioreactors, for large scale production of biofuels, drugs and other products, we need to be able to understand how substrates and cofactors enter the compartment and also how intermediates are confined to the lumen. Consequently, the study of the BMC shell is key to our understanding of how these compartments can be used in synthetic biology.

1.1.4. A Synthetic Approach to BMCs

The ability to compartmentalise reactions, and possibly whole pathways, is highly desirable, with many applications in metabolic engineering, nanotechnology and bioengineering. Microcompartments are an ideal method of introducing compartmentalisation into bacterial cells. Instead of having to rewrite or revise the genetic code to manipulate the metabolic activities of the host organism, the microcompartment is a pre-evolved system which already primarily functions as a metabolically active powerhouse of the cell. BMCs represent a comparitively simple solution to enhance cellular production of designer chemicals, vitamins, antibiotics, biofuels and non-native metabolites (Parsons et al. 2010). To engineer a separate vehicle for the compartmentalisation of a complex pathway, many factors need to be considered and the bioreactor must comprise specific chemical and physical properties. Firstly, the boundaries of the reactor should allow for selective diffusion, to permit substrates and products to pass whilst retaining the catalytic components and protecting them against degradation. The exterior of the bioreactor should be able to withstand changes to the cellular environment, such as pH and temperature and must be able to be used in a living system without stimulating an adverse cellular response. In addition the functional bioreactor

size must not exceed the nanometers range to allow the pathway to be subjected to a single microenvironment (Monnard 2003). This gives BMCs the leading edge for the potential use as a bioreactor; it meets all the specifications required and does not require *de novo* biochemically engineering as it exists in nature, with only minor re-designing needed to tailor the BMC to the desired use. It also has the added benefit of potentially allowing any reaction involving a toxic intermediate to be produced quickly, efficiently and inexpensively, in living organisms. It could therefore be used to improve the yield of chemical reactions and to lower the toxicity to the host cell (Bonacci et al. 2012).

Currently it is possible to produce empty, recombinant BMC shells in lab strains of *E.coli*. This has allowed a further understanding of BMCs and how they can potentially be utilised in industry. In addition, the recent discovery of a target sequence has allowed the targeting of non-native proteins to the BMC (Fan et al., 2010) see section 1.5 Recombinant Pdu Studies. This provides the potential to use these organelles to produce non-native metabolites in an environment where substrates, enzymes and cofactors are confined. The advantages of BMC use in industry are therefore substantial; the targeting of specific proteins to the compartment interior increases local concentrations of substrates and enzymes, this confinement has the potential to increase the yield of the end product while mitigating any toxic or volatile intermediates. This mitigation would allow a pathway, which would otherwise not be viable, to be executed by bacteria.

1.2. Carboxysomes

Carboxysomes were the first microcompartments to be discovered. They were initially visualised by electron microscopy in the cyanobacteria, *Phormidium uncinatum* in 1956 (Niklowitz & Drews 1956), and subsequently identified and isolated from the chemoautotroph *Halothiobacillus neapolitanus* as polyhedral bodies in 1973 (Shiveley, Ball & Kline 1973). Initially they were mistaken for viruses, but further research by Shiveley et al. indicated a role in carbon fixation via the Calvin cycle. It was found that these polyhedral inclusions contained the carbon dioxide-fixing enzyme

RubisCO; they were subsequently named carboxysomes due to their suggested involvement in CO_2 fixation. It has now been shown that carboxysomes do in fact play an integral role in enhancing autotrophic CO_2 fixation via the Calvin cycle and are widely distributed amongst both chemoautotrophs and cyanobacteria (Price et al. 2008).

Even though carboxysomes are fairly sophisticated in that they are large, multi-protein complexes, shown in Figure 1.3, they are the simplest of all characterised BMCs. The size of carboxysomes range between 80 and 150 nm in cross section and they are bounded by a thin 3-4 nm protein shell. They are composed of several thousand polypeptides consisting of 10 – 15 different types, totalling an overall mass of approximately 300 MDa (Yeates et al. 2007; Cheng et al. 2008).
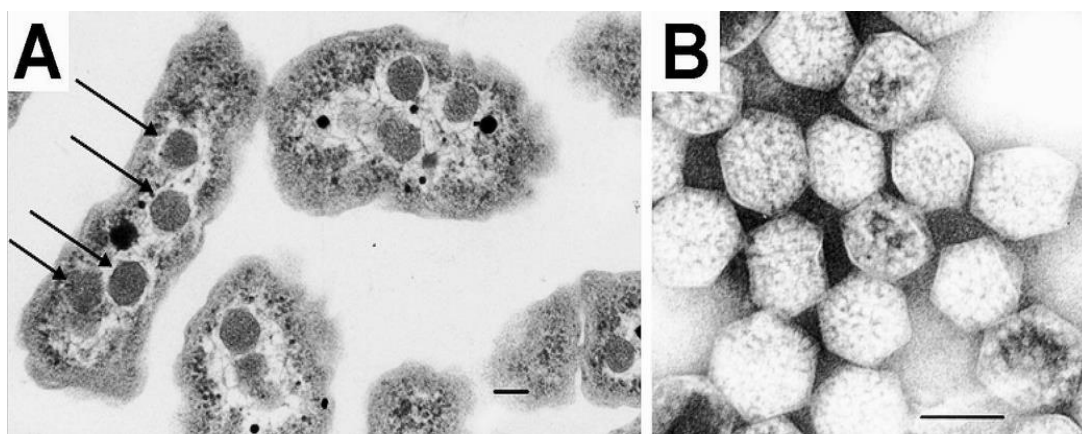
Figure 1.3 – TEM images of carboxysomes from *H. neapolitanus* A) Negatively stained thin sections of cells containing carbozysomes, highlighted by the arrows B) Purified negatively stained intact carboxysomes. The interior of the carboxysomes are packed with RuBisCO. Scale bars 100 nm. Adapted from (Tsai et al. 2007).

1.2.1. The Carboxysome Pathway

The carboxysome shell encases two distinct enzymes; carbonic anhydrase (CA) and ribulose bis-phosphate carboxylase monooxygenase (RuBisCO) (Shively et al. 1973; Fukuzawa et al. 1992). Within the confines of the microcompartment lumen, it was hypothesised that CA converts bicarbonate (HCO3-) to carbon dioxide (CO2). RuBisCO then converts CO2 and RuBP to two molecules of 3-phosphoglycerate (3-PGA) which then leaves the interior of the compartment,

through the selectively permeable shell, into the cell cytoplasm. This is the first step of the Calvin-Benson-Bassham cycle. It was suggested that CA would ensure that cytosolic bicarbonate was converted to CO2 at a concentration that would maintain optimum RuBisCO activity (Reinhold, Kosloff & Kaplan 1991). It has been shown that partially purified carboxysomes from two cyanobacterial strains are associated with CA activity (So et al. 2004). Although it is commonly recognised that CA is an essential component of a cellular carbon dioxide concentrating mechanism (CCM), the localisation of this enzyme or if many carboxysomes even comprise it was initially unclear (So et al. 2004).

Some early conclusions were drawn in 1989 by Price and Badger when the cytosolic levels of CA activity were raised, to test if CA needed to be localised within the carboxysome. It was found that firstly inorganic carbon must be present as bicarbonate rather than carbon dioxide, for the carboxysome to function. In addition, in carboxysome-containing cells, CA is absent from the cytosol but located with the carboxysome (Price & Badger 1989). Further research has shown that there are three classes of CA, α, β and γ; the expected evolutionary lineage to be found with carboxysomes. CcaA, is a carboxysome-associated member of the β class, which are widespread among *Bacteria*, *Archaea* and *Eucarya* domains. However, recently, So *et al*. have shown the existence of another lineage of CA (ε class), isolated from *H. neapolitanus*. It was demonstrated that this new CA, CsoS3, is a catalytically functional component of the carboxysome shell. It is predicted that carboxysomes from other species may contain this new lineage, as they contain homologues of the carbonic anhydrase CsoS3 (So et al. 2004). This may help to explain why, for so many years, the involvement of CA and its localisation in relation to the carboxysome has been so elusive.

The carboxysome is an essential part of the bacterial CCM. It is now recognised that when CO2 concentrations are low, carboxysomes are formed. The pathway begins with an active transport process that concentrates bicarbonate (HCO3-) within the cell cytoplasm. In the cytoplasm, HCO3- is maintained at a chemical non-equilibrium against carbon dioxide (CO2) through the absence of

CA activity in the cytosol (Price & Badger 1989; Price et al. 2008). Bicarbonate is the preferred form of inorganic carbon (Ci) as, compared to uncharged CO_2, it is 1000-fold less permeable to lipid membranes (Price et al. 2008). This would prevent CO_2 leakage out of cells. Subsequently, a carboxysome-associated CA converts the accumulated HCO_3^- to CO_2 and releases it within the carboxysomes. The carboxysome shell acts as a diffusion barrier to prevent the loss of CO_2. CO_2 then accumulates within the carboxysome lumen, in the location of RuBisCO (Cheng et al. 2008). RuBisCO subsequently catalyses the carboxylation of ribulose bisphosphate to form two molecules of 3-phosphoglycerate; this is the first step of the Calvin-Benson-Bassham cycle (Price et al. 2008).

1.2.2. Alpha and Beta-Carboxysomes

Currently two classes of carboxysome, which vary slightly in composition, have been identified. These have been termed alpha (α) and beta (β) carboxysomes. It is thought that each of these classes have evolved in parallel with a different phylogenetic group of RuBisCO; α-carboxysomes are associated with 1A RuBisCo and are found within chemoautotrophs and α-cyanobacteria, whereas β-carboxysomes are associated with 1B RuBisCO and are contained within β-cyanobacteria (Badger & Price 2003).

It is difficult to distinguish the difference between forms 1A and 1B of RuBisCo. In general form I enzymes are considerably diverse and are divided into four clades. Form IA and IB are typically known as the green forms as they are found in cyanobacteria and green algae whereas IC and ID are associated with red and non-green algae (Badger & Bek 2008). Both IA and IB enzymes are composed of a large catalytic subunit and a smaller subunit to form a hexadecameric structure consisting of eight copies of each protein; L_8S_8, or specifically $(L_2)_4(S_4)_2$ with a total M_r of 550,000 (Tabita 1999). Of forms IA and IB, the enzymes that are associated with carboxysomes are subgrouped into IAc and IBc. IAc RuBisCo is always associated together with a cluster of α-carboxysome genes and are thought to both be inherited by lateral gene transfer events. However Form IB is far less diverse than IA as β-cyanobacteria are the only bacteria to contain form IB of

RuBisCO and the enzyme genes may or may not be associated with the carboxysome gene cluster and could be located elsewhere in the genome (Badger & Bek 2008). Overall α and β- carboxysomes are thought to have similar architectural and mechanical properties but differ in the associated form of RuBisCO.
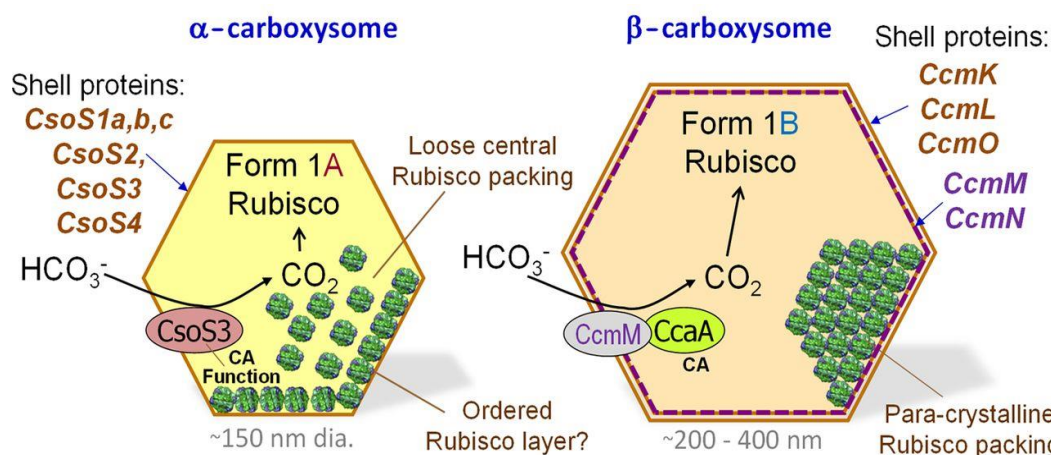
Figure 1.4. Diagrams showing the different components of α and β- carboxysomes, possible distribution of Rubisco within the carboxysomes and their comparative sizes. Adapted from (Rae et al. 2013)

1.2.3. Carboxysome Function

It is clear that the primary function of the carboxysome centres on the enzyme RuBisCO as it constitutes approximately 60% of the total carboxysome protein content, with the shell accounting for 17% (Cannon & Shively 1983). Therefore the key question is what metabolic purpose is there by packaging this carbon assimilation enzyme into the BMC? It is thought that the carboxysome either acts as a storage vessel to contain excess RuBisCO, or functions to enhance the kinetic ability of the enzyme (Gordon C Cannon et al. 2001). Studies have shown that when CO2 is limited, total cellular RuBisCO activity levels and the copy number of carboxysomes per cell increase (Beudeker et al. 1980). This gives some evidence that carboxysomes serve to increase the metabolic activity of the cell. They do this through several proposed methods:

(i) RuBisCO is commonly known as an inefficient enzyme, with a 9.6 fold higher specificity for O2 than CO2 in RuBisCO form I, the type present in all carboxysomes (Tabita 1999). This phenomenon

is known as photorespiration; an energetically wasteful process that involves the fixation of O2, instead of CO2, to RuBP by RuBisCO. Consequently it is thought that encasing this enzyme in a proteinaceous shell would differentially block oxygen from being catalysed to increase the efficiency of the enzyme by enhancing the carboxylase activity and excluding the competing substrate (Gordon C Cannon et al. 2001).

(ii) Bicarbonate accumulates in the cell cytoplasm, is converted to CO2 and released in the carboxysome lumen. Through this method the local concentrations are increased to generate a microenvironment of high CO2 levels in the carboxysome (Price et al. 2008). CO2 is prevented from diffusion through lipid membranes by releasing it directly into the selectively permeable carboxysome shell. By encasing RuBisCO in the same vicinity as CO2, the efficiency of carbon fixation by RuBisCO is increased and photorespiration is supressed (Cheng et al. 2008).

(iii) Similarly, the carboxysome shell is capable of differentiating between oxygen and carbon dioxide. It does this through charged pores which allow the passage of negatively charged molecules such as bicarbonate, a precursor of carbon dioxide, or 3-PGA, the end product of catabolism in the carboxysome, to enter the BMC whilst excluding molecules such as oxygen. These pores serve two purposes; to allow increased localised concentrations of CO2, increasing the efficiency of RuBisCO, but also to prevent the loss of energy during photorespiration by the exclusion of O2 (Gordon C Cannon et al. 2001).

Therefore, it could be considered that the carboxysome acts to improve the efficiency of the carbon assimilation enzyme, RuBisCO by providing a carbon dioxide concentrating mechanism (CCM)
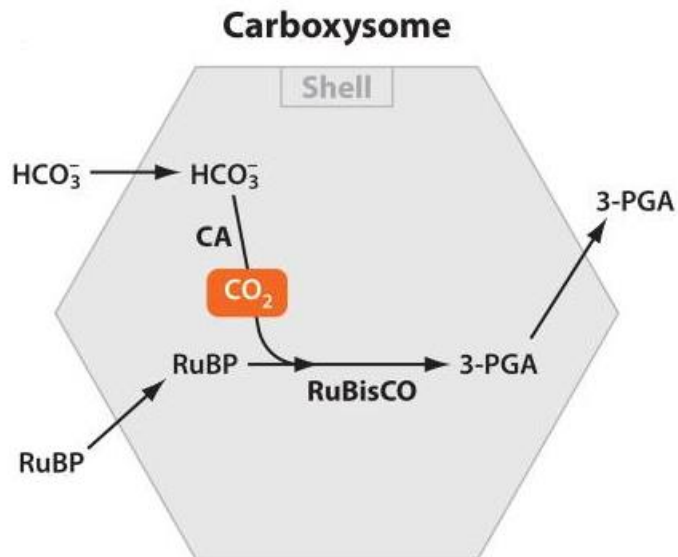
Figure 1.5. Model of the metabolic pathway of the Carboxysome: The carboxysome shell confines the enzymes required to convert bicarbonate (HCO$_3$-) to CO$_2$. RuBisCO then catalyses the carboxylation of ribulose 1,5-bisphosphate (RuBP) . The proposed function is to sequester CO2 and enhance its fixation. Adapted from (Yeates, Crowley & Tanaka 2010).

1.2.4. The Carboxysome Operon

It may appear that different proteins are associated with each form of carboxysome, however many protein components are conserved but the gene names can differ. The exceptions to this are the CsoS2 and CsoS3 proteins which are characteristic of α-carboxysomes whereas CcmM, CcmN and CcaA are specific to β-carboxysomes, as described in Table 1.1 below.

α-Carboxysomes		Role
Protein	CbbL	Form 1A RuBisCO large subunit
	CbbS	Form 1A RuBisCO small subunit
	CsoS2A	Associated with the shell, encoded by the same gene but different in level of glycosylation
	CsoS2B	
	CsoS3	Forms a novel type of CA and is tightly associated with the shell
	CsoS1A	Closely related in sequence, forms the bulk of the shell. Contains the BMC domains
	CsoS1B	
	CsoS1C	
	CsoS4A (OrfA)	Found to be a pentamer, may form vertices of the shell
	CsoS4B (OrfB)	

β-Carboxysomes		Role
Protein	RrcL	Form 1B RuBisCO large subunit
	RrbcS	Form 1B RuBisCO small subunit
	CcmK	BMC-domain proteins with homology to CsoS1, a major shell protein in the α-carboxysome
	CcmO	
	CcmL	Related in sequence to ScoS4A and B of the α-carboxysome and may also form the shell verticies
	CcmM	Restricted to β-carboxysomes. May function as organizing factors or in enzyme regulation. CcmM may act as a scaffolding protein to establish interactions between the protein shell and encapsulated enzymes (Yeates, Thompson & Bobik 2011)
	CcmN	
	CcaA (IcfA)	Carboxysome-associated carbonic anhydrase

Table 1.1 - The proteins associated with α and β-carboxysomes and the role they play in carboxysome formation and function.

1.2.5. The Carboxysome Shell Structure

The outer casing, or shell, is the most identifiable feature of the BMC. It is comprised of small proteins of around 100 amino acids and these shell forming proteins contain a BMC domain that are thought to form either the facets of the shell, or the pentameric vertices (G. C. Cannon & Shively, 1983; Kerfeld et al., 2005). Originally mistaken for virions, carboxysomes share many similarities with icosahedral viral capsids. They both contain multiple homologues of a small protein, either the

CsoS1 or CcmK proteins for α and β-carboxysomes respectively. Many copies of this small but distinct protein constitutes the shell of the carboxysome (Yeates et al. 2007). However several other shell proteins have been found, including; Cso4 in α-carboxysomes and CcmO and CcmL in β-carboxysomes (refs). To date, six carboxysome shell proteins have been crystallised. These include CcmK1, CcmK2 and CcmK4 from β-carboxysomes (Kerfeld et al. 2005; Tanaka et al. 2008; Crowley et al. 2008) and CsoSIA, CsoSIB and CsoSID from α-carboxysomes (Klein et al. 2009; Tsai et al. 2007). These structures have revealed that the protein monomers aggregate into hexameric tiles, giving the protein a convex and concave side. It was found that these hexamers formed a two-dimentional layer and that CcmK2 hexamers faced the same direction whereas CcmK4 hemamers alternated between convex and concave orientations (Kinney, Axen & Kerfeld 2011). Proteins from the α-carboxysome display the same convex/concave hexamer structure with uniform directionality. In addition CsoS4A and CcmL have been found to form pentameric structures (Tanaka et al. 2008). They also have concave/convex sidedness but unlike the hexameric proteins, they have a positive electrostatic potential. This is thought to be influenced by the presence of an 8-10 amino acid loop on the concave face of the pentamer, which is lacking in the hexamers (Kinney, Axen & Kerfeld 2011).

Structural studies, which have led to schematic modelling of the carboxysome shell, are thought to apply to other BMCs too. The shell domains are highly conserved, as well as the presence of hexameric and pentameric proteins. The hexamers contain a central pore of 4-7 Å and are thought to tile together to form the facets of the shell whereas the pentamers cap the vertices (Cai et al. 2014).

1.2.6. The Assembly of Carboxysomes

The individual carboxysome shell proteins have been shown to self-assemble into cyclic disc-shaped hexamers (Kerfeld et al. 2005). These hexamers are then able to fold together and form the icosahedral structure of the carboxysome shell. This shell assembly must somehow coincide with

the assembly of the cargo within. Until recently, the nature of shell protein assembly was largely unknown. It was suggested that both the shell proteins and cargo have the ability to self-assemble (Orus et al. 1995) but the mechanism for this was undetermined. There is evidence to suggest that the carboxysome shell proteins and its cargo are able to assemble together; partially assembled carboxysomes have been found to always contain both RuBisCO and shell proteins (Iancu et al. 2010). The data also suggests that the cargo must be able to self-assemble as RuBisCO is observed in the inner layers of the assembling compartment.

Studies carried out on isolated carboxysomes from *Synechococcus* revealed that there were several distinct stages to carboxysome formation visible by EM. These include the initial formation of ring-shaped structures, followed by electron-translucent inclusions that have the carboxysome shape and internal organisation of RuBisCO and lastly carboxysomes with an internal electron-translucent area. It was suggested that the electron—translucent inclusions are grouped molecules of RuBisCO and these were present at very early stages of carboxysome biogenesis. It was found that unfixed carboxysomes had a tendency to collapse, leaving the RuBisCO to be visualised by EM. This RuBisCo could be identified by its "doughnut" shape. Consequently, with high RuBisCO concentrations, it was possible to show that RuBisCO molecules tended to self-assemble, forming structures distinct to mature carboxysomes, without the presence of a carboxysome shell (Orus et al. 1995).

To support this, Cameron et al have shown that carboxysome biogenesis begins with the aggregation of RuBisCO; this initiation is dependent on CcmM, a protein thought to act as a scaffold between the carboxysome shell and the encapsulated enzymes (Cameron et al. 2013; Long et al. 2011). During this process, RuBisCO aggregates into a distinct foci, usually localised to a cell pole. The resulting nascent carboxysome is therefore comprised of disordered RuBisCO molecules that have not yet been enveloped by shell proteins. This gives further evidence that the carboxysome cargo self-assembles first, preceding its complete encapsulation by the carboxysome shell.

Furthermore it has been shown that partially formed carboxysomes can be visualised. Suggesting that RuBisCO is simultaneously aggregated and encapsulated (Cameron et al. 2013).

Overall, through live cell fluorescence microscopy and transmission electron microscopy (TEM), it has been shown that carboxysomes do in fact originate as small foci of self-assembling RuBisCO. This small aggregate of carboxysome cargo then grows over a timespan of hours, into a larger RuBisCO inclusion which is then encased abruptly by the colocalisation of shell proteins to the foci, establishing a protected internal environment (Cameron et al., 2013; A. H. Chen, Robinson-Mosher, Savage, Silver, & Polka, 2013).

The assembly process of BMCs are important to our understanding of how shell proteins and cargo interact to form the structure and package proteins inside. This can then be applied to engineered BMCs, allowing the biosynthesis of designer chemicals, drugs, biofuels and other products. So far the assembly of both Pdu and Eut BMCs remain completely unknown, however insights into the assembly of carboxysomes can help to advance research into the formation of BMCs as a whole due to possible similarities between these bacterial organelles.
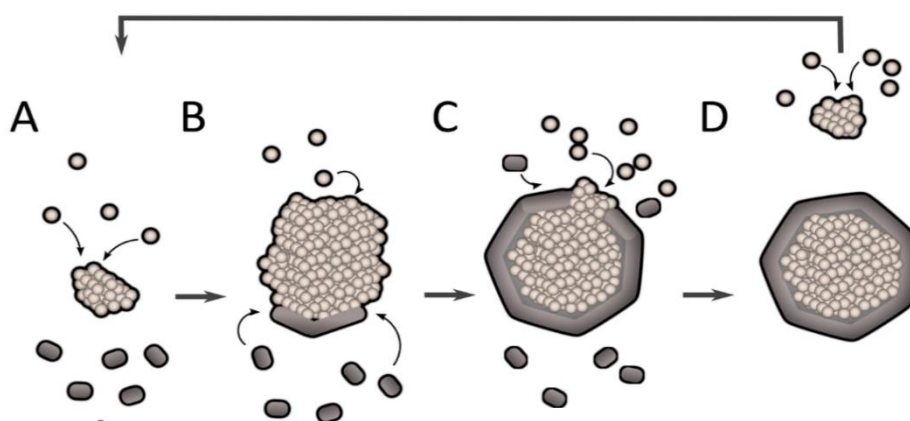
Figure 1.6. A proposed model for the self-assembly of carboxysomes: A) Aggregation of RuBisCO to form a "nucleus" occurs, B) As the RuBisCO "nucleus" reaches its full size carboysome shell proteins assemble around the RuBisCO, C) Shell assembly completes and the RuBisCO is sealed off from the cytosol, creating an oxidising environment, D) Formation of a new RuBisco "nucleus" takes place after completion of the previous carboxysome assembly. Adapted from (Chen et al. 2013).

1.3. Ethanolamine Utilisation Microcompartments

Ethanolamine is a product of the degradation of the bacterial and mammalian membrane component phosphatidylethanolamine and is produced in the gastrointestinal tract of mammals. Utilisation of ethanolamine allows a variety of bacteria, including the best-studied case *Salmonella*, as well as *Escherichia, Klebsiella, Pseudomonas, Actinobacteria, Clostridium, Mycobacterium* and *Enterococcus,* to inhabit diverse environments, such as the mammalian gut. Here the ethanolamine is derived from intestinal epitheial and bacterial cells as well as the host diet, as the catabolism of this amino alcohol can provide their sole source of carbon and nitrogen (Bradbeer 1965; Tsoy, Ravcheev & Mushegian 2009). This catabolic process involves a Cobalamin-dependent pathway and the necessary genes involved are clustered in the ethanolamine utilisation (*eut*) operon, including enzymes for ethanolamine degradation and carboxysome shell protein homologs (Chang & Chang 1975; Stojiljkovic, Bäumler & Heffron 1995).The initial evidence for the existence of Eut BMCs stemmed from the discovery of genes encoding shell proteins in *Salmonella enterica*, this led to the finding of genes for ethanolamine degradation clustered in the same operon (Stojiljkovic, Bäumler & Heffron 1995; Kofoid et al. 1999). Subsequent studies have shown that, during growth on ethanolamine, *S. enterica* forms BMCs (Shively et al. 1998).

Both the Eut and Pdu BMCs form less regular structures and do not resemble a regular icosahedron as closely as the carboxysome does (Figure 5) (Yeates, Thompson & Bobik 2011). It has been suggested that this is due to the differences in the vertex protein properties between the various BMCs (Yeates, Thompson & Bobik 2011). Nevertheless, the approximate size of the Eut BMC is similar to that of the carboxysome at 100 nm (Held, Quin & Schmidt-Dannert 2013). The Eut BMC is also considered to be more complex than that of the carboxysome, housing more enzymes for a degradation pathway that involves a volatile intermediate, as shown in Figure 1.7.

1.3.1. The Eut Pathway

Initially the eut pathway begins with the conversion of ethanolamine to ammonia and acetaldehyde; the enzyme involved is the Cobalamin-dependent ethanolamine ammonia lyase (EutBC) (Bradbeer 1965). Acetaldehyde can then be converted to acetaldehyde, which in turn is converted to acetyl-CoA, acetyl-phosphate and lastly to acetate. Acetaldehyde can alternatively be converted to ethanol. The conversion to acetate produces one molecule of ATP by substrate-level phosphorylation and involves the enzymes; acetaldehyde dehydrogenase (EutE), phosphotransacetylase (EutD) and acetate kinase, whose gene is outside of the *eut* operon. The conversion of acetaldehyde to ethanol is catalysed by an alcohol dehydrogenase (EutG) which maintains the NADH/NAD$^+$ balance (Kofoid et al. 1999; Roof & Roth 1988).
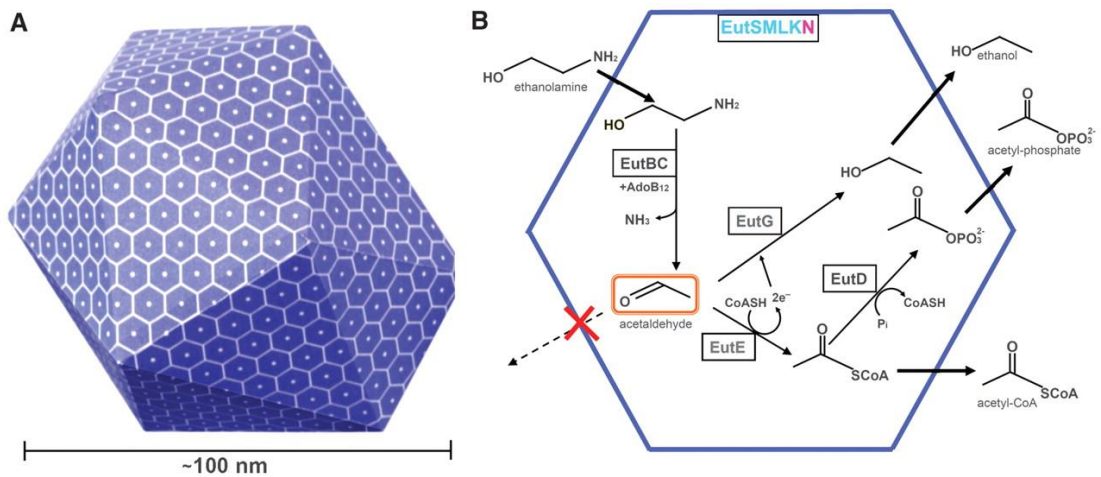
Figure 1.7. The Eut BMC: A) The irregular icosahedron structure of the Eut BMC is shown to be around 100 nm in diameter B) The degradation pathway of ethanolamine initiates with the conversion to acetaldehyde, a volatile intermediate that is confined in the BMC lumen. The products of this internalised pathway are ethanol and the acetate-producing intermediates acetyl-phosphate and acetyl-CoA. Adapted from (Tanaka, Sawaya & Yeates 2010).

S. enterica uses ethanolamine as a sole carbon and nitrogen source under aerobic conditions. In the presence of oxygen, the TCA cycle and glyoxylate shunt metabolise acetyl-CoA (Roof & Roth 1988). However under fermentative conditions *S. enterica* is only able to use ethanolamine as a sole nitrogen source but not as a sole carbon and energy source. This is because oxygen is required to divert pathway intermediates into biosynthetic reactions (Price-Carter, Tingey, Bobik, & Roth,

2001). Despite this, the degradation of ethanolamine provides additional ATP under anaerobic conditions when yeast extract is present to provide biosynthetic intermediates. In addition, when tetrathionate is accessible as a terminal electron acceptor, ethanolamine also provides a sole carbon and energy source during anaerobic respiration (Price-Carter et al., 2001).

1.3.2. The *eut* Operon

The Eut metabolosome from *S. enterica* and *E.coli* are encoded by an operon consisting of 17 genes. This includes 5 structural shell proteins; EutS, EutM, EutN, EutL and EutK, as well as enzymes of the ethanolamine degradation pathway mentioned above EutBC, EutE, EutD and EutG (Kofoid et al. 1999; Tanaka, Sawaya & Yeates 2010; Roof & Roth 1988). The operon also contains the genes *eutA* and *eutT* which encode the regulatory proteins, ethanolamine ammonia lyase reactivase and a corrinoid cobalamin adenosyltransferase that converts cob(I)alamin to Adenosylobalamin (Ado-B$_{12}$) .A positive regulatory protein encoded by *eutR* is required for transcription induction of the *eut* operon (Roof & Roth 1992). The operon also includes the gene *eutH*, which encodes a transport protein for ethanolamine that is important at a low pH (Penrod, Mace & Roth 2004). It has been suggested that *eutJ* encodes a chaperone protein, but the exact function is unknown (Kofoid et al. 1999). The functions of EutP and EutQ are also unknown, although EutP has shown to have sequence similarity to known GTPases (Kofoid et al. 1999).

1.3.3. The Eut Shell

There are at least five Eut structural shell proteins; these include EutS, EutM, EutN, EutL and EutK (Kofoid et al. 1999). Of these, *eutK*, *eutL*, *eutM* and *eutN* are essential to the formation of the metabalosome. Genetic studies have revealed that mutations in any of these essential genes disrupt the growth of *S. enterica* on ethanolamine; it results in the metabolosome shell being malformed, permitting acetaldehyde leakage that ultimately prevents growth due to the loss of carbon (Penrod & Roth 2006).

EutM is a 96-amino acid hexameric BMC domain shell protein. It forms flat, cyclic hexamers that fold into extended sheets. The crystal structure has revealed a central pore occupied by a sulphate ion (from the crystallisation buffer), which indicates that the pore may be used for the transport of small molecules (Tanaka, Sawaya & Yeates 2010). It is thought that due to its similarity to the major structural shell protein PduA; EutM is likely to be the major building block of the Eut metabolosome. In contrast, other Eut shell proteins were found to have unusual structural features, suggesting specialised functional roles (Tanaka, Sawaya & Yeates 2010).

EutL is the largest Eut BMC domain protein and forms a pseudohexameric trimer and is thought to have similarity to PduB. Each monomer is formed from a combination of two tandem, circularly permuted BMC domains (Sagermann, Ohtaki & Nikolakakis 2009; Tanaka, Sawaya & Yeates 2010). Interestingly, as previously mentioned, EutL presumably features a gated pore, located at the centre of the trimer, for metabolite transport (Tanaka, Sawaya & Yeates 2010). This idea is based on crystal structures that reveal both an open and closed pore conformation. These two different conformations arise from large movements (15 Å) in the loop residues when the pore is opening or closing. The open pore is large enough (between 8 and 11 Å) to transport enzymatic cofactors. It is thought that a cofactor binds to the closed pore which subsequently opens and allows the molecule to enter the BMC; the pore then closes. In addition to EutM, EutL crystallises in molecular layers, suggesting its role as a major structural component of the shell (Sagermann, Ohtaki & Nikolakakis 2009; Tanaka et al. 2008).

EutS is a 111 amino acid shell protein with an unusual structure. Unlike the typical BMC domain proteins that form flat hexamers, EutS consists of a 40° bend. This bend is presumed to allow EutS to form the edges of the shell that help the facets to join together, with a similar role to that of PduJ (Tanaka, Sawaya & Yeates 2010). It is thought that a single amino acid (G39), which is conserved amongst all EutS proteins, is responsible for the unusually bent structure. The crystal structure of a

G39V mutant was found to have a flat hexameric structure, giving evidence that this amino acid is important for the functional diversification of EutS (Tanaka, Sawaya & Yeates 2010).
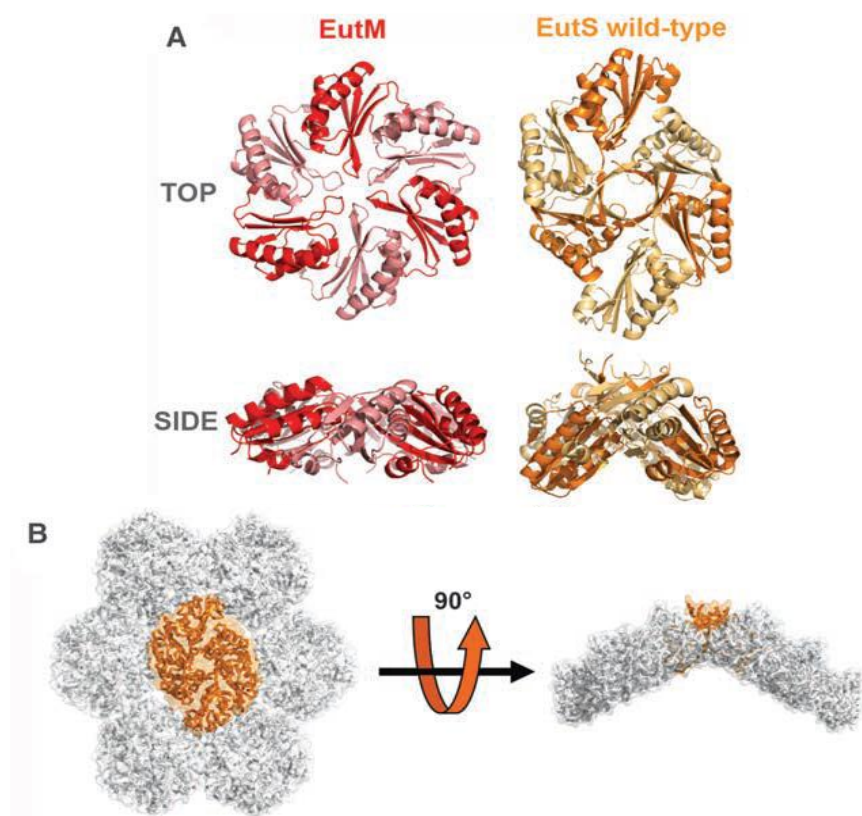
Figure 1.8. The structure of EutM and EutS. A) Side by side images of EutM and EutS structure, highlighting the 40° bend in the middle of EutS hexamer, in comparison to the flat EutM hexamer. B) A proposed model of how EutS (orange) may bring about curvature in a flat shell of hexamers, creating the vertices of the Eut BMC shell. Adapted from (Tanaka, Sawaya & Yeates 2010) .

EutK is a unique protein in the Eut BMC system. Unlike the other shell proteins, which have been reported to be either trimeric or hexameric, EutK was found to be monomeric in solution. In addition to the conserved BMC domain, it has also been found to include a 60 amino acid C-terminal extension, which contains a helix-turn-helix nucleic acid binding motif. Additionally this structure has a high positive charge, supporting its function in DNA/RNA binding, although its exact role is unknown (Tanaka, Sawaya & Yeates 2010).

EutN has a pentameric structure. Although it does not contain a BMC domain, it has sequence similarity to CcmL and CsoS4A, which are pentameric proteins in carboxysomes that are predicted toform the vertices of the BMC (Forouhar et al. 2007).

1.3.4. Eut Metabolosome Function

Eut BMCs are thought to play an essential role in the mitigation of the volatile ethanolamine degradation intermediate, acetaldehyde. By the encapsulation of this metabolic pathway, acetaldehyde is prevented from leaking into the cytoplasm where it could potentially cause damage to cellular components. Genetic tests have shown that *polA* (DNA repair polymerase) and *gsh* (glutathione biosynthesis) mutants are unable to grow on ethanolamine; it was proposed that this was due to the toxic build-up of acetaldehyde (Rondon, Horswill & Escalante-Semerena 1995; Rondon, Kazmierczak & Escalante-semerena 1995). In addition, due to the structural and functional similarities between the Eut and Pdu BMC systems, the proposed aldehyde toxicity of acetaldehyde and a role for the Eut BMC in encapsulating this intermediate has been suggested based on the toxicity of propionaldehyde and the Pdu BMCs primary function to mitigate this (Chowdhury et al., 2014).

Moreover, it has been suggested that the primary function of Eut BMCs is to prevent the loss of acetaldehyde as an essential carbon source. The vapour pressure of acetaldehyde is much higher than that of propionaldehyde and consequently, carbon loss due to volatility is likely to be more significant (Chowdhury et al. 2014).

1.4. Propanediol Utilisation Microcompartments

The research described later in this thesis focuses on the characterisation of Pdu BMCs. For many years, carboxysomes were considered to be the only known bacterial organelles. However, in 1994, a protein was found that had high sequence similarity to the carboxysome shell protein, CcmK (P Chen, Andersson & Roth 1994; T. A. Bobik et al. 1999). The homologous shell protein was subsequently named PduA and was found to be a major component of the Pdu shell. Bobik et al found that *S. enterica* forms BMCs similar in size and shape to carboxysomes when grown in the presence of 1,2-propanediol (1,2-PD), however when grown on other carbon sources these compartments do not form (T. A. Bobik et al. 1999). This led to the discovery of Pdu microcompartments, shown in Figure 1.9.
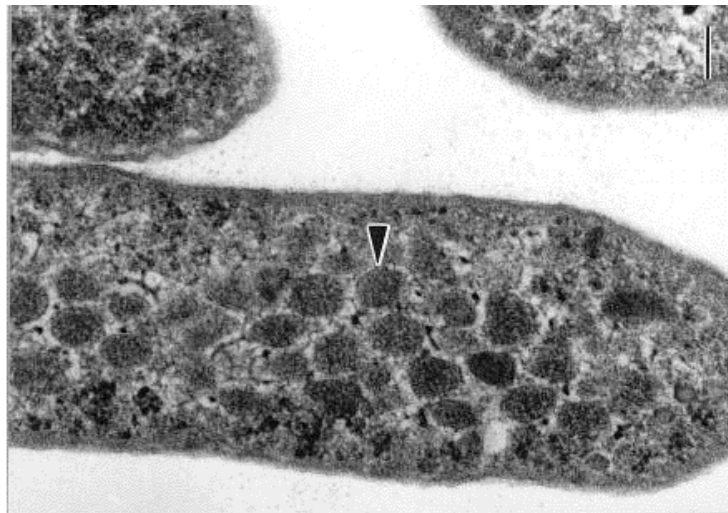
Figure 1.9. Pdu BMCs: TEM image of a thin section of *S. enterica* serovar Typhimurium LT2 grown on propanediol under aerobic conditions. BMCs can be seen throughout the cytoplasm; they are less regular in size and shape than carboxysomes and generally smaller. Scale bar 100 nm. Adapted from (G C Cannon et al. 2001)

The Pdu BMCs are polyhedral structures about 80-100 nm in diameter and were found to encapsulate enzymes necessary for the catabolism of 1,2-PD. Although they are a similar size and shape, Pdu BMCs are more complex than carboxysomes. They are estimated to comprise 18,000 polypeptides consisting of 18 -20 different types. The overall mass is projected to be twice that of carboxysomes at 600 MDa (Cheng et al. 2008).

Interestingly some bacterial strains, such as *Lactobacillus reuteri,* are able to utilise Pdu BMCs for the metabolism of glycerol as well as 1,2-PD due to the similarity between these three-carbon molecules (Pang et al. 2012).

1.4.1. Ecology of 1,2-PD degradation

The degradation of common plant cell wall sugars such as rhamnose and fucose, produces 1,2-PD under anaerobic conditions. In aquatic sediments and the large intestines of higher animals, the breakdown of these sugars leads to the release of 1,2-PD as a major product of the fermentation process (Obradors et al. 1988; Toraya, Honda & Fukui 1979). Enteric bacteria and bacteria in soil and aquatic environments are then able to use 1,2-PD as a carbon and energy source. Therefore through the production of BMCs, bacteria are able to use 1,2-PD for their metabolism, enabling them to occupy niches other bacteria can not, allowing them to live in competition-free microenvironments.

Genes associated with the formation of Pdu microcompartments have been found in various enteric and soil-inhabiting bacterial genera such as; *Salmonella, Citrobacter, Klebsiella, Shigella, Yersinia, Listeria, Lactobascillus, Lactococcus, Clostridium* and a species of *Escherichia coli* (E24377A) (Jorda et al. 2013; Bobik 2006; Cheng et al. 2008). The *pdu* gene clusters in these genera are highly conserved, suggesting that 1,2-PD degradation is dependent on the BMC (Cheng et al. 2008). It has been shown that the catabolism of 1,2-propanediol and ethanolamine is closely linked to intestinal proliferation and to bacterial virulence (Harvey et al. 2011), whilst more recently, studies have shown that 1,2-PD degradation is involved in enteric pathogenesis and is essential to the bacteria's ability to grow in the intestine (Staib & Fuchs 2014).

1.4.2. The *pdu* Operon

The genetic analysis of the catabolism of 1,2-PD by *S. enterica* identified a specific gene cluster involved in the Pdu pathway (Jeter 1990). This gene cluster, or *pdu* operon, was found to contain

23 genes; *pocR, pduF, pduABCDEGHJKLMNOPQSTUVWX* (P Chen, Andersson & Roth 1994; T. A. Bobik et al. 1999). These genes encode proteins necessary to form a functional BMC, including (I) structural proteins, (II) enzymes and (III) regulatory proteins. This comprises (I) the structural shell proteins, PduABJKNUT, (II) 1,2-PD degradative enzymes PduCDELPQW, (III) B_{12} recycling proteins, PduGHOSX as well as other Pdu BMC related proteins, PduM and PduV (P Chen, Andersson & Roth 1994; T. a Bobik et al. 1999).

Both the *pdu* and *cob* (cobalamin, B_{12}, biosynthesis) operons are found on the same regulon. This regulon is induced by 1,2-PD and controlled by the expression of two genes; *pocR* and *pduF*, located between the two operons (Chen et al. 1995). *pocR* encodes a positive transcriptional regulatory protein which mediates the induction of the regulon by 1,2-PD and *pduF*, encoding a diffusion facilitator which enables the transport of 1,2-PD (T. A. Bobik et al. 1999). PduF also comprises motifs that are associated with lipid membrane-binding and transmembrane channel proteins (Bobik et al. 1997; T. A. Bobik et al. 1999).

Coenzyme B_{12} is an essential cofactor for the first enzyme in the pathway, the diol dehydratase (PduCDE) (Jeter 1990) and therefore, growth on 1,2-PD is dependent on its availability. *S. enterica* is able to synthesise Cobalamin de novo, but only under anaerobic conditions (Jeter, Olivera & Roth 1984). This however, creates a paradox; *S. enterica* needs oxygen to catabolise 1,2-PD but cannot synthesise Cobalamin under aerobic conditions (Roth, Lawrence & Bobik 1996). However, it has now been established that tetrathionate can be used as an alternative terminal electron acceptor for both ethanolamine and 1,2-PD utilisation under anaerobic conditions, supporting the endogenous synthesis of Cobalamin (Price-Carter et al. 2001).

1.4.3. The Pdu Pathway

The catabolism of 1,2-PD involves a complex coenzyme B12-dependent pathway. It ultimately provides the cell with energy in the form of ATP and propionyl-CoA, an electron sink.

Following the uptake of 1,2-PD by the bacterial cell, 1,2-PD is transported into the BMC through the Pdu shell, presumably through a pore in the shell of the BMC.. Within the confines of the BMC, 1,2-PD is converted to propionaldehyde by the coenzyme Cobalamin-dependent enzyme, diol dehydratase (Toraya, Honda & Fukui 1979), formed of three protein subunits; PduC, PduD and PduE (Bobik et al. 1997). Propionaldehyde can found in both a reduced or oxidised form. Propionaldehyde dehydrogenase, PduP, catalyses an reduction reaction to convert propionaldehyde to propionyl-CoA where NAD^+ acts as a oxidising agent to accept the free electron, converting it to NADH (T. a Bobik et al. 1999). Propionyl-CoA leaves the BMC and is subsequently converted to propionyl-phosphate by a phosphotransacylase, PduL, and then to propionate by a reversible propionate kinase, PduW, producing one molecule of ATP (Toraya, Honda & Fukui 1979; Obradors et al. 1988; Jeter 1990). Propionyl-CoA can also enter the methyl-citrate pathway to release pyruvate as a carbon source and succinate, but only in aerobic conditions (Horswill & Escalante-semerena 1997). Alternatively, propionaldehyde can be oxidised by 1-propanol dehydrogenase, PduQ, to form 1-propanol; this reaction requires the coenzyme NADH to act as a reducing agent and donate an electron, forming NAD^+ (Toraya, Honda & Fukui 1979; Obradors et al. 1988).
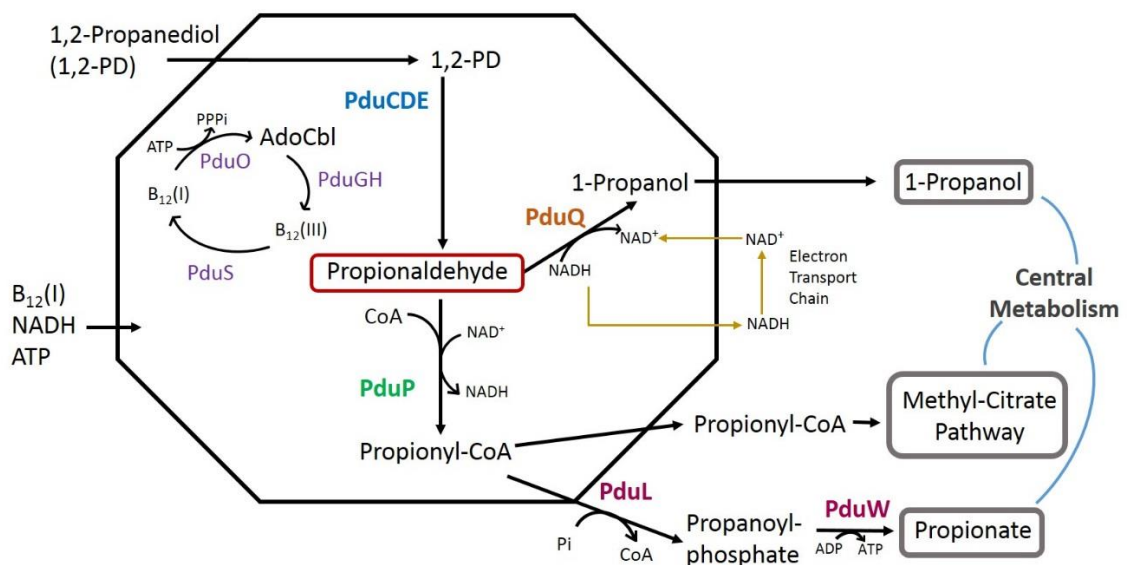
Figure 1.10. The pathway of 1,2-PD degradation. 1,2-PD enters the Pdu BMC through a selectively permeable protein shell and is degraded to propionaldehyde, a toxic intermediate that is sequestered in the BMC lumen. It is then catabolised to 1-propanol and propionyl-CoA, which leave the BMC and feed into central metabolism pathways in the cytosol.

Overall, the catabolism of 1,2-PD produces one molecule of ATP per propanediol molecule, as well as 1-propanol, propionyl-CoA and propionate. These products feed into central metabolism via other metabolic pathways. Even though the Pdu pathway can operate under aerobic or anaerobic conditions, 1-2-PD cannot produce a source of carbon (such as pyruvate) for biosynthetic reactions anaerobically. This is because the Methyl-Citrate pathway (see Figure 1.11 below) involves beta-oxidases that generate NADH + H$^+$ that require an electron transfer chain (Price-Carter et al. 2001). Therefore under anaerobic conditions, 1-2PD cannot be used as a solitary carbon and energy source.
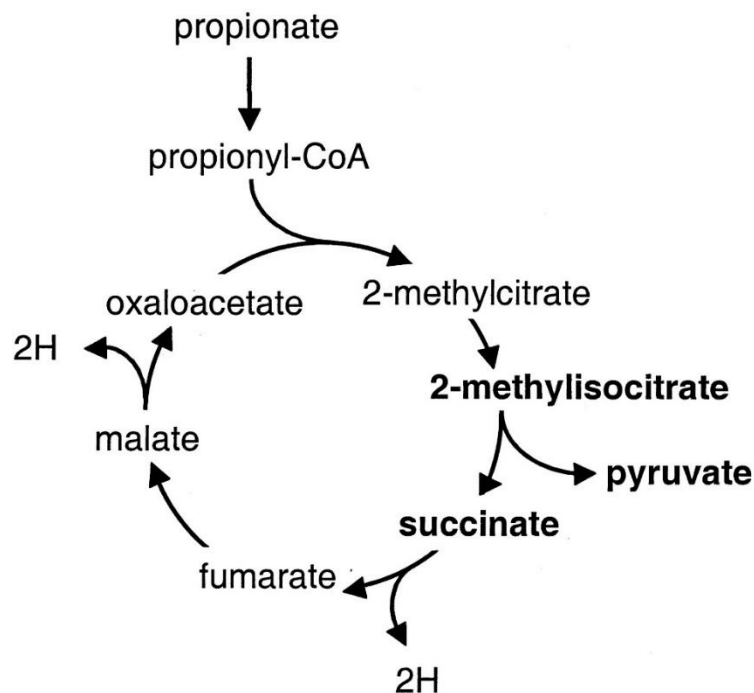
Figure 1.11. The Methyl-Citrate pathway, a key pathway for the metabolism for propionate under aerobic conditions. Adapted from (Salomons et al. 2000).

1.4.4. The Function of Pdu Microcompartments

Initially 1,2-PD catabolism may seem uncomplicated, but compartmentalisation of this pathway is essential for its viability due to the toxicity of the intermediate propionaldehyde. It has been suggested that the Pdu shell acts as a differential diffusion barrier to prevent the leakage of propionaldehde into the cell cytoplasm. Due to the high reactivity of this intermediate, compartmentalisation prevents damage to other cellular components (T. a Bobik et al. 1999). This is supported by the study of mutants unable to form the Pdu shell; it was found that propionaldehyde accumulated to toxic levels when grown on 1,2-PD (Sampson & Bobik 2008; Havemann, Sampson & Bobik 2002).

Another proposed function of the Pdu BMC is that compartmentalisation increases the local concentration of key enzymes, substrates and cofactors involved in the pathway to increase the efficiency of metabolic reactions. The Pdu BMC is more complex than that of the carboxysome as it contains linked metabolic enzymes and regulatory proteins to recycle the Adenosyl-Cobalamin. Therefore the need for concentrating the pathway at a molecular level is even greater.

1.4.5. Enzymology and Composition of the Pdu BMC

Of the 23 genes associated with the *pdu* operon, seven are known to encode proteins that are associated with the compartment shell; PduABJKNTU. Recently, Sinah et al have shown, through the use of PduM deletion mutants in *S. enterica* that PduM also localises with the BMC shell. Further evidence showed that when BMCs were purified and compared to the crude extract, PduM was enriched in the purified fraction, indicating that it is a component of the shell, however it is not required for the production of empty BMCs (Sinha et al. 2012). There is also evidence to suggest that PduV, a currently uncharacterised protein, is associated with the outer surface of the compartment shell; this is discussed later in chapter 1.6.

Other proteins encoded by the *pdu* operon form encapsulated enzymes, or enzyme subunits, which contribute to the catabolism of 1,2-PD. PduCDE forms the Cobalamin-dependent diol dehydratase

enzyme complex which catalyses the first step in the degradation pathway of 1,2-PD. Three further enzymes and enzyme complexes to support the role of PduCDE; diol dehydratase reactivase (PduGH), adenosyltransferase (PduO) and cobalamin reductase (PduS). These further enzymes function to recycle the Adenosyl-Cobalamin, the metabolically active form of Cobalamin associated with BMCs (Roth, Lawrence & Bobik 1996). During this recycling process, the central cobalt ion of cobalamin is reduced to Co(I), shown as B_{12}(I) in Figure 1.10, by cobalamin reductase, PduS. The Co(I) is a super-nucleophile that, along with the adenosyltransferase enzyme, PduO, facilitates the attachment of the adenosyl group from ATP (Walker, Murphy & Huennekens 1969). This reaction is unusual in that it releases triphosphate from the ATP molecule.

PduP, a propionaldehyde dehydrogenase, converts the toxic propionaldehyde to propionyl-CoA in the second metabolic stage of the pathway. PduP is a CoA-acylating enzyme and requires NAD^+ as a cofactor (Leal, Havemann & Bobik 2003). Interestingly, recent studies on *L. reuteri*, a bacteria that ferments glycerol to 3-hydroxypropionic acid (3-HP) also contains the enzyme PduP. This reaction involves the conversion of 3-HP to 3-hydroxypropionaldehyde (3-HPA), which is converted to 3-HP-CoA by PduP. This starts an enzymatic cascade involving PduL and PduW to produce ATP (Sabet-Azad et al. 2013), indicating a secondary role for some enzymes encoded by the *pdu* operon.

All of the metabolic enzymes discussed so far; PduCDE, PduS, PduO, and PduP have been shown to be encapsulated in the lumen of the BMC. However, the terminal enzymes of the Pdu pathway, PduL and PduW are located outside of the compartment and do not co-purify with it (Havemann & Bobik 2003).

Although it had previously been found that a phosphotransacylase (PTAC) was involved in 1,2-PD degradation, the enzyme involved had not been identified (Toraya, Honda & Fukui 1979; Obradors et al. 1988). However, it has been established that the *pduL* gene encodes an evolutionarily distinct PTAC, which is conserved and functions to convert propionyl-CoA to propionyl phosphate in the

Pdu pathway (Liu et al. 2007). Likewise, PduW is a terminal enzyme associated with the BMC, but located outside the confines of the lumen (Havemann & Bobik 2003). Bobik et al found that *pduW* had 87% similarity to the acetate kinase gene *ack* found in *S. enterica*, idnetifying PduW as a propionate kinase that converts propionyl phosphate to propionate (T. a Bobik et al. 1999).

PduQ was found to be related to alcohol dehydrogenases in 1999 by Bobik *et al* and has since been found to catalyse the conversion of propionaldehyde to 1-propanol (T. a Bobik et al. 1999). More recently, studies have shown that PduQ from *S.enterica* is iron-dependent and is located in the BMC, unlike two other terminal enzymes PduL and PduW. Through a series of *in vitro* and *in vivo* studies, Cheng et al have also identified that the main function of PduQ is to recycle NADH to its oxidised form, NAD^+ within the confines of the BMC. This allows PduP to be supplied with its cofactor, NAD+ internally within the Pdu BMC. However, studies also indicated the regeneration of NAD+ can occur via the electron transport chain. This requires the movement of NADH and NAD+ across the semi-permeable Pdu shell (Cheng et al. 2012), as shown in Figure 1.10.

Bioinformatic studies have shown that *pduX*, the last gene in the *pdu* operon, encodes an ʟ-Threonine kinase (Rodionov et al. 2003). Fan et al showed that PduX converts ʟ-threonine to ʟ-threonine-phosphate in *S. enterica*, a precursor for the nucleotide loop of Ado-Cobalamin (Fan & Bobik 2008). This means it is directly involved in *de novo* synthesis of Ado-Cobalamin. In addition PduX was the first enzyme identified that phosphorylates free ʟ-threonine (Rodionov et al. 2003).

Overall, the Pdu BMC encases at least 6 enzymes, comprising 9 different proteins; PduCDE, PduGH, PduO, PduP, PduQ and PduS. A further three enzymes have been found to associate with the BMC but are not located within the lumen, these are PduL, PduW and PduX.

1.4.6. Formation of the Pdu BMC

The way in which Pdu shell proteins assemble to form the icosahedral structure of the BMC remains unresolved. Further study into BMC formation needs to take place to understand fully the potential

of BMCs in synthetic biology and biotechnology. However, a recent study into the formation of the recombinant carboxysome shell has led to the finding that the internal cargo, RuBisCO, is capable of self-assembly; this initiates carboxysome formation and results in the carboxysome shell proteins constructing around the cargo (Cameron, Wilson, Bernstein, & Kerfeld, 2013; A. H. Chen, Robinson-Mosher, Savage, Silver, & Polka, 2013). However, the Pdu BMC is a more complex system, with more proteins involved and a larger number of internalised enzymes, substrates and cofactors. Due to the striking similarities between the two BMCs, it is feasible to conceive that Pdu BMC formation could use a similar model involving the self-aggregation of internalised components which is subsequently enveloped by the Pdu shell proteins. This remains unclear as the Pdu BMC has been shown to encapsulate enzymes that contain a specific targeting sequence. This sequence can be recombinantly used to target other enzymes and proteins to the BMC (see section 1.5.1). The need for a targeting sequence could indicate that the Pdu BMC shell structure may form *before* some of the enzymes are encapsulated, although it could be possible for initiation of compartment formation to begin with the self-aggregation and assembly of several specific encapsulated proteins.

1.4.7. The Pdu Shell

BMCs shells are typically composed of 5 – 10 proteins that contain a specific BMC domain (see chapter 1.1.1). Recent crystallography studies have given insights into how Pdu BMC proteins assemble to form the organelle shell and also the function of these proteins (Crowley et al. 2008; Kerfeld et al. 2005; Tanaka et al. 2008; Havemann, Sampson & Bobik 2002; Pang et al. 2014). Several features of the BMC shell make it specialised to its function. At least three properties of shell proteins are important for the function of the bacterial organelle; the proteins must interact with each other to form a layer which surrounds the BMC, they must form essential interactions with internal components of the organelle and also allow the movement of molecules across the shell (Crowley et al. 2008).

The current model of the Pdu BMC suggests that it is composed of at least seven different proteins; PduA, PduB, PduJ, PduK, PduN, PduT and PduU (Cheng et al. 2011). It is also thought that the shell could contain another protein, PduM, as it was found that a deletion mutant lacking the *pduM* gene produced BMCs with irregular size and shape, although its exact role is unclear (Sinha et al. 2012). In addition, due to two translation start sites, *pduB* is translated into two separate proteins of varied lengths, PduB (28kDa) and a shorter isoform, PduB' (24kDa) which differs by 37 residues (Havemann & Bobik, 2003). These shell proteins were initially identified by their DNA sequence similarity to proteins required for carboxysome formation, in particular PduA, PduJ, PduK and PduT proteins that have similarity to shell proteins of the carboxysome (T. A. Bobik et al. 1999; Shively et al. 1998).

PduA, PduB, PduB' and PduJ are considered to be the major components of the Pdu BMC shell, constituting 7.5, 12.8, 12.1 and 11% of purified Pdu organelles from *S. enterica*, as determined by densitometry of 2D electrophoresis (Havemann & Bobik 2003). The minor shell components were determined to be PduK, PduN, PduT and PduU, with protein percentages of 1.6, not determined, 1.6 and 1.5% respectively (Havemann & Bobik, 2003). Parsons et el demonstrated that organelle formation was dependent on the concentration of the shell proteins; if these proteins were overproduced in an *E. coli* strain containing the *pdu* operon, the resulting BMCs were abnormal (Parsons et al. 2008).

Studies have also been carried out to determine which of these shell-associated proteins are essential to the structure of the BMC. It has been shown that deletion of shell protein genes generally have two main phenotypes when grown on 1,2-PD; propionaldehyde toxicity and faster growth when cobalamin is limiting (Havemann, Sampson & Bobik 2002; Sampson & Bobik 2008) This is characteristic of the non-functional BMCs when *pduB* and *pduB'*, *pduJ* or *pduN are deleted*, indicating that they are essential structural proteins required for complete and intact organelle formation. In addition, when the *C. freundi pdu* operon is expressed in *E. coli*, a *pduA* deletion mutant is unable to form BMCs in this system, indicating that it could be essential to the formation

of the BMC (Parsons et al. 2008). However, later studies using the endogenous *S. enterica pdu* operon suggest then when *pduA* is deleted, the resulting strains appear to have intermediate phenotypes; they form larger organelles and produce an intermediate level of toxicity by propionaldehyde (Cheng et al. 2011). When *pduK*, *pduT* or *pduU* were deleted, the BMC structure was not impaired and growth on 1,2-PD was not severely influenced (Cheng et al. 2011). Previous work on recombinant, empty Pdu compartment shells (ie BMC's only containing shell proteins) showed that not all of these proteins are necessary to form the BMCs in *E.coli*. The minimum shell components required to form the empty organelle were found to be PduA, PduB, PduB', PduJ, PduK and PduN (Parsons et al. 2010).

X-ray crystal structures of Pdu shell proteins have revealed flat, 6-fold hexamers that package in a tile-like formation and form layers, as shown in Figure 1.2 (Crowley et al. 2008; Pang et al. 2014). Most of these crystallised hexamers, with the exception of PduU, have distinct openings along the central axis. These openings are thought function in molecular transport and act as pores. These pores have been found to differ in size and charge, depending on the residues surrounding the opening (Kerfeld et al. 2005; Crowley et al. 2010).

As with the Eut BMC it is proposed that the BMC protects the cell from propionaldehyde, the toxic intermediate formed from the conversion of 1,2-PD by PduCDE, a diol dehydrase. This is thought to be the main function of the Pdu BMC; to mitigate the toxicity by acting as a barrier to prevent diffusion and subsequent DNA damage (T. A. Bobik et al. 1999).

1.4.7.1. PduA
PduA is a 94 amino acid residue shell protein of the Pdu organelle that has been estimated to comprise 16% of the total shell (Havemann & Bobik 2003), rendering it a major component. It was originally identified due to its similarity to CcmK, a carboxysome shell protein (T. A. Bobik et al. 1999; P. Chen, Andersson & Roth 1994). PduA was first shown to be part of the Pdu shell in 2002 by Havemann, Sampson and Bobik (Havemann et al., 2002). They did this through immunogold

labelling of *S. enterica* cells using anti-PduA antibodies and subsequent visualisation by electon microscopy. It was found that the majority of gold particles localised to the periphery of the Pdu organelles, indicating that PduA is a shell component. They also showed that a *pduA* deletion mutant was unable to form intact BMCs, characterising PduA as an essential protein for the formation of compartments (Havemann, Sampson & Bobik 2002). However this strain was actually a double deletion mutant lacking both *pduA* and *pduB* and further studies showed that a single *pduA* mutant forms enlarged BMCs with similar appearance to that of the wild type (Cheng et al. 2011). Interestingly it was later found that in recombinant, empty Pdu BMCs expressing the minimum number of shell proteins required, when *pduA* is deleted the resulting BMCs formed are elongated and filamentous and no longer resembled intact microcompartments (Parsons et al. 2010). In addition, when PduA was overexpressed in *E.coli*, without the other Pdu proteins, the structures formed were ordered nanotube-like arrangements in the cell cytoplasm unlike the structure of intact whole BMCs (Parsons et al. 2010; Pang et al. 2014).

PduA has a single BMC domain and the crystal structure reveals that monomers package into a symmetrical hexamer on the six-fold axis of symmetry. It is shaped like a hexagonal disc, similar to shell protein hexamers from other BMCs (Crowley et al. 2010). The hexamer has an opening in the centre of the disc which is a defining feature of BMC shell proteins and is thought to serve as a central pore to facilitate the selective movement of molecules across the shell (Crowley et al. 2010; Kerfeld et al. 2005). These hexamers have been shown to group tightly into higher order structures, namely uniform molecular sheets, with edge-edge interactions between hexameric units (Crowley et al. 2010).

Through these findings, it was suggested that PduA potentially functions as a shell protein transporter for 1,2-PD (Havemann & Bobik 2003; Havemann, Sampson & Bobik 2002; Crowley et al. 2010). This proposed function is consistent with the high abundance of PduA, from isolated BMCs, compared with the other shell proteins (Havemann & Bobik 2003; Havemann, Sampson & Bobik

2002). In addition, the properties of the central PduA pore gives further evidence for its function in 1,2-PD transport. The exposed atoms forming the pore during crystallography show many hydrogen bond donors and acceptors. This could favour the transport of the relatively hydrophilic 1,2-PD over propionaldehyde, which presents only one hydrogen bond acceptor and no donors, subsequently limiting its loss from the BMC (Crowley et al. 2010). Also, it has been reported that *pduA* deletion mutants are still able to form enlarged functional BMCs, but when cultured on 1,2-PD, there was a period of interrupted growth (Havemann, Sampson & Bobik 2002; Cheng et al. 2011), this reinforces its role as a 1,2-PD transporter as opposed to a shell support protein. Further evidence stems from a crystallisation study that has captured a substrate analog, glycerol (similar to 1,2-PD), bound to the central pore of a PduA mutant (Pang et al. 2014). This supports the view that substrates, in particular 1,2-PD, can enter the organelle via the central pore of PduA.

Alternatively, PduA interacts with many of the other shell proteins and could therefore potentially act as a scaffold for BMC biogenesis. It has been shown to interact with PduB, PduJ, PduK, PduN and PduU (Parsons et al. 2010).

1.4.7.2. PduB

PduB is synthesised in two forms due to the presence of two translation start sites on the polysistronic mRNA (Parsons et al. 2008). Essentially, *pduB* is two overlapping genes expressed in the same reading frame. This produces two different proteins, PduB and PduB' of 28 and 24 kDa respectively (Havemann & Bobik 2003). The significance of the two different forms of PduB have not yet been established.

Together, PduB and PduB' make up over 50% of the total Pdu shell protein mass, at 27% and 25% respectively (Chowdhury et al. 2014). This indicates that it has an important role in the structure and integrity of the compartment shell. Studies have provided evidence for this; *pduBB'* deletion mutants produced a strain with no visible BMCs from several hundred examined cells, indicating

that PduB and PduB' are essential for the formation of the BMC. In addition, a single polar body was observed in ~20% of cells, consisting of aggregated BMC components (Cheng et al. 2011). Interestingly, despite the high abundance of PduBB' in the Pdu shell, the only other shell protein it was found to interact with, by nickel affinity chromatography pull-down assays, was PduA (Parsons et al. 2010).

The crystal structure of PduB from *L. reuteri* has been solved. Three PduB subunits assemble into a trimer with pseudo-hexameric symmetry, as a result of each subunit containing a tandem BMC repeat. In total 18 ligands have been found to bind to the trimeric PduB structure; of these 17 were glycerol and one was an acetate ion. One of these glycerol ions was found to bind to the central pore of the trimeric structure and three glycerol molecules occupy each of the subunit channels with the others binding at the chains (Pang et al. 2012).

The PduB trimer subsequently forms higher order structures by packaging into uniform molecular sheets, similar to that of PduA and PduT and are thought to form the facets of the BMC. However, unlike other Pdu shell protein, PduB contains subunit pores with the ability to bind glycerol. The abundance of glycerol bound to sites around the concave face of PduB suggests that it is involved in glycerol transport; the crystal structure shows that residues lining the pore have affinity for glycerol molecules and could act as a substrate channel. It is thought that due to the structural similarity, size and hydrogen bonding potential between glycerol and 1,2-PD, the subunit channels are likely to be a transport mechanism for 1,2-PD. It has also been suggested that propionaldehyde may not pass through the pores due to the different hydrogen-bonding potential of the aldyhyde group compared with that of the hydroxyl group; aldehydes accept two hydrogen bonds in planar arrangement whereas alcohols can donate one and accept two hydrogen bonds with tetrahedral geometry. There are at least two sites located in the PduB structure which display these characteristics, providing evidence that it is able to act as a semi-permeable barrier to prevent the

loss of the toxic aldehyde from the BMC but permit the transport of 1,2-PD across the shell (Pang et al. 2012).

In addition, the glycerol molecule bound to the central pore contains flexible loops above and below it. When glycerol is bound, the loops are locked closed. This suggests that it could be a ligand-gated channel that could prevent aldehyde efflux but allow the transport of glycerol and possibly 1,2-PD into the BMC (Pang et al. 2012).

1.4.7.3. PduJ

The crystal structure of PduJ has not yet been solved, however PduJ shares 86% sequence similarity to PduA, indicating a similar structure and role in the BMC shell (Crowley et al. 2010). Interestingly, PduA and PduJ share 100% similarity over the pore-lining residues, 37-40, suggesting that their function in the shell is identical. In contrast to PduA, a *pduJ* deletion mutant forms elongated compartments, suggesting improper closure of the BMC (Cheng et al. 2011; Chowdhury et al. 2014). This may infer that PduJ forms the edges that join the BMC facets together for complete closure of the organelle. This is supported by the relatively high abundance of PduJ, comprising 11% of the total BMC protein. In addition, a *pduJ* deletion mutant was shown to prevent the formation of BMCs in 57% of cells; where no BMC-like structures we seen. In 22% of cells of cells, elongated structures were observed, supporting the role of PduJ as an essential structural component of the Pdu shell (Cheng et al. 2011).

1.4.7.4. PduK

Although the structure of PduK has not been solved, it is clear that the sequence contains a predicted iron-sulphur (Fe-S) cluster binding motif in the carboxyl terminal domain of the protein, namely [CNLCLDPKCPRQKGEPRTLC] (Crowley et al. 2010). This C terminal extension makes PduK larger than most of the other shell proteins, with the exception of PduBB', at 160 amino acids in length. The function of this Fe-S cluster is unclear; it was proposed that the C terminus could be

involved with a specific targeting sequence that enables enzymes to be targeted to the interior of the BMC, however, it has since been shown, through the use of PduK C terminal truncations, that the N terminus of PduK is involved with targeting peptides to the organelle lumen (Lawrence et al. 2014).

Interestingly, PduK seems to interact with many proteins in the *pdu* operon, including PduA, PduT, PduM, PduV and PduP, although it's exact function has not yet been determined (Parsons et al. 2010; Lawrence et al. 2014). A recent study has shown that through the use of PduK C-terminal truncations, the N-terminus of PduK mediates protein encapsulation into the BMC through an interaction with the targeting peptide P18 (see section 1.5.1) (Lawrence et al. 2014). However the role of the C-terminal extension is currently unclear, although it is thought to facilitate the binding of other Pdu proteins, cofactors or enzymes.

It was found that a *pduK* deletion resulted in the formation of aggregates of BMCs (Cheng et al. 2011). These aggregates occurred in ~52% of the cells studied. However they differed from the polar bodies observed in PduBB' deletion mutants; in PduK deletion strains, aggregates appeared to be composed of BMCs with shell structures present. Polar bodies observed in PduBB' deletions seemed to lack any defined structures. Further studies also showed that these PduK deletion aggregates were fully functional demonstrating that PduK is not essential to the function of the BMC, but does have an effect on its localisation and perhaps its solubility (Cheng et al. 2011). In addition the *pduK* deletion had no effect on propionaldehyde toxicity or growth on 1,2-PD. It has been suggested that PduK has a role in the spatial organisation of BMCs in the cell, or a role in BMC segregation during cell division (Cheng et al. 2011).

1.4.7.5. PduN

Currently, it is understood that bacterial organelles are comprised of sheets of hexameric shell proteins that are subsequently folded into polyhedral facets, forming the faces of the BMC (Kerfeld et al. 2005). These facets are thought to be joined by a pentameric protein present at the vertices

of the polyhedral shell (Tanaka et al. 2008). These pentameric proteins are smaller than the other hexamers and belong to family of similar presumed vertex proteins with a distinct sequence and structure. However, although crystal structures of hexameric proteins support this model, studies of vertex proteins remain inconclusive (Wheatley et al. 2013).

Proteins associated with vertex family include; EutN, PduN, CcmL and CsoS4. Of these proteins, CcmL and CsoS4 (carboxysome proteins) have been found to be pentameric, however EutN has revealed a hexameric quaternary structure that is almost hexagonal in shape (Tanaka, Sawaya & Yeates 2010). However a recent study has found that EutN does have a pentameric assembly (Wheatley et al. 2013).

This provides evidence that PduN is very likely to form a pentameric arrangement that helps the BMC to close by establishing the vertices of the structure, although it has not yet crystallised. A study using a pduN deletion mutant found that in ~90% of cells, BMCs were irregular and had abnormal shapes, they were also subject to propionaldehyde toxicity during growth on 1,2-PD, indicating that PduN is essential for the proper formation and closure of the BMC (Cheng et al. 2011).

1.4.7.6. PduT

PduT accounts for approximately 3% of the total content of the Pdu BMC shell, constituting it as a minor component of the shell (Cheng et al. 2011). It is a unique shell protein in that it contains tandem BMC domains with a novel fold variation; it is known to assemble as a pseudohexomeric homotrimer (Crowley et al. 2010). The crystal structure reveals that PduT does not form extended two-dimensional layers that other shell proteins do. Instead interactions formed between the edges of the hexamers bury half the surface area that PduA does. This may be a control mechanism to limit the incorporation of PduT in the shell, allowing it to interact with other Pdu proteins (Crowley et al. 2010).

The crystal structure of PduT has also revealed a site at the central pore for a [4Fe-4S] cluster to bind (Crowley et al. 2010). Interestingly, this cluster is accessible from both sides hinting at a role in electron transfer across the BMC shell, or for the regeneration of Fe-S centers in the BMC lumen (Crowley et al. 2010; Chowdhury et al. 2014). Each subunit of the trimer provides a cysteine residue which are included in the ligands for the metal cluster, however the fourth ligand to the iron molecule was not identifiable. Furthermore, two additional cysteine residues (C108 and C136) located in close proximity in domain II may form a disulphide bond. It is thought that the formation of this disulphide link may alter the conformation of PduT. This could cause a redox-sensitive change to the central pore. Considering the putative function of PduT in electron transport; the role of this shell protein could be to support PduS, which mediates the reduction of B_{12} by providing one electron to the central cobalt atom (Cheng & Bobik 2010).

1.4.7.7. PduU

PduU is a minor Pdu shell protein; it is not abundant and is non-essential for the formation and function of the Pdu metabolosome (Havemann & Bobik 2003; Cheng et al. 2011). As expected, PduU has a hexameric form but unusually, the permuted BMC fold is circular. Instead of forming well-packaged hexagonal layers, PduU tends to form strips of hexamers.

A unique feature of PduU in comparison to the other shell proteins is the presence of a six-stranded, parallel β-barrel produced by the amino terminus on the other side of the disk forming an extended tail (Crowley et al. 2008; Tanaka, Sawaya & Yeates 2010). This β-barrel allows the central PduU pore region to be capped (Crowley et al. 2008). The appearance of β-barrels in transmembrane proteins usually consist of at least 12 strands and function to create pores for molecular transport (Schulz 2002), however the centre of the PduU β-barrel is occluded and therefore unlikely to have a role in transport. There is some speculation that this occluded conformation could open under certain conditions to allow the transport of small molecules, however due to an unusual deep cavity with several hydrophobic residues, on the face of PduU opposite the β-barrel, it has been suggested that PduU could form several, currently unknown, molecular interactions and/or present a specific

enzyme binding site (Crowley et al. 2008; Chowdhury et al. 2014). A recent study has demonstrated, through protein-protein interaction modelling, that the PduU β-barrel is likely to interact with the N-terminus of PduV. Experimental data has confirmed, using a bait and prey method, that PduV and PduU do interact (Jorda et al. 2015). This interaction suggests that PduU plays a role in the possible spatial organisation of Pdu organelles in the cell.

Studies have been carried out using a recombinant system involving the expression of shell proteins alone to form empty Pdu organelle shells. When *pduU* was deleted from this system, there was no effect on the BMC shells (Parsons et al. 2010). Studies using the complete *pdu* operon also confirm that *pduU* deletion mutants produce BMCs with normal formation and the majority of cells (~90%) contained BMCs similar to that of the wild type (Cheng et al. 2011). In addition, when *pduU* deletion mutants were grown on 1,2-PD with limiting B_{12}, the growth rate of cells was similar to that of the wild type in limiting $B_1$2. This demonstrates that PduU is nonessential for the formation of Pdu BMCs and does not affect the mitigation of propionaldehyde toxicity as growth was not impaired (Cheng et al. 2011). This suggests a specialised functional role for PduU in the BMC shell, such as facilitating molecular transport.

1.4.7.8. PduM

The role of PduM is completely unknown. There is no distinguishable BMC domain, causing it to be overlooked as a shell protein and there are no other identifiable motifs. Sequence analysis shows that it is unrelated to proteins of a known function, but a GenBank search reveals that there are over 200 PduM homologs among many genera, including those currently known to produce Pdu BMCs.

Studies have indicated that PduM could possibly be a structural component. SDS-PAGE and Western Blot analysis of BMCs from wild type *S. enterica* versus a *pduM* deletion strain shows that PduM from the wild type is present in the fraction containing purified BMCs; the band is not present in the purified fraction from the deletion strain. In addition overproduction of PduM caused the

formation of BMCs to be impaired. EM of the deletion mutant indicated that PduM is required for the formation and assembly of Pdu BMCs, however growth rates of the mutant indicated that there was no effect on 1,2-PD metabolism. It has therefore been suggested that PduM may be a structural component of the Pdu BMC, but has no catalytic function (Sinha et al. 2012). Despite these findings, more research needs to be undertaken to determine the exact location and function of PduM in the Pdu BMC.

1.5. Recombinant Pdu studies

The potential uses of BMCs in synthetic biology, metabolic engineering, nanotechnology and bioengineering are vast, with many possible applications. (see section 1.1.4). That being said, the capability to engineer recombinant BMCs can not only advance our understanding of these unique bacterial organelles, but also help us to realistically apply BMCs to a system that can produce them easily, cheaply and quickly, in order for them to be used in an industrial setting.

In order to do this, BMCs have been designed in a recombinant system whereby empty compartment shells can be expressed in lab strains of *E.coli*. These empty shells can then be used in various ways to further our knowledge of how the system works and also how BMCs can be applied.

Thus far, the Pdu compartmentalisation system is thought to be promising for further use as a recombinant vessel for biosynthetic pathways. This is because it contains the most diverse range of shell proteins, to allow many different enzymes and metabolites to be encapsulated. In comparison, carboxysomes are formed from fewer shell proteins and generally pack the interior with RuBISCo. This means the targeting of diverse pathways to the interior of the BMC may prove to be difficult due to the limitations of the shell and also the specialised luminal environment.

Currently it is possible to express empty Pdu shells in *E.coli*. This allows further study on the formation of the Pdu BMC and shell proteins, but also allows the exploration of protein targeting to the BMC.

Parsons *et al* have shown that empty Pdu BMCs, containing the BMC domain shell proteins PduABJKNUT, are capable of forming complete, delimited compartments (Figure 1.12B), although PduU and PduT were found to be non-essential to the formation of intact BMCs. Analysis of the crude extract of E.coli cells expressing the empty shells revealed protein bands corresponding to that of the shell protein sizes by SDS-PAGE. In addition this protein complex could be separated from other cytoplasmic protein by ultracentrifugation on a sucrose gradient (Figure 1.12A). Furthermore, this study showed that immunogold labelling of these delimiting compartments using an anti-PduA primary antibody clearly demonstrates that these structures are that of the Pdu shells, see Figure 1.12C (Parsons et al. 2010).
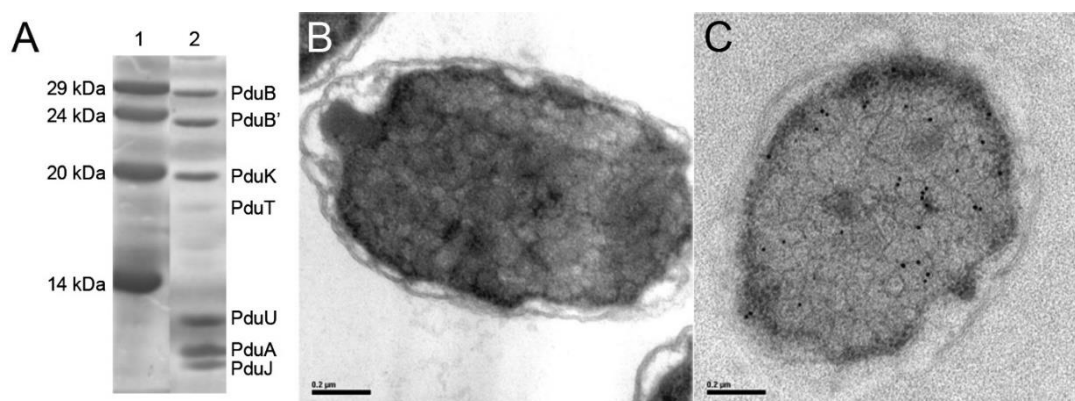
Figure 1.12. The synthesis of empty Pdu BMCs containing the shell proteins PduABJKNUT A) SDS-PAGE of the protein extract of cells expressing empty BMCs after sucrose gradient utracentrifugation (lane 2) against a protein standard (lane 1) PduN cannot be seen, but is thought to have low expression, consistent with its role as a vertex protein. B) TEM thin sections of *E.coli* cells expressing Pdu Shells, individual comparments can be seen C) Immunogold labelling of thin sections of E.coli expressing pduABJKNUT, cross-reacted with anti-PduA antibodies and a secondary antobidy conjugated to 15 nm gold particles. The particles can be seen to localise at the boundaries of the BMCs, consistent to PduA's role as a major structural shell protein. Sourced from (Parsons et al. 2010) with permissions.

1.5.1, Targeting Proteins to the Compartment

Further to the production of empty organelles, Parsons *et al* have also show that proteins can be targeted to the shell, in a step forward to our understanding of how BMCs can be utilised in synthetic biology. By the use of PduC, PduD and PduV as delivery vehicles, GFP was localised to the empty BMC. Moreover, depending on the targeting protein, GFP could be differentially targeted to the outside of the BMC shell, or to the compartment interior; live cell imaging revealed that proteins can be directed to the BMC lumen with PduC or PduD, or to the outer surface with PduV. It was also shown that the first 42 amino acids of PduV were capable of protein targeting, although the exact sequence is still unknown (Parsons et al. 2008).

Moreover, research on the use of luminal enzymes to target proteins to the BMC has identified ~20 amino acid N-terminal extensions containing specific targeting sequences. The first to be identified was that of PduP from *S. enterica*; it was found that the first 18 amino acids were sufficient for encapsulating GFP inside the BMC (Fan et al., 2010). Subsequently, further studies revealed that the first 18 amino acids of PduD also acted as a targeting sequence and was able to direct protein to the interior of the BMC (Fan & Bobik 2011). Although interactions that facilitate transport across the proteinaceous shell remain largely unknown, specific amino acids have been identified as important for shell binding. E7, I10 and L14 of PduP is required for the initial binding to PduA and subsequent encapsulation. It has been suggested that E5, L8 and I12 are the analogous targeting residues in the N terminus of PduD (Sargent, F. a Davidson, et al. 2013). It has been found that these PduP targeting sequence residues, which are located on the face of an α-helix, bind to the C-terminal helix of PduA and PduJ (Fan et al. 2012). Recent *in vitro* studies of Pdu BMCs from *Citrobacter freundii* have found that the PduP targeting sequence mediated encapsulation through an interaction with PduK (Lawrence et al. 2014). The variance in identified shell protein for PduP interaction could highlight the differences between Citrobacter and Salmonella systems, or could indicate that PduP interacts with several shell proteins.

However, targeting sequences must only count for one method of directing an enzyme to the BMC as other BMC-associated proteins lack extensions that could contain targeting sequences, and no obvious sequences have been detected in these proteins (Chowdhury et al. 2014).

1.5.2. Targeting Pathways to the Pdu BMC

As a relatively new area of research, there is a lot of interest in how targeting peptides can be used to direct protein to the BMC. In particular, synthetic 18 amino acid long peptides, from the N terminus of PduP or PduD have been have been used to target protein into the lumen of purified, empty BMC shells (Lawrence et al. 2014). This gives vast potential for the use of targeting peptides and recombinant BMCs for the biosynthesis of entire pathways. Indeed, it has already been shown that the use of these targeting sequences to tag both pyruvate decarboxylase and an alcohol dehydrogenase in an *in vivo* empty BMC system, can create an ethanol bioreactor in the interior of the Pdu BMC. Moreover, results showed that strains containing these modified BMCs produced elevated levels of ethanol compared with strains that did not contain bacterial organelles (Lawrence et al. 2014).

1.6. The Spatial Organisation of Pdu BMCs

Microcompartment dynamics in a growing and dividing cell remains largely elusive. However there must be a mechanism to ensure daughter cells obtain BMCs when a cell divides. Live cell imaging using time lapse microscopy has demonstrated that fluorescently-labelled Pdu BMCs associate with filamentous structures in the cell and, through an unknown mechanism, are able to move across these filaments. It has been shown that these filaments are comprised of or at least associated with PduV by live cell imaging (Parsons et al. 2010).

1.6.1. An introduction to PduV, Structure and Function

PduV is one of the few Pdu-related proteins whose function is completely unknown. It is a relatively small protein, 150 amino acids in length and approximately 16 kDa. The structure is currently unknown but is predicted to contain four helices as well as a beta sheet (Figure 1.13). To form filaments, it would be necessary for PduV to polymerise, although the orientation and specific interactions during protein polymerisation is completely unknown. However it is uncertain if PduV is able to freely form filaments, or if it attaches to other protein in the cytosol.
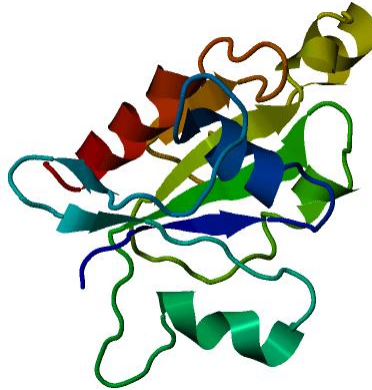
Figure 1.13. Predicted model for the structure of a PduV monomer. Based on a target-template sequence similarity alignment of 22%, using the Protein Model Portal.

Studies have given insights into the role PduV may have; by the use of live cell imaging, PduV-GFP was seen to localise to filaments in the cell cytoplasm, which were often associated with mCherry-tagged Pdu BMCs (Parsons et al. 2010). This indicates that PduV either forms filamentous structures, or localises to pre-existing filaments in the cell. These filaments have been shown to associate with BMCs and this interaction is thought to play a crucial role in the dynamics of the organelle.

It has also been shown that PduV can direct protein to the BMC; a PduV-GFP fusion was found to largely associate with the empty BMC shells by immunogold labelling (Parsons et al. 2010). It was subsequently found, through the use of PduV C terminal truncations, that the N terminal region was responsible for targeting to the BMC (Parsons et al. 2010). In addition, further experiments showed that, while enzymes seemed to localise to the interior of the BMC, PduV was seen to

localise to cup-like structures on the outer surface of the shell (Parsons et al. 2010). This indicates that PduV is likely to interact on the outer surface of the compartment, as opposed to being internalised.

Furthermore, dynamic movement observed during time-lapse microscopy clearly shows interaction between Pdu BMC shells and PduV-lined filaments; results indicated that PduV may be involved in the regulation of the spatial distribution of BMCs in growing cells (Parsons et al. 2010).

1.6.2. PduV interactions

An initial study carried out by Parsons *et al* identified possible interactions between PduV and other proteins, in particular the Pdu shell. It was found, through pull-down assays, that PduV did not appear to co-elute with any of the major shell proteins, PduA, PduB, PduJ or PduK (Parsons et al. 2010). Subsequent data however, revealed that PduV may possibly interact with PduK (unpublished data).

A recent study identified, through protein-protein interaction modelling, that PduV is likely to interact with the shell component PduU. This was also shown experimentally using target and bait fusions (Jorda et al. 2015). It was also predicted that the N-terminal region of PduV binds to the PduU β-barrel directly, this is consistent with previous data, revealing that the N terminus of PduV is responsible for targeting to the BMC (Jorda et al. 2015; Parsons et al. 2010).

1.6.3. Putative GTPase activity

Interestingly PduV has been found to have some sequence similarity to members of the Ras-like GTPase superfamily. Parsons et al have also revealed that preliminary data have shown that purified pduV has weak GTPase activity (Parsons et al., 2010). However the exact nucleotide binding site has not been identified. This putative GTPase activity gives some similarity to other cytoplasmic, filament-forming proteins such as MreB and FtsZ, the bacterial homologs of actin and tubulin which are known to require nucleotide binding for their polymerisation.

1.7. Aims

In comparison to carboxysomes and other BMCs the Pdu system is a fairly new discovery, and as such there are still many key questions that need to be addressed. Through a multi-disciplinary approach the work described in this thesis aims to provide further information regarding some off these questions. The first question to be investigated was the possible interaction between PduV and PduK. The aim of theis work was to use fluorescence microscopy to see if it was possible to visualise the interaction between the two, with the potential to quantify this interaction through the use of FRET or FLIM FRET. Following this, truncated forms of PduK were to be used to try and determine which region of the protein is required for the interaction with PduV. The seoncd, and largest portion of the work has focussed on advancing the techniques used to visualise Pdu BMCs by fluorescence microscopy, and using this to try and gain further insights into the formation of the shell and investigate if any other shell proteins interact with PduV. The first part of this work aimed to determine which shell proteins can be tagged with fluorophores whilst still appearing to retain functionality. In doing so this work also revealed further information about the role each shell protein plays in the formation and stablitiy of the BMC shell, as well as possible regulation of PduV filament formation and length. It was hoped that these interractions could be further investigated using FRET/FLIM FRET but sadly this was not possible. The third and final question was to further understand the function of PduV. This work centred on investigating the conditions in which Pduv forms filament like structures and providing further evidence for PduV possessing GTPase activity through the use of mutations in the predicted GTP binding region.

Chapter 2: Materials and Methods

2.1. Materials

2.1.1. Chemicals

Unless otherwise stated, chemicals were purchased from Sigma-Aldrich. Other products were purchased from manufacturers as follows; IPTG and ampicillin from Melford Laboratories Ltd, chelating sepharose from Amersham Biosciences, QIAprep Spin Miniprep Kit, QIAquick Gel Extraction Kit and 50 x TAE buffer from QIAGEN GmbH, T4 DNA ligase and restriction enzymes from Promega and New England Biolabs Inc (NEB). Tryptone, yeast and bacterial agar were purchased from Oxoid Ltd, FastStart HF PCR System from Roche Diagnostics GmbH, Yeast Protein Extraction Reagent (YPER Plus) from Pierce, 30% acrylamide and bis-acrylamide solution and 5 X sample loading buffer and HyperLadder 1 kb from Bioline.

2.1.2. Bacterial Strains

Bacterial strains used for either DNA cloning purposes (JM109/DH5α) or protein expression (BL21 (DE3)/ BL21 (DE3) pLysS) were purchased from Novagen, Invitrogen or Promega.

Strain	Description	Source
JM109	endA1, recA1, gyrA96, thi, hsdR17 (rk-, mk+), relA1, supE44, Δ(lac-proAB), [F′ traD36, proAB, laqIqZΔM15]	Promega
BL21 (DE3)	F- ompT gal dcm lon hsdSB(rB- mB-) λ(DE3 [lacI lacUV5-T7 gene 1 ind1 sam7 nin5])	Novagen
Bl21 (DE3) pLysS	F- ompT gal dcm lon hsdSB(rB- mB-) λ(DE3) pLysS(cmR)	Novagen
DH5α	F-φ80lacZΔM15Δ(⊠lacZYA-argF)U169 recA1 endA1 hsdR17(rk-, mk+) phoA supE44 thi-1 gyrA96 relA1 λ-	Invitrogen

Table 2.1. List of bacterial strains used in this study.

2.1.3. Plasmids

Plasmid	Description	Source
pET14b	Over-expression N-terminal His-tag fusion protein vector with T7 promoter, Amp*R*	Novagen
pET23b	Over-expression C-terminal His-tag fusion protein vector with T7 promoter, Amp*R*	Novagen
pET3a	Over-expression vector with T7 promoter, Amp*R*	Novagen
pLysS	contains T7 lysozyme gene, Cm*R.* used in lDE3 lysogenic hosts to suppress basal expression from the T7 promoter	Novagen
pET14b-pduV	*pduV* is an NdeI/SpeI fragment	Warren Lab
pET23b-pduV-gfp	*pduV* is an XbaI/SacI fragment, GFP is a SacI/EcoRI fragment	Warren Lab
pET3a-pduV-cerulean	*pduV* is an NdeI/SpeI fragment, *cerulean* is a SacI/SpeI fragment	This Study
pET3A-pduV(G8A)-cerulean	*pduV(G8A)* is an NdeI/SpeI fragment, Cerulean is a SacI/SpeI fragment	This Study
pET3A-pduV(G13A)-cerulean	*pduV (G13A)* is an NdeI/SpeI fragment, *cerulean* is a SacI/SpeI fragment	This Study
pET3A-pduV(K14A)-cerulean	*pduV(K14A)* is an NdeI/SpeI fragment, *cerulean* is a SacI/SpeI fragment	This Study
pET3A-pduV(T43A)-cerulean	*pduV(T43A)* is an NdeI/SpeI fragment, c*erulean* is a SacI/SpeI fragment	This Study
pLysS-mCherry-pduA-BJKNU	*mcherry* is an XbaI/NdeI fragment, subsequent *pdu* genes cloned as XbaIII/HindIII fragments using link and lock	Warren Lab
pLysS-mCherry-pduA-BJKNUT	*mcherry* is an XbaI/NdeI fragment, subsequent *pdu* genes cloned as XbaIII/HindIII fragments using link and lock	Warren Lab
pLysS-pduV-cerulean	*pduV-cerulean* is a HindIII/XbaI fragment.	This Study
pET3a-pduK-Ypet	*pduK* is an NdeI/SpeI fragment. y*pet* is an SpeI/BamHI fragment.	This Study
pET3a-Ypet-pduK	*ypet* is an AseI/SpeI fragment. *pduK* is an NdeI/SpeI fragment.	This Study
pET3A-pduABJNU	*pdu* genes cloned as XbaIII/HindIII fragments using link and lock	Warren Lab
pET3A-pduABJNU-pduK-Ypet	*pduK-ypet* is an XbaI/HindIII fragment.	This Study
pET3a-pduABJNU-Ypet-pduK	*ypet-pduK* is an XbaI/HindIII fragment	This Study
pET3a-pduA	*pduA* is an XbaIII/HindIII fragment	Warren Lab
pET3a-pduAB	*pdu* genes closed as XbaIII/HindIII fragment	Warren Lab
pET3a-pduABJ	*pdu* genes closed as XbaIII/HindIII fragments using link and lock	Warren Lab

pET3a-pduABJK	*pdu* genes closed as XbaIII/HindIII fragments using link and lock	Warren Lab
pET3a-pduABJKN	*pdu* genes closed as XbaIII/HindIII fragments using link and lock	Warren Lab
pET3a-pduABJKNU	*pdu* genes closed as XbaIII/HindIII fragments using link and lock	Warren Lab
pET3a-pduABJ-pduK-Ypet	*pduK-ypet* is an XbaI/HindIII fragment	This Study
pET3a-pduABJ-Ypet-pduK	*ypet-pduK* is an XbaI/HindIII fragment	This Study
pET3a- pduABJ-pduK-Ypet-pduN	*pduN* is an XbaI/HindIII fragment	This Study
pET3a- pduABJ-pduK-YpetN-pduU	*pduU* is an XbaI/HindIII fragment	This Study
pET3a-pduABJ-Ypet-pduK-pduN	*pduN* is an XbaI/HindIII fragment	This Study
pET3a-pduABJ-Ypet-pduKN-pduU	*pduU* is an XbaI/HindIII fragment	This Study
pET3a-pduN	*pduN* is an NdeI/SpeI fragment	Warren Lab
pET3a-pduK96	*pduK96 is an XbaI/HindIII fragment*	This Study
pET3a-pduK119	*pduK119 is an XbaI/HindIII fragment*	This Study
pET3a-pduK133	*pduK133 is an XbaI/HindIII fragment*	This Study
pET3a-pduK96-pduN	*pduK96 is an XbaI/HindIII fragment*	This Study
pET3a-pduK119-pduN	*pduK119 is an XbaI/HindIII fragment*	This Study
pET3a-pduK133-pduN	*pduK133 is an XbaI/HindIII fragment*	This Study
pET3a-pduK96N-pduU	*pduU is an XbaI/HindIII fragment*	This Study
pET3a-pduK119N-pduU	*pduU is an XbaI/HindIII fragment*	This Study
pET3a-pduK133N-pduU	*pduU is an XbaI/HindIII fragment*	This Study
pLysS-mCherry-PduABJK	*mcherry* is an XbaI/NdeI fragment, subsequent *pdu* genes cloned as XbaIII/HindIII fragments using link and lock	Warren Lab
pLysS-mCherry-PduABJ-pduK96NU	*pduK96NU* is an AatII/HindIII fragment	This study
pLysS-mCherry-PduABJ-pduK119NU	*pduK119NU* is an AatII/HindIII fragment	This study
pLysS-mCherry-PduABJ-pduK133NU	*pduK133NU* is an AatII/HindIII fragment	This study
pET3a-mCherry (N-terminal)	*mcherry* is an AseI/SpeI fragment	This Study
pET3a-mCherry (C-terminal)	*mcherry* is an NdeI/SpeI fragment	This Study
pET3a-mCherry-pduA	*pduA* is an NdeI/SpeI fragment	This Study
pET3a-mCherry-pduA-pduB	*pduB* is an XbaI/HindIII fragment	This Study
Pet3A-mCherry-pduAB-pduJKNU	*pduJKNU* is an AscI/HindIII fragment	This Study
pLysS-pduA-pduB-mCherry	*pduB-mcherry* is an NdeI/SacI fragment	This Study
pLysS-pduAB-mCherry-pduJ	*pduJ* is an XbaI/HindIII fragment	This Study
pLysS-pduAB-mCherryJ-pduKNU	*pduKNU* is an StuI/HindIII fragment	This Study
pLysS-pduA-mCherry-PduB	*mcherry-pduB* is an NdeI/SpeI fragment	This Study
pLysS-pduA-mCherry-PduB-PduJKNU	*pduJKNU* is an AscI/HindIII fragment	This Study
pET3a-pduJ-mCherry	*pduJ-mcherry* is an NdeI/SacI fragment	This Study
pET3a-pduAB-pduJ-mCherry	*pduJ* is an XbaI/HindIII fragment	This Study
pET3a-pduAB-pduJ-mCherry-pduKNU	*pduKNU* is an StuI/HindIII fragment	This Study
pET3a-mCherry-pduJ	*mcherry-pduJ* is an NdeI/SpeI fragment	This Study
pET3a-PduAB-mCherryPduJ	*mcherry-pduJ* is an XbaI/HindIII fragment	This Study
pET3a-PduAB-mCherryPduJ-pduN	*pduN* is an XbaI/HindIII fragment	This Study
pET3a-PduAB-mCherryPduJN-pduU	*pduU* is an XbaI/HindIII fragment	This Study
pET3a- pduN-mCherry	*pduN-mcherry* is an NdeI/SacII fragment	This Study
pET3a-PduABJK-PduN-mCherry	*pduN-mcherry* is an NdeI/SacI fragment	This Study
pET3a-PduABJK-PduN-mCherry-PduU	*pduU* is an XbaI/HindIII fragment	This Study
pET3a-mCherry-pduN	*mcherry-pduN* is an NdeI/SpeI fragment	This Study
pET3a-PduABJK-mCherryPduN	*mcherry-pduN* is an XbaII/HindIII fragment	This Study
pET3a-PduABJK-mCherryPduN-PduU	*pduu* is an XbaII/HindIII fragment	This Study

pET3a- pduU-mCherry	*pduU-mcherry* is an NdeI/SacII fragment	This Study
pET3a-PduABKJN-PduU-mCherry	*pduU-mcherry* is an XbaI/HindIII fragment	This Study
pET3a-mCherry-PduU	*mcherry-pduU* is an NdeI/SpeI fragment	This Study
pET3a-PduABJKN-mCherry-PduU	mcherry-pduU is an XbaI/HindIII fragment	This Study

Table 2.2. List of plasmids used in this study.

2.1.4. Primers

All primers were supplied from Invitrogen Life Technologies.

Primer Name	Sequence	Restriction Enzyme Site
PduA Forward	GGC CAT ATG CAA CAA GAA GCG TTA GG	NdeI
PduV G8V Forward	ATA ATG CTA ATT GTC CCC AGC CAG TGC	N/A
PduV G8V Reverse	GCA CTG GCT GGG GAC AAT TAG CAT TAT	N/A
PduV Forward	GGC ATT AAT AAA CGC ATA ATG CTA ATT GGC CCC	AseI
PduV Stop Reverse	GCC ACT AGT TCA CAT ATG TTT TGT GAG ACA	SpeI/NdeI
PduB Reverse	GGC ACT AGT TCA GAT GTA GGA CGG AC	SpeI
Ypet Forward	CG ATT AAT ATG GTG AGC AAA GGC GAA GAG CTG	AseI
Ypet Reverse	Tgatcaaaagtatac gaatatctcgagcaagtacgggagccc	SpeI/NdeI
mCherry Forward 1	GCATTAATATGGTGAGCAAGGGCGAGGAGGAT	AseI
mCherry Reverse 1	GCACTAGTTTTCATATGCTTGTACAGCTCGTCCATGCCGCC	NdeI/SpeI
mCherry Forward 2	GCCATATGTTTGAGCTC ATGGTGAGCAAGGGCGAGGAG	NdeI/SacI
mCherry Reverse 2	GCACTAGT TCACTTGTACAGCTCGTCCATGCCGCC	SpeI
Cerulean Forward	GCATTAATTTTCCATGGATGGTGAGCAAGGGCGAGGAGCTG	AseI/NcoI
Cerulean Reverse	GCCATATGCTTGTACAGCTCGTCCATGCCGAGAGT	NdeI
PduJ Reverse	GCGAGCTCTGCGGATTTAGGTAAAATGGCTTCAACGTC	SacI
PduU Reverse	TAGAGCTCTGTCCGGGTGATGGGACAGGCGGTAAAA	SacI
PduA Forward	GGCCATATGCAACAAGAAGCGTTAGGA	NdeI
PduA Reverse	GGCGAGCTCGCTAATTCCCTTCGGTAAGA	SacI
PduB Forward	GGCCATATGAGCAGCAATGAGCTG	NdeI
PduB Reverse	GGCGAGCTCGATGTAGGACGGACGATCGTTT	SacI
PduJ Forward	GGCCATATGAATAACGCACTGGGACTG	NdeI

PduJ Reverse	GCGGAGCTCTGCGGATTTAGGTAAAATGGCTTCAACGTC	SacI
PduN Forward	GGCCATATGCATCTGGCACGGGTT	NdeI
PduV N Reverse	GGCGAGCTCACGAGAAAGCGTGTCGACAAT	SacI
PduU Forward	GGCCATATGGAAAGACAACCCACC	NdeI
PduU Reverse	TTTGAGCTCTGTCCGGGTGATGGG	SacI
GFP Forward 1	CCG GAG CTG ATG AGC AAA GGA GAA GAA CTT	SacI
GFP (His) Reverse	CCG CCG ACT AGT AAA GAA TTC TTA GTG ATG GTG ATG GTG	SpeI/EcoRI
GFP Forward 2	GCG AGC TCA TGA GCA AAG GAG AAG AAC	SacI
GFP Stop Reverse	GCG CGC GAA TTC AAA ACT AGT TCA AAT TTG TAC AGC TCA	SpeI/EcoRI
PduV G13A Forward	C AGC CAG TGC GCT AAA ACG TCA C	N/A
PduV G13A Reverse	G TGA CGT TTT AGC GCA CTG GCT G	N/A
PduV K14A Forward	C CAG TGC GGT GCA ACG TCA CTC A	N/A
PduV K14A Reverse	T GAG TGA CGT TGC ACC GCA CTG G	N/A
PduV T43A Forward	ACA ACG ATA GAC GCA CCG GGT GAA TAT	N/A
PduV T43A Reverse	ATA TTC ACC CGG TGC GTC TAT CGT TGT	N/A

Table 2.3. List of primers used in this study.

2.1.5. Media and solutions for bacterial work

Luria-Bertani (LB) broth:

Tryptone   10 g

Yeast extract   5 g

NaCl   5 g

The broth was made up to 1 L with dH$_2$O and autoclaved

Luria-Bertani (LB) agar:

15g of Bacterial agar were added to 1 L of LB broth and then autoclaved

Super optimal broth (SOB) Medium:

Tryptone   2 g

Yeast extract   0.5 g

NaCl   0.05 g

Made up to 90 ml with dH$_2$O

1 ml of 250 mM KCl solution was then added to SOB medium and adjusted to pH 7.0. This was

consequently made up to 100 ml with dH$_2$O and then autoclaved. 0.5 ml of 2 M MgCl$_2$ solution

was added after cooling.

Antibiotics

Ampicillin: 50 mg/ml stocks were made by dissolving ampicillin in dH$_2$0, and was used at a working

concentration of 50 µg/ml.

Chloramphenicol: 34 mg/ml stocks were made by dissolving chloramphenicol in ethanol, and was

used at a working concentration of 34 µg/ml.

2.1.6. Media and solutions for DNA work

<u>TAE Buffer</u>

Tris	40 mM
Acetic Acid	20 mM
EDTA	1 mM

2.1.6.1. Solutions for immobilized metal ion affinity chromatography (IMAC)

<u>Charge Buffer</u>

$NiSO_4$	0.1%

<u>Binding Buffer</u>

Tris-HCl, pH 8.0	20 mM
NaCl	100 mM
Imidazole	5 mM

<u>Wash Buffer 1</u>

Tris-HCl, pH 8.0	20 mM
NaCl	100 mM
Imidazole	50 mM

<u>Wash Buffer 2</u>

Tris-HCl, pH 8.0	20 mM
NaCl	100 mM
Imidazole	100 mM

Elution Buffer

Tris-HCl, pH 8.0	20 mM
NaCl	100 mM
Imidazole	400 mM

Strip Buffer

EDTA	100 mM
NaCl	100 mM
Tris-HCl, pH 8.0	20 mM

2.1.6.2. Solutions for BMC isolation

No Salt Solution

20 mM Tris-HCL pH 8.0

Normal Salt Solution

20 mM Tris-HCL pH 8.0

20mM NaCl

High Salt Solution

20 mM Tris-HCL pH 80.0

80 mM NaCl

2.1.6.3. Solutions for protein SDS-PAGE

1x Running Buffer:

Tris-HCl	25 mM
Glycine	250 mM
SDS	0.1%

Coomassie Blue (500ml)

Glacial acetic acid   250 ml

Coomassie blue   0.6 g

SDS   0.1 g

Tris-HCl   0.25 g

Glycine   0.15 g

Made up to 500 ml with dH_2O.

SDS-Loading Buffer (5x)

Tris-HCl pH 6.8   50 mM

SDS   2%

Glycerol,   10%

β-Mercaptoethanol   1%

EDTA   12.5 mM

Bromophenol Blue   0.02%

2.1.6.4. Composition of SDS gels

Protein samples were analysed by gel electrophoresis, using 15% SDS-PAGE acrylamide gels, as shown in table 2.4 below.

	15% Resolving Gel		5% Stacking Gel
Water	1.75 ml	**Water**	7 ml
1.5 M Tris pH 8.7	3.75 ml	**1 M Tris pH 6.8**	1.25 ml
10% SDS	0.1 ml	**10% SDS**	50 µl
30% Acrylamide	4 ml	**30% Acrylamide**	1.7 ml
APS	0.1 ml	**APS**	50 µl
TEMED	15 µl	**TEMED**	15 µl

Table 2.4. Composition of SDS gels.

Protein samples were mixed with 5x protein loading buffer and boiled at 95 °C for 5 minutes. Samples were then run at 200 Volts for 1 hour in SDS running buffer alongside Kaleidoscope Prestained Standards (Bio Rad) or SeeBlue Pre-stained Protein Standard (Invitrogen). Protein bands were visualised by Coomassie Blue staining.

2.1.6.5. Solutions for Western Blot

PBST Buffer

NaCl	137 mM
KCl	2.7 mM
Na_2HPO_4	100 mM
KH_2PO_4	2 mM
Tween	0.25%

Alkaline Phosphatase Pre-Incubation Buffer

NaCl	100 mM
Tris pH 9.6	100 mM
$MgCl_2$	5 mM

<u>Blotting</u>

SDS-PAGE gels were run as described above and a protein transfer was then undertaken onto to Immun-Blot PVDF membrane (Bio Rad) using a Trans-Blot SD Semi-Dry Transfer Cell (Bio Rad) following the manufacturer's protocols at 15 Volts for 30 minutes. The membrane was then blocked by PBST + 3% milk at room temperature for 1 hour. The membrane was then incubated in PBST + 3% milk including the primary antibody (anti-mCherry -Roche) at a 1 in 1000 dilution for 1 hour. The membrane was then washed 4 times in PBST at room temperature with 10 minutes for each wash step. The membrane was then incubated in PBST + 3% milk including the secondary antibody (Anti-mouse alkaline phosphatase -Sigma) at a 1 in 5000 dilution for 1 hour. The membrane was again washed 4 times in PBST. The membrane was then washed in the alkaline phosphatase pre-incubation buffer and subsequently developed using 2 ml of BCIP/NBT substrate until bands were visible. The reaction was then stopped by washing with water to prevent over-development.

2.2. Microbiological methods

2.2.1. Sterilisation

All media and buffers were sterilized for 15 minutes at 121° C /1 bar pressure in an autoclave, unless they contained temperature sensitive components. In this case buffers were filter sterilised using a 0.2 μm pore size Minisart syringe filter (Sartorius).

2.2.2. Bacterial Growth

2.2.2.1. Plate cultures

Baceterial cells were either spread or streaked onto agar plates supplemented with appropriate antibiotics which were incubated at 37 °C overnight.

2.2.2.2. Liquid Cultures

Liquid cultures were either inoculated with a single colony from an agar plate or inoculated with a sample from an overnight starter culture (at 1:100 dilution factor). These cultures were then incubated at a temperature of 25 °C, 30 °C or 37 °C, shaking at 180 rpm.

2.2.3. Preparation of competent cells

DH5α, JM109, DH10β or Bl21-DE3 *E. coli*, were streaked out onto LB agar plates and incubated at 37 °C overnight. 5 ml of LB medium was then inoculated with a single colony and grown shaking at 37 °C at 220 rpm overnight. 50 ml of fresh LB medium was then inoculated with 0.5 ml of the starter culture and grown at 37 °C shaking at 180 rpm until the culture had an optical density of 0.6-0.8 at 600 nm. The cells were then cooled on ice for 10 minutes, before being centrifuged at 2700 rpm at 4 °C for 10 minutes. The pelleted cells were then resuspended in 10 ml of ice cold 0.1 M CaCl$_2$/10% glycerol solution and incubated on ice for 15 minutes. Cells were again centrifuged at 2700 rpm at 4 °C for 10 minutes and the pelleted cells were resuspended in 1 ml of 0.1 M CaCl$_2$/10% glycerol solution. Cells were then dispensed into 50 µl aliquots and stored at -80 °C.

2.2.4. Transformation of competent cells

50 µl of competent bacterial cells were defrosted on ice and inoculated with 1 µl of DNA . The cells were then incubated on ice for 20 minutes before being heat shocked at 42 °C for 60 seconds. Cells were then incubated on ice for 2 minutes with 200 µl of SOC media subsequently added to the cells, followed by incubation at 37 °C shaking at 220 rpm for 30 minutes. The cells were then spread LB agar plates supplemented with appropriate antibiotics.

2.2.5. Production of recombinant protein

BL21-DE3 competent cells were transformed with the plasmid containing the gene(s) for the protein to be purified. 3-4 colonies were then inoculated into 5 ml of LB media with the appropriate antibiotic and grown shaking at 37 °C at 220 rpm overnight. This 5 ml starter culture was then diluted down into 500 ml of fresh LB. The cells were grown shaking at at the required temperature at 220 rpm until the optical density at 600 nm was between 0.4-0.5. IPTG was then added (100 mg/litre) in order to activate transcription from the T7 promoter located on the plasmid. Cells were grown for between overnight after induction at 18 °C and then harvested by centrifugation at 4000 rpm at 4 °C for 30 minutes.

2.2.6. Lysis of Bacteria

2.2.6.1. Sonication of cells

Harvested cells were lysed by sonication using a Sonics Vibracell Ultrasonic processor, with 6x 30 sec bursts at 50% power with 30 second breaks between each burst. The sonicated cells were then centrifuged at 17,500 rpm for 15 min at 4 °C and the supernatant was retained.

2.2.6.2. YPER treatment of cells

1 g of cell pellet was re-suspended in 10 ml YPER Plus supplemented with 1 tablet of Complete Protease Inhibitor Cocktail and Benzonase® Nuclease (5 µl per 10 ml YPER). The lysate was agitated on a mechanical rocker at room temperature for 3 hours.

2.2.7. Protein Purification

2.2.7.1. Nickel Column

Proteins tagged with 6-Histidine residues were purified by immobilized metal ion chromatography using Chelating Sephraose Fast Flow resin loaded with Nickel. All protein purifications were carried out at room temparture, however all protein samples were kept on ice and all buffers (as described in Section 2.1.6.1) had been stored at 4 °C and subsequently kept on ice. A column was prepared by adding 5 ml of Chelating Sephraose Fast Flow (GE Life Sciences) to a syringe with a valve attached. The column was then prepared allowing 30 ml water to flow through the column and then charged with 30 ml of Charge buffer containing 0.1% $NiSO_4$. The column was then equilibrated with with 50 ml of Binding buffer. The protein extract after sonication was passed through the column and the flow through collected. Any unbound proteins were washed off of the column by passing through 50 ml of Binding buffer followed by 25 ml of Wash buffer I and then followed by 25 ml of Wash buffer II. The flowthrough was collected for each of these washes. The protein was then extracted from the column with 30ml of Elution Buffer, with this elution collected in 1 ml fractions and stored at 4 °C. The column was then cleaned for subsequent purfications by washing with 50 ml of Strip Buffer.

2.2.7.2. Microcompartment purification using YPer Plus

BL21(DE3) strains containing plasmid DNA for Pdu microcopmartment shell expression were cultured in 200 ml LB (at 37 °C, shaking at 160 rpm) to an OD600 of 0.8 and protein production was induced with 400 μM IPTG at 18 ºC overnight (shaking at 160 rpm). The cells were harvested by centrifugation for 10 minutes at 4 °C at 2683 x g. 1 g wet cell pellet was re-suspended in 10 ml YPER Plus (Pierce) supplemented with 1 tablet of Complete Protease Inhibitor Cocktail (Roche) and 1250 units Benzonase® Nuclease (5 μl per 10 ml YPer). The lysate was incubated for 3 hours at room temperature and gently agitated using a shaking platform.

The lysate was pelleted for 5 min at 11,300 x g, 4°C. Supernatant 1 and pellet 1 were collected. Pellet 1 contained the microcompartments and was re-suspended in 2 ml 20 mM Tris-HCl, pH 8.0, 20 mM NaCl. The suspension was centrifuged at 4 °C for 5 min at 11,000 x g and supernatant 2 and pellet 2 were collected. Supernatant 2 contained the microcompartments. The NaCl concentration of supernatant 2 was raised to 80 mM by addition of 5 M NaCl (24 μl of 5M NaCl in 2 ml supernatant 2). Supernatant 2 was then centrifuged at 4 °C for 5 min at 11,000 x g and supernatant 3 and pellet 3 were collected. Pellet 3 (containing the microcompartments) was re-suspended in 1 ml of 20 mM Tris-HCl, pH 8.0 and clarified by centrifugation (4 °C for 5 min at 11,000 x g). The final supernatant should contain the purest microcompartments. 10 μl of total lysate, S1, P1, S2, P2, S3 and 5μl of P3, final supernatant and final pellet were loaded onto 15 % SDS gels. This method has been published by Lawrence et al. 2014.
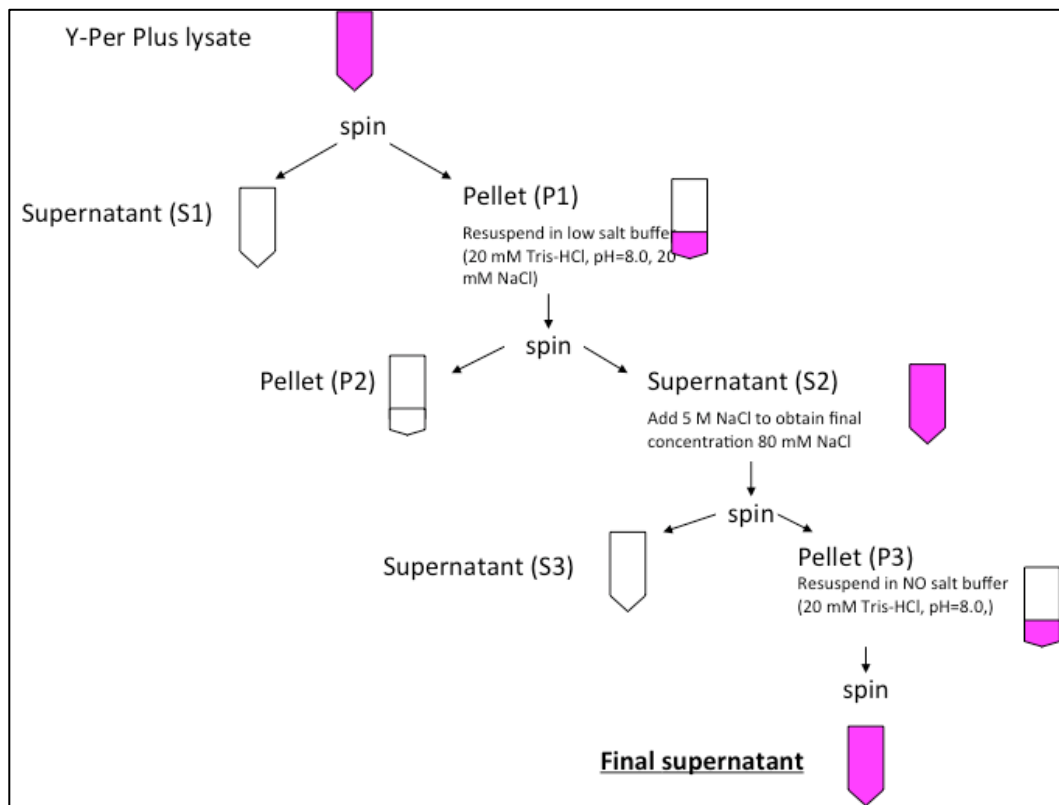
Figure 2.1. Diagram summarising the microcompartment purification process.

2.3. Molecular Biological Methods

2.3.1. PCR reactions

All PCR reactions were performed in an Eppendorf AG 22331 PCR machine. The basic PCR reaction

and the cycles used are outlined as follows:

	With DMSO	**Without DMSO**
ddH$_2$O	32.5 µl	37.5 µl
10 x PCR Buffer (Roche with 18 mM MgCl^2	5 µl	5 µl
DMSO	5 µl	-
5 mM dNTPs	2 µl	2 µl
10 µM 5' Primer	2 µl	2 µl
10 µM 3' Primer	2 µl	2 µl
DNA Template	1 µl	1 µl
Taq polymerase	1 µl	1 µl

Table 2.5. Composition of typical PCR reactions

Step	Temperature	Time	Cycles	Process
1	95 °C	2 mins	1	Initial denaturation of template DNA
2	95 °C	30 secs		Denaturation of DNA
3	50-60 °C	30 secs	35	Annealing of primers
4	72 °C	1 min per 1000 bp		Elongation
5	72 °C	5 mins	1	Final Elongation

Table 2.6. Typical PCR conditions

Once the PCR reaction was completed the product was subjected to agarose gel electrophoresis.

2.3.1.2. Overlap Mutagenesis PCR

In order to generate PduV mutations described in section 6.2.2.2, overlap mutagenesis PCR was used, as described by (Hoa et al. 1989). This method uses 2 sets of primers and 2 rounds of PCR reactions to generate the target gene with the desired mutation. In the first round of PCR reactions the gene is amplified from the template DNA using two flanking primers master primers (1 and 2) that amplify from the 5' end of both strands, and two internal primers (1M and 2M) that introduce the desired mutation. The two flanking primers are also used to introduce restriction sites to allow the insertion of the mutated gene into an expression vector. During the second PCR when the strands of products 1 and 2 and 1M and 2M are denatured the strands with 3' complementary generated using primers 1M and 2M will anneal. Primers 1 and 2 will then amplify this to generate the full length target gene containing the desired mutation. This is shown in Figure 2.2 below.
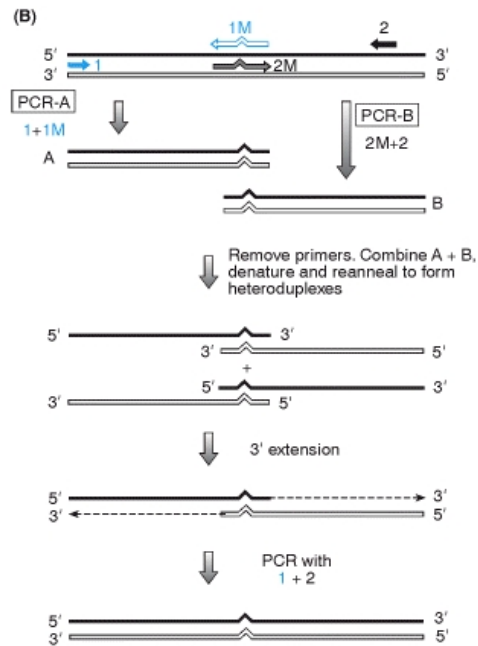
Figure 2.2. Schematic to show the process for overlap mutagenesis PCR. Figure adapted from (Mccullum et al. 2010).

2.3.2. Electrophoresis of DNA

DNA was visualised for cloning purposes by running agarose gels. 1% agarose gels were made using 1x TAE and 1 µl of ethidium bromide (10 µg/ml) was added per 1 ml of gel. The DNA sample was then run alongside 5 µl of Bioline Hyperladder at 70 volts for 1 hour and DNA bands were visualised by exposure to ultraviolet light on a transilluminator.

2.3.3. Isolation and purification of a DNA fragment

The DNA band of interest was excised from an agarose gel using a scalpel blade. Purification was carried out using Qiagen QIAquick® gel extraction kit following the manufacturer's protocol with their reagents.

2.3.4. Isolation of plasmid DNA

5 ml of LB media with appropriate antibiotics was inoculated with a single colony from a transformation plate and grown shaking at 37 °C at 220 rpm overnight. Plasmid DNA isolation was then carried out using a Qiagen Qiaprep Spin Miniprep Kit following the manufacturer's protocol with their reagents.

2.3.5. Ligation of DNA

Vector and insert DNA were digested with the relevant restriction enzymes as described

in Section 2.3.6. The ligation of DNA fragments into the vector was carried out at 4 °C.

Typical ligation reaction:

Insert 5 µl

Vector 3 µl

10x Rapid Ligation buffer (Promega) 1 µl

T4 DNA Ligase (Promega) 1 µl (= 1 U/10 µl)

2.3.6. Restriction digest of DNA

Plasmid DNA was digested using the relevant enzymes. The optimal buffer was chosen according

to either the Promega or New England Biolabs information provided. The reactions were incubated

for 2 hours at the temperature required by the restriction enzyme before being subjected to

electrophoresis.

	Single Digest	Double Digest
ddH$_2$O	6 µl	5 µl
10 x Buffer	1 µl	1 µl
Restriction Enzyme 1	1 µl	1 µl
Restriction Enzyme 2		1 µl
Plasmid DNA	2 µl	2 µl

Table 2.7. Composition of a typical restriction digest.

2.3.7. Cloning into vectors

2.3.7.1. Link and Lock method

Many of the constructs generated in this study were produced using the 'link and lock' multiple

cloning method (Mcgoldrick et al. 2005). This method of cloning allows multiple genes to be cloned

consecutively into the same construct through the use of the same restriction sites. This was

achieved using using SpeI/XbaI, which have compatible cohesive ends, and HindIII. In this process the SpeI/XbaI sites are destroyed leaving only one XbaI and SpeI site in the newly formed constructs to allow insertion of the next gene.

2.4. Biochemical methods

2.4.1. Bradford assays

The Bradford assay is dependant on coomassie blue G250 binding to proteins, especially to arginyl and lysyl residues. In the presence of protein, the absorbance the dye moves fro the red cationic form (470 to 550 nm) to the blue anionic form (590 to 620 nm). As a result the quantity of the protein can be estimated by measuring the amount of coomassie in the blue form at 595 nm (Bradford, 1976). The coomassie blue dye from BioRad was added to diluted protein solution. The reaction was left at room temperature and the OD595 was measured. A standard curve was generated with bovine serum albumin (5, 10, 15, 20 and 25 mg) amd this was used to determine the protein conetration of the purified sample.

2.4.2. GTPase Assay

Two different assays were used to try and measure the GTPase activity of PduV. The first was a a photometric ATP/NADH coupled assay, as described in (Hess & Wurster 1970). Later, a more recently described assay using Anitmony was used, as described in (Bartolommei, Moncelli & Tadini-Buoninsegni 2013).

2.5. Imaging analysis

2.5.1. Live cell imaging

Samples were visualised using an Olympus IX81 microscope with PlanApo 150x OTIRFM-SP 1.49 NA lens mounted on a PIFOC z-axis focus drive (PhysikInstrumente, Karlsruhe, Germany), and illuminated using LED light sources (Cairn Research Ltd, Faversham, UK) with appropriate filters (Chroma, Bellows Falls, VT). An Optisplit device (Cairn Research Ltd) was used to allow simultaneous acquisition of multiple wavelengths. Samples were visualised using a ProEM CCD (Princeton

Intruments) camera, and the system was controlled with Metamorph software (Molecular Devices). Each 3D-maximum projection of volume data was calculated from 21 z-plane images, each 0.2 μm apart, using Metamorph software. During live-cell imaging, cells were mounted onto agar pads on glass slides and fitted onto an ASI motorised stage (ASI, Eugene, OR) on the above system. All live-cell imaging was undertaken using LB media supplemented with appropriate antibiotics at room temperature. Once acquired, deconvolution of images was carried out using Autoquant software and figures prepared using Microsoft Powerpoint, where adjustments to contrast or brightness were applied uniformly to the entire image. All filters used were supplied by Chroma, Vermont,USA and detail of excitation and emission filters are in Table 2.8 below.

Fluorophore	Excitation Filter	Emission filter
Cerulean	ET436/20x	ET480/40m
GFP	ET480/20x	ET510/20m
Ypet	ET500/20x	ET535/30m
mCherry	ET580/25x	ET625/30m

Table 2.8. Excitation and emission filters used to visualise Cerulean, GFP, Ypet and mCherry fusion proteins.

2.5.1.1 Design of FRET Experiments to Explore the Interaction Between PduV and PduK

Initially, to determine if there is an interaction between PduV and PduK, the common FRET pairs Ypet (a derivative of YFP) and Cerulean (a derivative of CFP) were chosen as fluorescent tags. Cerulean has an excitation peak at 433 nm and emits light at 475 nm while Ypet has excitation and emission peaks at 517and 530 respectively, shown in Figure 3.1. This makes the use of these proteins highly advantageous in fluorescent live cell imaging. If the localisation of Cerulean and Ypet are within a distance of 10 nm, the excitation of Cerulean will cause an emission of Ypet signal. This is due to the overlap of the two spectra. Cerulean acts as a donor fluorophore, when excited to a higher energy state, instead of returning to the ground state by energy emission, energy is transferred to Ypet, the acceptor molecule and consequently Ypet signal is emitted as it returns to the ground state. In theory the best FRET pairs are the ones that have higher spectral overlap.

However, this causes problems with background fluorescence and spectral bleed-though (SBT), where even if FRET is not occurring, the donor signal may still be seen on excitation of the acceptor. For this reason Cerulean and Ypet make good FRET pairs with a Förster distance overlap of 4.9 nm as opposed to GFP and Ypet, for example, which have a larger overlap of 5.6 nm as shown in Figure 2.3 (Kaminski, Rees & Schierle 2014).
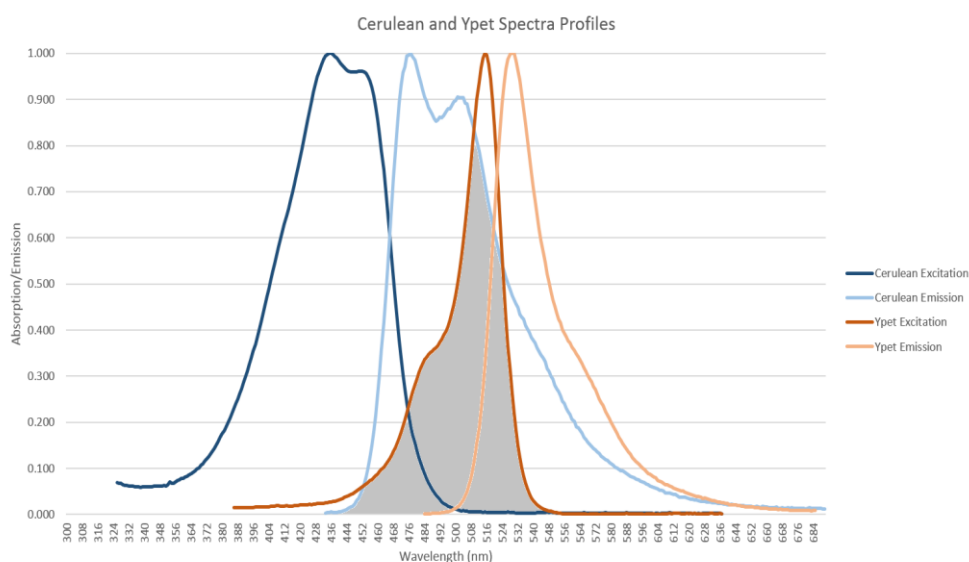
Figure 2.3. Cerulean and Ypet Spectra Profiles. The excitation and emission profiles of Cerulean and Ypet are shown, with peaks for absorbance and emission at 517 and 530 for Cerulean and 433 and 475 for Ypet respectively. The area of overlap between Cerulean emission and Ypet excitation is shown in grey and is known as the spectral overlap, or Förster distance (Ro). The Forster distance is used to determine the FRET efficiency, i.e. the fraction of energy that is transferred to the acceptor, for each donor excitation event. It is therefore used to decide on the best fluorophore pairs to use for FRET. An overlap between the two spectra is necessary to ensure that energy can transfer between two fluorophores if within a distance of 10 nm from each other, however if the overlap is too small the FRET efficiency would be too low. If the overlap is too high, background fluorescence or spectral bleed-though (SBT) can occur.

2.5.2. TEM conventional

2.5.2.1. Preparation of samples

A 5 ml culture of *E. coli* (JM109 or BL21(DE3)pLysS) producing proteins of interest was grown overnight at 37 ºC. The cells were harvested by centrifugation at 4,000 x g at 4 °C for 10 minutes, re-suspended in 2 ml of 2 % paraformaldehyde, 0.5 % glutaraldehyde in PBS and fixed for 1 hour at

room temperature. Traces of the fixing solution were then removed by twice washing the cells with

1 ml of PBS. The samples were then resuspended in the primary stain, 1 % osmium tetroxide, and

incubated at room temperature for 1 hour. The samples were twice washed with PBS prior to

dehydration. Dehydration was accomplished by subjecting the sample to a solvent gradient (Table

2.9).

Composition	Solvent	Time (minutes)
70%	Ethanol	20
100%	Ethanol	20
100%	Ethanol	30
100%	Propylene Oxide	30
100%	Propylene Oxide	30
50:50	Propylene Oxide:Embedding medium	60
100%	Embedding medium	180

Table 2.9. The solvent gradient used for the dehydration of samples for electron microscopy.

The embedding medium used was Agar Low Viscosity Resin and the constituents for a block of

medium hardness is shown in Table 2.10. The samples were placed in 0.5 ml embedding tubes and

centrifuged for 10 minutes at 4000 x g to concentrate the cells to the tip and incubated at 60 ºC

overnight to polymerise.

Component	Mass
LV Resin	48 g
VH1 Hardener	16 g
VH2 Hardener	36 g
LV Accelerator	2.5 g

Table 2.10. Low viscosity resin constituents used to produce a block of medium hardness

2.5.2.2. Sectioning and visualisation of samples

Specimens were thin sectioned at a thickenss of ~80nm with a glass knife on an RMC MT-6000-XL

ultramicrotome. Sections were collected on copper grids and post-stained with 5 % uranyl acetate

for 30 minutes at 60 ºC and 0.1 % lead citrate for 10 minutes at room temperature. Sections were

then observed and photographed with a JEOL-1230 transmission electron microscope.

2.5.3. TEM immuno-labelling

For immunogold labelling of PduV-GFP, BL21(DE3) cells expressing PduV-GFP and the associated BMC shell were embedded in Agar Low Viscocity Resin. A 5 ml culture of *E. coli* (JM109 or BL21(DE3)pLysS) producing proteins of interest was grown overnight at 37ºC. The cells were harvested by centrifugation at 4,000 x g at 4 °C for 10 minutes, re-suspended in 2 ml of 2 % paraformaldehyde, 0.5 % glutaraldehyde in PBS and fixed for 15 minutes at room temperature. Fixed cells were then washed three times in 1 ml of PBS. Dehydration of the cells was again accomplished by subjecting the cells to a solvent gradient, (Table 2.11).

Composition	Solvent	Time (minutes)
30%	IMS	120
60%	IMS	120
90%	IMS	Overnight
100%	Dried Ethanol	60
100%	Dried Ethanol	60
100%	Dried Ethanol	60
1:1	Ethanol:Resin	60
1:2	Ethanol Resin	60
100%	Resin	60
100%	Resin	Overnight

Table 2.11. The solvent gradient used for the dehydration of samples for immuno-labelled electron microscopy.

The samples were then placed in embedding tubes and centrifuged for 10 minutes at 4000 x g to concentrate the cells to the tip and incubated at 60 ºC overnight to polymerise. Sections were then cut as described in section 2.5.2.2 and, placed on copper grids. Immunolabelling was achieved by the following method; The grids were washed in TBST (20 mM Tris, 500 mM NaCl, 0.05% Tween-20, 0.1 % BSA, pH 7.4), blocked in 2 % fish gelatine in TBST for 30 minutes and incubated for 1 hour with the primary antibody (1:100 anti-GFP rabbit IgG) (Gullick Lab, University of Kent). The grids were washed in TBST and incubated with goat anti-rabbit IgG immunogold conjugate, 15 nm gold particles (British Biocell) 1:50 for 30 minutes. Finally the samples were washed in TBST, then millipore water and were then dried. Samples were then stained and visualised as described in Section 2.5.2.2.

2.5.4. AFM

Samples were visualised using a Bruker Multimode 8 scanning probe microscope. Purified BMCs were mounted on hydrophobic MICA by incubating 20 µl of purified BMCs on the surface for 5 minutes. 2.5 % (v/v) glutaraldehyde in PBS buffer was then used to fix the sample, and this was then dried using nitrogen gas. Images were collected in air using the peakforce tapping mode with peak-asyst air cantilever probe (Bruker) with a nominal spring constant of 0.4 N/m. Images were then processed using the supplied Nanoscope software.

2.5.5. Experiment Design

When microscopy analysis was used for investigative purposes at least 3 slides were examined in all experiements to ensure any findings were both accurate and repeatable, and not simply as a result of biological variation. In addition to this, when drawing conclusions from microscopy analysis it was ensured that at least 50 cells were imaged.

Chapter 3: Exploring possible interactions between the PduK and PduV

3.1. Introduction

The potential ability to utilise recombinant shells to produce designer chemicals, drugs and biofuels relies on our understanding of the structure of the shell, as well as the properties of the shell proteins that form it. The Pdu shell is the second best-studied of all known BMCs, after the carboxysome. However, very little is known about the assembly of proteins to form the Pdu BMC structure or how small molecules are transported across the shell. Currently it is known that the essential proteins involved in recombinant Pdu shell formation are PduA, PduB (expressed as two isomers, PduB and PduB'), PduJ, PduK and PduN. The addition of PduU to the complement of PduABJKN resulted in the formation of slightly larger BMCs. However the functional role of these shell proteins within the BMC still remains largely unknown, see section 1.4.7.

Previous studies have given insights into the phylogenetic relationship between shell proteins and identified which other shell proteins interact with other shell proteins. Interestingly PduA appears to interact with all of the essential shell proteins. The other proteins were shown to interact only with PduA, with the exception of PduK which co-purified with PduT by IMAC (Parsons et al. 2008). Further studies carried out by Dr S. Frank revealed that PduK also co-purified with PduV, a protein thought to be involved in the spatial organisation of the Pdu BMC (unpublished data). Furthermore, overexpression of PduK in *E. coli,* cells housing PduA-X, displayed a single large aggregate complex that still contained the delimiting structure of the BMC; this indicates that overexpression prevented the spatial separation of the organelles, but did not affect the BMC structure (Parsons et al. 2008). This leads to the question: what is the role of PduK in the BMC shell?

One potential role for PduK is for the protein to help facilitate the transport of molecules into the BMC through an interaction with the P18 targeting sequence (Lawrence et al. 2014). The C-terminus of PduK is unique to shell proteins in that it contains an extension that harbours an amino-acid sequence containing 3 cysteine residues, reminiscent of a motif associated with the presence of an iron-sulphur centre. However no evidence has been shown that this region of the protein does

indeed house such a redox centre. A recent study found that a BMC shell that lacks PduK has a similar phenotype to that of PduK overexpression described above – protein aggregates can be seen, but these contained defined shell structures. It was also found that a *pduK* deletion had no effect on propionaldehyde toxicity or growth on 1,2-PD (Cheng et al. 2011). Although PduK is considered to be an essential shell protein, its exact function is currently unknown. It is likely that PduK is involved in several processes, such as mediating the internalisation of molecules and facilitating the distribution of BMCs throughout the cell cytoplasm, through an interaction with PduV.

This investigation aims to characterise further the role of PduK in the recombinant Pdu shell. To do this, fluorescence live cell imaging was used to identify possible interactions between PduK and PduV and to determine if PduK is involved in the distribution of BMCs in the cell, as previous studies have suggested. In addition, through the use of C-terminal PduK truncations, the role of the C-terminal extension in the spatial organisation of BMCs was investigated. In order to identify protein-protein interactions by live cell imaging it was necessary to engineer protein fusions whereby PduK and PduV were tagged with fluorophores to allow visualisation by microscopy. However in so doing, it was also necessary to determine if the resulting protein fusions were functional, i.e. if compartments containing tagged PduK could still form, and if tagged PduV still associated with filaments. Any loss of function due to fluorescent tags could generate artefactual results that may be difficult to interpret.

3.2. Results

3.2.1. Cloning of fluorescent tag-fusions

Initially, to determine if there is an interaction between PduV and PduK, the common FRET pairs Ypet (a derivative of YFP) and Cerulean (a derivative of CFP) were chosen as fluorescent tags. Genes for expression of these flurophores where cloned into expression plasmids with either *pduV* or *pduK* as described below.

3.2.1.1. Cloning *pduV-cerulean*

pduV was originally sourced from the *pdu* operon of *Citrobacter freundii* by Dr J Parsons (Parsons et al. 2008). For this study, *pduV* was sub-cloned into *pET3a* using the restriction sites 5' NdeI and 3' SacI. The c*erulean* gene was subsequently fused onto the 3' end corresponding to the C-terminus of PduV , as it has previously been shown that tagging PduV on the N terminus inhibits function (Parsons et al. 2010). The *cerulean* was sourced from (Rizzo et al. 2004) and primers were designed containing the restriction sites 5' SacI and 3' SpeI. After PCR and subsequent digest to remove extra bases, *cerulean* was ligated with *pduV,* as outlined in Section 2.3.5. The resulting plasmid is shown in Figure 3.1. PduV-Cerulean was also later sub-cloned into the chloramphenicol resistant plasmid *pLysS*, in order to co-express with ampicillin-resistant plasmids containing other *pdu* genes. This was sub-cloned by restriction digests of *pLysS-(pduN)* and *pET3a-pduV-cerulean* with XbaI and HindII. The *pduV-cerulean* fragment was then ligated with *plysS* and transformed into JM109 competent cells as outlined in Section 2.2.4. JM109 cells were then cultured from the transformation plate and grown overnight at 37 °C, as described in Section 2.2.2.1. To harvest the plasmid, Qiagen Minipreps were carried out and the DNA was test digested to ensure the genes had been inserted correctly into the plasmid, as outlined in Section 2.3.6. This cloning method was unaltered throughout the cloning process.
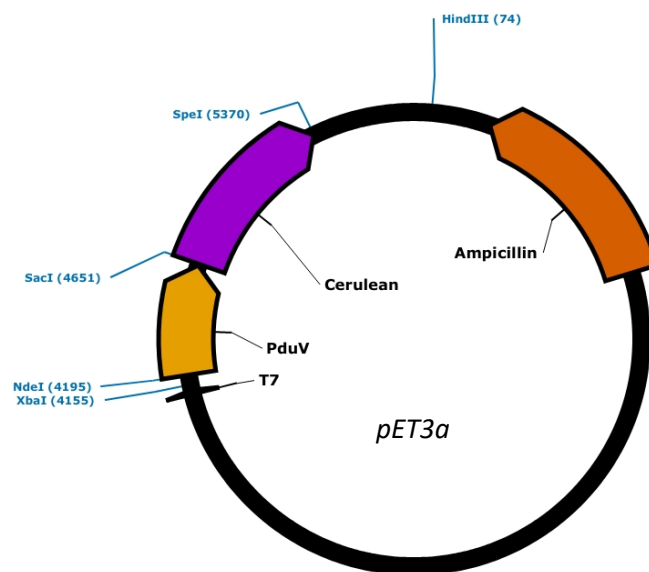
Figure 3.1. Plasmid map of *pET3a-pduV-cerulean*. Length is 5786 bp and plasmid contains an ampicillin resistance gene.

3.2.1.2. Cloning *pduK* fusion tags

It was not known if tagging PduK on the N- or C- termini had any effect on the formation of Pdu BMCs. Consequently, two separate constructs were engineered in order to tag PduK separately on both the N and C terminus with Ypet. For the N-terminal tag, *ypet* was amplified by PCR using primers containing a 5' AseI and 3' SpeI and NdeI (See Table 2.3). The digested *ypet* PCR product was cloned into the 5' NdeI, 3' SpeI of *pET3a*, locking the gene in the plasmid with the compatible sites AseI and NdeI, which are subsequently destroyed when ligated together. *pduK* was then sub-cloned after *ypet* using the 5' NdeI and 3' SpeI sites. C-terminal tagged PduK was engineered by the PCR of *ypet* with the restriction sites 5' SpeI, 3' BamHI. *ypet* was then ligated behind *pduK* in a *pET3a* plasmid. *pduK* was re-cloned by PCR in order to remove the stop codon and ligated with the *pET3a* plasmid using the NdeI and SpeI sites, (Figure 3.2).
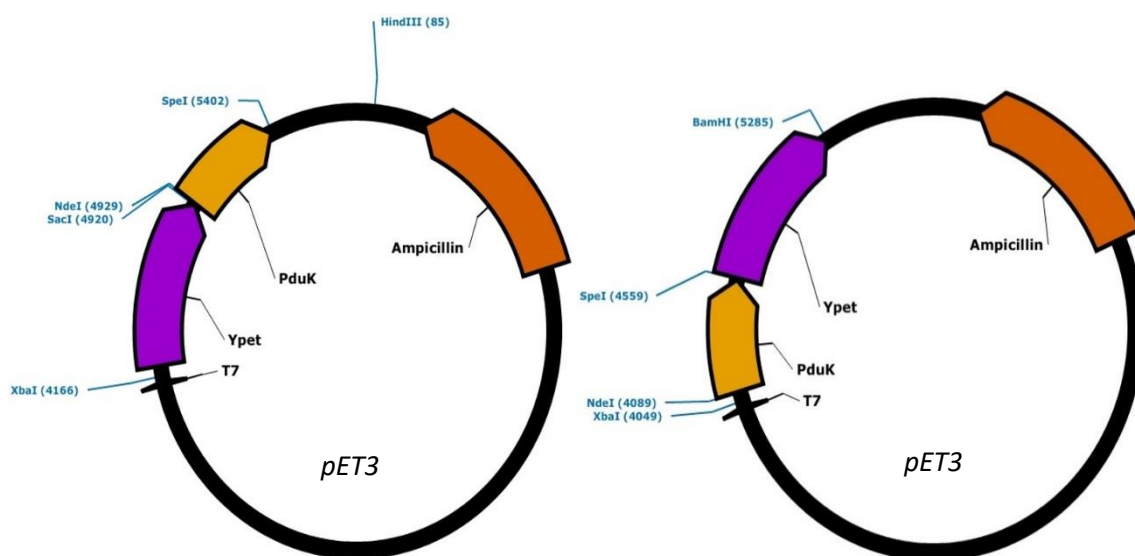
Figure 3.2. Plasmid maps of engineered constructs containing *ypet* and *pduK*. A) *pET3a-ypet-pduK*. Total plasmid length is 5807 bp B) *pET3a-pduK-ypet.* Total plasmid length: 5798

3.2.1.3. Cloning *pduK* fusions at the end of the Pdu BMC construct

It was necessary to engineer a construct containing a fluorophore-tagged PduK as well as genes required for recombinant Pdu shell formation. This is because initial results revealed that when

PduK-Ypet and Ypet-PduK were co-produced with PduV-Cerulean, the function of PduV was impaired as filaments were no longer visible. In addition tagged-PduK alone appeared to aggregate at the cell poles, (data not shown). Therefore the expression of BMCs are necessary to determine possible interactions between PduV and PduK.

Previously it has been shown that changing the order of the shell protein genes, by inverting the minimal shell protein assembly to give *pduN-K-J-B-A* resulted in the appearance of aberrant structures. However due to ease of cloning, *pduK* fusion genes were added to the end of the BMC construct *pET3a-pduABJNU*, outlined in Table 2.2. To do this, *pduK-ypet* and *ypet-pduK* were restricted with XbaI and HindIII, to cut the fragment from the plasmid. These fragments were ligated with *pET3a-pduABJNU* restricted with SpeI and HindIII as shown in Figure 3.3. The compatible cohesive ends of SpeI and XbaI allows the fusion gene to be inserted into the construct after the genes corresponding to other shell proteins.
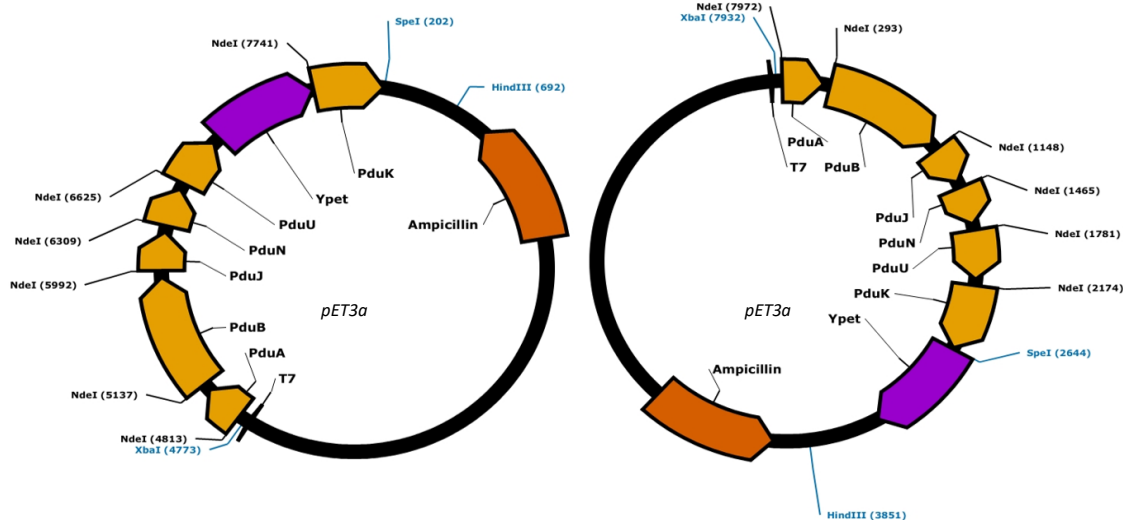
Figure 3.3. Plasmid map of *pET3a-pduABJNU-ypet-pduK* and *pET3a-pduABJNU-pduK-ypet*. This construct contains the *pduK* fusion tags, *pduK-ypet* and *ypet-pduK* integrated after the other genes required to form the BMC shell. Total plasmid length: 8091

3.2.1.4. Integration of *pduK-ypet* with genes for the BMC shell.

Live cell imaging revealed that BMCs do not form correctly when expressed from a construct that has a *pduK* fusion cloned after the genes encoding the other shell proteins, however images revealed that PduABJNU-K-Ypet contained BMCs that were more similar to the control than PduABJNU-Ypet-K (Figure 3.6.). To investigate further the effect of gene order on the formation of BMCs and the effect this has on PduV, *pduK-ypet* was integrated in the normal gene order; PduABJ-K-Ypet-NU by the 'Link and Lock' process.

Initially pET3a-pduABJ (See Table 2.2) was restriction digested with SpeI and HindIII. *pET3a-pduK-ypet* was also digested, with the restriction enzymes XbaI and HindIII. The fragment ends were joined by ligation, with XbaI and SpeI forming a new site as they have compatible cohesive ends. As a result, the previous XbaI/SpeI site is destroyed, locking the genes with the plasmid and allowing further genes to be sub-cloned into the plasmid using the same restriction sites. The *pET3a-PduABJ-K-Ypet* plasmid was restricted with SpeI and HindIII, and *pduN* was cut from pET3a with the restriction enzymes XbaI and HindIII. Once again the fragments were ligated, resulting in the formation of a new restriction site and the destruction of XbaI/SpeI. Finally *pET3a-PduU* was restricted with XbaI and HindIII and ligated into *pET3a-PduABJ-K-Ypet-N* that had been digested with SpeI and HindIII. This process resulted in the construct shown in Figure 3.4.
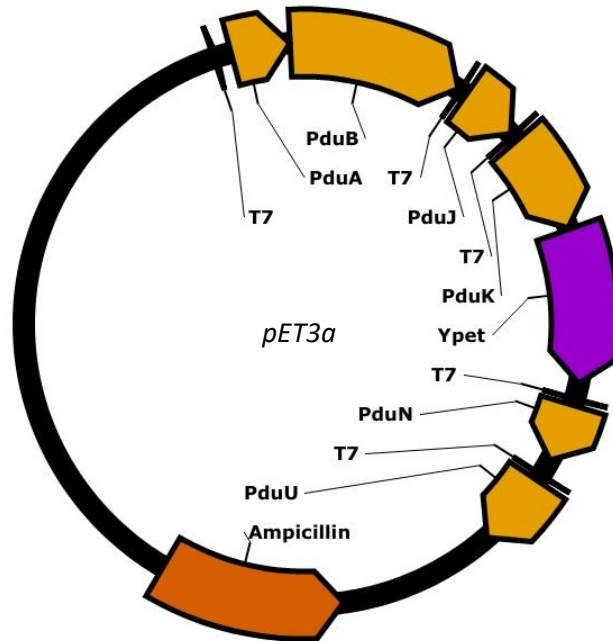
Figure 3.4. Plasmid map of *pET3a-pduABJ-pduK-ypet-NU*. This construct contains the *pduK* fusion tag, *pduK-ypet* integrated in the correct order of genes required to form the BMC shell. Total plasmid length: 8091

3.2.2. Microscopy analysis to characterise a proposed interaction between PduK and PduV

The recombinant shell protein constructs, expressed in *E. coli* and used in this study consists of genes that encode the proteins necessary to form the BMC shell. These genes were derived from the *pdu* operon of *Citrobacter freundii* and include; *pduA, pduBB', pduJ, pduK, pduN,* and *pduU.* Expression of these genes produced empty BMCs that were similar in size and shape to the wild type compartments produced in *S. enterica* (Parsons et al. 2008). In addition, studies have also been carried out using empty, recombinant Pdu BMC shells containing mCherry-labelled PduA. These mCherry-PduABJKNU compartment shells were also very similar to the wild-type Pdu shells and formed intact structures of approximately 100 nm in diameter (Parsons et al. 2010).

As well as the shell proteins required to form an empty BMC, PduT is associated with the BMC but its role within the BMC is not known. It is considered to be a non-essential component of the shell as described in Section 1.4.7.6. Therefore, an investigation was initiated to determine whether or

not the addition of PduT had any effect on the localisation or formation of filaments. In addition, the effect of tagging PduV with a fluorophore was investigated. Previously, studies had been carried out to give insights into the function of PduV. From this it was known that PduV can be tagged on the C-terminus with GFP however, no other PduV fusion tags have been explored (Parsons et al. 2010).

In order to examine the functionality of PduV-Cerulean, the presence of filaments and the distribution of mCherry-tagged empty microcompartment shells were examined by fluorescence microscopy. It is necessary to express PduV-Cerulean in conjunction with BMC shells for filamentous structures to be observed. In the absence of Pdu BMC shells, PduV-Cerulean can be seen to localise only at the cell poles in inclusion-like foci (Parsons et al. 2010).

3.2.2.1. Visualisation of the PduV-Cerulean fusion tag with Pdu BMC shells

PduV-Cerulean was expressed with empty Pdu shells in order to investigate the effect of a C-terminal Cerulean tag. Two separate *E. coli* BL21 (DE3) strains were engineered. The first contained the plasmids *pLysS-mCherry-PduABJKNUT* and *pET3a-pduV-cerulean* and the second contained the plasmids *pLysS-mCherry-PduABJKNU*, and *pET3a-pduV-cerulean.* For the purpose of live cell imaging, cultures (25 mL) were inoculated from a starter culture containing one colony from a double transformation. The cultures were then grown at 37°C to mid-log (OD_{600} of between 0.4 and 0.6), see Section 2.2.2.2, and mounted on an agarose pad and were then visualised by microscopy, see Section 2.5.1.
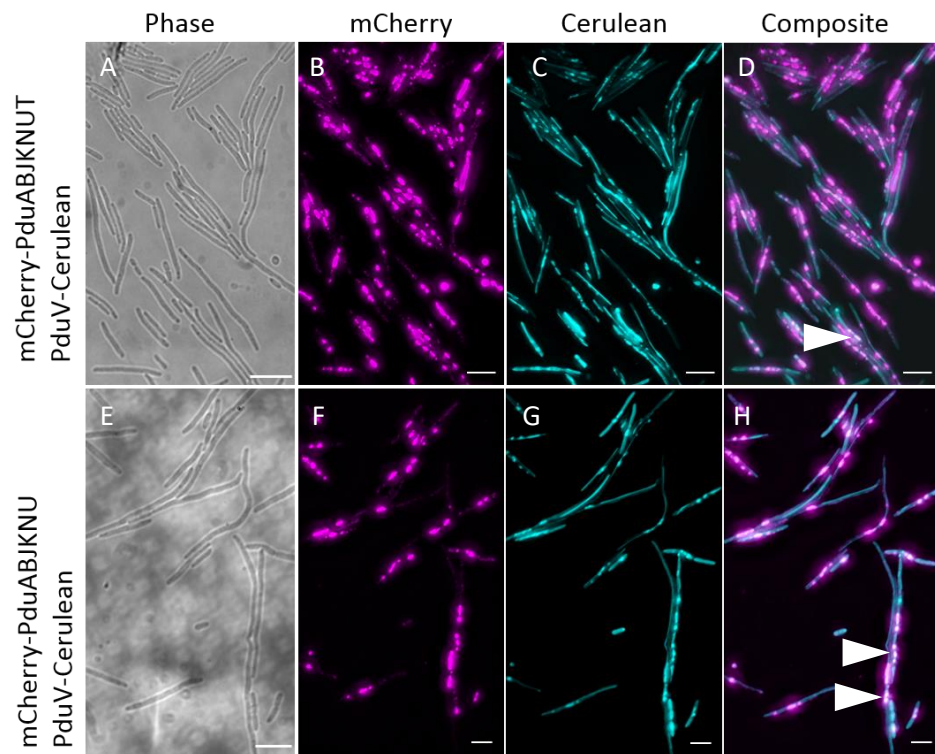
Figure 3.5. Comparison when PduV-Cerulean is co-expressed with BMC shells that either contain or lack PduT. Live cell images acquired show the Phase, mCherry, Cerulean and Composite signals. The *E.coli* strains visualised include **A-D** – mCherry-PduABJKNUT, PduV-Cerulean and **E-H** – mCherry-PduABJKNU, PduV-Cerulean. Colocalisation between empty BMC shells and PduV can be seen in both samples (white arrows), however the level of colcalisation appeared reduced when PduT was present in the empty BMC shell (Top Image). Scale Bar: 5 μm

Elongated cells have previously been visualised when recombinant Pdu BMCs are expressed in *E. coli* (Parsons et al. 2010; Sargent, F. A. Davidson, et al. 2013) presumably as they exert a stress response. Figure 3.6 is consistent with this observation and shows that the cells were elongated in strains co-producing PduV-Cerulean in conjunction with either mCherry-PduABJKNU or mCherry-PduABJKNUT. PduV-Cerulean was observed in filamentous structures in both of these strains and was also seen in discrete foci throughout the cytoplasm, often co-localised with the empty BMC shells (as shown by arrows). The distribution of the microcompartments also appeared unaffected when PduV was labelled with Cerulean. mCherry-tagged Pdu BMCs were distributed throughout

the cytoplasm of the cell in discrete foci, corresponding to previous results observed by Parsons et al (Parsons et al. 2010).

Interestingly, the level of co-localisation appeared visibly reduced in the presence of PduT at the end of the empty microcompartment construct. This is shown by the white foci in the composite image of Figure 3.6, which represents co-localisation between the Cerulean and mCherry signal. As a result of the reduction in co-localisation, all future experiments were carried out with empty microcompartments lacking PduT.

3.2.2.2. The effect of fusing Ypet to PduK on BMC formation and interaction with PduV-Cerulean by live cell imaging

In order to examine the possible interaction between PduK and PduV, fluorescence microscopy was initially carried out with BL21 (DE3) strains containing *pLysS-PduV-Cerulean* and either *pET3a-pduK-ypet* or *pET3a-ypet-pduK* (images not shown). Microscopy images showed that both PduV-Cerulean and the Ypet-labelled PduK localised to the cell poles. The Cerulean and Ypet signal seemed to co-localise but this may be a result of insoluble-protein aggregation and the formation of packed inclusions. To explore the possible interaction between PduK and PduV, it was therefore necessary to include genes for Pdu shell protein expression to prevent protein aggregation and visualise individual foci. As a result, due to ease of cloning, *pduK-ypet* and *ypet-pduK* were sub-cloned at the end of the shell construct, see Section 3.2.1.3.

BL21 (DE3) strains co-producing PduV-Cerulean and either PduABJNU-K-Ypet or PduABJNU-Ypet-K were grown at 37°C by inoculation of a culture (25 mL) from an overnight starter culture containing cells from one colony of a double transformation agar plate. The cells were grown to mid-log (OD$_{600}$ 0.4-0.6) and visualised by microscopy as outlined in Section 2.5.1.

Results, from the images in Figure 3.7, showed that when PduV-Cerulean was co-expressed with empty BMC shells containing a PduK-Ypet or Ypet-PduK fusion, there were no obvious elongated

filamentous structures. Short linear structures were observed in some of the cells (as indicated by the white arrow heads), although these shorter filaments were not as prevalent as filaments seen in the mCherry-PduABJKNU control. To quantify this, strains were imaged by microscopy and the number of filaments in 200 cells from each strain were counted in MetaMorph (Section 2.5.1). A moderate number of filaments, at 53 per 200 cells were observed in images of the strain expressing PduABJNU-K-Ypet and PduV-Cerulean, whereas only 24 filaments were seen when PduABJNU-Ypet-PduK and PduV-Cerulean were co-expressed. However both of these were markedly reduced when compared to the control where 241 filaments were counted in 200 cells; with many cells containing multiple filaments.

Interestingly, the fluorescent foci of BMCs containing PduK fusions were much larger compared to that of mCherry-PduABJKNU shells. Compartments of PduABJNU-Ypet-PduK were not distributed as evenly throughout the cytoplasm as the control and individual compartments, represented by discrete foci of Ypet fluorescence signal, were not observed (Figure 3.6). In comparison, PduABJNU-K-Ypet BMCs appeared to be more evenly distributed compared with the N-terminal PduK tag and discrete foci were visible, as indicated by the circled cell in Figure 3.6.

Overall, as seen in Figure 3.7, PduV and PduK appeared to co-localise, as suggested by the green tint in the composite images. However it is difficult to assess whether the BMCs had formed correctly, incorrect folding could lead to the exposure of residues that would not normally be revealed and may cause interactions that would not normally occur. The higher number of filaments observed with PduABJNU-K-Ypet and visualisation of discrete foci suggests that shell protein may be folded correctly to form intact compartment structures when the C terminus of PduK is tagged as opposed to the N terminus.

The method of Pdu BMC shell protein assembly is currently unknown and the effect of reordering the genes encoding shell proteins was largely also unknown. The result of cloning *pduK* at the end

of the shell construct may have inhibited possible assembly processes. For this reason, PduK-Ypet was incorporated in the recombinant Pdu shell construct in the same gene order as the *pdu* operon from *C. freundii*.
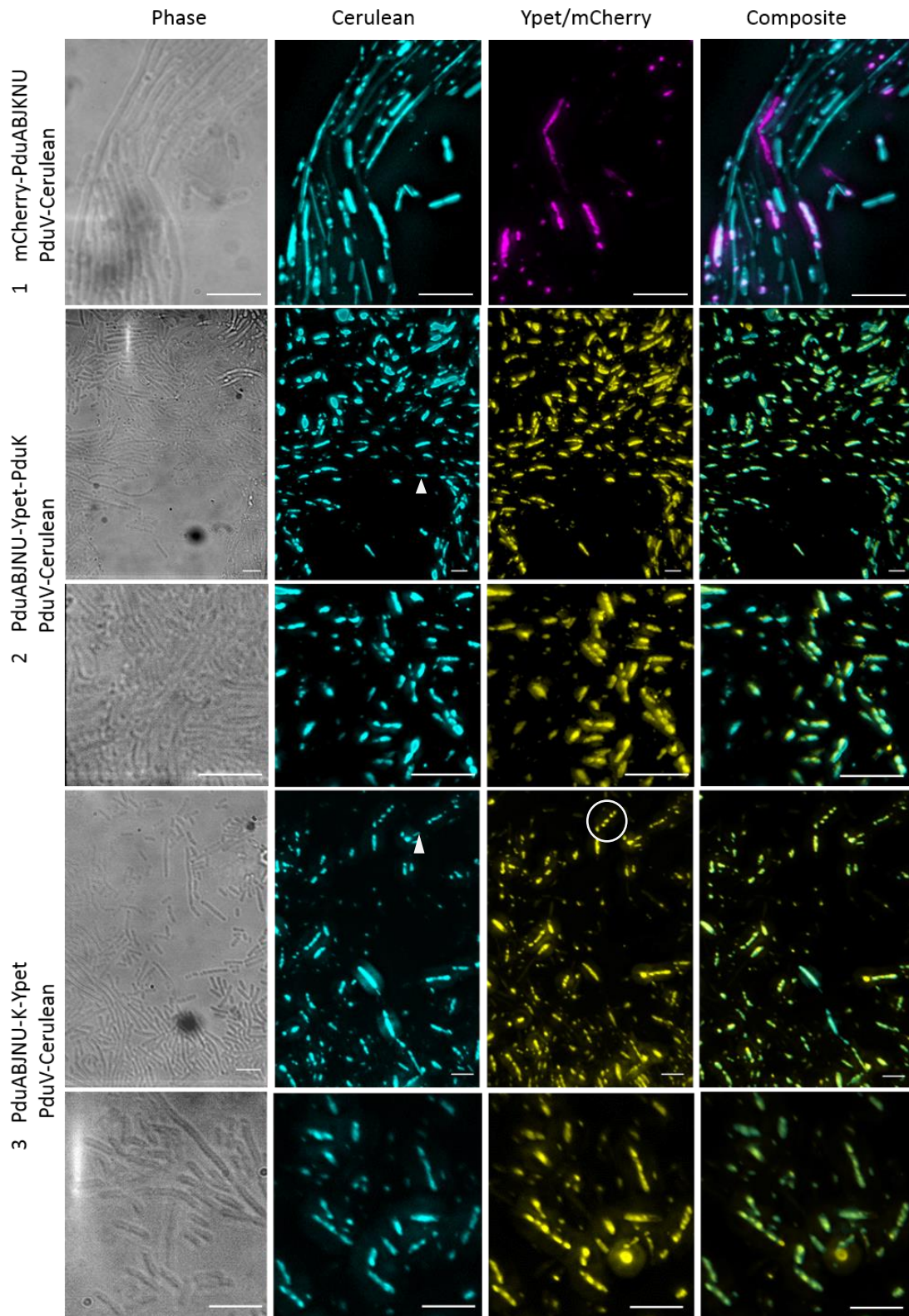
Figure 3.6. Effect of tagging PduK on BMC formation and PduV function. Live cell images acquired show the Phase, Ypet or mCherry, Cerulean and Composite signals. The *E. coli* strains visualised include PduV-cerulean co-expressed with 1) mCherry-PduABJKNU 2) PduABJNU-Ypet-PduK 3) PduABJNU-K-Ypet. Two corresponding images are shown for strains 2 and 3, with the bottom images zoomed in to visualise structures more clearly. The expression of BMC shells containing PduK with Ypet fused to either the N

or C terminus appeared to greatly reduce the presence of filamentous PduV-Cerulean filaments. Occassionally short filamentous structures were observed (white arrows). BMC shells containing Ypet-PduK were not distributed as evenly throughout the cytoplasm as the control and discrete foci of Ypet fluorescence signal, were not observed. However BMC shells containing PduK-Ypet appeared to be more evenly distributed discrete foci were visible, as indicated by the circled cell. In both cases PduK and PduV did appear to colacalise Scale Bar: 5 μm

3.2.2.3. Exploring possible interactions between PduK and PduV by live cell imaging

To explore the possible interaction between PduV and PduK, *pduK-ypet* was cloned in the functional BMC shell gene order. A BL21 (DE3) *E.coli* strain was engineered to contain the plasmids *pET3a-PduABJ-K-Ypet-NU* and *pLysS-pduV-cerulean*. Cells were then grown for microscopy at 37°C in 25 ml cultures by inoculation from an overnight starter culture as described in Section 2.2.2.2 and visualised by live cell imaging at an OD600 of between 0.4 and 0.6 (mid-log).

Fluorescent images in Figure 3.8 showed that the incorporation of *pduK-Ypet* with the rest of the shell genes resulted in the appearance of elongated filaments containing PduV-Cerulean. These filaments were not visible when strains expressing tagged *pduK*, reordered to the end of the shell construct, were studied (see Section 3.2.2.2). This suggests the need for shell proteins to be expressed in a particular order for PduV to function. Despite the presence of elongated filaments, similar to that observed with the mCherry-PduABJKNU BMC control, the BMCs present in the PduABJ-K-Ypet-NU strain in some cases appeared to aggregate and amassed in large, bright foci indicating that the shells did not form correctly with the fluorophore-tagged PduK.
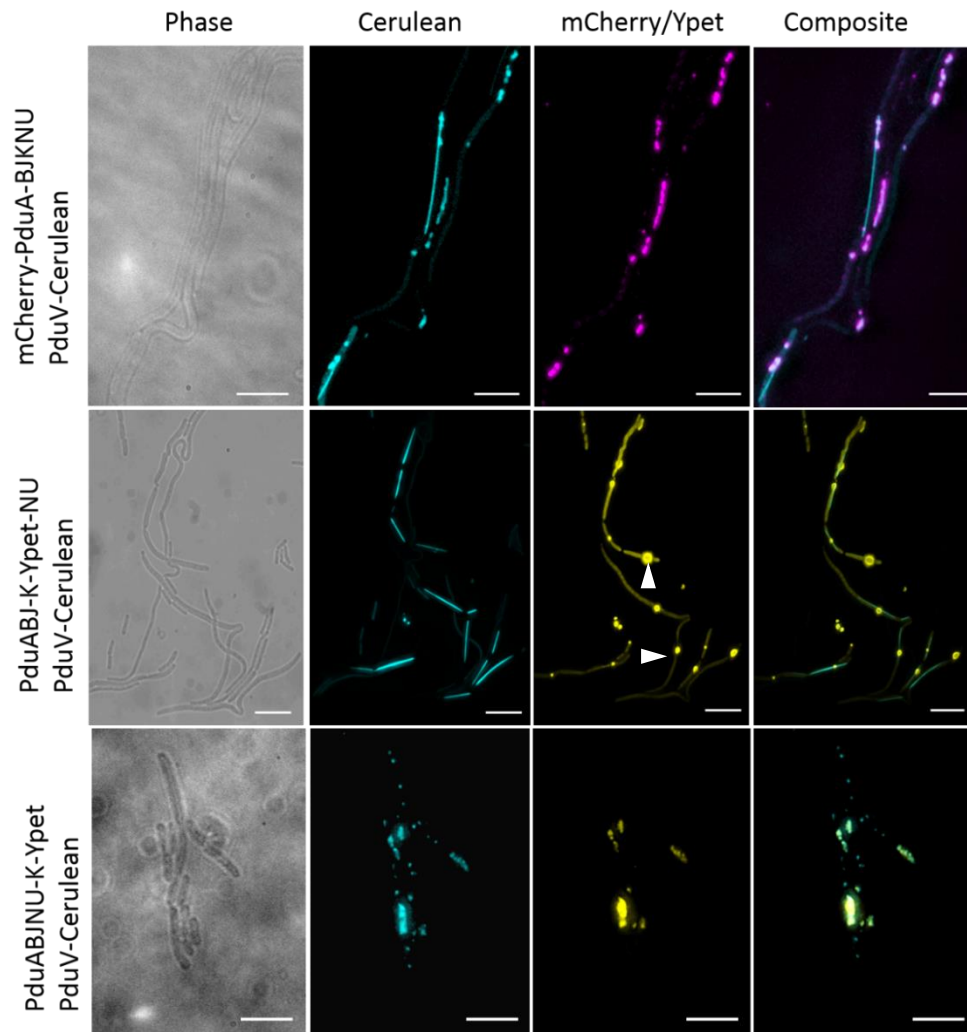
Figure 3.7. Exploring the interaction between PduK and PduV. Live cell images acquired show the Phase, Ypet or mCherry, Cerulean and Composite signals. The *E. coli* strains visualised include PduV-cerulean co-expressed with 1) mCherry-PduABJNU 2) PduABJK-Ypet-NU 3) PduABJNU-PduK-Ypet. The cloning of PduK-Ypet into the correct positon in the Pdu operon resulted in the formation of PduV-Cerulean filament similar ot that in the control sample, however the BMC shells accumulated into large foci, suggesting they shells were not forming correctly (White Arrows). Scale Bar: 5 μm

3.2.2.4. The formation of the BMC shell with tagged PduK

To investigate the structure of BMCs formed when PduK is labelled with Ypet, cells were thin sectioned and visualised by TEM. BL21 (DE3) cells were transformed with the engineered BMC constructs. Starter cultures were then grown overnight at 37°C by inoculation using several colonies from the transformation plate. Larger 100 ml cultures were then grown by inoculation from the starter culture (1:100), at 37°C until an OD_{600} of 0.8 was reached. The cultures were subsequently

induced, as outlined in Section 2.2.5, and grown overnight at 19°C. Cells were spun down and prepared for thin sectioning and visualisation by TEM as described in Section 2.5.2.
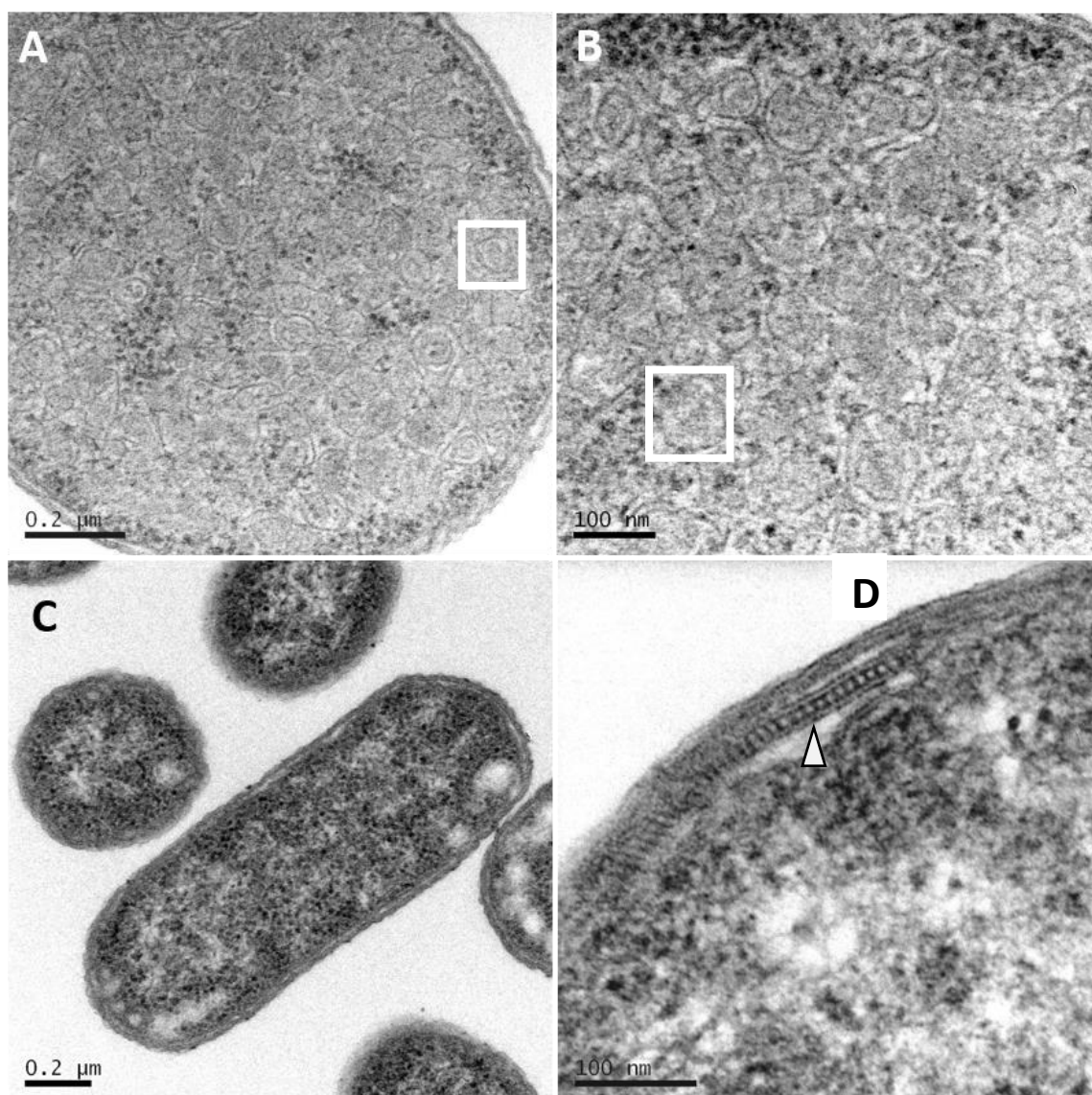
Figure 3.8. Examining the effect of tagging PduK on BMC formation. TEM analysis of whole cell thin sections of cells expressing mCherry-PduABJKNU (A & B), a negative control of BL21 (DE3) pLysS cells (C) and cells expressing PduABJ-K-Ypet-NU (D). BMC shells were observed in control cells as expected (white squares in panes A and B) and were not observed in then negative control. However when PduK-Ypet was incorporated into the Pdu operon BMC shells were not observed (Pane D). However elongated tube like arrangements we observed near the cell wall in apprxoximately 10% of cells, as shown by the white arrow.

Results showed that compartments from the control strain expressing mCherry-PduABJKNU BMCs, Figure 3.8 (A & B), are able to form intact structures that vary in size between 70 – 100 nm, measured using ImageJ software. These compartments appear less regular than wild-type *S. enterica* Pdu BMCs, however, this may be a result of the angle of sectioning. Cells were densely packed with BMCs and as a result were enlarged in both width and length. The shells of the BMC can be seen as electron dense strands that close to form the intact, empty, compartment. Cellular components such as ribosomes and DNA can be seen around the edges of the cell, or packed in discrete areas, separate from that of the densely packaged BMCs. A negative control strain, Bl21 (DE3) *pLysS* was grown at the same time and subjected to the same growth and TEM sectioning conditions. No compartment-like structures were observed in this control, as shown in Figure 3.8 (C).

Interestingly, TEM of thin sections of cells containing PduABJ-K-Ypet-NU showed very similar results to that of the negative control, BL21 (DE3) *pLysS,* shown in Figure 3.8 (D) BMC-like compartments were not present in any of the cells visualised (n=200), although some cells (~10%) contained unusual patterned structures. These structures were highly uniform, consisting of elongated, narrow tube-like arrangements that comprised outer, delimitated walls with a segmented interior. In addition many cells contained inclusion bodies. These structures were not present in the negative control and are likely to be due to the expression of PduABJ-K-Ypet-NU. This experiment was carried out twice and the same result was observed on both occasions.

3.2.3. Analysis of the role of PduK in the BMC shell

It was found that PduK-fusions prevented the formation of the BMC shell. The role that PduK has on a recombinant Pdu system was then explored. Two *E.coli* strains were created that harboured the genes necessary for shell formation but lacked *pduK*; (1) *pET3a-mCherry-pduABJNU* with *pLysS-pduV-cerulean* and (2) *pET3a-mCherry-pduABJNU* alone. These strains were visualised by live cell imaging and TEM to determine: the localisation of PduV in relation to the BMC, the presence of

PduV-Cerulean associated filaments and also the effect on BMC formation in the absence of PduK

in a recombinant system.

3.2.3.1. Co-localisation between the shell and PduV; exploring the role of PduK's role in this interaction

Strains were grown for fluorescent live cell imaging including; mCherry-PduABJKNU PduV-Cerulean

as a positive control for BMC formation and PduV function as well as mCherry-ABJNU and PduV-

Cerulean. These were grown in the same conditions as previous cultures, at 37°C in a 180 rpm

shaking incubator until a cell density of OD_{600} 0.4-0.6 was reached. Cells were then mounted and

visualised as described in Section 2.5.1.
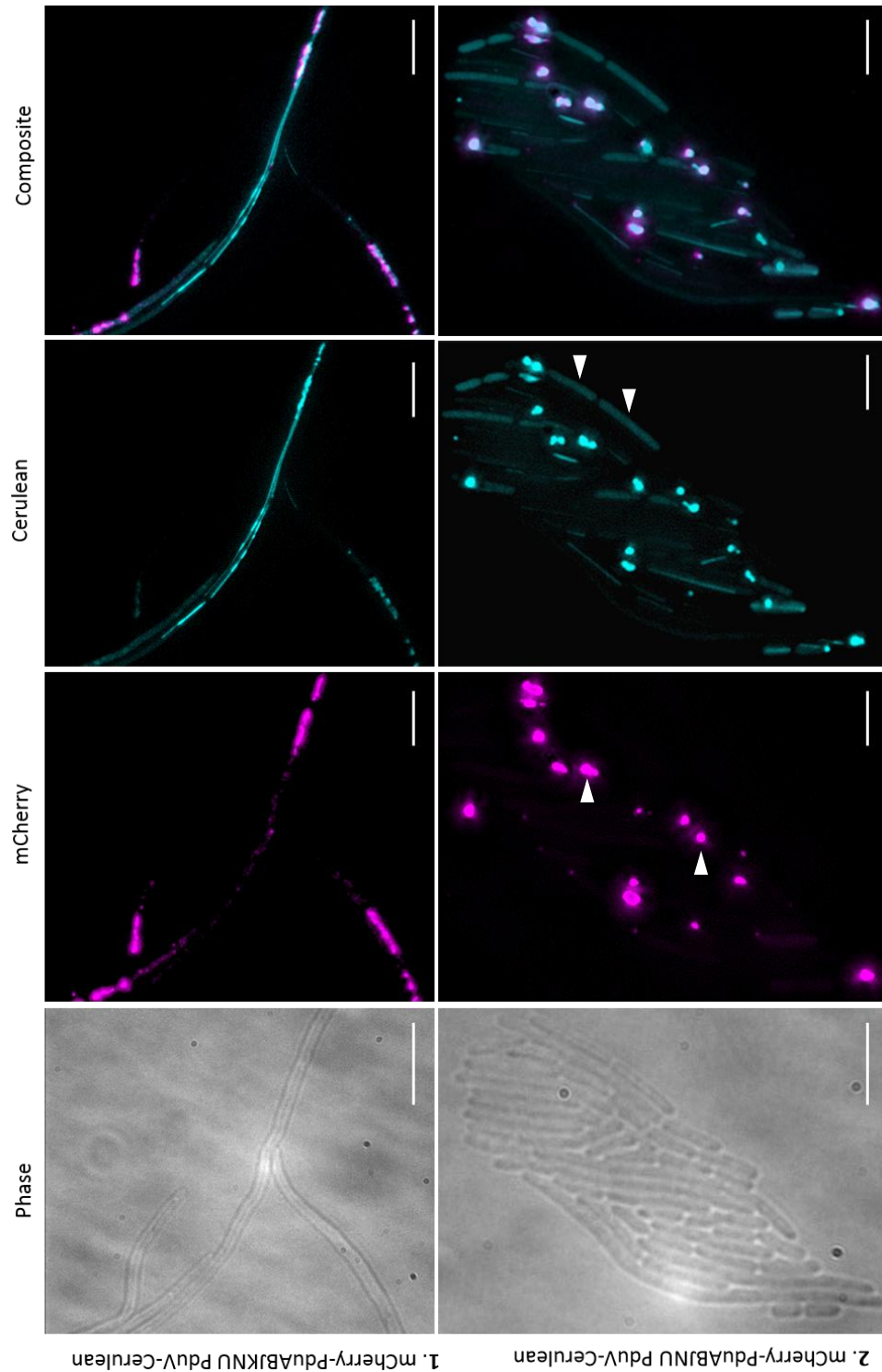
Figure 3.9. Exploring the necessity of PduK in the interaction between PduV and BMCs. Live cell images acquired show the Phase, mCherry, Cerulean and Composite signals. The *E.coli* strains visualised include **Top Row** mCherry-PduABJKNU and PduV-Cerulean and **Bottom Row** – mCherry-PduABJNU, PduV-Cerulean. The absence of PduK resulted in the BMC shells accumulating into large foci (white arrows), however there was co-localisation between PduV-Cerulean and these BMC shells. It is unclear if this was due to the two interacting or was a result of protein aggregation. Scale Bar: 5 μm.

Compared to the control strain, images showed that cells co-expressing mCherry-ABJNU and PduV-Cerulean produced large BMCs, as indicated by the bright mCherry foci. Each cell appears to have only a few spots of compartment localisation, and the signal intensity indicates that the BMCs may be clumped together. This suggests that the BMC shells did not form correctly and are likely to be aggregated.

Cerulean signal shows that PduV accumulated into large foci compared with the control (Figure 3.9). These foci had a high signal intensity and PduV-Cerulean filaments were barely visible. However, the filaments that are observed are similar to those in the control and indicate that PduV is still able to either polymerise to form filaments, or attach to pre-existing filaments in the cell. The Cerulean signal appeared to be more cytoplasmic than the control. The results also revealed that recombinant BMCs lacking PduK were still able to co-localise with PduV. This can be seen in Figure 3.9, where mCherry signal and Cerulean signal overlap in the composite image. This indicates that either PduK is not essential for the interaction between the Pdu shell and PduV or that the proteins have aggregated together.

3.2.3.2. BMC shell formation in BMCs lacking PduK

Live cell imaging results suggests that PduV is able to associate with Pdu BMC shells that lack PduK. However it was unclear if the resulting compartments were able to form correctly. To investigate this further, mCherry-PduABJNU BMCs were expressed in BL21 (DE3) cells. Cultures were grown at 37 °C to an OD_{600} of 0.8, induced and grown overnight at 19°C. Cell were then harvested and prepared for thin sectioning as outlined in Section 2.5.2.

A control strain, mCherryPduABJKNU, grown on the same day and in the same conditions revealed intact compartments from TEM imaging. The BMC shells were ~100 nm in diameter and identical to previous TEM images of this strain, Figure 3.10. Interestingly, cells expressing PduABJNU formed a variety of structures. Larger compartments can been seen, demonstrated by the white square in image B, ranging in diameter from 80-150 nm. Some of these structures did not appear intact as

the shell border was not entirely delimited, with gaps visible. In addition to these large malformed BMCs, strands of protein filaments could be seen wrapped around the periphery of the cell, on the cytosolic side of the cell membrane, as shown by the white arrow. This suggests that the larger mCherry foci seen in this strain by fluorescence microscopy could either be large disconnected BMCs, aggregated shell protein, or a combination of both.
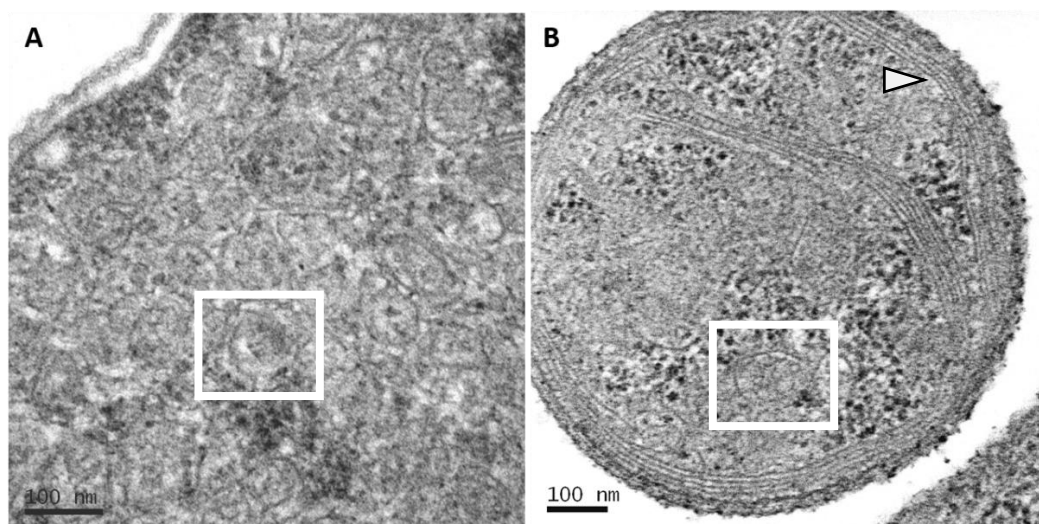
Figure 3.10. Examining the role of PduK in the formation of BMCs. TEM analysis of whole cell thin sections of cells expressing mCherry-PduABJKNU (A) or PduABJNU (B). The absnce of PduK resulted in the formation of larger, incomplete BMC shells (white square). In addition bundles of protein filaments were observed around the cytosolic side of the cell membrane.

3.2.5. Recombinant BMCs with PduK C-terminal truncation variants

PduK is known to contain a C-terminal extension of approximately 70 amino acids. The role of this extension is unknown, although it has been proposed to house an iron-sulphur centre. Like all characterised shell-proteins, PduK contains a BMC domain, located in the N-terminus of the protein. The BMC domain identifies the protein as a shell component and mediates the interaction with other shell constituents to form the structure of the compartment.

By the use of C-terminal PduK truncations, the role of this extended region can be characterised. Little is currently known about the C-terminal extension of PduK however previous studies using PduK truncations have demonstrated that the P18 targeting peptide directs protein to the BMC through an interaction with the N terminus of PduK (Lawrence et al. 2014). Although this does not

provide any clues about the function of the extended region, it does show how the use of such truncations can provide insights into the role that PduK may have in the BMC shell.

To identify any possible interaction between PduK and PduV, BMC shells containing PduK C-terminal truncations were engineered; this involved integrating the PduK truncated variants into the shell construct. Three novel constructs were generating by integrating a stop codon after amino acid residues 133,119 and 96 giving rise to the variants PduK*133, PduK*119 and PduK*96. Full length PduK is 160 amino acids in length, with the C-terminal extension spanning from 90-160 amino acids (Crowley et al. 2010).

In this study, BMCs were engineered to contain an mCherry tag, allowing compartment visualisation by fluorescent microscopy. Strains containing the BMC variants were co-produced with PduV-Cerulean to determine if the C-terminal extension of PduK has any effect on the localisation or function of PduV.

3.2.5.1. Cloning *pduK* truncations with the genes necessary for shell formation in a recombinant system

Three PduK truncations of total amino acid lengths of 133,119 and 96 were provided by Dr Andrew Lawrence. To further characterise the co-localisation between PduV and PduK, it was necessary for the *pduK* truncations to be integrated in the correct order with the other structural shell genes.

In order to do this, the following restriction digests were set up: pET3a-*PduK** with SpeI, HindIII and pET3a-*pduN* with XbaI and HindIII. Due to the compatible nature of XbaI and SpeI, when ligated together, *pduK* and *pduN* fragment ends were joined in a manner that could not be further restricted at the site of joining, it is therefore said to be 'locked'. This new pET3a-*pduK*N* plasmid was further digested with restriction enzymes SpeI, HindIII; pET3a-*pduU* was also restricted with XbaI and HindII. *pduU* was then ligated with pET3a-*pduK*N* to link and lock the genes together.

Subsequently, pET3a-*pduK*NU* was restricted with AatII, which cuts in *pduK*, and HindIII. The *pduK*NU* fragment was ligated with pLysS-mCherry-*pduABJK* that had been digested with the same

restriction enzymes. Consequently *pduK* was partially replaced with the appropriate truncated form of the gene.

3.2.5.2. Fluorescence microscopy of BMCs containing truncated variants of PduK co-expressed with PduV-Cerulean

BL21 (DE3) strains co-producing PduV-Cerulean with either BMCs with full length PduK (control strain) or with BMCs containing the truncated PduK variants were grown in 25 ml cultures from inoculation by an overnight starter culture. Initially cells were grown at 37°C to an OD_{600} of 0.6-0.8 and visualised by microscopy. This experiment was repeated twice. In addition, cells were also grown at 28 °C to assess if results were due to the rate of cell growth, although for stains containing BMC shells with C-terminal truncations, growth temperature did not affect the outcome and the results were found to be identical.

Compared with a strain expressing BMCs with full length PduK, mCherry-PduABJK*NU BMC shells appeared aggregated, as demonstrated by the larger, brighter mCherry foci, Figure 3.11. They were not distributed throughout the cell as evenly as the control strain. Visually, mCherry-PduABJK*96NU BMCs appeared to more similar to the control compartments than either mcherry-PduABJK*119NU or mCherry-PduABJK*133NU. The distribution of the shells were more spread out and the foci of mCherry signal did not appear as enlarged. In strains expressing mcherry-PduABJK*119NU and mCherry-PduABJK*133NU BMC shells, the mCherry foci were large, with fewer per cell than the other strains. In addition the foci can be seen to at the poles of the cell, indicating that the shell proteins are likely forming inclusion bodies; this suggests that the BMCs may not be folding correctly, Figure 3.11.

The presence of PduV differed in strains containing the various BMC PduK truncation variants. PduV filaments and foci were present in the control strain, Figure 3.11. PduV foci in the control strain were distributed throughout the cell, with a similar size to the BMC foci and appeared largely associated with the mCherry signal of the BMCs. PduV foci in the PduK*96 truncation variant strain

were similar to that of the control. In comparison, PduV foci in the PduK*119 and 133 BMC variants were much larger, a similar size and shape to the enlarged BMCs and often localised to the poles of the cell. Despite the enlarged BMCs and PduV-cerulean foci in some strains, PduV-Cerulean foci still co-localised with the BMCs, as is shown by the white overlap signal in the composite images of Figure 3.11.
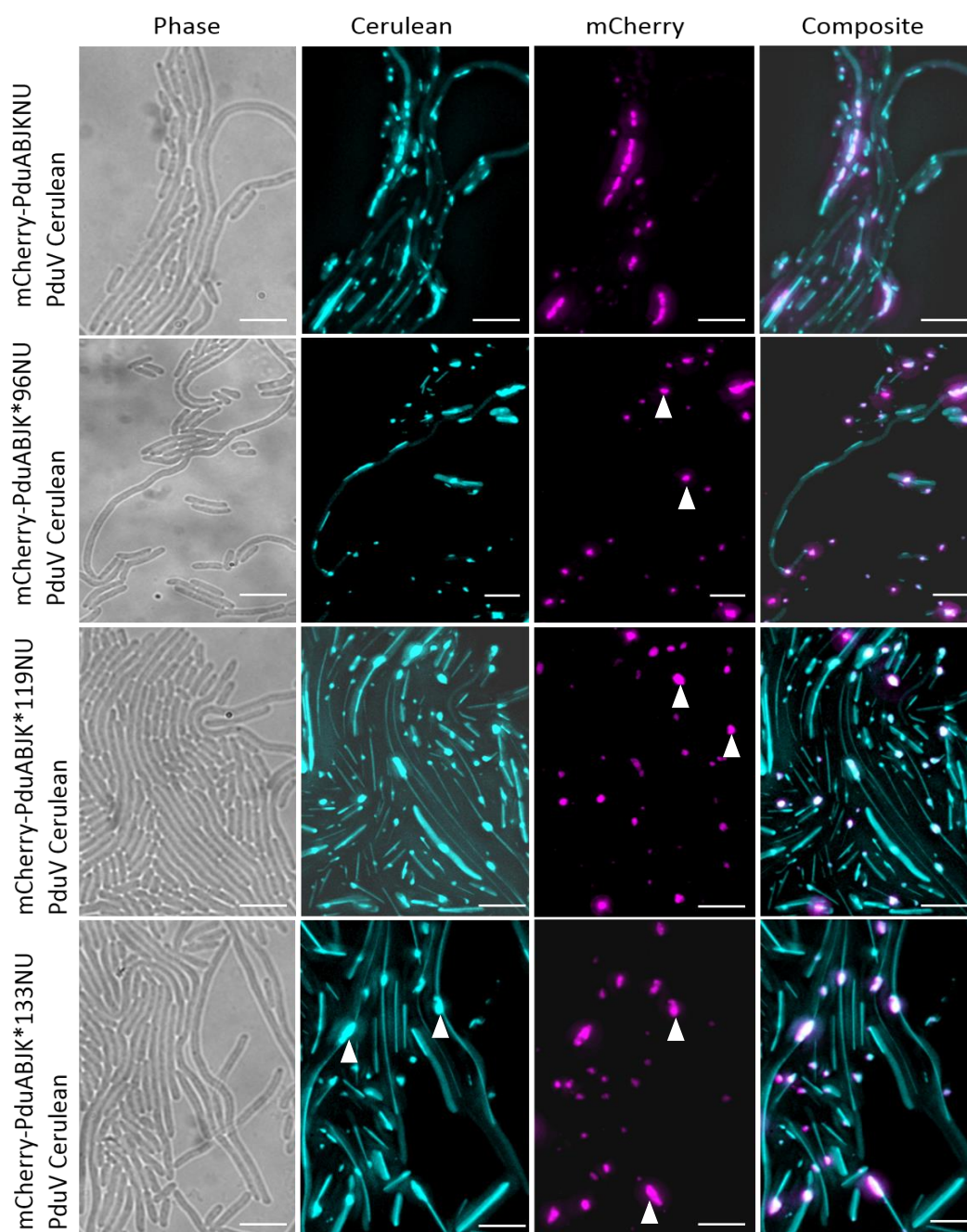
Figure 3.11. Exploring the effect of truncating PduK on the distribution of BMCs and their interaction with PduV**.** Live cell images acquired show the Phase, mCherry, Cerulean and Composite signals. The *E.coli* strains visualised include **Top Row** mCherry-PduABJKNU, **Second Row** mCherry-PduABJK*96NU, **Third row** mCherry-PduABJK*119NU and **Bottom Row** – mCherry-PduABJK*133NU, all with PduV-

Cerulean. The truncation of PduK resulted in the BMC shells aggregating into larger, brighter foci, which were not distrubted throughout the cell as evenly as in the control (white arrows), however this effect appeared more severe in cells expressing PduK*119 or PduK*133. In addition, a similar effect was ovserved with PduV, with the expression of PduK*119 or PduK133 resulting in large accumulations of PduV (white arrows). Pdu V filaments also appeared longer in these two strains. Scale Bar: 5 μm

Unexpectedly, PduV-associated filaments appeared to vary in length. The control and also mCherry-PduABJK*96NU strains contained both shorter filaments and longer ones. However, strains with the PduK truncated variants, mCherryPduABJK*119NU and mCherryPduABJK*133NU, contained filaments that seemed considerably longer (Figure 3.11). To evaluate this difference, images were analysed in MetaMorph in order to measure accurately and compare the filament length for each strain.

3.2.5.3. Filament length analysis

BL21 (DE3) strains co-expressing PduV-Cerulean with A) mCherry-PduABJKNU (full length PduK as a control sample), B) mCherry-PduABJK*96NU, C) mCherry-PduABJK*119NU and D) mCherry-PduABJK*133NU were grown for microscopy. Starter cultures were set up from one colony of a double transformation plate and grown as outlined in Section 2.2.2.2. Subsequent cultures (25 mL) were set up and grown at both 37°C and 28 °C to an OD_{600} of between 0.4 and 0.6. Results shown are of the analysis of images from *E.coli* growth at 37°C from >200 cells.

Cells were mounted on an agarose pad, and visualised by live cell imaging outlined in Section 2.5.1. Images were then processed in MetaMorph software to calibrate distance per pixel and allow the accurate measurement of filament length. Data for filament length was collected in Microsoft Excel and grouped to be able to plot a histogram. OriginLab was subsequently used to plot the data to a LogNormal fit.

Results show that when fitted to a LogNormal distribution, the peak PduV-Cerulean-associated filament length with BMCs containing full-length PduK is 2.365 μm. The histogram demonstrates that filament length ranges from approximately 0.5 μm to 14 μm. The shape of the histogram for PduV-Cerulean-associated filaments with a PduK*96 BMC variant is very similar to the control, as is the range of filament length. The peak length for PduK*96 is also very similar to full length PduK, at 2.429 μm, a difference that does not appear to be significant, (Figure 3.12).

Peak filament lengths with BMCs containing PduK*119 and 133 variants were higher than both the control and PduK*96 BMC strains, at 3.519 and 4.341 μm respectively. This amounts to filament length increases from the control sample of 48.8 and 83.6% for PduK*119 and 133 strains respectively. This shows that filament length is nearly 1.5 x and 2 x longer in these strains compared to the control. The shape of the LogNormal distribution also differs with these samples compared to PduK*96 and the control. The fit had a shoulder on the right of the distribution curve, indicating that a higher number of filaments were longer in length. This is also shown by the range of filament length which is as high as 22 μm for PduK*133 BMCs. T-Testing was also carried out which showed that the difference in filament length between cells expressing PduK*96 and the control cells was not statistically significant, whilst the difference in filament length between cells expressing PduK*119 or PduK*133 and the control cells was statistically significant, (Table 3.1). Raw data can be found in Appendix 1.
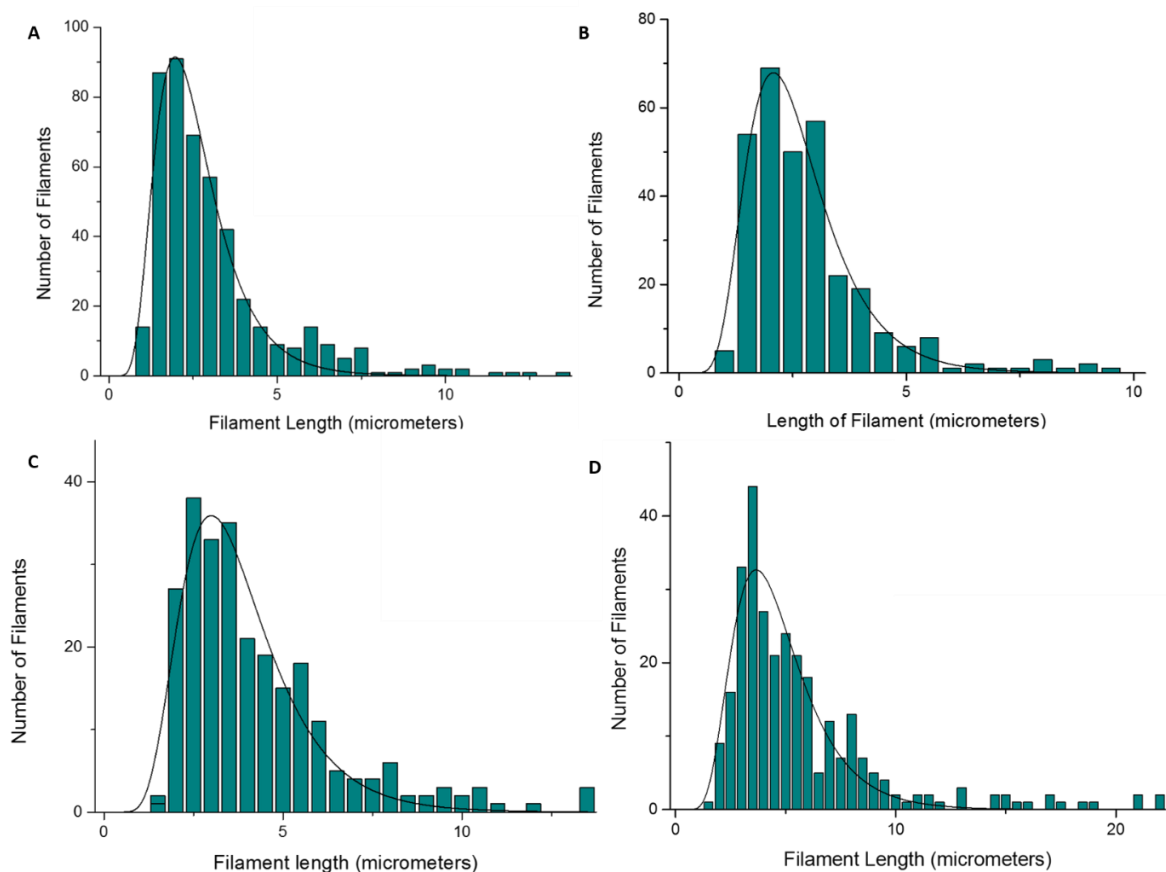
Figure 3.12. Exploring the effect of truncating PduK on the length of PduV filaments. Graphs showing the distribution of PduV filaments lengths in cells expressing (A) mCherry-PduABJKNU, (B) mCherry-PduABJK*96NU, (C) mCherry-PduABJK*119NU   and (D) mCherry-PduABJK*133NU. PduV-Cerulean filaments were on average longer when shells containing PduK*119 or PduK*133 were expressed. There was also a much larger range of filament lengths in cells expressing PduK*133.

BMC Variant	Peak Filament Length	T-Test
Length of PduK (amino acids)	(µm)	
A) Full length PduK (160)	2.365 ± 0.05	
B) PduK*96 (96)	2.429 ± 0.06	0.137976361
C) PduK*119 (119)	3.519 ± 0.10	9.92263×10^{-13}
D) PduK*133 (133)	4.341 ± 0.12	3.08972×10^{-21}

Table 3.1. Exploring the effect of truncating PduK on the length of PduV filaments. Table showing the peak length of PduV filaments lengths in cells expressing (A) mCherry-PduABJKNU, (B) mCherry-PduABJK*96NU, (C) mCherry-PduABJK*119NU and (D) mCherry-PduABJK*133NU and T-Test results to analyse the significance of the difference from the control sample. PduV-Cerulean filaments were on

average longer when shells containing PduK*119 or PduK*133 were expressed and T-Testing showed the difference to from the control strain to be statistically significant.

Overall the variability of PduV-associated filament length suggests that the C-terminus of PduK may interact with PduV. BMCs with PduK C-terminal truncations appear to be related to the increase of PduV-Cerulean-associated filament length. The length of filaments are similar with full-length PduK BMCs and a PduK truncated variant of 96 amino acids (total length). This is surprising as longer length PduK truncated variants, PduK*119 and PduK*133 are associated with longer filaments, even though a higher proportion of the protein remains.

3.2.5.4. TEM analysis to determine if truncated PduK BMC variants form intact compartments

Fluorescence live cell microscopy images revealed that BMCs containing PduK truncations did not appear to form correctly. Compared to the control strain, which contained BMC shells with full-length PduK, the truncated variants appeared aggregated, with larger mCherry foci that localised to the cell poles rather than distributed throughout the cell (Figure 3.11). To explore the formation of Pdu compartment shells containing truncated PduK, BL21 (DE3) strains were grown and prepared for TEM thin sectioning as outlined in Section 2.5.2. These strains expressed only the BMCs containing either full length PduK, mCherry-PduABJKNU (control strain) or truncated PduK variants; mCherry-PduABJK*96NU, mCherry-PduABJK*119NU or mCherry-PduABJK*133NU. None of the strains co-expressed PduV-Cerulean. Cell sections were then stained and visualised by electron microscopy, as described in Section 2.5.2.2.

TEM images revealed that the control strain, expressing Pdu BMC shells with full length PduK formed complete, intact structures ranging from ~80-100 nm in diameter. These compartments were identical to the Pdu BMCs visualised previously in Section 3.2.4. In comparison, BMCs containing truncated PduK varied in size and shape and tended to form shells that were not completely intact. mCherry-PduABJK*96NU BMCs were much larger than that of the control (Figure

3.13), ranging from ~100-200 nm in diameter. The majority of these shells appeared to be broken, containing an opening where the two ends of the shell failed to meet, this is shown by the white arrows in Figure 3.13 (B). mCherry-PduABJK*119NU shells appeared malformed, with several layers of shell protein wrapped around, in a spiral-like structure, where the BMC was unable to close. The size of the shells varied from ~80-150 nm with the vast majority of the shells remaining fractured. Similarly, mCherry-PduABJK*133NU BMCs appear completely malformed. Shell protein strands can be seen to form spiral structures that fail to close to form completed compartments. These structures are ~80-200 nm in diameter and do not have a consistent or defined shape.

Overall TEM results show that BMCs containing truncated PduK variants form broken, malformed structures that tend to be larger than control Pdu shells. Interestingly, despite the increase in size, compartments formed with the PduK*96 truncation are most similar to the control in shape and structure. In comparison the other BMC variants form incomplete, spiralled structures that mostly fail to close.
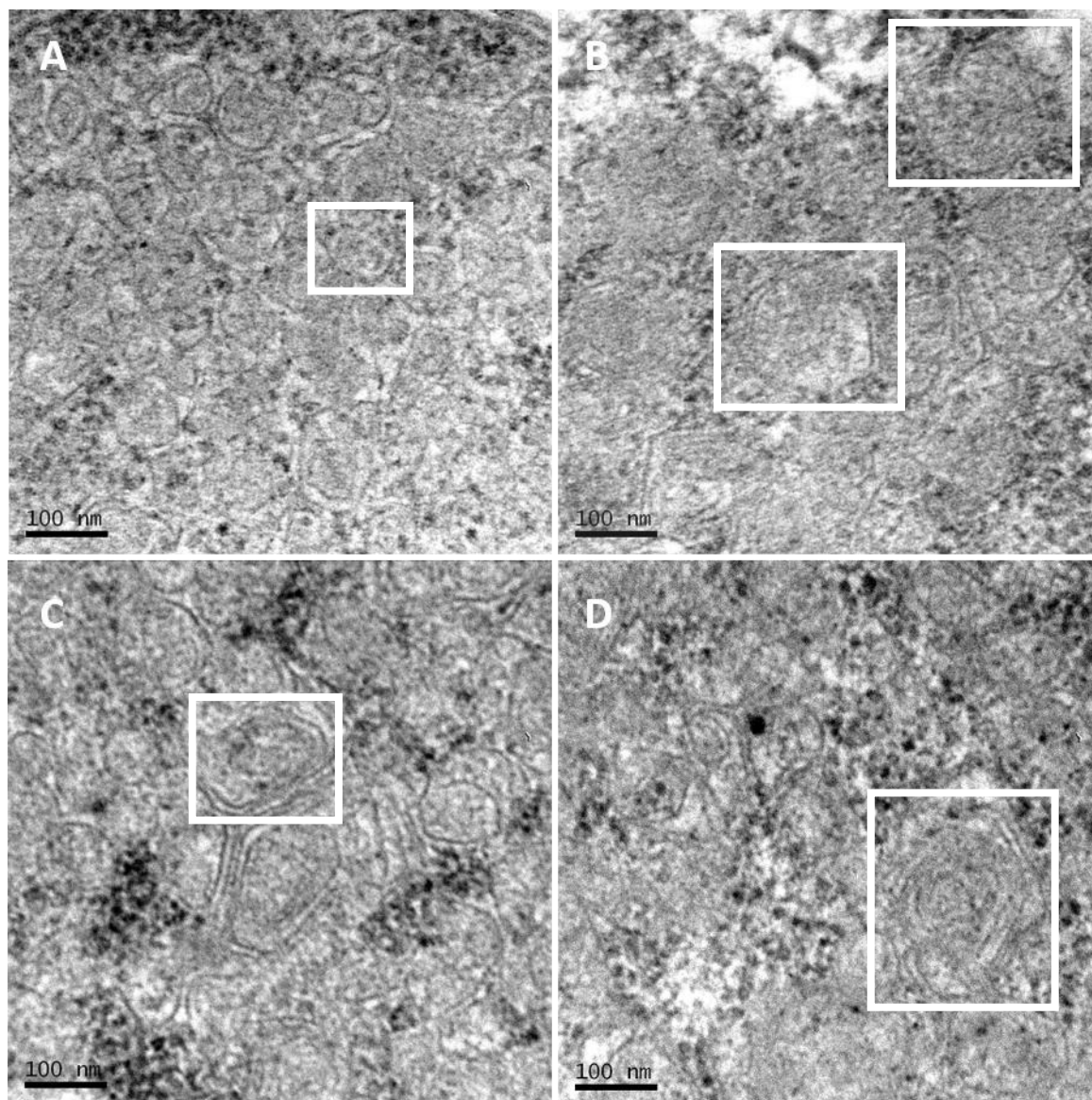
Figure 3.13. Examining the effect of truncating PduK on BMC formation. TEM analysis of whole cell thin sections of cells expressing (A) mCherry-PduABJKNU, (B) mCherry-PduABJK*96NU, (C) mCherry-PduABJK*119NU and (D) mCherry-PduABJK*133NU. BMCs containing truncated PduK varied in size and shape and tended to form shells that were not completely intact. The expression of truncated PduK variants resulted in much larger BMC shells being formed. In the case of PduK*96 the majority of the shells appeared to be broken, containing an opening where the two ends of the shell failed to meet, as seen in cells highlighted by white squares. The sells varied in size from 100-200 nm. PduK*119 shells appeared malformed, with several layers of shell protein wrapped around, in a spiral-like structure, where the BMC was unable to close (white square). The size of the shells varied from ~80-150 nm with the vast majority of the shells remaining fractured. Similarly, mCherry-PduK*133 shells appear completely malformed. Shell protein strands can be seen to form spiral structures that fail to close to form completed compartments (white square). These structures are ~80-200 nm in diameter and do not have a consistent or defined shape.

3.3. Discussion

The aim of the research described in this chapter was to develop the tools and reagents that were required to be able to monitor physiological *in vivo* interactions between PduK and PduV. Does PduV specifically interact with one region of PduK to allow the region-specific localisation of BMCs within the bacterial cell? In aiming to address this key fundamental question a large array of plasmids has to be constructed to reflect the various permutations and combinations of shell proteins to allow this interaction to be probed fully. In so doing a number of further essential discoveries were made about the requirements for BMC function.

Key to the success of being able to draw meaningful conclusions form this research is the ability to detect BMCs by either live cell imaging or by TEM of sectioned cells. There is a clear requirement for PduK within the normal formation of BMCs. The absence of this protein gives rise to aberrant structures that are not fully formed. More surprising is the observation that PduK has to be present in the natural order of shell-encoding proteins for the BMC to take shape correctly. Previous work has shown that the reversal of the full set of genes for empty shell synthesis resulted in the formation of aberrant structures similar to those observed in the absence of PduA (Parsons et al. 2010). However it was thought this affect was mainly due to the importance of PduA in shell formation, making contacts with the other shell proteins. However the finding that the translocation of just one shell protein gene to the end of the operon suggests that the protein, as it is being made has to interact under the appropriate conditions with the correct shell proteins to allow completion of the structure. More recently it has been shown that the position of *PduJ* within the operon directly affects its function (Chowdhury et al. 2016). Such an "ordered" synthesis may underline some of the higher order quaternary structure organisation of this remarkable macromolecular complex.

From bio-informatics we know that PduK represents a BMC-shell protein domain of about 110 amino acids that is tethered to an "unknown" C-terminal extension. The natural thought would be

that the C-terminal region would be associated with biding either internalized protein cargo, binding external facing proteins (such as PduV) or the uptake/control of external substrates. The N-terminal region would therefore be involved in forming the structural hexameric tile that forms a key component of the facet of the overall structure. It was surprising therefore to discover that none of the C-terminal truncations of PduK were able to replace PduK within the minimal shell-gene repertoire for empty BMC formation (*pduABJKN)*. Moreover the truncated variants revealed structures, upon thin sectioning, suggesting that the BMC was unable to close properly. The presence of these "open" BMCs suggests that PduK actually has an important role to play in closing the structure, perhaps by generating a bend or fold along one of the edges of the BMS, in a similar way to the envisaged role for PduU. This finding has the potential to signiciantly change the way in which the structure of Pdu proteins is interpreted as it had previopusly been thought that it was the BMC-shell protein domain that was key for the structural role of Pdu proteins. Now we can see that other regions within the protein can also bekey to them carrying out their structural roles.

Although the research was successful in generating the required variety of tools and reagents for this study, the research was ultimately unsuccessful in attaining its original goal of detecting specific PduV-PduK interactions. This was caused by the fact that addition of either N- or C- extensions to PduK resulted in forms of PduK that could not replace wild type PduK. Any tagged form of PduK was found to prevent proper formation of BMCs and thus would not reflect the normal situation. Such an effect could not have been predicted from the outset of this research, especially given the observation that wild type BMCs are easily observed with a tagged version of the more abundant PduA. However as will be seen in subsequent chapters, many shell proteins are sensitive to modification.

Chapter 4: Effect of mCherry fusions on BMC formation and the interaction with PduV

4.1. Introduction

The function of the bacterial microcompartment is completely dependent on its outer shell. *Salmonella enterica* expressing mutant Pdu shell proteins which prevent proper formation of the Pdu compartment shell, were found to accumulate propionaldehyde to levels that induced 20-30 hours of growth arrest and resulted in DNA damage (Cheng et al. 2011). This highlights the importance of the shell to the role of the BMC in sequestering toxic intermediates. Although it is evident that BMC shell mutants, lacking any one of the essential genes, *pduA,B,J,K or N* were unable to form intact, delineated compartments, the exact roles of these shell proteins are largely unknown (Cheng et al. 2011). Studies have provided insights into roles that these proteins may have in the formation of the organelle, or specific roles in protein localisation, see section 1.4.7 (Lawrence et al. 2014; Wheatley et al. 2013; Havemann, Sampson & Bobik 2002; Sargent, F. A. Davidson, et al. 2013).

The formation of the Pdu shell remains largely elusive, although it is beleived that the shell undergoes a self-assembly process. Recombinant empty BMCs, consisting of PduABJKNU(T) expressed in *E.coli* are able to form in the absence of any other Pdu proteins (Parsons et al. 2008). This differs from the carboxysome assembly process which involves the simultaneous aggregation of cargo (RuBisCo) which is subsequently encapsulated by the shell proteins. Therefore despite structural and functional similarities it appears the process of shell formation differs greatly between the two, with the carboxysomes dependence of the presence of it's cargo not being replicated in the case of the Pdu Microcopmartment. Although little is understood about this formation process of the Pdu shell, the proteins that form it have been investigated.

As previously described, in section 1.4.7, PduA, PduBB' and PduJ are the most abundant proteins found within fully formed BMCs, with PduK, PduN, PduT and PduU constituting a smaller proportion of the shell (Havemann & Bobik 2003). Altering the expression levels of any of the shell proteins, including those that are major and even minor components of the compartment, can cause the

BMC to misfold, forming unusual, broken structures (Parsons et al. 2008). This is integral to the function of the BMC, as the shell not only allows substrates, cofactors, coenzymes and products to enter or exit the organelle, it also acts to confine intermediates within the lumen to increase the efficiency of reactions and prevent toxicity to the cell. Therefore, understanding the role of each of these proteins, how they interact with other components to assemble the compartment structure and how they are distributed in the cell, especially during cell division, is important for their use as metabolosomes for specific pathways.

Previous research have investigated the effect of tagging various shell proteins with fluorophores. An N-terminal PduA fusion expressed with the other genes necessary for recombinant empty BMC shell formation, mCherry-PduA-BJKNU, results in the formation of intact shell structures and BMC formation with this modified version of PduA was not impaired (Parsons et al. 2010). In addition a C-terminal GFP fusion with PduN was able to rescue the formation of intact BMCs when co-expressed with PduABJKU, suggesting that PduN-GFP does not hinder the integration of PduN in the shell. Conversely, an N-terminal GFP fusion did not rescue the formation of BMCs suggesting that PduN function was impaired (Parsons et al. 2010). Similarly, results shown in chapter 3 of this thesis have shown that when PduK was tagged on either the N or C terminus, compartments were no longer able to form, as described in section 3.2.2.2. Aside from PduA, PduN, and now PduK, no other Pdu shell proteins have been tagged with fluorophores or analysed by fluorescence microscopy.

In order to provide insights into each of the shell components, proteins were tagged on the N- and C- termini with mCherry, creating two separate constructs in each case, with the exception of PduK which does not form intact BMC shells when tagged. These tags were integrated into the gene order from the *C. freundii* operon and expressed in *E. coli*. The expression and formation of compartments in each case aimed to give structural information on how the shell component is integrated into the compartment – if tagging either end of the protein disrupts the formation of the shell clues could

be provided into the importance of the terminus in the interaction with other components to assemble the compartment structure. Limited experiments were carried out with PduABJ**K-mCherry**-N-U as studies had shown that this fusion tag is non-functional.

This study also aims to investigate the interaction between shell proteins and PduV-Cerulean through live-cell imaging. By tagging each shell protein with mCherry, the localisation between red and blue signal can be visualised and consequently, interactions between each shell component and PduV can be investigated.

4.2. Results

4.2.1. Cloning of individual fluorescently tagged shell proteins

Genes encoding shell proteins were tagged with mCherry. This involved production of nine novel

constructs (numbers 2-10), listed in Table 4.1 below.

Construct ID	Shell protein tag	Completed construct
1	mCherry-PduA	pLysS-**mCherry-PduA**-BJKNU *
2	PduA-mCherry	pET3a-Pdu-**A-mCherry**-BJKNU
3	mCherry-PduB	pLysS-PduA-**mCherry-**B-JKNU
4	PduB-mCherry	pLysS-PduA-**B-mCherry**-JKNU
5	mCherry-PduJ	pET3a-PduAB-**mCherry-J**-KNU
6	PduJ-mCherry	pET3a-PduAB-**J-mCherry**-KNU
7	mCherry-PduN	pET3a-PduABJK-**mCherry-N**-U
8	PduN mCherry	pET3a-PduABJK-**N-mCherry**-U
9	mCherry-PduU	pET3a-PduABJKN-**mCherry-U**
10	PduU-mCherry	pET3a-PduABJKN-**U-mCherry**

Table 4.1. Engineered constructs that encode BMCs containing a mCherry-tagged shell protein.

* This construct has been shown to form intact BMCs when expressed and has therefore been used as a

control in this study.

Initially *mCherry* was amplified by PCR from *pLysS-mCherry-PduABJKNU* with the addition of the

following restriction sites: N-terminal - 5' AseI, 3' NdeI, SpeI and C-terminal – 5' NdeI, SacI 3' SpeI .

The presence of the extra restriction sites is to allow gene insertion between NdeI and SpeI for the

N-terminal *mCherry* tag and between NdeI and SacI for the C-terminal *mCherry* tag. After restriction

digestion (AseI, SpeI for N-terminal *mCherry* and NdeI, SpeI for C-terminal *mCherry*) to remove extra

bases and create the 5' and 3' overhangs, the *mCherry* N and C terminal PCR fragments were ligated

into *pET3a*, which had been restricted with NdeI and SpeI. Ligation of the N-terminal *mCherry*

fragment with pET3a ultimately destroys the 5' restriction site by the joining of the cohesive ends of AseI and NdeI. This allows the insertion of genes that encode shell proteins between the NdeI and SpeI sites behind *mCherry*. Once ligated with pET3a, both N- and C- terminal tags were sequenced to ensure that no mutations had been introduced.

Each of the genes encoding the shell proteins; PduA, PduBB', PduJ, PduK, PduN and PduU were subcloned from *pET3a*. The genes had been originally cloned after PCR from *C. freundii* by Dr Josh Parsons with the restriction sites 5' NdeI and 3' SpeI. These *pET3a-pdu* constructs were restricted with NdeI and SpeI, to cut out the *pdu* gene which was subsequently ligated with the compatible NdeI and SpeI ends of the *pET3a-mCherry* fragment. This created *pET3a-mCherry-pdu** constructs where the asterisk represents the gene for the shell constituent.

Genes encoding Pdu shell proteins to be ligated at the C-terminus of *mCherry* were amplified by PCR from the corresponding pET3a-pdu* construct as a template, with the addition of a 3' SacI restriction site instead of SpeI at the end of the gene. The 5' NdeI site remained the same. The primers used are listed in Table 2.3. PCR fragments, restricted with NdeI and SacI were ligated into the C-terminal *mCherry* construct; *pET3a-mCherry,* which had also been restriction digested with the same enzymes, to create the plasmid, *pET3a-pdu*-mCherry*. The mCherry and Pdu fusions tags were then cloned with the other genes necessary for recombinant shell formation. The Link and Lock method of cloning was used to subclone genes into the same plasmid, see Section 2.3.7.1.

4.2.1.1. PduA
An N-terminal PduA mCherry tag, *pLysS-PduAmCherry-BJKNU*, engineered by Dr Josh Parsons, was used in this study, see Table 2.2.

The C-terminal PduA tag was engineered as above, to create a *pET3a-pduA mCherry* construct. Subsequently, *pduB* was subcloned from *pET3a* by restriction with XbaI and HindIII. *pET3a-mCherry-pduA* was also restriction digested with SpeI and XbaI and the fragments were ligated. Due to the

compatible cohesive ends of XbaI and SpeI, these sites can join to create the construct *pET3a-pduA-mCherry-PduB* by the Link and Lock method.

pduB contains the restriction site AscI, which is only present in that gene once and is not present in *pET3a*. By the restriction digest of AscI and HindIII sites of both *pET3a-pduA-mCherry-PduB* and *pET3a-mCherry-pduABJKNU,* the plasmids can be cut in the middle of *pduB* allowing the rest of the Pdu shell-encoding genes to be cloned behind it. This forms the shell protein construct: *pET3a-pduA-mCherry-PduBJKNU.*

4.2.1.2. PduB

A C-terminal PduB-mCherry tag was constructed as described in Section 4.2.1. *pduB-mCherry* was subcloned with *plysS-pduA* by the Link and Lock method to produce the construct; *pLysS-pduAB-mCherry*. To subclone the shell constituents *pduJKNU* at the end of the construct, firstly, *pduJ* had to be added to the plasmid. To do this, *pduJ* was cloned at the end of the construct by Link and Lock using XbaI and SpeI as well as HindII. A restriction site StuI, unique to *pduJ* in both constructs; *pLysS-mCherry-PduABJKNU* and *pLysS-pduAB-mCherry-pduJ* was used, along with HindIII, to cut in the middle of *pduJ* and introduce the remaining shell genes to engineer the construct: *pLysS pduAB-mCherry-JKNU*.

 The N-terminal PduB tag was created as described in Section 4.2.1 *mCherry-pduB* was subcloned with *pLysS-pduA* by the Link and Lock method. Subsequently *pLysS-pduA-mCherry-pduB* was restriction digested with AscI, which cuts the plasmid once within PduB as well as HindIII. *pLysS-mCherry-PduABJKNU* was restricted with the same enzymes and the fragments were ligated to form the completed construct: *pLysS-pduA-mCherry-pduB-JKNU*.

4.2.1.3. PduJ

pET3a-mCherry-pduJ was engineered as described in Section 4.2.1 *mCherry-pduJ* was subcloned by the Link and Lock method, with *pET3a-pduAB* (Table 2.2). *pET3a-pduAB-mCherry-pduJ* and *pLysS-*

mCherry-PduABJKNU were then restricted with StuI and HindIII and ligated to construct the plasmid: *pET3a-pduAB-mCherry-J-KNU*.

To engineer *pET3a-pduAB-J-mCherry-KNU*, pduJ-mCherry was subcloned with *pET3a-PduAB* by the Link and Lock method. Each consecutive gene was then cloned after the last by Link and Lock from *pET3a* plasmids containing each gene, as described in Table 2.2. The Link and Lock method is described in Section 2.3.7.1.

4.2.1.4. PduN

pET3a-mCherry-pduN and *pET3a-pduN-mCherry* were cloned as described in Section 4.2.1. The *pduN* tags were restricted using XbaI and HindIII and subsequently ligated with *pET3a-pduABJK* which had been restriction digested with SpeI and HindIII (Link and Lock method, Section 2.3.7.1). For both engineered constructs, *pduU* was subcloned by the Link and Lock method resulting in: *pET3a-pduABJK-mCherry-N-U* and *pET3a-pdu-ABJK-N-mCherry-U*.

4.2.1.5. PduU

As with all shell protein fusions, *pET3a-mCherry-pduU* and *pET3a-pduU-mCherry* were cloned as described in Section 4.2.1. The fusion tags were subcloned by a restriction digest with XbaI and HindIII and then ligation with *pET3a-pduABJKN*, which had been restricted with SpeI and HindIII (Link and Lock method). This resulted in the following constructs: *pET3a-PduABJKN-mCherry-U* and *pET3a-PduABJKN-U-mCherry*.

4.2.2. Optimisation of protein production

This investigation aimed to analyse the protein content of strains expressing the genes for the BMC tagged-shell protein variants by SDS PAGE and Western Blot analysis. However, growth of each strain under identical growth conditions revealed that protein production may differ depending on the plasmid used to engineer the BMC constructs. The colour of the cells within the various cultures appeared to vary depending on the plasmid used; *pLysS* or *pET3a*.

4.2.2.1. Effect of plasmids on protein production

When strains containing each construct were grown for expression studies, the colour of cells were observed. The production of fluorescent proteins is known to cause the colour of cells to change, depending on the properties of the fluorophore. For example, when cells expressing Ypet-tagged PduK were grown for live cell imaging, Section 3.2.2.2, the cell pellet had a dark yellow appearance. In this case, cells expressing mCherry were expected to have a magenta colouration, however only certain strains seemed to generate the expected appearance.

Cultures of BL21(DE3) cells (200 mL) containing each of the tagged-BMCs listed in Figure 4.1 (C) were grown at 37°C. This experiment was initially carried out to investigate the protein content of purified BMCs containing tagged-shell proteins. The cultures were inoculated from an overnight starter culture to an OD_{600} of 0.05. The starter cultures were in turn inoculated with ~4 colonies from a fresh transformation plate. The 200 mL cultures were induced with IPTG when an OD_{600} of 0.8 was reached and the cultures were transferred to a shaking platform at 19°C overnight.

The following day, the colour of the cultures were observed; 2 mLs of culture were transferred to a 2 mL Eppendorf and an image was taken, Figure 4.1 (A).
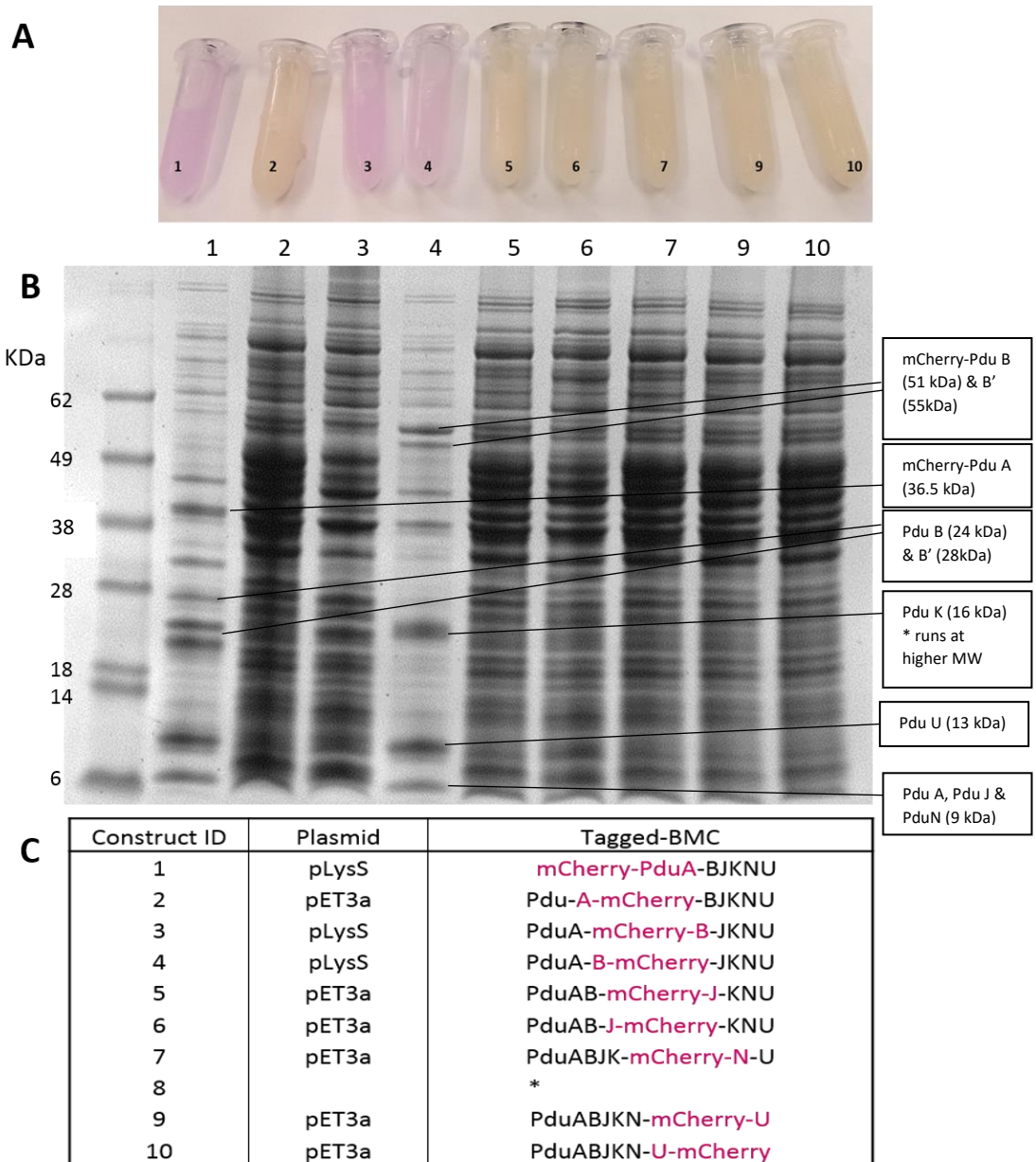
Figure 4.1. The colour of cells expressing constructs from either pET3a or pLysS compared to the observed protein profile. Cell samples were taken from a culture grown at 19 °C overnight after induction for the imaging of cell colouration. Cells from the cultures were then pelleted, resuspended in Ypet solution and incubated for 3 hours. Samples of the cell lysate were then taken for SDS PAGE analysis A) The difference in the colour of cells expressing each construct was imaged. Cells expressing mCherry-tagged BMC variants from a pLysS plasmid (constructs 1,3 and 4) appear magenta compared to cells expressing tagged-BMCs from pET3A. B) 15% SDS PAGE of cell lysates after exposure to Yper detergent C) Table displaying each of the corresponding construct ID numbers from A and B, note Construct 8 is

not present in either A or B as it was cloned at the end of the study for a complete data set. Previous studies had already identified that tagging PduN on the C terminus was unsuccessful, see Section 4.1.

Interestingly only three of the nine samples were magenta and these three strains contained a *pLysS* construct with the others involving shell genes cloned with *pET3a*. Even though the colouration of cells differed when mCherry-tagged shell proteins were expressed from the two varying plasmids, earlier studies in Section 4.2.2.2 showed that all of the mCherry-tagged proteins were still produced from both plasmids. However the effect of the two different plasmids on the amount of protein expressed, causing a change in cell colour, was unclear.

The cells were pelleted and exposed to a protein extraction reagent solution for 3 hours as described in the BMC purification method, outlined in Section 2.2.7.2 Samples were then taken for SDS PAGE analysis after treatment with YPer; 1 mL of cells were spun down and resuspended in 50 μL of 1 X PBS buffer and then prepared for SDS according to Section 2.1.7.4.

Figure 4.1 (B) shows that shell proteins were a lot more visible in lanes 1, and 4 and slightly clearer in lane 3 compared to the other lanes which appeared to contain many more proteins. These lanes contained cell lysates of proteins expressed from *pLysS* constructs. The band pattern for constructs: 2, 5, 6, 7, 9 and 10, all cloned into *pET3a*, appeared identical. Although all lanes contained samples of a crude cell lysate, the band pattern of *pET3a* constructs were very different to that observed in Figure 4.3. This could be due to several factors such as protein extraction treatment or growth conditions due to a larger culture. Nevertheless, the results demonstrate that the production of shell proteins was higher, with less background protein production by *pLysS* constructs compared with *pET3a*.

To ensure that the results are comparable, it was necessary to maintain consistency between constructs and minimise differences in expression patterns because of the plasmid used. Differences in expression due to the design of the constructs were not anticipated due to the same

promotor, T7, being present in both plasmids. To explore the difference in cell colouration, *pET3a-pdu-A-mCherry-BJKNU* was re-cloned into a *pLysS* vector. This involved restriction of sequenced *pET3a-pduA-mCherry* construct with XbaI and HindIII and the subsequent ligation with *pLysS-pduU* which had been restricted with the same enzymes, removing the gene already cloned in the plasmid. The succeeding gene encoding PduB was then cloned after the fusion by Link and Lock, see Section 2.3.7.1. *pLysS-pdu-A-mCherry-B* and *pET3a-pdu-A-mCherry-BJKNU* were restriction digested with AscI and HindIII to cut in the middle of *pduB* and replace the fragment with the rest of the shell genes, forming *pLysS-pdu-A-mCherry-BJKNU*.

Three BL21(DE3) strains containing the constructs: *pLysS-mCherry-PduA-BJKNU*, *pLysS-pdu-A-mCherry-BJKNU* and *pET3a-pdu-A-mCherry-BJKNU* were grown in 25 mL cultures at 37°C to an OD_{600} of ~0.6. Cells were then induced with IPTG and grown at 19 °C for 2 hours as described in Section 2.2.5. A 1 mL cell culture sample was taken for each strain, cells were centrifuged at 4000 rpm for 1 min and resuspended in 50 µL of 1 X PBS buffer. The samples were then denatured as outlined in Section 2.1.7.4 and run on a 15% SDS gel, as shown in Figure 4.2.
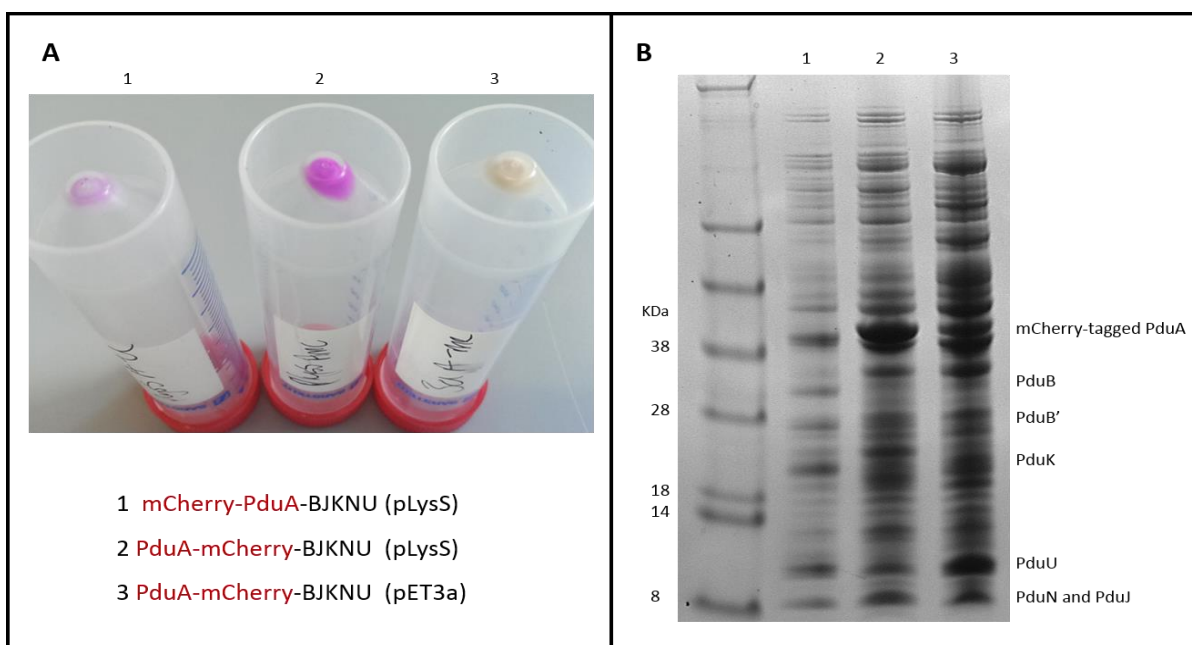
Figure 4.2. Comparison of cells expressing BMCs with a C-terminal mCherry-tagged PduA cloned with pLysS or pET3a. Expected molecular weights of the Pdu proteins expressed had previously been identified (Parsons et al. 2010). A) Cell pellets from a 25 mL cell culture demonstrate the colour of cells

expressing an mCherry-tag. Interestingly cells expressing mCherry-PduA-BJKNU and PduA-mCherry-BJKNU cloned with pLysS were magenta compared to cells expressing PduA-mCherry-BJKNU from a pET3a plasmid. B) 15% SDS PAGE gel of cell samples taken from the corresponding cell pellets in image A.

Figure 4.2 (A) shows that tagged-BMCs expressed from a *pLysS* plasmid are associated with a magenta colouration of cells. In comparison, the same genes expressed from a *pET3a* vector did not cause cells to become coloured. This is consistent with previous results that showed strains expressing *pLysS* constructs were magenta compared to strains expressing genes from *pET3a*, Figure 4.1. SDS PAGE, image B Figure 4.1, revealed that shell proteins were visible in the control strain expressing *pLysS-mCherry-PduA-BJKNU*. Bands appeared darker, indicating a higher protein concentration, in lanes 2 and 3 for PduA-mCherry BMCs, however this could be due to differences in cell density of the cultures. In addition, lanes 2 and 3 appear to contain many more bands.

The results of the SDS gel analysis are largely inconclusive; the expression of shell proteins when bacterial cells are examined by SDS are not clearer depending on plasmid. Lanes 2 and 3 representing *pLysS-pduA-mCherry-BJKNU* and *pET3a-PduA-mCherry-BJKNU* appeared to have many contaminating bands making individual shell proteins difficult to determine, but again this could be due to the higher density of the cell culture. This result differs from that of previous expression studies in Section 4.2.2.2 and may be due to overloading of protein on the gel. The band pattern is identical in both gels, and darker bands corresponding to those visualised previously in Figure 4.1 can still be seen.

Overall it is clear that bacterial strains containing BMC genes cloned with pLysS appear magenta in colour when cultured. This differs from strains containing BMC variants expressed from a pET3a plasmid which appear normal in colour. It was difficult to draw definitive conclusions on how the plasmid affected BMC protein expression when alalysis protein content by SDS-PAGE when whole cell lysates were analysed due to the amount of protein bands visualised by SDS.

4.2.2.2. Protein expression after induction

Results have shown that the plasmid used may affect the expression of protein, causing colouration in cell cultures. To investigate further protein expression of each strain, cells were cultured and samples taken at specific time-points after induction. The protein content of the cells were analysed by SDS PAGE and Western Blots to determine if firstly, all shell proteins were visible when induced, and secondly, if protein expression increased over time.

BL21(DE3) competent cells were transformed with the completed constructs listed in Table 4.1. Several colonies from the same transformation plate were used to inoculate a 5 ml starter culture. The starter culture was grown overnight as described in Section 2.2.2.2. A larger LB culture (250 mL) was inoculated with the starter culture (1:100 dilution) and grown at 37 °C until an OD_{600} of 0.8 was reached. The cultures were then induced with IPTG, as outlined in Section 2.2.5, and grown at 19°C overnight.

After induction with IPTG, 1 mL of cell culture was taken for SDS PAGE and Western Blot analysis at varying time-points: straight after induction (0 hours), 1 hour after induction, 2 hours after induction and overnight. An OD_{600} of the cultures were taken and then the cells were harvested by centrifugation at 4000 rpm for 1 min. Each cell sample was diluted by addition of 1 x PBS according to the OD_{600} to ensure that each cell sample was the same density allowing for any change in protein production after induction to be visualised. Samples were run on pre-cast SDS gels, as described in Section 2.1.7.4 and were also analysed by Western Blotting as described in Section 2.1.7.5, using anti-mCherry to identify the tagged shell protein. The SDS-PAGE gels and western blots were produced using cell samples taken at the same times on the same days to ensure consistency. The corresponding molecular mass of tagged shell proteins are listed in Table 4.2 below.

	Molecular mass, KDa	
	Untagged Shell Protein	mCherry-Tagged Shell protein
PduA	9.5	36.5
PduB	24	51
PduB'	28	55
PduJ	9	36
PduK	16 *	43
PduN	9	36
PduU	13	40

Table 4.2. The molecular weights of untagged shell protein compared with mCherry-tagged shell proteins.

* PduK usually runs at ~20KDa on an SDS PAGE gel

Figure 4.3 shows SDS gels and Western blots from cells expressing BMCs containing a mCherry shell protein fusion. Each lane consists of whole cell extracts from strains expressing the BMC mCherry-tagged variants. Empty BMC shells containing PduA with an N-terminal mCherry tag, (Image A) appeared to show an increase in protein production which can be seen from lanes 0-O/N with bands for the shell proteins visible, as labelled, however PduN is not detectable by SDS PAGE due to its low abundance. In addition it is not easy to determine which band PduJ may be due to the lowest detectable marker band being 15 KDa. The corresponding western blot, image E, clearly shows the presence of mCherry-PduA expression, which again appeared to increase over time after induction with IPTG.

In comparison, expression of the other constructs do not appear to involve an increase in shell protein production as seen with mCherry-PduA BMCs, with the exception of image B which shows BMCs formed with mCherry-PduB.

Image B, Pdu-A-mCherry-BJKNU, appeared to show an increased expression of predominately mCherry-PduA, with no noticeable increase in the expression of other shell proteins. The corresponding western blot, image F, confirms the presence of mCherry-PduA and the apparent increase in expression over time. The SDS gel of BMCs with mCherry-PduB, image C, provides no noticeable band of tagged shell protein, however the western blot validates that mCherry-PduB is expressed, image G. Interestingly there is only one band when PduB is tagged on the N terminus, compared with the two bands visualised in the western blot for the PduB C-terminal tag, image H. Both mCherry-PduB and mCherry-PduB' bands are visible by SDS PAGE, image D. PduK appears to run higher, between 20 and 25 KDa but this may be due to the samples not running as far on the gradient gel. Likewise when all SDS gels were examined, the position of PduK was variable, below 20KDa when PduN-mCherry was analysed and higher than 20 KDa with mCherry-PduB.

Expression of tagged PduJ, both N- and C- terminus did not appear to increase over time, although the bands for other shell proteins appeared to increase, Figure 4.3 (A) and (B). This is repeated by the western blots, images D and E, which show faint bands that appear not to increase in density over time for mCherry-PduJ and have only a slight increase over time with expression of PduJ-mCherry.

Expression studies were not carried out with BMCs containing mCherry-PduN as it had been previously found that an N-terminal PduN tag did not produce fully formed, functional microcompartment shells.

Protein production appeared to increase slightly over time when PduU was tagged on the N- or C-terminus, Figure 4.3 images O and P. All shell proteins were visible and matching western blots, images Q and R also showed that tagged PduU was expressed and that expression of PduU-mCherry appeared to increase over time. Although bands were visible for mCherry-PduU at all timepoints, it was difficult to see a correlation of band density. The bands did not get darker over time suggesting that protein production had not increased, with the sample taken overnight (O/N) appearing to be a lot fainter than the other bands, despite the SDS gel indicating that there may have been an increase in protein production.

Overall, expression studies revealed that all bands representing shell proteins were visible. However, an apparent increase in protein expression over time, after induction, was only observed with some of the strains, most noticeably in Figure 4.3 (A), (B) and (D), corresponding to BMC tagged variants expressed from constructs; pLysS-mCherry-pduA-BJKNU, pLysS-pduA-mCherry-BJKNU and pLysS-pduA-B-mCherry-JKNU. Interestingly all of these BMC variants are expressed from a pLysS plasmid and appear to show larger increases in protein production after induction compared with the pET3a plasmids, with the exception of (pLysS) PduA-mCherry-B-JKNU which does not appear to show a protein increase over time.
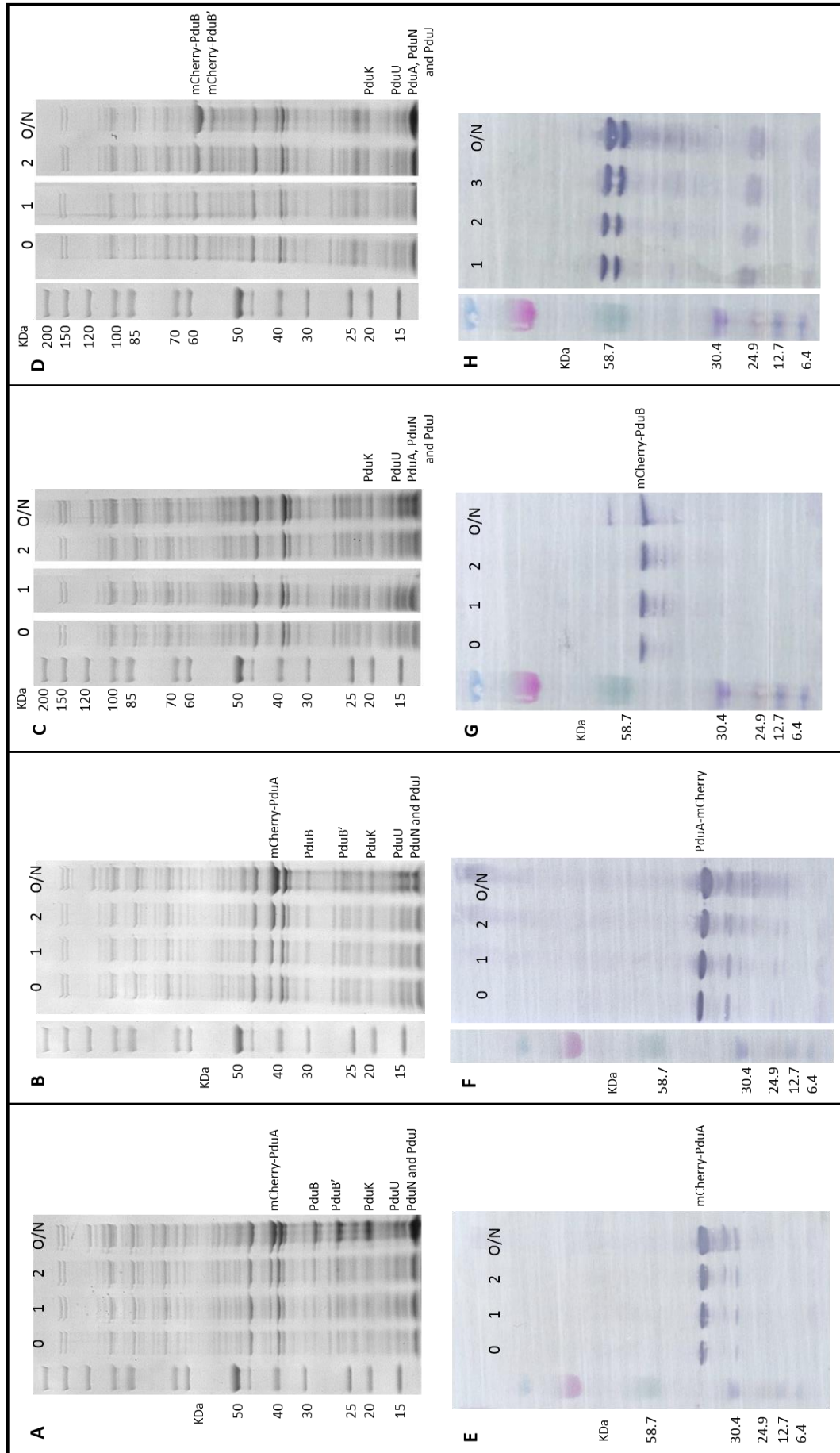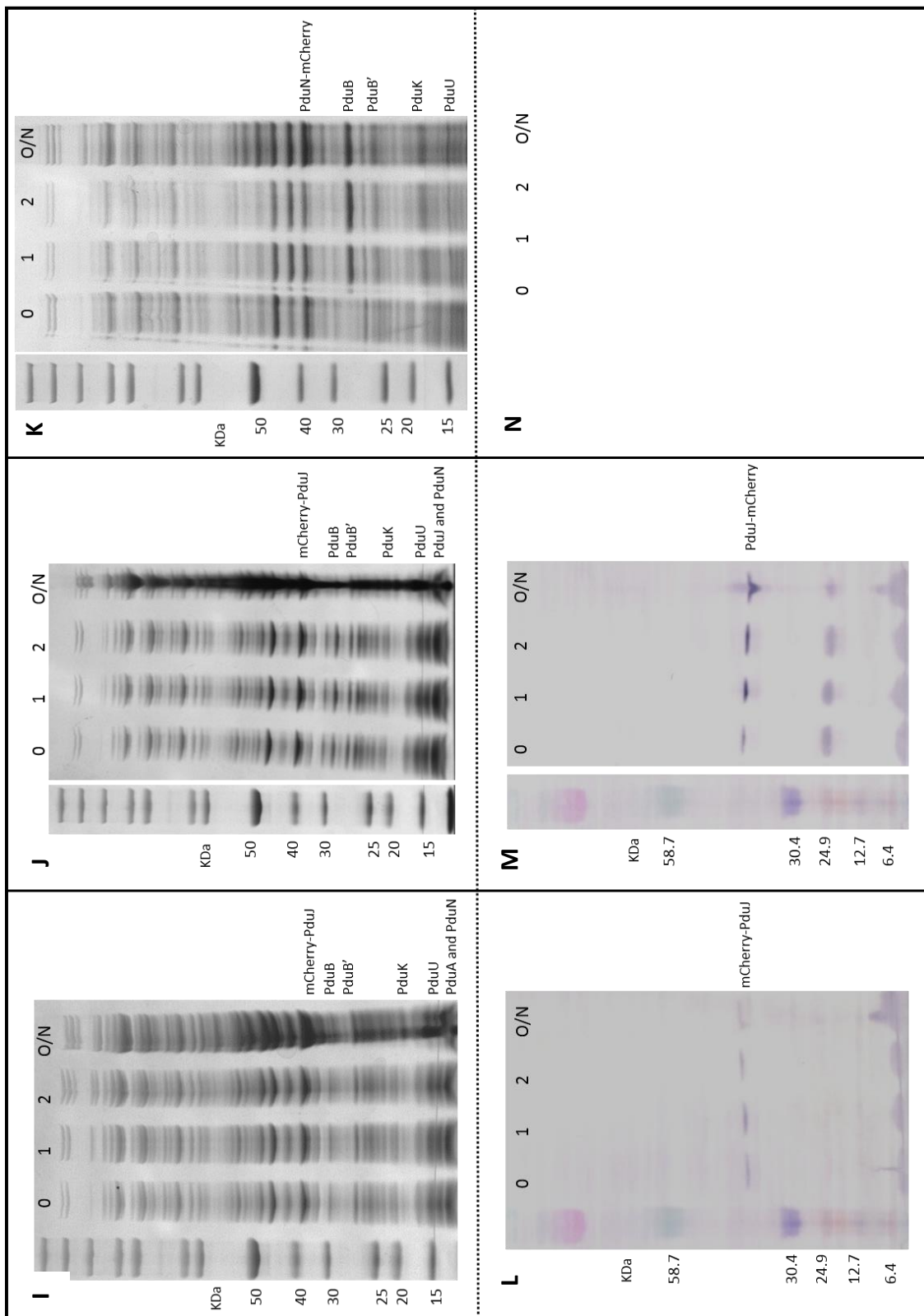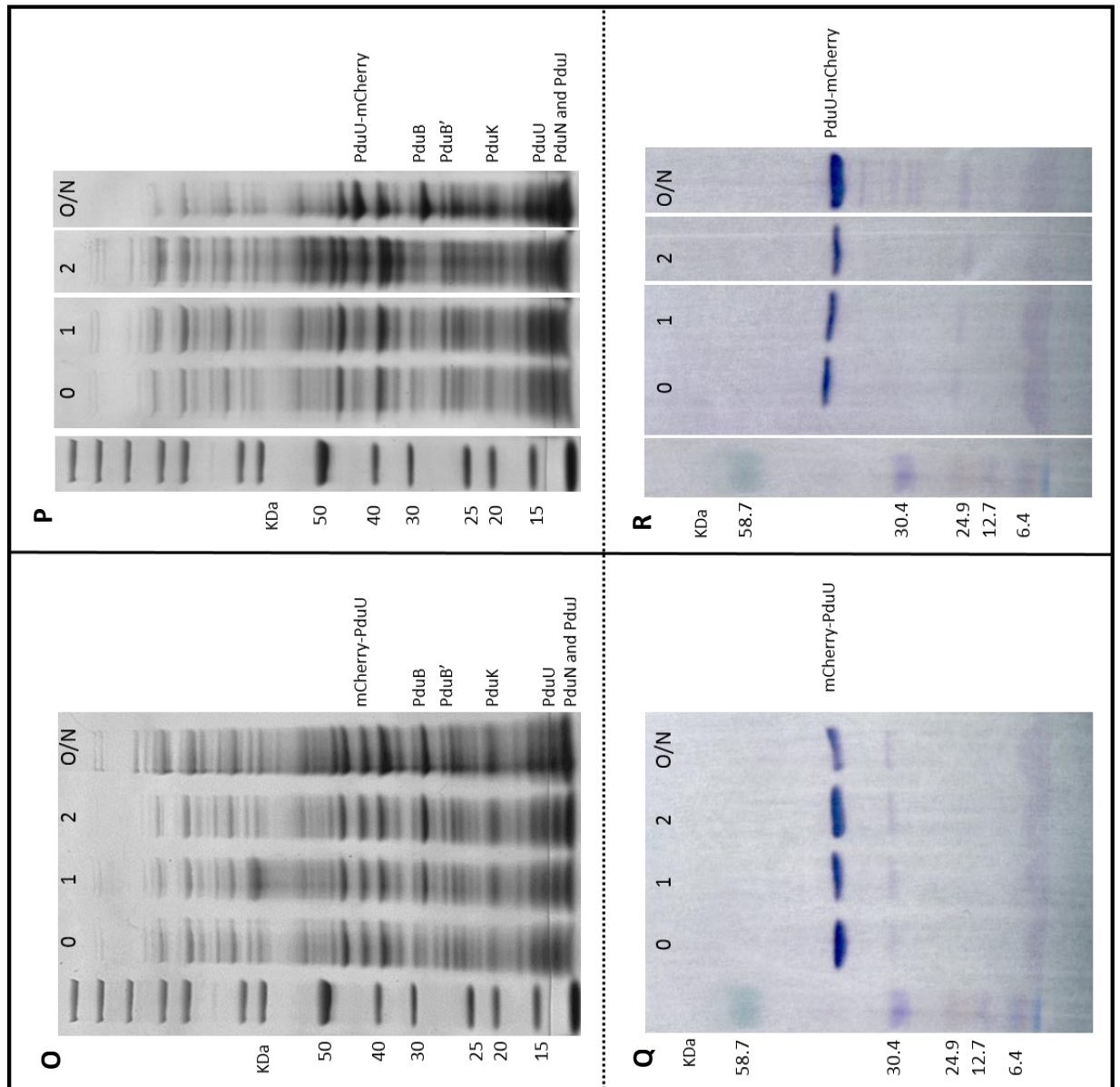
Figure 4.3. SDS PAGE and Western blot analysis of protein expression directly after induction (0 hours), 1 and 2 hours after induction and also overnight (O/N). SDS samples were equally loaded by measuring the OD_{600}, pelleting the cells and resuspending in 1 x PBS buffer and lamelli buffer. Samples were then run on 15% gels. For each of the following, SDS gels and western blots (anti-mCherry) of BL21(DE3) cells a construct for the expression of shell protein-tagged BMC variants in either *pET3a* or *pLysS* are shown: A) and B) (plysS) mCherry-PduA-BJKNU, C) and D) (pLysS) PduA-mCherry-BJKNU, E) and F) (pLysS) PduA-mCherry-PduB-JKNU, G) and H) (pLysS) PduA-B-mCherry-JKNU I) and J) (pET3a) PduAB-mCherry-J-KNU K) and L) (pET3a) PduAB-J-mCherry-KNU M) and N) (pET3a) PduABJK-N-mCherry-U O) and P) (pET3a) PduABJKN-mCherry-U Q) and R) (pET3a) PduABJKN-U-mCherry

4.2.2.3. Effect of expressing BMCs in strains also containing an empty pLysS plasmid

Results have suggested that constructs cloned with *pLysS* show a larger increase in protein expression after induction. In addition strains expressing proteins encoded by genes from a pLysS plasmid involve a magenta colouration of *E. coli* cells.

To explore the role of *pLysS* in protein production, two strains were produced consisting of *pET3a-pduAB-**mCherry-J**-KNU* and *pLysS* as well as *pET3a-pduAB-**J-mCherry**-KNU* and *pLysS*. These strains were cultured alongside strains containing *pET3a* BMC constructs alone to compare the effect of adding *pLysS* to the cells.

Strains were produced by the transformation of BL21(DE3) *pLysS* cells with each of the pET3a constructs. In addition BL21(DE3) cells were transformed with the same constructs for comparison of expression without pLysS. Several colonies from the transformation plate were used to inoculate a 5 mL starter culture. The starter culture was grown overnight as described in Section 2.2.2.2. A larger LB culture (250 mL) was inoculated with the starter culture (1:100 dilution) and grown at 37 °C until an OD_{600} of 0.8 was reached. The cultures were then induced with IPTG, as outlined in Section 2.2.5, and grown at 19°C overnight. 1 mL cell samples were taken for western blotting at 0 hours, 1 hour, 2 hours after induction and also overnight (O/N). An OD600 was taken for each sample and cells were pelleted at 4000 rpm in a microcentrifuge. The cell pellets were then diluted with 1 x PBS according to the optical density to ensure gels were equally loaded, Any differences in protein concentration was therefore due to expression and not cell density, see Section 2.1.7.4. Samples were then run on a 15% SDS PAGE gel and western blots were carried out using anti-mCherry, as outlined in Section 2.1.7.5.
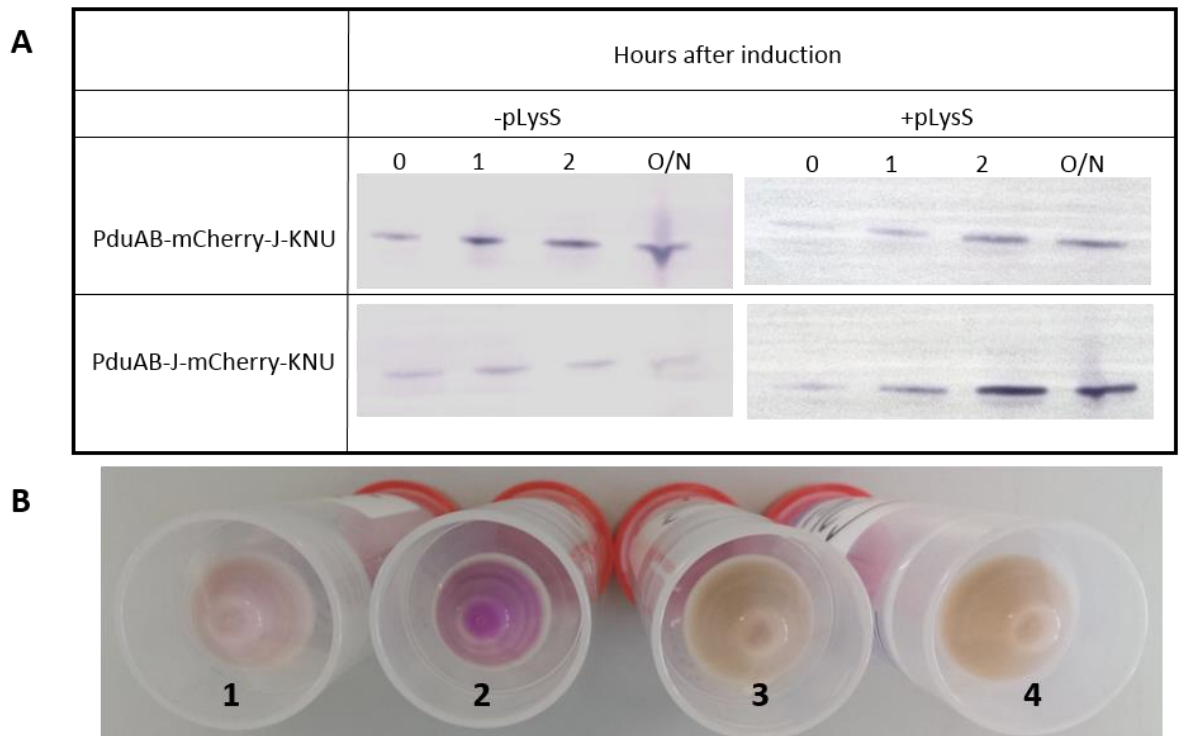
Figure 4.4. Difference in protein expression between cells containing a pET3a mCherry-tagged BMC construct with and without pLysS. A) Western Blot analysis using anti-mCherry of mCherry-tagged PduJ BMCs expressed with and without pLysS. Samples were taken at time-points after induction with IPTG. B) The colour of the cells overnight were also recorded 1- PduAB-mCherry-J-KNU with pLysS, 2- PduAB-J-mCherry-KNU with pLysS, 3- - PduAB-mCherry-J-KNU without pLysS and 4- PduAB-J-mCherry-KNU without pLysS. Cells expressing BMC variants in the presence of empty pLysS were pink or magenta indicating higher mCherry expression.

Figure 4.4 (A) shows western blots of mCherry tagged-PduJ BMCs grown in both the presence and absence of pLysS. Without pLysS it is difficult to establish an increase in mCherry-tagged PduJ over time, although from 0 to 1 hours after induction for mCherry-PduJ, an increase in band density is seen (Figure 4.4). There is no apparent increase in protein synthesis with PduJ-mCherry in the absence of pLysS and the bands for each time-point appear similar in density. In comparison, strains containing tagged BMCs as well as the empty pLysS vector show an increase in protein expression over time after induction for both mCherry-tagged PduJ BMCs, with far more protein present in overnight samples compared to samples taken at the time of induction. This suggests that the addition of empty pLysS plasmids to strains containing BMC variants increases the production of

shell proteins after induction. This shows a similar pattern to tagged shell protein constructs that were cloned with pLysS directly.

Similarly, the colour of cell pellets were recorded, shown in Figure 4.4 (B). Strains containing pLysS were either pink or purple compared to strains lacking plysS. In addition to the western blot findings, this demonstrates that the addition of an empty pLysS plasmid effected protein synthesis. Results therefore indicate that the addition of pLysS to bacterial strains containing tagged-BMC variants cloned with pET3a, increase protein production when induced.

4.2.2.4. Effect of plasmids on BMC purification

Results have shown that although there appears to be a difference in the expression of mCherry-tagged shell proteins encoded by pET3a and pLysS constructs, shown by the colour of cells, SDS gels are not as clear-cut. It is difficult to conclude, by SDS PAGE of whole cell extracts, if the plasmid had any effect on overall protein expression.

Previous western blot analysis demonstrated that BMC tagged shell constructs cloned with pLysS generally showed a greater increase in protein after induction compared with pET3a constructs. Furthermore, the addition of empty pLysS plasmid to strains containing pET3a BMC constructs rescued the expression of shell protein after induction with a higher increase in expression over time compared to strains lacking pLysS.

To investigate further protein expression levels, strains containing mCherry-tagged shell protein BMC variants cloned with pET3a, in the presence and absence of pLysS were grown for BMC purifications. SDS PAGE gels were carried out to compare the amount of purified protein with each strain and to determine if pLysS addition had any effect. In this way, the purification method could therefore be optimised.

BL21 (DE3) pLysS and BL21 (DE3) competent cells were transformed with pET3a constructs: 5,6,8,9 and 10 listed in Table 4.1. Several colonies were picked from each transformation plate and used to inoculate 5 mL starter cultures. The starter cultures were grown overnight and subsequently used to inoculate 250 mL cultures (1:100). These cultures were then grown at 37°C and induced when an OD_{600} of 0.8 was reached. The cultures were then transferred to a shaking platform at 19°C and grown overnight. This process is outlined in Section 2.2.5. The following morning, cells were harvested and BMCs were purified according to the original, unaltered Yper reagent method which involves purification with varying concentrations of salt, as described in Section 2.2.7.2 Samples were taken for each step of the purification protocol, prepared for SDS PAGE analysis and run on a 15% gel as outlined in Section 2.1.7.4. Results are shown in Figure 4.5.

Figure 4.5 demonstrates each step of the BMC purification process for strains containing mCherry-tagged BMC constructs cloned with *pET3a*, in the absence and presence of *pLysS*. Interestingly, all purifications carried out from strains containing empty pLysS have visible shell protein in the final clarified supernatant fraction. In comparison, purifications carried out with only the BMC construct expressed have far less protein present in the final fraction. In addition the number of shell proteins visible are lower without pLysS present. For example, only mCherry-PduJ is visible Figure 4.5 (A), compared with mCherry-PduJ, PduB, PduB' and PduK clearly visible in the purified fraction shown in Figure 4.5 (B). This is the case for all gels, with the exception of mCherry-PduU BMCs, image G. In the absence of pLysS, the final fraction clearly contains shell proteins and there appears to be no large difference between purifications of this BMC variant with or without pLysS.

The reason why purifications seem to differ so dramatically between proteins expressed with and without pLysS is unclear. Some of the strains differ in protein content after a 3 hours exposure to Yper, depending on whether pLysS was present or not, as can be seen when cell lysate fractions of the SDS gels are compared. Shell protein bands do not appear to be visible in the cell lysate fraction in the absence of pLysS, images A and C, with mCherry-tagged PduJ BMCs. In comparison, when

pLysS is present, bands corresponding to each shell protein can be seen, and the shell protein band intensities are higher. Individual bands can be seen in cell lysate fractions with and without pLysS for PduN-mCherry BMCs, however the band intensities are higher in image F, indicating that there was higher protein synthesis with pLysS. It is difficult to compare the cell lysate fractions of mCherry-tagged PduU gels, due to overloading, nonetheless bands corresponding to shell proteins can be seen in images H and J, with pLysS, and are less noticeable in images G and I.

When the protein fractions are compared, pellets 2 seemed to contain a large amount of protein that is lost in the purification method. After the addition of low salt buffer and subsequent centrifugation, see Section 2.2.7.2, BMCs should have remained in the supernatant. However, a lot of shell protein, for all strains, appear to pellet when centrifuged. In addition, in the absence of pLysS, more protein is present in the clarification pellet compared to the clarification pellets when pLysS is present. Overall the final BMC purification fraction contains less contaminating bands and more shell proteins with higher band intensities when pLysS was present in the bacterial strains.
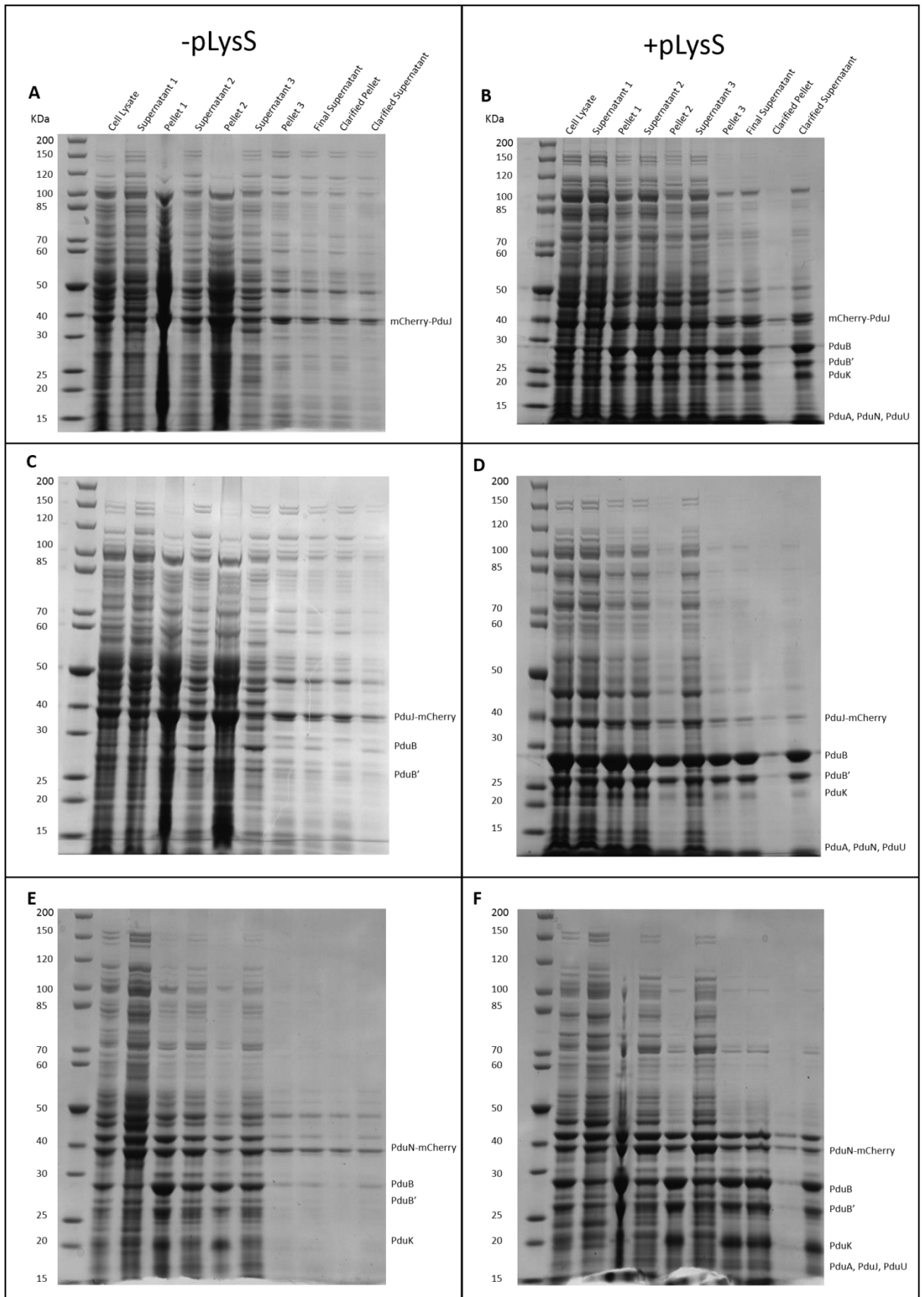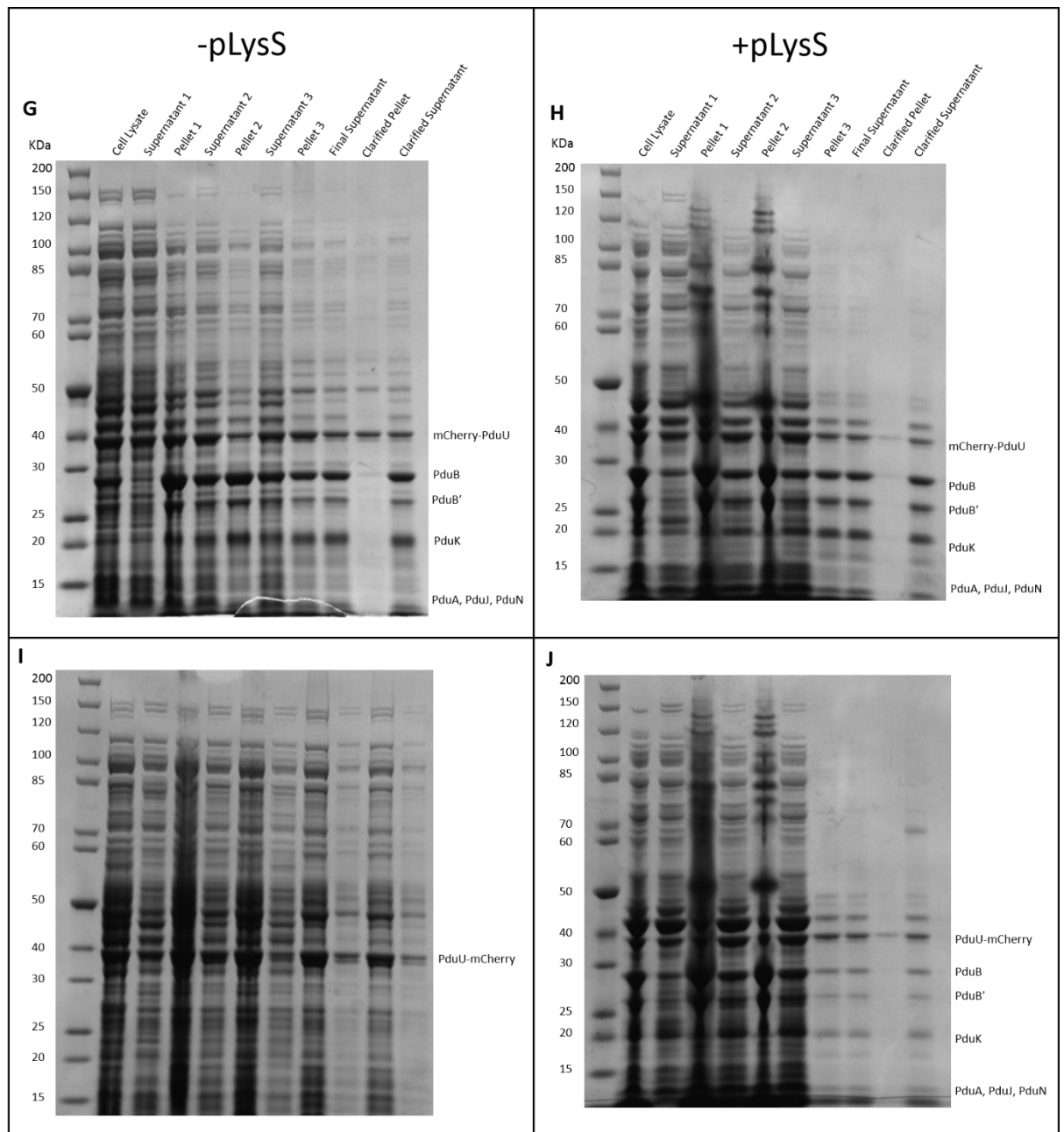
Figure 4.5. SDS PAGE analysis of tagged-BMC shell purification with and without pLysS. Each strain was grown in identical conditions and strains expressing the same tagged-shell protein with and without pLysS were cultured on the same day to minimise variation in protein expression due to growth conditions. BMCs were purified according to the Yper method (Section 2.2.7.2) and samples were taken for SDS PAGE analysis at each stage. Only constructs cloned with pET3a were studied. An N terminal PduN tag was not investigated at this construct was cloned later A) and B) PduAB-mCherry-J-KNU with and without pLysS C) and D) PduAB-J-mCherry-KNU E) and F) PduABJK-N-mCherry-U G) and H) PduABJKN-mCherry-U and I) and J) PduABJKN-U-mCherry.

As a result of the effect of pLysS on protein expression, future studies were carried out with both pLysS and pET3a constructs in each strain, with BMC shell proteins expressed from one of the plasmids. Adding pET3a to strains containing BMC constructs cloned with pLysS was to ensure that the cellular environment as well as the expression levels would be similar in each strain.

4.2.3. Optimisation of the purification protocol

It is evident that the addition of pLysS to cells expressing BMCs with tagged-shell proteins leads to a higher BMC yield when purified. However, when attempting the purification process with BMC shells containing either PduA-mCherry, mCherry-PduB or PduB-mCherry the process failed. All of these BMC variants were expressed from a pLysS plasmid. Therefore, further optimisation of the purification protocol was necessary. It is uncertain why some mCherry-tagged BMCs were able to purify better than others and may indicate that the shells form incorrectly with some tags as opposed to others.

In addition purification repeats led to variable results; it was often difficult to purify mCherry-tagged BMC shells, which made subsequent visualisation by TEM inconsistent. To limit the variability, the cell growth conditions and purification protocol were optimised for mCherry-tagged BMCs.

4.2.3.1. Effect of growth temperature

To determine if temperature affects the expression of BMC shells and subsequent protein purification, cultures of BL21(DE3) cells containing *pLysS-pduA-mCherry-BJKNU* as well as empty *pET3a* plasmid were grown at 18°C and, 28°C. This strain was chosen for optimisation as previous BMC purifications from this strain were unsuccessful, with little or no purified shell protein present in the final fraction (data not shown). Live cell imaging results showed that the size and location of BMC foci were similar to that of the mCherry-PduA-BJKNU BMCs, which are known to form correctly, therefore, BMC purification would give further insights in to the formation and structure of this mCherry-tagged BMC variant.

Cell cultures (250 mL) were inoculated from the same 5 mL starter culture. The starter culture was inoculated from several colonies of a single transformation plate. Cultures were then grown to an OD of 0.8 and induced with IPTG. All cultures were then grown overnight at 19°C. BMCs were then purified according to Section 2.2.7.2 and samples were taken for SDS PAGE analysis. SDS gels of BMCs purified after initial growth at 18°C and 28°C were then compared to SDS gels of growth at 37°C, which had previously resulted in no purified BMCs visualised by TEM from the final purified fraction.

Purifications show that cells grown at a lower temperature result in a higher amount of protein expression (Images A and B, Figure 4.6), however, the resulting purified BMC fraction is not pure with many unknown contaminating bands. In comparison, cells grown at 37°C, Image C, express more shell protein and the final fraction is considerably purer, as shown in Figure 4.6. As a result of temperature studies, it was decided to continue growth at 37°C for subsequent purification experiments.
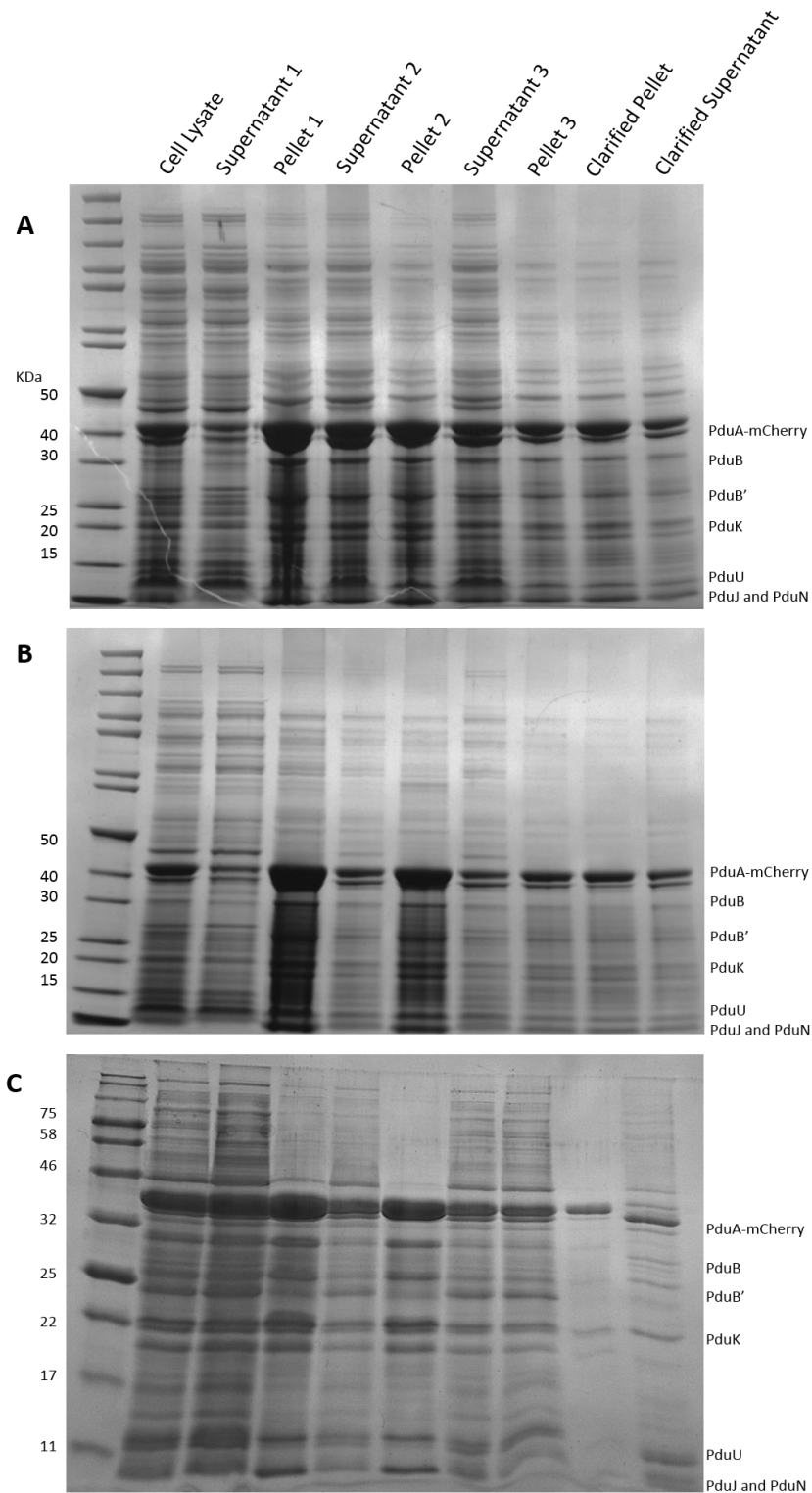
Figure 4.6. The purification of PduA-mCherry-BJKNU BMCs after growth at varying temperatures. BL21(DE3) pET3a cells expressing BMCs with C-terminally tagged PduA from a pLysS vector, were grown at 18°C and 28°C from the same starter culture. BMCs were purified by the Yper method, with samples from each stage of the purification retained for SDS analysis. This was compared to a previous SDS gel of PduA-mCherry BMCs grown at 37°C. 15% SDS gels are as follows: A) Cells expressing PduA-mCherry BMCs grown at 18°C B) 28°C C) 37°C

4.2.3.2. Minimisation of protein loss in Pellet 2

The efficiency of BMC purifications were variable depending on the mCherry-tagged shell protein expressed. However, it was commonly observed that a large amount of shell proteins were present in pellet 2 of the purification process leading to lower levels of shell protein in the final fraction. This is shown in Figure 4.5, which demonstrates that purification of all mCherry-tagged BMC variants included a large loss of protein at the pellet 2 stage.

Although the reason why shell proteins pelleted at that stage of purification is unclear, the speed of centrifugation as well as expression levels of the shell proteins were identified as factors that may have contributed to the loss of shell protein in the BMC purification. In order to reduce the amount of protein lost in pellet 2, centrifugation speed after low salt buffer was added was reduced to 4000 rpm, however this did not affect the amount of protein in the pellet (data not shown). In addition the level of protein production was reduced by culturing cells at 37°C and inducing with one quarter of the normal IPTG used (100 µM). However this also had little effect.

Having shown that the BMC purification process could not be easily optimised to reduce the amount of shell protein in pellet 2 without the need for changing buffer composition, it was decided to continue using the BMC purification method as described in Section 2.2.7.2. The aim of tagged-BMC purification was to analyse the formation, morphology and stability of isolated BMC shells outside of the cellular environment by TEM.

4.2.3.3. Optimisation of BMC visualisation by TEM

Previously, recombinant BMCs expressed in *E. coli* cells have been isolated and visualised by TEM. In addition, native Pdu BMCs produced in *Salmonella enterica* have been purified using an alternative method to the protocol used in this study and the resulting purified compartments have been visualised. This study aims to analyse recombinant mCherry-tagged Pdu BMCs by TEM, to determine the effect of the mCherry tag on the formation of microcompartment shells.

Initially BL21(DE3) strains containing empty pET3a as well as tagged shell protein constructs, *pLysS-mCherry-PduA-BJKNU* or *pLysS-PduA-mCherry-PduBJKNU* were cultured for BMC purification according to Sections 2.2.2 and 2.2.5, with growth at 37°C and induction with IPTG to a final concentration of 100 µM. The BMCs were then isolated following the Yper purification method outlined in Section 2.2.7.2, and samples were taken for SDS PAGE analysis at each stage of the purification process. The final clarified supernatant was subsequently dried onto a copper grid, fixed and negative stained for TEM, according to Section 2.5.2.2.

Results of SDS PAGE showed that purified shell proteins were present in the final clarified supernatant. However, when analysed by TEM, BMC shells were not visualised. Membranous material as well as negatively stained proteins were seen for both mCherry-PduA-BJKNU and PduA-mCherry-BJKNU samples, but BMC shells were not observed. This could be due to an impure fraction used for TEM analysis, with contaminating proteins making shells difficult to visualise. However the SDS gels show that shell proteins are the most abundant in that fraction. The lack of BMC shells could also be due to the method of preparation of visualisation by TEM, involving fixation with glutaraldehyde and numerous wash steps which could either prevent the adhesion of BMC shells to the surface of the grid, or subsequently cause them to be washed off.

As previously described in Section 4.2.3.2, a large amount of shell protein is found at the pellet 2 stage of the purification process, and results in decreased shell protein in successive fractions. To try and improve shell protein observation by TEM, pellet 2 from the same purification was prepared for thin sectioning according to the same protocol used for whole cell thin sectioning, as described in Section 2.5.2. This resulted in a vast improvement in the visualisation of BMC shells. As shown in Figure 4.7, clear BMC-like structures can be seen with shells containing mCherry-PduA or PduA-mCherry. However, PduA-mCherry-BJKNU shells appeared malformed and broken; the size and shape of shells were varied, in contrast to mCherry-PduA-BJKNU shells which were fairly uniform. There were more shells present with the mCherry-PduA tag whereas there appeared to be other

proteins in the PduA-mCherry sample. The difference between the TEM results of the two mCherry-tagged BMCs is likely to be a result of the placement of the mCherry tag and its effect on the formation of the BMC.

Overall this method has been applied to two shell protein tags, one of which, mCherry-PduA-BJKNU is known to form intact BMC shells. The method was shown to be successful in visualising the structure of tagged shells and was therefore applied to all further mCherry-tagged BMC purifications.
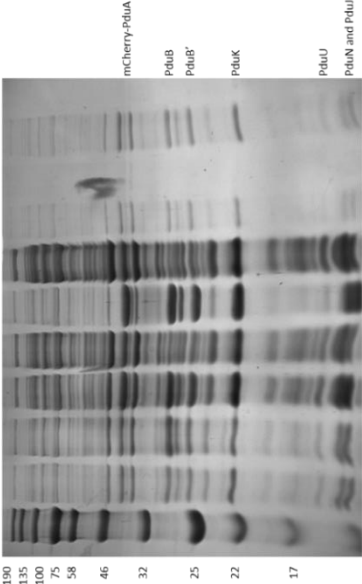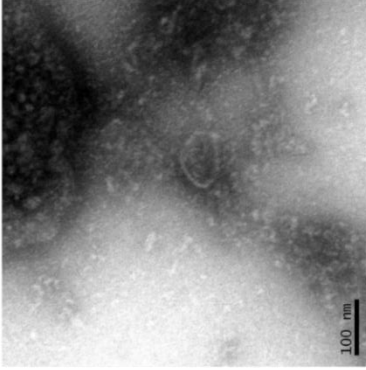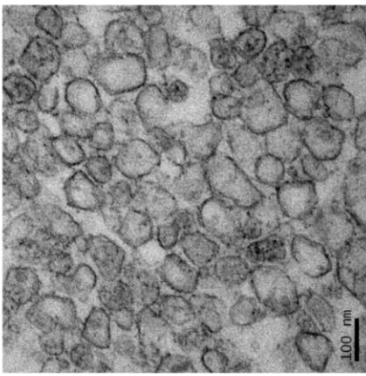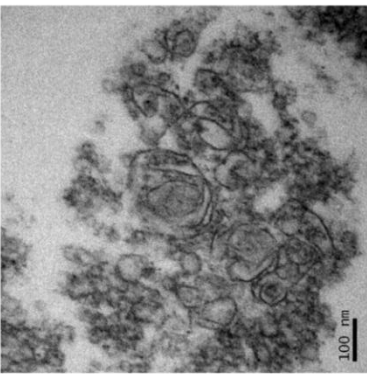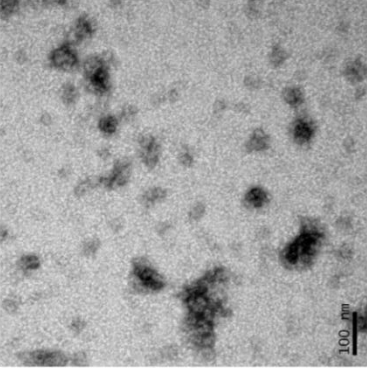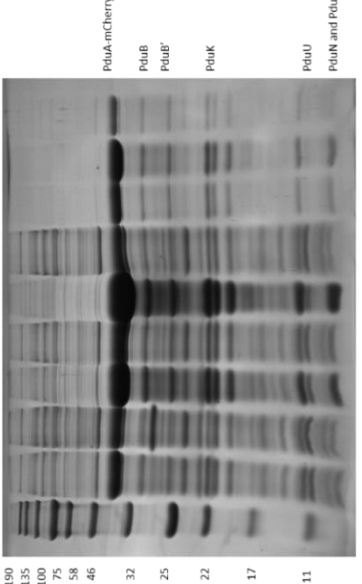
Figure 4.7. Optimisation of TEM visualisation of mCherry-tagged BMCs. BL21(DE3) pET3a cells expressing mCherry-tagged PduA BMCs were grown overnight as described in section xxx and purified according to the Yper method. 15% SDS PAGE gels of the BMC purifications are shown for mCherry-PduA-BJKNU and PduA-mCherry-BJKNU tagged-shell variants, shown in the first column. The purified fraction of BMCs were then dried onto a copper grid for TEM analysis, depicted in column 2, however, no shell-like structures were visualised. Pellet 2 of the purification method was then fixed and prepared for thin sectioning and then observed by TEM, shown in column 3.

4.2.4. The formation of mCherry-Tagged PduB BMCs

4.2.4.1. BMC purification as an indication of correct formation

Previously, BMC purifications of compartments with mCherry-tagged shell proteins expressed from pET3a plasmids were carried out in the presence and absence of pLysS. Results showed that purifications were more efficient, with a higher level of shell proteins in the final fraction in the presence of and empty pLysS plasmid in the bacterial strain. Further purifications of mCherry-tagged PduA BMC variants were carried out for optimisation studies and TEM analysis and despite protein being lost in pellet 2, the final purification fraction contained predominately shell proteins. The purification of mCherry-tagged PduB was repeatedly unsuccessful. BL21(DE3) cells were transformed with *pET3a* and either *pLysS-pduA-mCherry-B-JKNU* or *pLysS-pduA-B-mCherry-JKNU*. Several colonies were used to inoculate overnight starter cultures, which were subsequently used to inoculate 250 mL cultures of LB, containing ampicillin and chloramphenicol, as described in Sections 2.2.2.2. Cells were grown at 37°C. When an OD_{600} of 0.8 was reached, protein synthesis was induced with IPTG (100 μM) and then grown overnight as outlined in Section 2.2.5. Cells were harvested the following morning and purified according to the Yper method in Section 2.2.7.2. Samples of purification fractions were taken for SDS PAGE analysis, as shown in Figure 4.8.
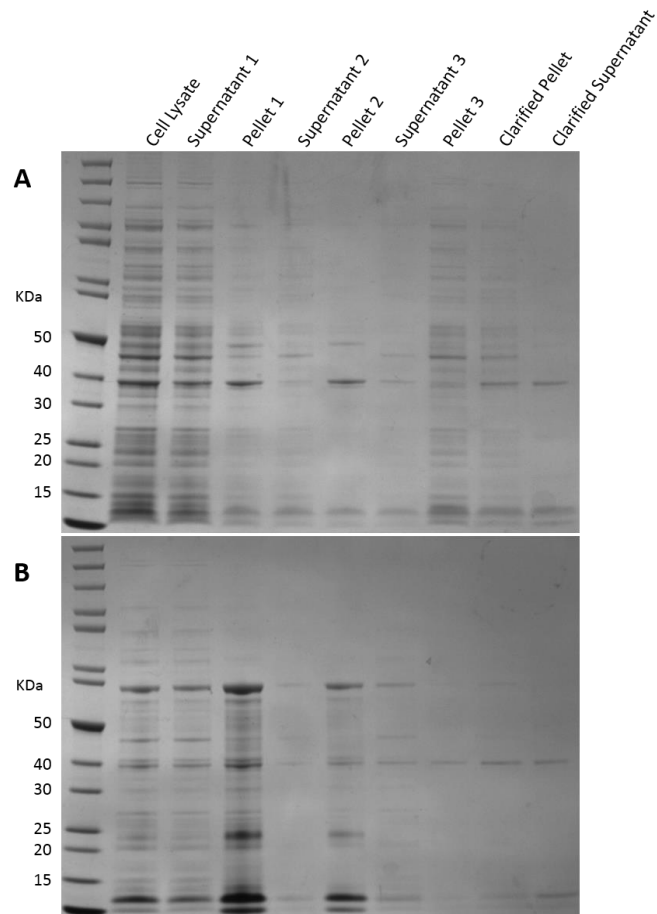
Figure 4.8. Purification of mCherry-tagged PduB BMCs. BL21(DE3) pET3a cells expressing either PduA-mCherry-B-JKNU or PduA-B-mCherry-JKNU were grown overnight and purified using the Yper method. Samples were collected for SDS PAGE analysis and 2 µl of each fraction in 2 x sample buffer were run on a 15% SDS gel. A) Purification of PduA-mCherry-PduB-JKNU B) Purification of PduA-B-mCherry-JKNU

SDS PAGE analysis of mCherry-tagged PduB purifications revealed that proteins were lost at each stage of the purification process. For the mCherry-PduB purification, proteins were predominantly lost in supernatant 1, pellet 3 and the clarified pellet. Shell proteins were mainly lost in pellet 1 and pellet 2 for PduA-B-mCherry-KNU BMCs. This difference in protein loss in each fraction could highlight differences between the formation of BMCs depending on the N- or C- terminal PduB tag. Overall there was an absence of shell proteins in the final purified fraction. This was very different to all of the other shell protein tags, where protein was visible to the end of the purification, despite some being lost in fractions. In this way, it was hypothesised that PduB fusions with mCherry failed

to form BMCs when the other shell proteins were also expressed. Therefore the purification process acted as an indicator for the formation of intact BMC shells.

4.2.4.2. Insights into the morphology of tagged-PduB BMCs by TEM and live cell imaging

To explore the formation of mCherry-tagged PduB shells further, live cell imaging and TEM thin sectioning was carried out.

BL21(DE3) strains containing pET3a and either; pLysS-mCherry-PduA-BJKNU, pLysS-PduA-mCherry-PduB-JKNU or pLysS-PduA-B-mCherry-JKNU were grown in 250 mL cultures at 37 °C until an OD_{600} of ~0.6 was reached. Cells (1 mL) were then taken from the culture and pelleted by centrifugation for live cell imaging as outlined in Section 2.5.1. IPTG (100 µM) was then added to the cell culture to induce the expression of BMCs and cell samples were taken 2 hours after induction for live cell imaging and also thin sectioning and subsequent visualisation by TEM. Results are shown in Figure 4.9.

Live cell imaging of the control strain expressing mCherry-PduA-BJKNU, known to form complete, intact BMC shells demonstrated individual foci spread throughout the cytoplasm in cell before induction. Some cells were elongated, but there were also shorter cells present too. After induction, cells were elongated and many foci of mCherry signal were present in each cell. This corresponds to the TEM thin sections observed 2 hours after induction which show intact BMC shells approximately 100 nm in diameter.

Interestingly, cells expressing PduA-mCherry-B-JKNU were associated with one inclusion body at one pole of the cell; there did not appear to be more than one inclusion per cell, with the exception of cells that were dividing, as observed by live cell imaging. There was little difference between cells visualised at the two different time points, except that cells appeared longer after induction. Thin sectioning of whole cells fixed 2 hours after induction revealed identical results to that of live cell imaging; cells contained and inclusion body at the pole; no BMC-like structures were visualised. This

indicated that an N-terminal PduB tag did not form any structures that resembled BMC shells when expressed with the other Pdu shell proteins.

In comparison, a C-terminal PduB tag was very different to the N-terminal tag when expressed with the shell proteins necessary to form BMCs. PduA-B-mCherry-JKNU localised throughout the cell cytoplasm before induction, as can be seen by live cell imaging in Figure 4.9. The mCherry signal was completely cytoplasmic with no distinct foci visible. There appeared to be a variety of cell lengths with some elongated cells and some shorter cells. Live cell imaging 2 hours after induction showed similar results. The mCherry signal was completely cytoplasmic. This indicated that the formation of BMC shells containing PduB-mCherry was impaired. TEM analysis of thin sections of cells taken 2 hours after induction confirmed that there were no obvious intact BMC shells present. Throughout the cell cytoplasm, distinctive areas of low electron density can be seen. These areas are commonly observed with BMC shells, as can be seen in the mCherry-PduA-BJKNU-expressing cells, however in this case, definite shell outlines cannot be distinguished easily. Strands of shell proteins can be observed, as indicated by the white arrows in Figure 4.9, although these strands did not fold into completed shell structures. These data indicate that tagging PduB with mCherry in either the N- or C- termini results in a lack of BMCs when expressed with the other shell proteins. Consequently, further studies with m-cherry tagged PduB were not carried out.
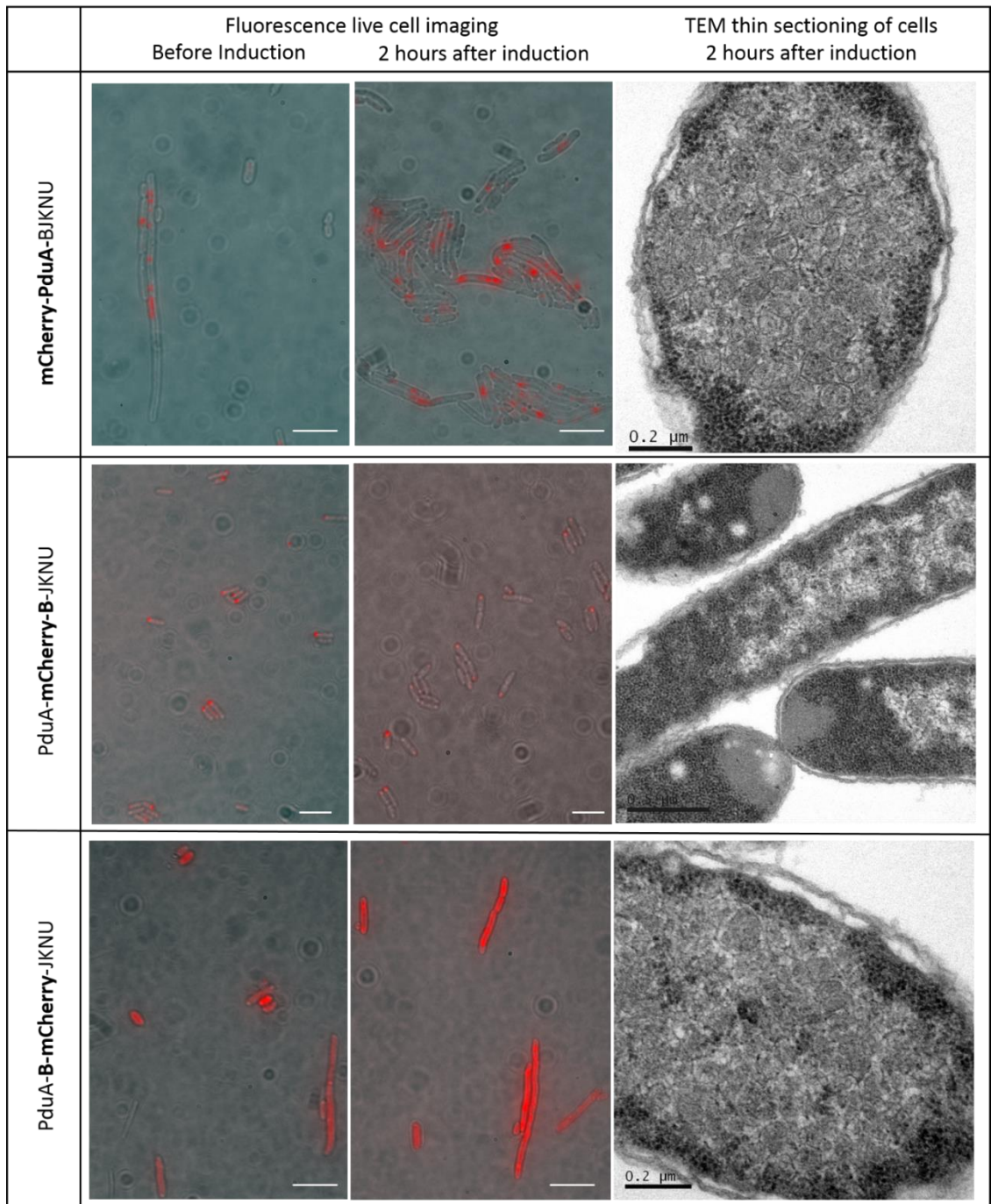
Figure 4.9. Analysis of the formation of mCherry-tagged BMCs. BL21(DE3) *pET3a pLysS-pduA-mCherry-B-JKNU* and BL21(DE3) *pET3a pLysS-pduA-B-mCherry-JKNU* were analysed by live cell imaging directly before induction and also 2 hours after induction and TEM thin sectioning of whole cells 2 hours after induction. Scale bar represents 5 μm in fluroescence microscopy images and 0.2μm in TEM images.

4.2.5. Effect of tagging shell proteins with mCherry on BMC shell formation

Live cell imaging and TEM thin sectioning provided insights into the morphology of BMC shells when PduB was tagged with mCherry. To explore the morphology of shells with each of the other shell protein tags, fluorescence microscopy and TEM was carried out directly before induction with IPTG, at an OD_{600} between 0.6 and 0.8 as well as 2 hours after induction, with an OD_{600} of approximately 1.2 In addition the mCherry-tagged BMC variants were purified and pellet 2 was prepared for thin sectioning as previously described in Section 2.5.2 so isolated BMC can be visualised.

Strains containing mCherry shell constructs and an additional plasmid, either pLysS or pET3a for the reasons described in Sections 4.2.2.1 and 4.2.2.3 were grown from starter cultures, which in turn had been inoculated from several colonies from a fresh transformation, as outlined in Sections 2.2.2.2. Cultures (500 mL) were grown at 37°C until an OD of ~0.6 was reached. Cells were then harvested for both live cell imaging and thin sectioning as described in Sections 2.5.1 and 2.5.2.1. The cell cultures were then induced with 100 µM of IPTG and the temperature was dropped to 19 °C. After 2 hours of growth, cells were harvested for live cell imaging and thin sectioning again, the approximate OD600 of the cultures were ~1.2 at this stage. The cell culture was then left overnight at 19 °C. Cells were then pelleted by centrifugation and resuspended in Yper for BMC purification, as described in Section 2.2.7.2. Pellet 2 of the BMC purification was then prepared for thin sectioning using the same protocol as whole cell thin sectioning described in Section 2.5.2. Live cell imaging data is shown in Figure 4.10 and TEM results are shown in Figure 4.11.

4.2.5.1. Live cell imaging of whole cells at time points

Live cell imaging results show a phase image with mCherry overlap. This allows the analysis of the location of the mCherry-tagged BMCs in relation to the cell. Before induction, it is easier to visualise individual foci in the cell cytoplasm. Foci are most distinctive in the control sample, mCherry-PduA-BJKNU. Cells also appear elongated in this strain, which is common for cells expressing BMCs,and likely represents a stress response. After induction the control strain appears longer, with many

more foci spread throughout the cell. The foci also appear brighter. In comparison cells expressing PduA-mCherry-JKNU appear shorter before induction than the control strain. There are fewer mCherry foci per cell than the N-terminally tagged PduA BMC strain before induction and the foci appear bigger, indication either larger sized BMCs, or aggregated protein. Two hours after induction, the cells observed are longer in length and the mCherry signal is spread in areas within the cytoplasm, rather than in discrete foci, although some brighter foci-like signal can be seen. From these results, it is unclear whether PduA-mCherry tagged-BMCs form intact shells, however live cell images reveal that the fluorescent signal is unlike that of the control strain.

Similarly, the mCherry-PduJ BMC strain contained individual foci of mCherry signal spread throughout the cytoplasm before induction. However, the cells observed appeared to vary in width, with some appearing to be wider than those previously visualised in the control strain. This was also true for cells after induction and cells were elongated in length both before and after induction. After induction, the mCherry signal was more cytoplasmic, although the patches of signal did not spread the length and width of the cell. It was difficult to establish discrete BMC foci, similar to the PduA-mCherry strain.

Interestingly, a strain expressing PduJ-mCherry BMCs was hard to visualise by fluorescence microscopy. This was because the mCherry signal bleached extremely quickly and therefore made it highly difficult to take an image. The images for a strain containing PduJ-mCherry BMCs before and after induction appeared to contain mCherry signal in the cytoplasm, although the presence of foci could not be established.

In a strain expressing mCherry-PduN, before induction large foci were observed at the poles of the cell, suggesting the mCherry-PduN was accumulating in inclusion bodies. After 2 hours of induction with IPTG, a noticeable difference was observed. There was a drastic reduction in the number of large foci observed at the cell poles, with the mCherry signal now a lot more dispersed throughout

they cytoplasm. Some cells exhibited a slight accumulation of mCherry-PduN however there was no real pattern to this, and was not forming discrete foci.

A similar observation was made when looking at PduN-mCherry. Before induction large foci were again observed at the cell poles, with very little cytoplasmic signal. After induction, there was an increase in the cytoplasmic signal, and there was a reduction in the number of large large foci at the cell poles, however this was not to the same extent as that observed with mCherry-PduN.

Discrete foci of mCherry signal could be observed in a strain expressing PduABJKN-mCherry-U BMCs before induction. There was a little background mCherry signal as shown by the faint red signal present throughout the cells. After induction the background signal was more obvious, where expression of shell proteins increased. The mCherry signal was brighter than before induction and more signal was present in the cytoplasm, rather than in discrete foci, although areas within the cell contained higher levels of signal compared to others. In these areas of high signal intensity, discrete foci could be visualised, but the overall fluorescence pattern was very different to that of the control strain.

In comparison a PduU-mCherry expressing strain contained predominantly cytoplasmic signal before induction. Occasional bright foci of mCherry signal were visible, however, after induction the mCherry signal appeared to be brighter and completely cytoplasmic. Cells expressing mCherry-tagged PduU on either the N- or C- terminus were elongated with a fixed cell width, similar to that of the control strain. However, it was unclear if mCherry-tagged PduU BMCs were able to form intact shell structures from the live cell imaging data as the fluorescent signal was largely cytoplasmic. This indicated that either shells were unable to form or that the mCherry-tagged shell protein was not being incorporated into the shell structure.
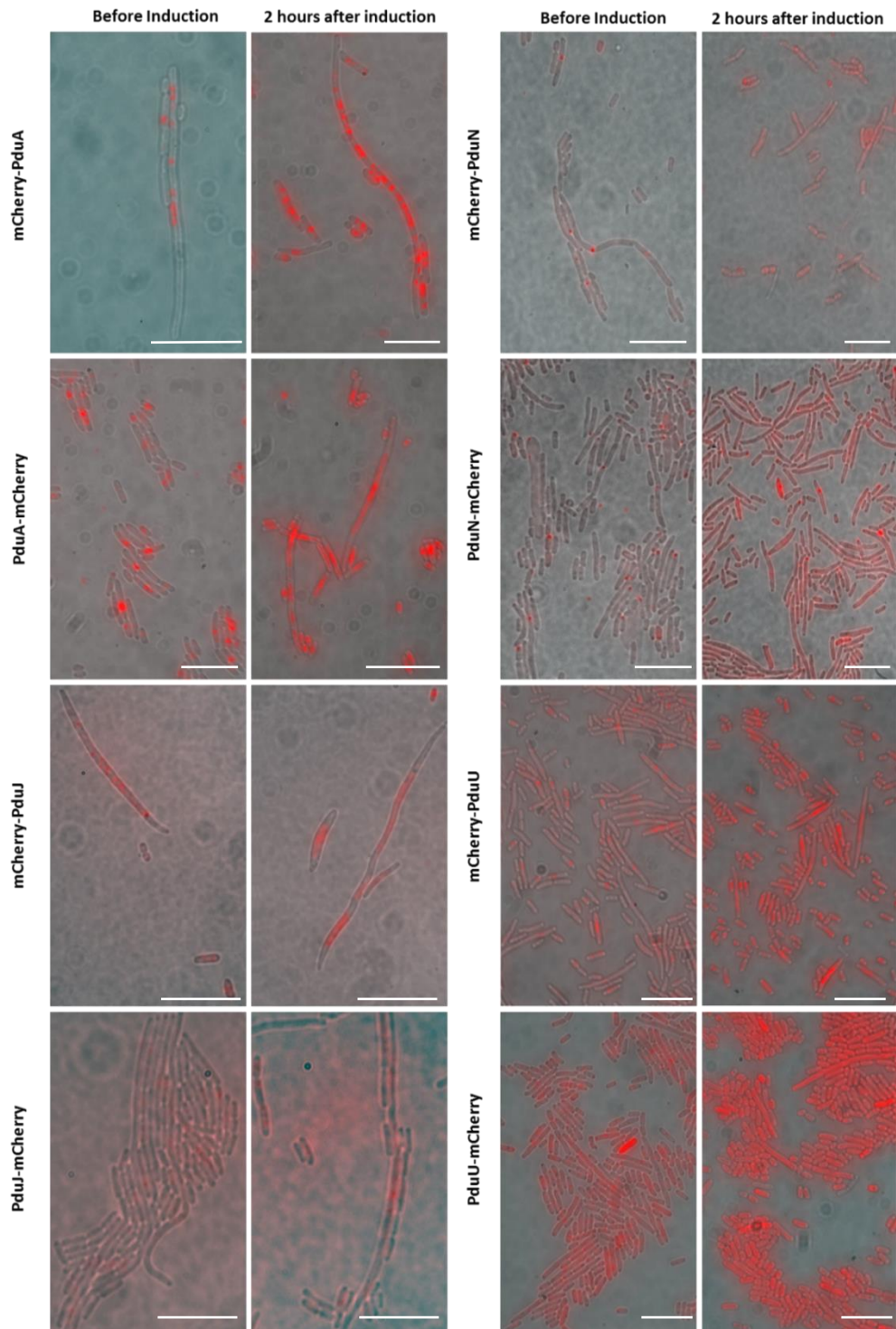
Figure 4.10. Analysis of the formation of mCherry-tagged BMCs. BL21(DE3) pET3a pLysS-mCherry-pduA-B-JKNU, BL21(DE3) pET3a pLysS-pduA-mCherry-BJKNU, BL21(DE3) pLysS pET3a-pduA-mCherry-B-JKNU, BL21(DE3) pLysS pET3a-pduAB-mCherry-JKNU, BL21(DE3) pLysS pET3a-pduABJ-mCherry-KNU, BL21(DE3) pLysS pET3a-pduABJK-mCherry-N-U, BL21(DE3) pLysS pET3a-pduABJKN-mCherry-U, BL21(DE3) pLysS pET3a-pduABJKN-mCherryU, BL21(DE3) pLysS pET3a-pduABJKN -U-mCherry, were analysed by live cell imaging directly before induction and also 2 hours after induction. Scale bar represents 5 μm.

4.2.5.2. TEM of whole cells at time points

4.2.5.2.1. mCherry-tagged PduA

TEM images of strains expressing shell constructs containing a mCherry-fusion tag are shown in Figure 4.11. Before induction, mCherry-PduA BMCs can be seen in distinctive patches with low electron density. The outlines of BMC shells can be observed, with some shells partially formed. After induction many more BMCs can be seen throughout the cytoplasm rather than in discrete patches. The majority of BMC shells are intact and the size of shells is fairly consistent (~100 nm). Although some spiral-shaped, rose-like shells were observed, these were not commonly visualised. When mCherry-PduA BMCs were isolated by thin sectioning of pellet 2 of the purification process, empty BMC shells were visualised. These shells were fairly uniform in shape and size, ranging from 80-100 nm. No spiralled structures were seen in the isolated TEM sections, although some broken or partly formed BMCs were present.

Initially from live cell imaging data, it appeared that a C-terminal PduA fusion was similar to that of the N-terminal tag. However a strain expressing PduA-mCherry formed structures that were different to mCherry-PduA BMCs, which are known to form correctly. Similar patches associated with BMC shells were observed in cells visualised before induction, although unlike mCherry-PduA BMCs, shell protein outlines were not visible at all in these patches before induction. Two hours after induction BMC shell borders were observed in similar grey patches although they were not as well defined as that of mCherry-PduA BMCs, and the majority appeared broken or only partly formed. There were also inclusion body-like areas located in the cytoplasm. This indicated that BMCs tagged with mCherry at the C terminus of PduA did not form correctly. Furthermore, isolation of PduA-mCherry BMC shells revealed primarily unfolded strands of shell proteins as well as occasional intact BMCs, although these varied greatly in size and shape. In comparison to an N-terminal PduA fusion tag, the C-terminal tag produced mostly malformed, partly formed or broken structures.

4.2.5.2.2. mCherry-tagged PduJ

Live cell imaging of BL21(DE3) *plysS* cells expressing PduAB-mCherry-J-KNU revealed large foci spread throughout the cytoplasm (Figure 4.10). TEM analysis of cells before induction show small distinct areas of aggregated shell protein. These aggregatedstrands are fairly indistinct and difficult to visualise, but are highlighted by the white arrows in Figure 4.11. After induction, many more structures are present in the cell cytoplasm. Shells are well defined and some appear intact with the size ranging from 70 – 130 nm in diameter. However many shells appear broken as the two strand ends do not meet, as demonstrated by the white arrow heads. In comparison to mCherry-PduA BMC, there appears to be a larger proportion of broken shells with the PduJ tag, indicating that formation of BMCs is impaired.

Interestingly, thin sections of mCherry-PduJ BMCs, taken from pellet 2 of the purification, revealed a network of protein strands, thought to be unfolded shell protein do to its similar appearance to the shells visualised *in vivo*. No BMC shell structures were observed by TEM in the isolated BMC thin sections. The growth and purification of this strain was repeated and identical protein strands were visualised. It is unclear why BMC shells were not observed when thin sectioning of whole cells 2 hours after induction as well as live cell imaging indicated that there were intact shells present. The inability to purify intact BMC shell structures observed in thin sections of whole cells hints at either the instability of mCherry-PduJ shells outside of the cellular environment, or the vigorous process of preparation for thin sectioning may cause the intact and partially formed shells to completely unfold.

A table-style figure with columns: "Before induction (OD600 ~0.6)", "2 hours after induction (OD600 ~1.2)", "Isolated BMCs". The left vertical label reads: "BMCs expressing shell protein PduABJKNU with one of the shell proteins tagged with mCherry as follows: mCherry-PduA / PduA-mCherry / mCherry-PduJ / PduJ-mCherry". Scale bars 0.2 μm.
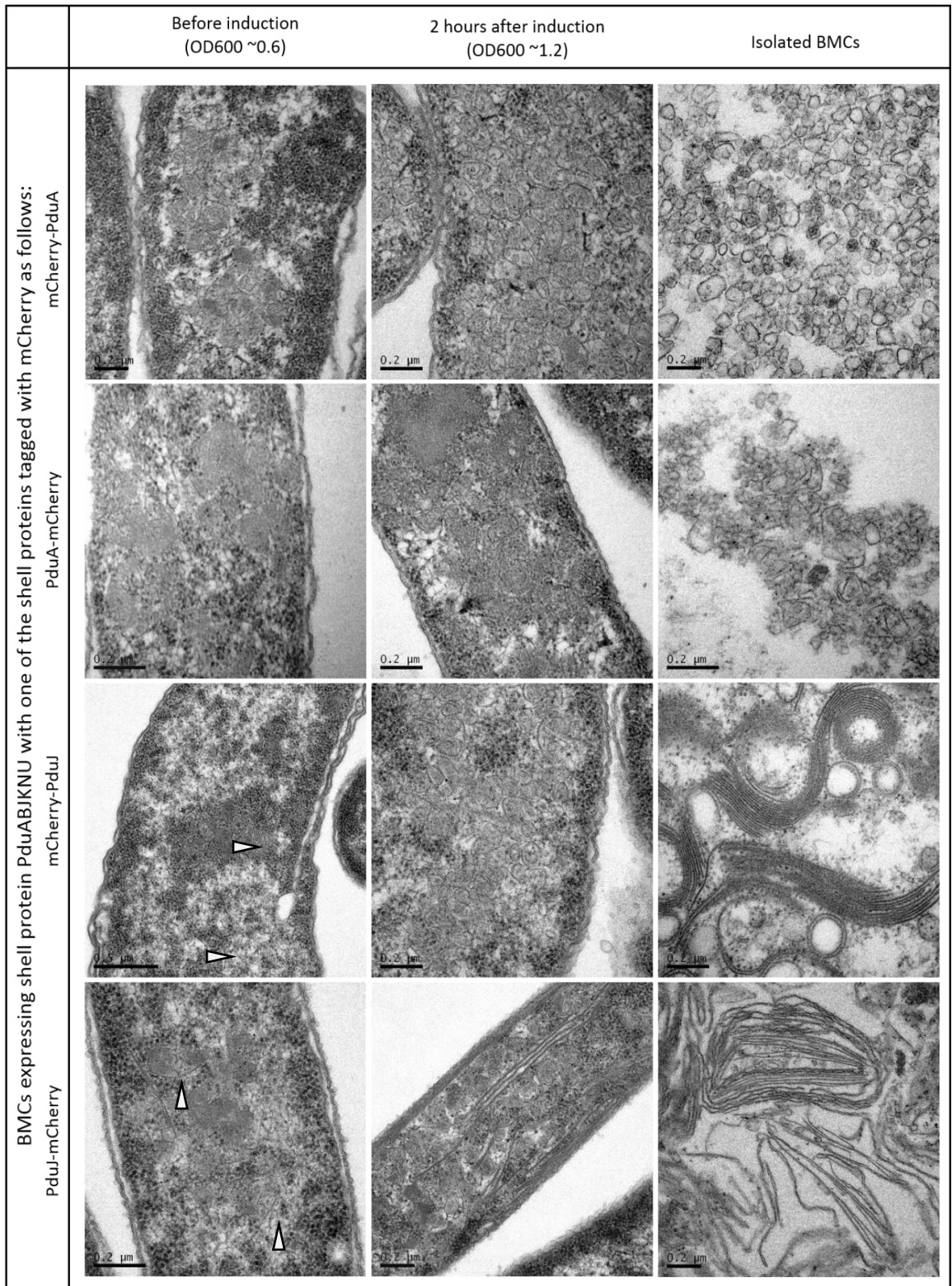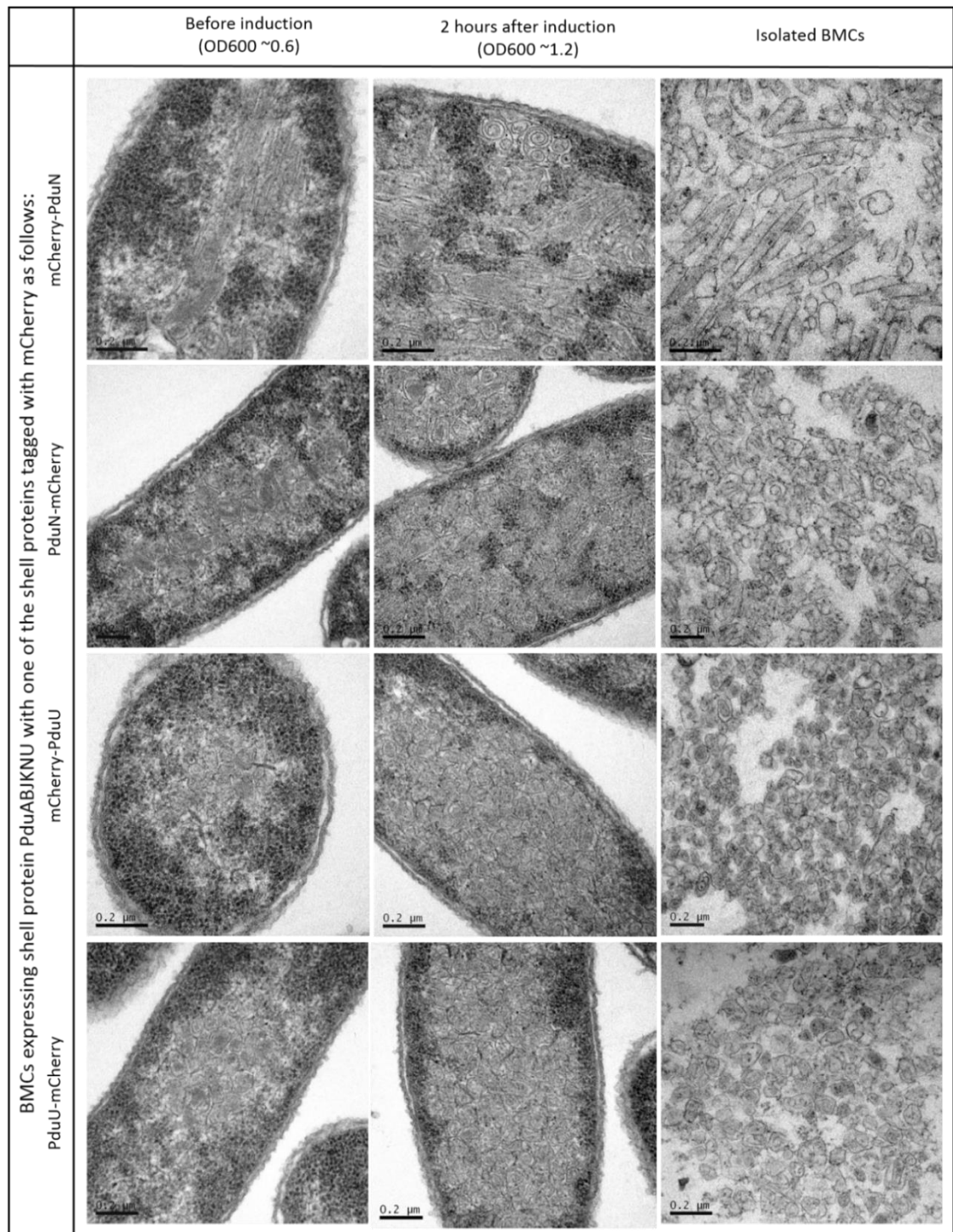
Figure 4.11. TEM analysis of whole cell thin sections and thin sections of pellet 2 from the purification process. The BL21(DE3) pET3a cells analysed include the expression of mCherry-PduA-BJKNU (first pane), PduA-mCherry-BJKNU (first pane), PduA-mCherry-PduB-JKNU and PduA-B-mCherry-JKNU. BL21(DE3) pLysS cells include the expression of: PduAB-mCherry-J-KNU (first pane), PduAB-J-mCherry-JKNU (first pane), PduABJK-mCherry-N-U (second pane), PduABJK-N-mCherry-U (second pane), PduABJKN-mCherry-U (second pane) and PduABJKN-U-mCherry (second pane). Samples were taken at 2 time points, directly before induction and 2 hours after induction to compare BMC formation stages. BMCs

were then isolated by the purification method and thin sections of pellet 2 were visualised by TEM, shown in the right-hand column.

It has already been shown in Section 4.2.3.3 that visualisation of the purified fraction of BMCs could not easily be observed by TEM. Therefore, to investigate the stru0cture of mCherry-PduJ BMC shells further, Atomic Force Microscopy (AFM) was used with a hydrophobic MICA surface as outlined in Section 2.5.4. PduAB-mCherry-J-KNU shells were compared to that of mCherry-PduA-BJKNU, shown in Figure 4.12. mCherry-PduA-BJKNU BMCs can clearly be visualised, with a size range of between 75-150 nm, as measured in ImageJ (n=200). In comparison, a variety of structures are present in the mCherry-PduJ purification. The majority of protein appears aggregated and the presence of BMC shells cannot be definitively determined.

mCherry-PduA-BJKNU   PduAB-mCherry-J-KNU
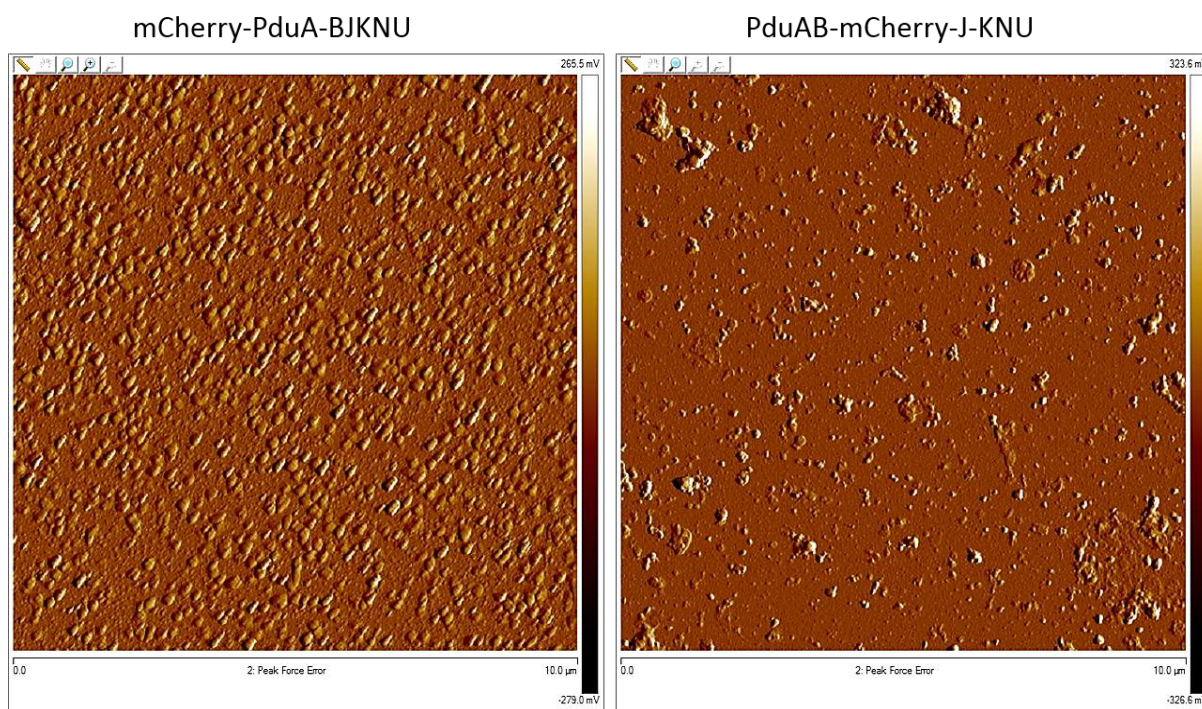
Figure 4.12. Atomic Force Microscopy images of purified mCherry-tagged BMCs. mCherry-PduA-BJKNU and PduAB-mCherry-J-KNU were purified and dried on a hydrophobic MICA surface. They were subsequently analysed by AFM.

Overall live cell imaging and thin sections of whole cells indicate that PduAB-mCherry-J-KNU BMCs are associated with the formation of both intact shells, as well as malformed or broken shell

structures. The shape and size of BMCs are more varied than that of mCherry-PduA BMCs and the visualisation of isolated BMCs shell structures has not been possible. Visualisation by TEM thin sections of pellet 2 was unsuccessful, with long strands of shell protein visible but no icosahedral shell structures. Furthermore AFM of purified mCherry-J BMCs showed aggregated proteins, but no long shell protein strands, nor intact shell structures were observed.

Similarly the visualisation of PduJ-mCherry BMCs by live cell imaging was difficult due to the quick bleaching of mCherry signal. When visualised by TEM before induction, patches associated with shell protein can be seen. Although there were no intact BMC shells present, strands resembling unfolded shell proteins were visualised, as highlighted by the white arrowheads in Figure 4.11. Some curved strands were visualised, although these did not close to form the shell structures. Thin sections of pellet 2 revealed similar linear structures to those observed *in vivo*. Strands thought to be unfolded shell protein were visualised and no intact BMCs were seen. These data indicate that neither N- nor C- terminally tagged PduJ forms intact BMC shells when co-expressed with proteins necessary to form completed structures.

4.2.5.2.3. mCherry-tagged PduN
TEM thin sectioning images of BL21(DE3) *pLysS* cells expressing PduABJ-mCherry-PduN-U revealed unique structures dissimilar to any of the other shells containing an mCherry fusion tag. These structures, as demonstrated in Figure 4.11, were elongated and tubular and were present in cells both before induction as well as after induction. Before induction, these elongated BMCs can be seen in distinct areas in the cell cytoplasm and appear to be open-ended without closure to form an intact structure. After induction, in addition to the tube-like BMCs located throughout the cytoplasm, spiralled BMC shells were also present. TEM of isolated mCherry-PduN shells, once again revealed the presence of tubular BMC shells, the majority of which did not appear to have shell protein at either end of the tubular structure. Interestingly, these elongated, open-ended shells were fairly consistent in width, ranging from 35 nm to 55 nm, measured using ImageJ software.

Cells expressing the C-terminal tagged PduN BMC variant were analysed by TEM and were found to contain mostly intact delineated shells before induction. These shells were fairly regular in size, around ~120 nm, however, the shape tended to be inconsistent with the formation of rounded structures as well as more regular BMC-like structures similar to those observed with mCherry-A-BJKNU BMCs. After induction cells were packed with irregular, misshaped and broken BMC shells. It was difficult to visualise any intact structures. This indicates that formation of PduN-mCherry BMCs was dependent on shell protein concentration, with the overproduction of shell proteins resulting in a lack of intact structures.

4.2.5.2.4. mCherry-tagged PduU

Live cell imaging of tagged-PduU BMCs revealed that discrete foci could be seen before induction in some cells, but after induction the mCherry signal was largely cytoplasmic, although foci could still be visualised, especially with the N terminal tag. However TEM thin sectioning results before and after induction were very interesting. For both PduU-tagged BMCs, before induction discrete areas of BMC shells were observed. BMCs appeared to be intact and regular in size and shape. After induction, cells were packed with intact shells, ranging from ~60 – 150 nm in size. Shells appeared very similar to those observed in the control strain, BL21(DE3) *pET3a pLysS-mCherry-PduA-BJKNU* and are therefore considered to be forming intact BMC structures. The difference in live cell imaging between tagged-PduU BMCs and the control is therefore unclear, however this could be due to mCherry expression levels or the difference in abundance of PduA compared with PduU.

As previously mentioned, it is unclear if mCherry-tagged PduU is incorporated into the BMC structure, as the live cell imaging results revealed that the signal was largely cytoplasmic.

4.2.8. Immuno-gold labelling of thin sections of whole cells and isolated BMCs

To determine if the mCherry-tagged shell protein was incorporated into the BMC shell, and to also investigate the location of the mCherry-tagged shell protein in the BMC structure, immuno-gold

labelling was carried out from both thin sections of whole cells as well as isolated BMCs. This involved growing cell 250 ml cell cultures from inoculation by an overnight starter culture and growth at 37°C in a shaking incubator at 180 rpm. Cultures were induced when an OD 600 of 0.6 – 0.8 was reached. After induction with 100 μM IPTG, cells were grown at 19°C for 2 hours. 25 ml of cells from each culture were then harvested by centrifugation at 4000 rpm and then fixed for TEM thin sectioning and immuno-gold labelling according to Section 2.5.3. In addition, the remaining ~200 ml cell cultures were grown overnight, and purified as described in Section 2.2.7.2. Pellet 2 of the purification process was then prepared for immuno-gold labelling using the same protocol as whole cell Immuno-gold labelling. The strains initially grown for TEM include: BL21(DE3) pET3a *pLysS-mCherry-pduA-BJKNU*, BL21(DE3) *pET3a pLysS-pduABJKNU* and BL21 (DE3) *pLysS pET3a-pdu-ABJKN-mCherry-U.*

Results of immuno-gold labelling using an anti-mCherry polyclonal antibody does not appear to be conclusive. It has been found that there are several limitations when using this method to analyse BMC shells either *in vivo* or *in vitro*. The negative control shown in Figure 4.13, image A, lacking exposure to the primary antibody, does not appear to have any unspecific binding. When ~100 cells were observed, <5 cells had any gold particles at all, and those that did had a maximum of 2 particles per cell. This indicated that there was very little unspecific binding. However the second negative control, containing a construct with BMC shells, but no mCherry tag, revealed gold labelling surrounding the outer membrane of the cell wall, Image B. There was no gold labelling within the cell cytoplasm or attached to BMC shells. When cells expressing mCherry-PduABJKNU were imaged, some gold label localised to the outer membrane of the cell, however gold labelling could be seen in discrete areas with low electron density, Image C. These areas are highly likely to contain BMCs, however staining was not possible as the density of the gold particles was lost, making it the visualisation of the labelling compared to the location of the shells unattainable.

In comparison, labelling of Pdu-ABJKN-mCherry-U BMCs resulted in more gold particles associated with the outer membrane of the cell compared to the BMC shells in the cytoplasm, Image D. Gold particles associated with areas of low electron density were thought to have attached to the mCherry-PduU component of the shell. However as the sections could not be stained in the same way as conventional TEM, it was difficult to visualise both the location of the gold and the BMC shells in the same cell.

Similarly, immuno-gold labelling of isolated BMC shells were inconclusive. The location of BMC shells compared to the gold could not be determined due to the staining method. Unfortunately due to time contraints this experiement was only carried out once. Further optimisation of the immuno-gold labelling of thin sections is therefore required.
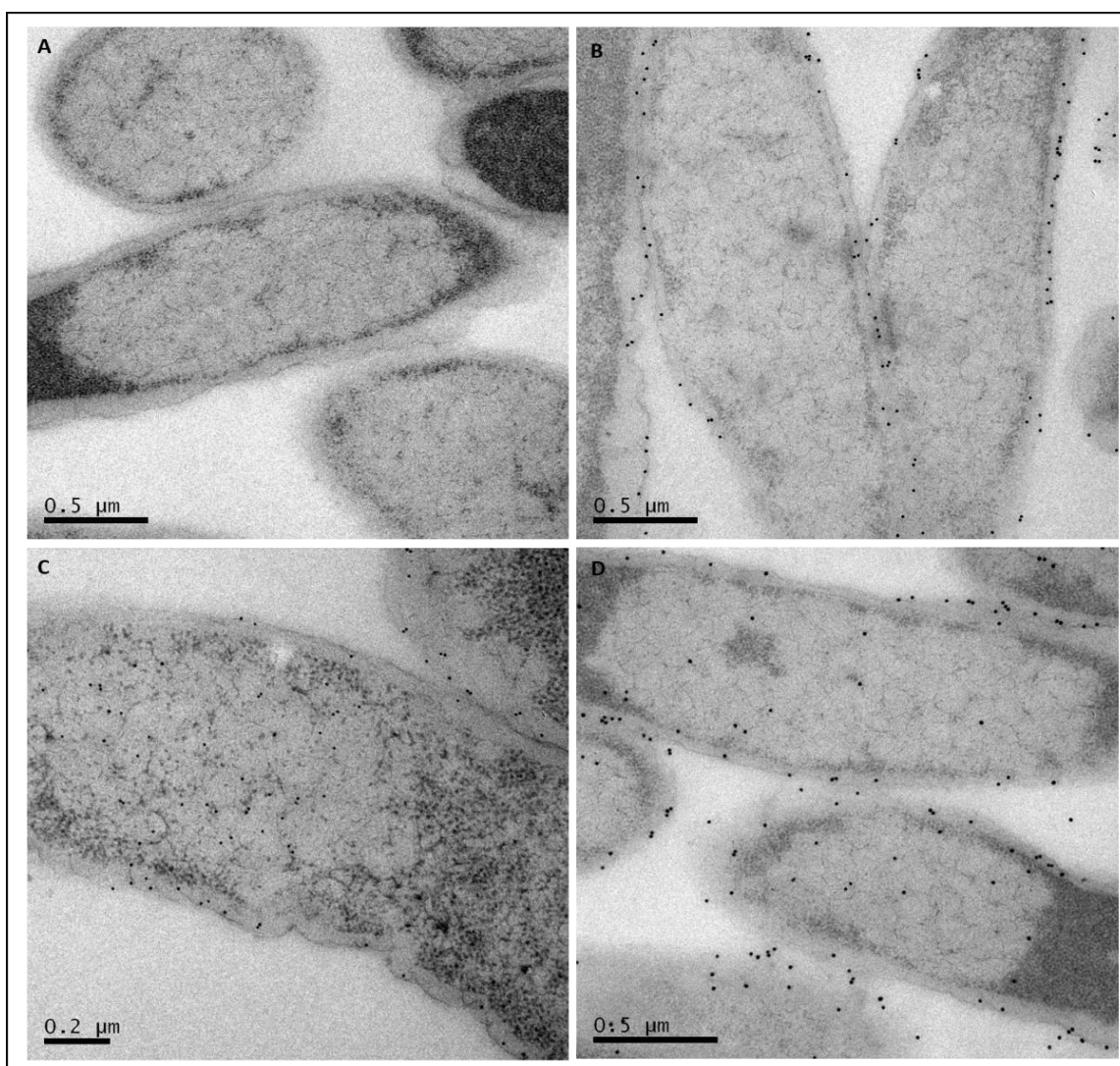
Figure 4.13. TEM thin sections of whole cells prepared for immune-gold labelling using 15 nm gold particles conjugated to an anti-Rabbit secondary antibody. The primary antibody used was anti-mCherry. A) Negative control of BL21(DE3) *pET3a pLysS-mCherry-pdu-ABJKNU* with no primary antibody used in the labelling process, B) Negative control, BL21(DE3) *pET3a pLysS -pdu-ABJKNU* with no mCherry present to test for unspecific antibody binding, C) Positive control BL21(DE3) *pET3a pLysS-mCherry-pdu-ABJKNU* including primary antibody D) BL21(DE3) *pET3a pLysS-pdu-ABJKN-mCherry-U.*

4.2.9. Co-expression with PduV-Cerulean

To investigate the relationship between PduV and the BMC shell, mCherry-tagged BMCs were expressed with PduV-Cerulean. Live cell imaging was subsequently used to study the respective localisation of mCherry and Cerulean fluorescent signal. The BMC tagged-variants studied involve those that were found to form similar structures to that of the control, mCherry-PdA-BJKNU. These include shells comprised of the following shell protein tags: PduA-mCherry, mCherry-PduJ, PduJ-mCherry, mCherry-PduN, PduN-mCherry, mCherry-PduU and PduU-mCherry.

Initially, FRET was going to be used to determine possible interactions between the shell proteins and PduV. However due to supervisory problems it was not possible to carry out these experiments to achieve a complete data set. Preliminary experiments explored the comparative localisation of PduV and PduA by FLIM FRET, suggesting that the two were located within a small distance (a few nm) of one another.

FLIM FRET differs from traditional FRET in that the FRET effect is determined by a shortening of the lifetime of the donor flurophore rather than the measurement of the emission intensity of the acceptor fluorophore. This allows for greater precision as traditional emission based measurements can be susceptible to other external factors such as variations in protein expression.

4.2.9.1. Live cell imaging results of PduV with each tagged shell protein

To explore the localisation and presence of PduV and PduV-associated filaments in comparison to mCherry-tagged shell proteins, BL21(DE3) cells co-expressing PduV-Cerulean with each mCherry-

tagged BMC were visulaised by live cell imaging. Strains were grown in 5 mL starter cultures overnight from several colonies on an agar plate, as outlined in Section 2.2.2.2. The starter culture was then used to inoculate 25 mL of LB media and the resulting cultures were grown at 37°C until an OD_{600} of between 0.4 and 0.6 was reached. Cells (1 mL) were then harvested and prepared for live cell imaging with agar pads, as outlined in Section 2.5.1.

mCherry-tagged BMCs have previously been described earlier in the chapter (4.2.5.1). BMC variants from strains co-expressing PduV-Cerulean appear to be very similar to those previously described, with the exception of PduABJKN-mCherry-U. The mCherry signal from this strain, with N-terminally tagged PduU, localises to highly enlarged foci with some background cytoplasmic signal when co-expressed with PduV-Cerulean, Figure 4.14. In comparison foci visualised in a strain expressing the mCherry-PduU tag in the absence of PduV appeared smaller and more evenly distributed throughout the cell. This difference could be a result of a possible interaction between PduU and PduV. Live cell imaging results of the overlap image of PduV-Cerulean and mCherry-PduU shows clear colocalisation between the two fluorescent signals, indicating an interaction between PduU and PduV. This is shown by the white foci as the arrowheads demonstrate. Interestingly there are no PduV filaments in this strain, indicating that an N terminal PduU tag impairs the function of PduV, although the mechanism for this is unknown. PduV also appears to be largely cytoplasmic, shown by the Cerulean signal spread throughout the cells. This could be due to the inability of PduV to polymerise into a filamentous structure or attach to other filaments in the cell.

Similarly there are no PduV filaments in the C terminally tagged PduU, with the majority of the Cerulean signal localising throughout the cell cytoplasm. The mCherry signal in this strain also appears to be largely cytoplasmic, as was the case with the strain expressing PduABJKN-U-mCherry BMCs without PduV-Cerulean (Figure 4.10). However TEM analysis revealed that BMC shells were able to form intact structures when PduU was tagged with mCherry. This indicates that either the cells are packed with BMC shells causing cytoplasmic signal, or not all of the mCherry-tagged PduU

is incorporated into the BMC structure. Results also suggest that PduV is somehow prevented from forming or attaching to as filaments were not visible when PduV-Cerulean was co-expressed with PduU-mCherry BMC variants. Similar to the N-terminal PduU tag, PduV-Cerulean localisation in the PduU-mCherry strain is associated with a high background level of Cerulean signal in the cytoplasm. Some of the signal localises to discrete foci, which in the composite image can be seen to mostly overlap with mCherry foci in the cell. This suggests that even though PduV function may be impaired due to the complete lack of filaments, PduV is still able to localise to BMCs when PduU is tagged.

Interestingly, in addition to PduU, BMC shells formed with mCherry-tagged PduJ are associated with impaired PduV function. A strain co-expressing PduAB-mCherry-J-KNU with PduV-Cerulean is shown in Figure 4.15. Markedly, filaments appear highly elongated in this strain with filaments often spanning the length of the cell. In comparison there are no PduV-Cerulean associated filaments present with the PduJ-mCherry BMC tag. However despite the lack of filaments, unlike the PduU tags, PduV does not appear to be cytoplasmic as when co-expressed with mCherry-tagged PduJ, but instead localises predominantly to discrete foci that overlap with the localisation of mCherry signal in the composite image. Therefore, despite the presence of either elongated filaments, or no filaments at all, BMCs formed with tagged PduJ are still seen to localise with PduV-Cerulean, which is also the case with tagged PduU. The reason why there is an absence of filament formation or an elongation in filament length is currently unknown.

BMCs formed with the mCherry-tagged shell proteins; PduA-mCherry and mCherry-PduN and PduN-mCherry contain structures very similar to that of the control strain with mCherry-PduA when co-expressed with PduV-Cerulean. Although the localisation of mCherry signal is different to that of the control, as described in Section 4.2.5.1, filamentous structures were visualised in all three strains. In addition to filaments, PduV was also seen in foci which were evenly distributed throughout the cells in strains expressing BMCs variants with PduA-mCherry and mCherry-PduN

tags. The PduN-mCherry BMC strain appeared to have a higher level of cytoplasmic PduV-Cerulean signal; although filaments were still present there was a large reduction in the number of PduV-Cerulean foci per cell. The mCherry signal in the PduN-mCherry strain was also largely cytoplasmic, with a few larger foci per cell rather than many, evenly distributed smaller foci. This indicates that the localisation of PduV corresponds to the localisation of the BMCs, especially when the Cerulean and mCherry images are overlapped showing co-localisation of BMCs with PduV foci. PduV-Cerulean was also shown to co-localise with BMC shells containing either PduA-mCherry or mCherry-PduN.

Overall, co-expression of mCherry-tagged BMCs with PduV-Cerulean leads to varying results depending on the specific shell protein that is tagged, as well as the terminus that mCherry is fused to. PduV-Cerulean is seen in linear structures in strains containing; mCherry-PduA, PduA-mCherry, mCherry-PduJ, mCherry-PduN and PduN-mCherry. BMCs with a C-terminal PduJ tag as well as PduU tagged on either terminus with mCherry do not contain filaments when co-expressed with PduV-Cerulean. Interestingly, cells expressing BMCs with mCherry-PduJ were associated with highly elongated PduV filaments. These data suggest that both PduJ and PduU are involved in an interaction nbetween the BMC and PduV, or the polymerisation of PduV into filaments. Disruption of this process by the addition of an mCherry protein fusion led to either the absence of linear structures or elongated filaments.

Composite

mCherry

Cerulean

Phase

A

B

mCherry-PduA-BJKNU

PduA-mCherry-BJKNU

Composite | mCherry | Cerulean | Phase

PduAB-mCherry-J-KNU

PduAB-J-mcherry-KNU

PduABJK-mcherry-N-U

PduABJK-N-mcherry-U

Composite   mCherry   Cerulean   Phase
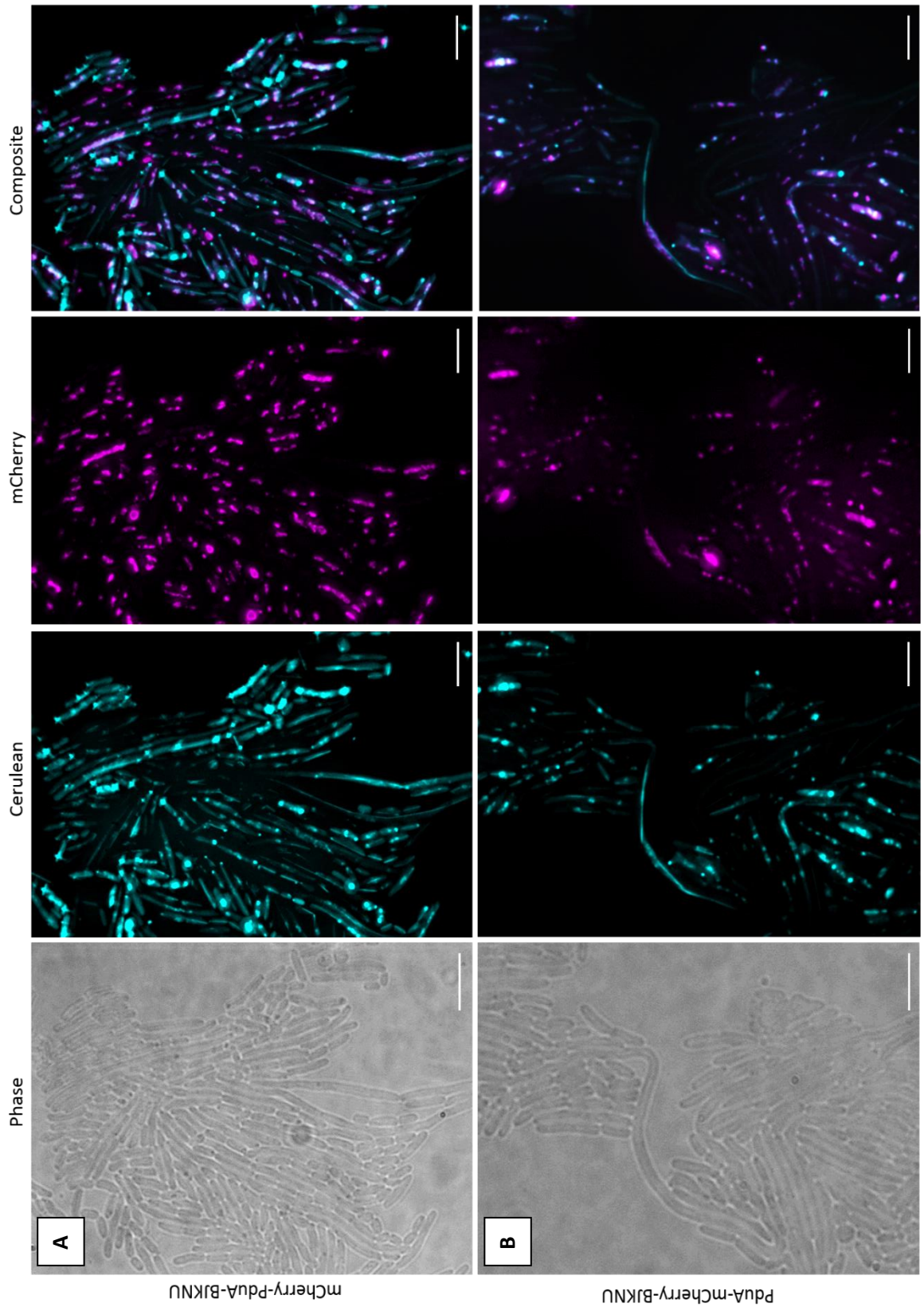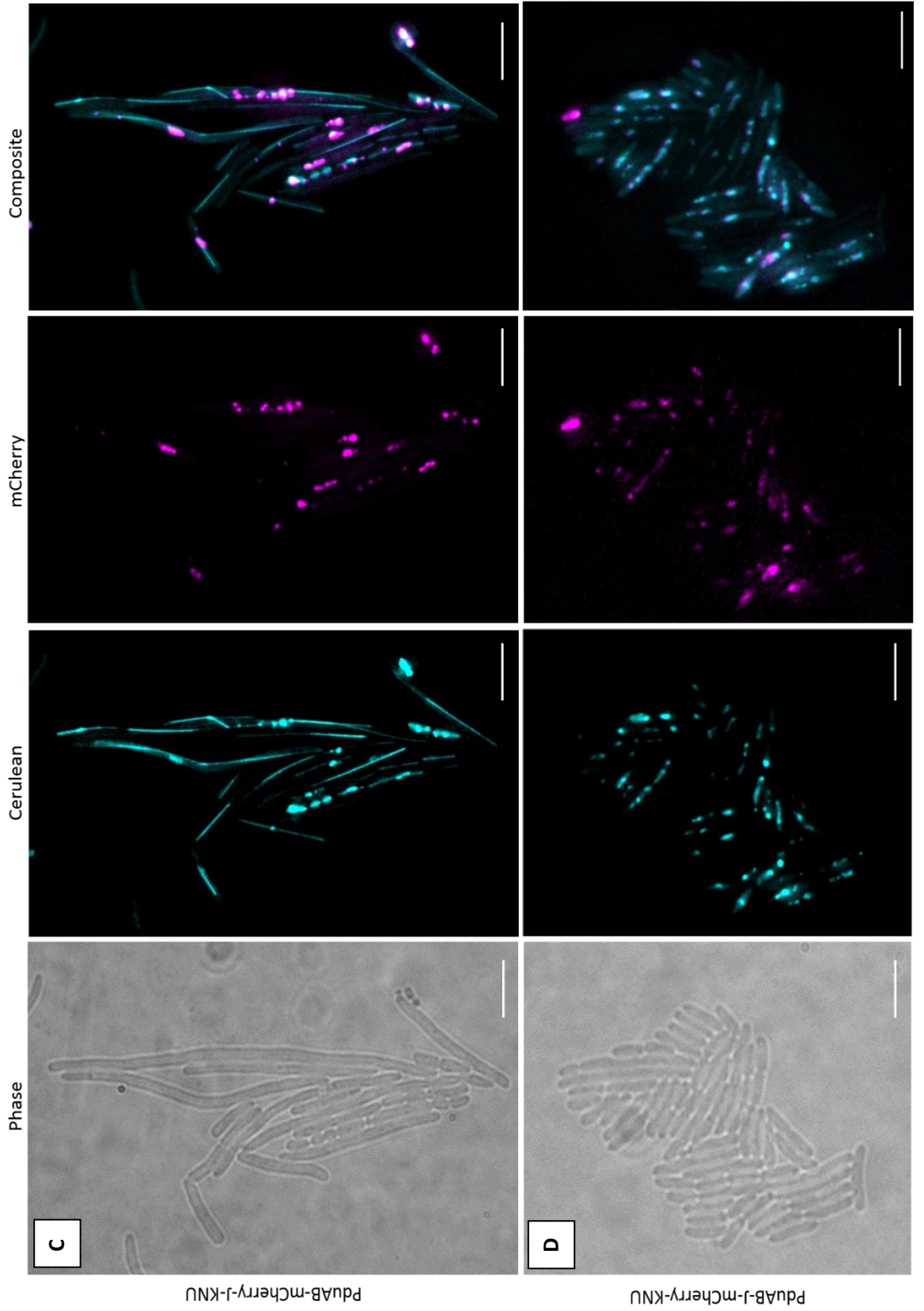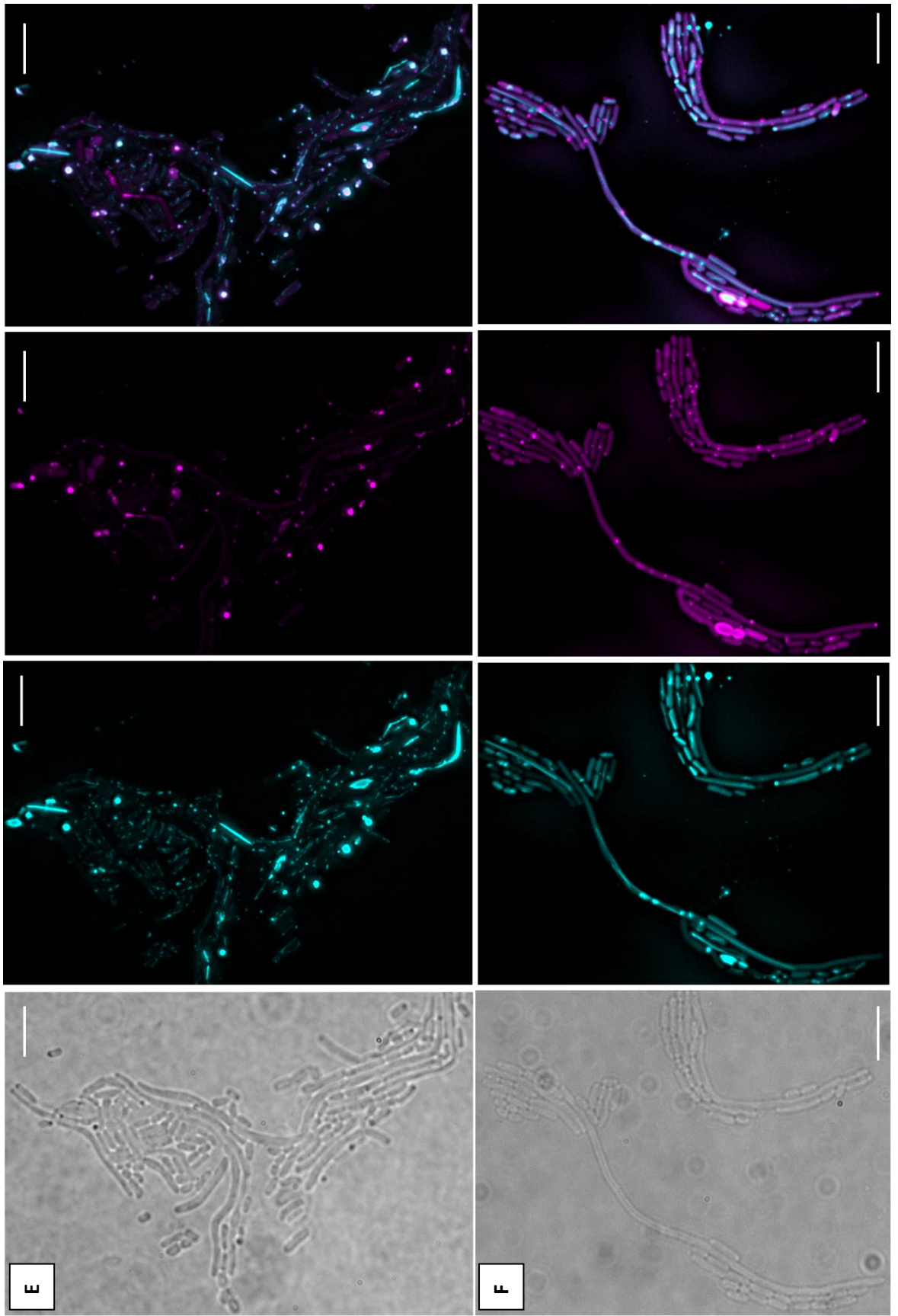
PduABJK-N-mcherry-U
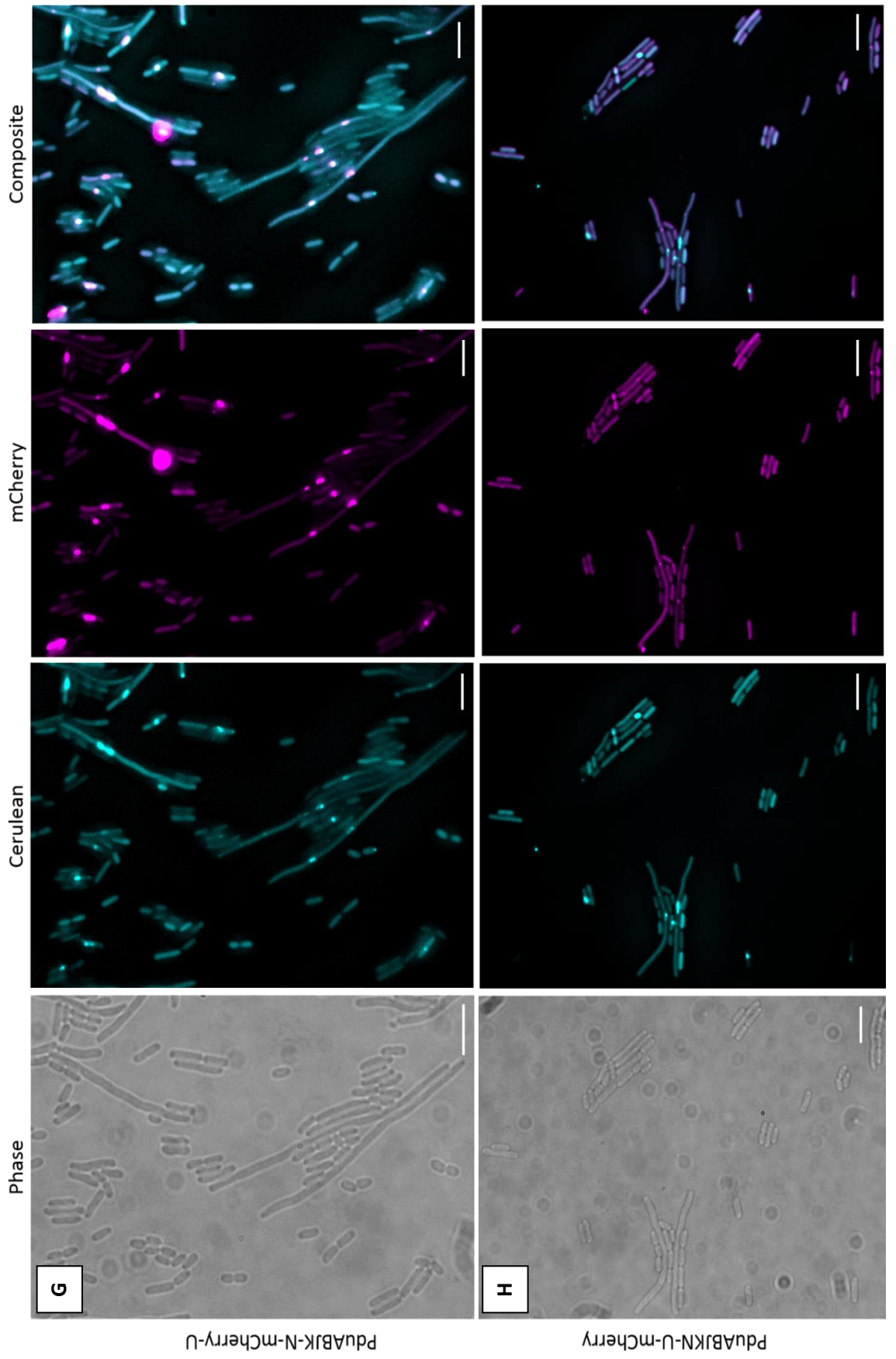
PduABJKN-U-mcherry

Figure 4.14. Investigating the effect of each mCherry tagged empty BMC variant on the localisation and organisation of PduV within the cell. **A)** BL21(DE3) *pET3a-pduV-cerulean pLysS-mCherry-pduA-B-JKNU*, **B)** BL21(DE3) *pET3a-pduV-cerulean pLysS-pduA-mCherry-BJKNU,* **C)** BL21(DE3) *pLysS-pduV-cerulean pET3a-pduAB-mCherry-JKNU,* , **D)** BL21(DE3) *pLysS-pduV-cerulean pET3a-pduA-mCherry-B-JKNU,* **E)** BL21(DE3) *pLysS-pduV-cerulean pET3a-pduABJK-mCherry-N-U,* **F)** BL21(DE3) *pLysS-pduV-cerulean pET3a-pduABJKN-mCherry-U,* **G)** BL21(DE3) *pLysS-pduV-cerulean pET3a-pduABJKN-mCherryU,* **H)** BL21(DE3) *pLysS-pduV-cerulean pET3a-pduABJKN -U-mCherry,* were analysed by live cell imaging directly before induction and also 2 hours after induction. Scale bar represents 5 μm.

4.2.9.2. PduV filament length analysis

Whilst looking at the effect of tagging each Pdu MCP component with mCherry on the localisation of PduV, it was noticed that in some of the strains where filaments were observed, the length of these filaments varied from that of the control strain expressing mCherry-PduA. In order to examine this in more detail, images were then processed in MetaMorph software to calibrate distance per pixel and allow the accurate measurement of filament length. Data for filament length was collected in Microsoft Excel and grouped to be able to plot a histogram. OriginLab was subsequently used to plot the data to a LogNormal fit. The plots for this data, as well as a summary of the effect of mCherry tags on filament formation is shown in Figure 4.15 below.

Results show that when fitted to a LogNormal distribution, the average PduV-Cerulean-associated filament length with BMCs containing mCherry-PduA is 2.16 μm (n=369). The histogram demonstrates that filament length ranges from approximately 1 μm to 9 μm. Tagging PduA at the C-terminus had no immediately noticeable effect on PduV filament length within the cell. When analysed the filament length was found to increase to 2.53 μm (n=209). To determine whether this was a statistically significant increase, a two tailed, unpaired Student's T-Test was carried out between the two complete data sets, and using a level of significance (*p*) value of 0.05 it was found this was not a statistically significant difference (p=0.69). When looking at the histogram, it was noted that the range of filament lengths was greater, with filaments up to 14 μm observed.

The addition of an mCherry tag to the N-terminus of PduJ had a visible effect on the length of PduV-Cerulean-associated filaments, with the filaments clearly being much longer. When analysed it was found that the average length was 4.95 µm (n=316), with filament lengths ranging from 1 µm to 29 µm, over 3 times longer than that observed with filaments containing mCherry-PduA. Again to determine whether this was a statistically significant increase, a Student's T-Test was carried out (between this dataset and that of mCherry-PduA) and it was found this was a statistically significant difference (p=1.57 x10^{-29}).

PduN provided a very interesting finding, with the effect on PduV-Cerulean-associated filaments varying depending upon where PduN was tagged. The addition of mCherry to the C-terminus had little effect, with the average length increasing to 2.50 µm (n=242). However Student's T-Testing revealed that this was a statistically significant difference (p=0.0004). The range of filament lengths was also less spread out, ranging from 0.5 µm to 9µm. The addition of an mCherry tag to the N-terminus of PduN resulted in PduV-Cerulean-associated filaments being much shorter. The average filament length was reduced to 1.02 µm (n=99), which Student's T-Testing revealed to be a statistically significant finding (p=8.65 x10^{-53}), while filament lengths ranged from 0.3 µm to 2.9 µm.

A summary of all average filament lengths, Standard Errors of Mean (SEMs) and filament length ranges is shown in Figure 4.15(B). The finding that the addition of a fluorophore to the Pdu shell proteins could affect the length of PduV, and that this effect could differ based on whther the flurophore was at the N or C terminus of the shell protein was of interest as it suggested that there could be as yet unidentified regulatory mechanisms in the formation of PduV filaments. The fluorescent tagging could potentially either be directly affecting the interaction of the tagged shell protein with PduV, or perhaps the effect it is having on the structure/formation of the BMC shells is in turn affecting the regulation of PduV filement length.

A

PduAB-mCherry-J-KNU Pduv-Cerulean
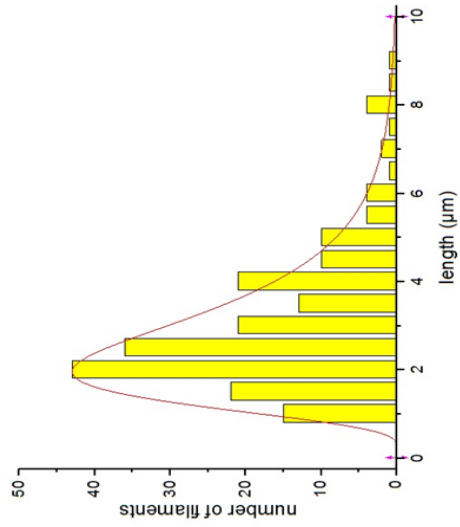
PduA-mCherry-BJKNU Pduv-Cerulean

mCherry-PduA-BJKNU Pduv-Cerulean

PduABJKN-mCherry-U Pduv-Cerulean
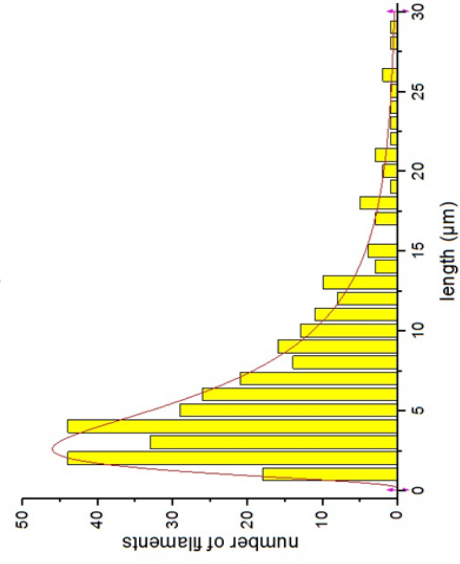
PduABJK-mCherry-N-U Pduv-Cerulean
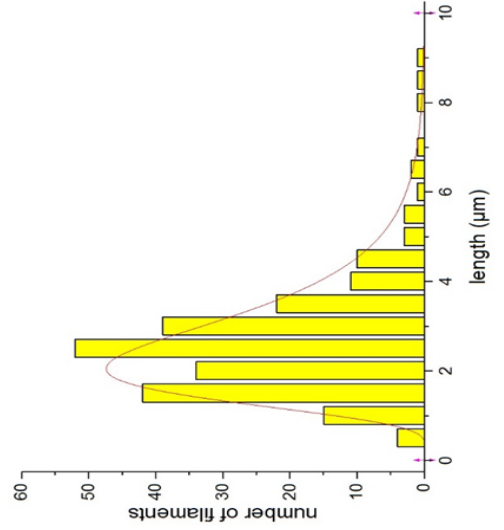
B

Tagged Pdu Protein	Average Filament Length (μm)	Filament Length Range (μm)
mCherry-PduA	2.16 ± 0.05	1-9
PduA-mCherry	2.53 ± 0.19	0.5-14
mCherry-PduJ	4.95 ± 0.36	1-29
PduJ-mCherry	No Filaments	N/A
mCherry-PduN	1.02 ± 0.03	0.3-2.9
PduN-mCherry	2.50 ± 0.11	0.5-9
mCherry-PduU	No Filaments	N/A
PduU-mCherry	No Filaments	N/A

Figure 4.15. The effect of tagging shell proteins of the Pdu MCP on the length of PduV associated filaments in the cell. A) Histograms showing the range in length of PduV-Cerulean-associated filaments in cells expressing mCherry-PduA, PduA-mCherry, mCherry-PduJ, mCherry-PduN and PduN-mCherry. Line of best fit was plotted using a LogNormal plot. B) Table showing the average filament length (with Standard Error of Mean (SEM)), and the range of filament lengths when each mCherry tagged variant is expressed in the Pdu shell.

4.2.10. Analysis of PduV with as, aBj, abjk, abjkn, abjknu, microscopy results

Previous studies have shown that the presence of PduV associated filaments within *E. coli* is dependent upon the expression of empty Pdu BMC shells (Parsons et al. 2010). However, it is not known whether it is the presence of the whole shell, or certain shell proteins which are required. To explore this a series of experiments were carried out using constructs expressing different shell proteins to determine which were necessary for filament formation. PduV-Cerulean was co-expressed in cells expressing PduAB, PduABJ, PduABJK, PduABJKN and PduABJKNU. Strains were grown in 5 mL starter cultures overnight from several colonies on an agar plate, as outlined in

Section 2.2.2.2. The starter culture was then used to inoculate 25 mL of LB media and the resulting cultures were grown at 37°C until an OD_{600} of between 0.4 and 0.6 was reached. Cells (1 mL) were then harvested and prepared for live cell imaging with agar pads, as outlined in Section 2.5.1.

As expected, when expressed in the presence of PduABJKNU (the previously described empty shell) PduV-associated filaments were observed and PduV was distributed to Foci throught the cell, as shown in Figure 4.16. When expressed in the presence of PduAB and PduABJ, no filaments were observed and PduV was shown to be cytoplasmic and often accumulating to one intense Foci. Interestingly when PduABJK was expressed filaments were observed, which are highlighted by white arrows in Figure 4.16. This suggested that it was perhaps PduK that was required for PduV to either associate with pre-existing filaments, or to polymerise to form filaments. It was expected that filaments would also be observed in the presence of PduABJKN, however surprisingly no filaments were observed w0ith PduV accumulating into large, intense foci, again shown in Figure 4.16.
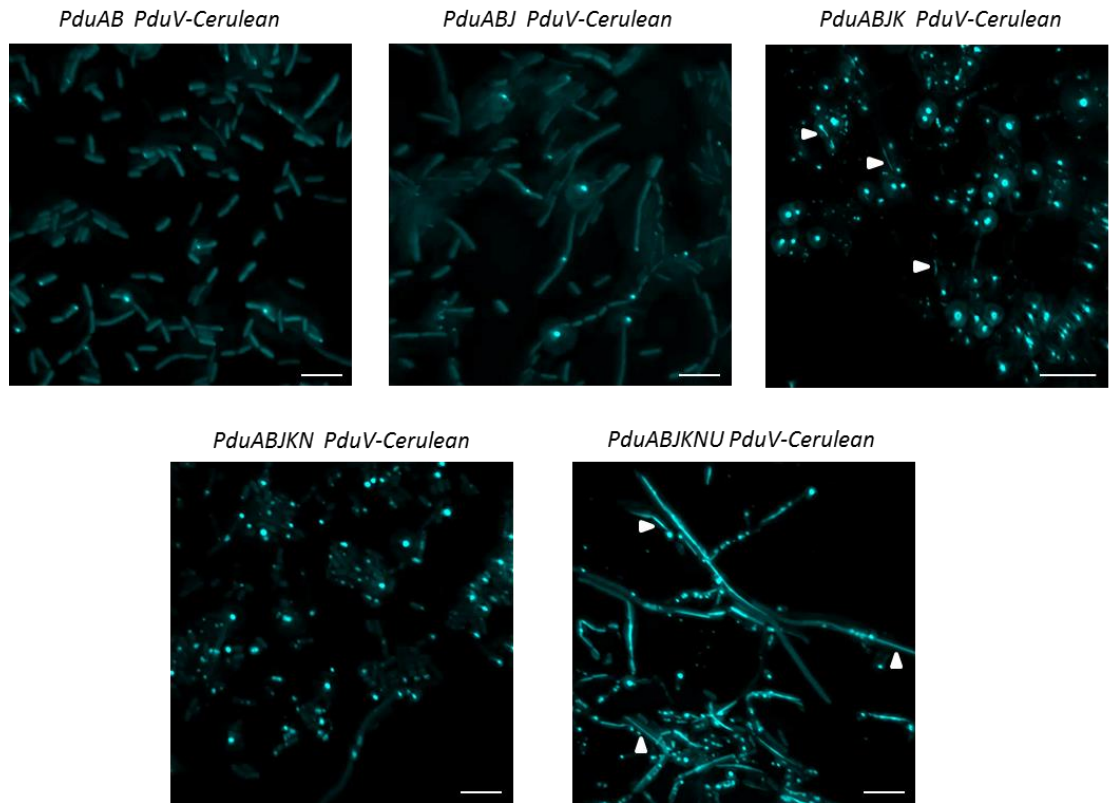
Figure 4.16. Investigating which Pdu shell proteins are required for the presence of PduV-associated filaments. L21(DE3) *pET3a-pduV-cerulean pLysS-pduAB*, BL21(DE3) *pET3a-pduV-cerulean pLysS-pduABJ,* BL21(DE3) *pLysS-pduV-cerulean pET3a-pduABJK,* BL21(DE3) *pLysS-pduV-cerulean pET3a-pduABJKN* and BL21(DE3) *pLysS-pduV-cerulean pET3a-pduABJKNU,* were analysed by live cell imaging. White arrows highlight the presence of PudV filaments. Scale bar represents 5 μm.

4.3. Summary

It became clear from the characterisation of PduK that fusions of YFP to either the N- or C- terminus of the protein prevented the protein from participating in the correct folding of the BMC. Although the fusion of mCherry to the N-terminus of PduA allowed for its correct incorporation into a folded BMC, it seemed prudent to investigate whether any of the remaining shell proteins could be tagged with a fluorescent protein. In this respect it was decided to investigate the effect of fusing mCherry to either the N- or C- terminus of PduB, J, N and U. In terms of being able to use super-resolution approaches to investigate the structure of BMCs it is important to know which shell proteins can be modified.

To address this problem required a significant amount of recombinant DNA technology. Firstly each of the genes for the various shell proteins had to be engineered such that the gene encoded for an mCherry fusion at either the N- terminus or C-terminus. These engineered shell protein constructs then had to be cloned into a plasmid containing genes for the other shell proteins. Moreover the genes for the shell proteins had to be cloned in the order of *pduABJKNU.* Only after this had been accomplished would it be possible to look at the effect of the fusions upon BMC formation.

The cloning allowed unexpected and frustrating observations to be made. Uppermost among these was that differences could be seen when the genes were incorporated into either a *pET3a* or *pLysS* vector (Figure 4.2). Normally *pET3a* is the main vector that would be used for expression studies. In contrast *pLysS* has been used as a compatible plasmid to allow for the use of two plasmids in *E. coli.* The vector was developed so as to allow the production of lysozyme, which acts as a natural repressor of the T7 polymerase. However what was observed in the studies reported herein was that more successful production of BMCs was observed either when the BMC shell genes were cloned into *pLysS,* or it was co-transformed with the genes on a *pET3a* plasmid (Figure 4.4 and 4.5). A study of the protein profile of strains containing either *pET3A* or *pLysS* variants showed that protein synthesis was successful in both cases, but BMC formation was more favoured in the presence of *pLysS*. It may be that lysozyme helps to reduce the activity of the T7 promoter, reducing stress within the *E. coli* cell and allowing more successful folding of the BMCs. This could also explain why more fluorophore is observed with *pLysS,* as the reduced cell stress response allows for more correct folding of the fluorophore. However it is interesting to note how difficult it is to get standardisation of expression within the *E. coli* system.

The construction of the various shell protein-mCherry fusions eventually allowed for a full characterisation of the various strains harbouring the relevant constructs. What was most interesting to observe was that really only the mCherry-PduA and mCherry-PduU constructs allowed proper BMC formation (Figure 4.11). All other combinations resulted in formation of

aberrant structures. This highlights how fortunate it was that the mCherry-PduA worked, as this was the first such fusion to be made. However it also highlights that the attachment of the comparatively bulky mCherry to the shell proteins generally results in mal-formation of the compartment, presumably through either improper folding or through steric hindrance in the "tiling" that takes place to make the shell.

The most interesting observations of the effects of the mCherry-fusions on BMC formation came from the images of the isolated BMC fractions (Figure 4.11). In fact, it proved technically challenging to isolate the BMCs, but the purification was made slightly eaiser due to the colour associated with the presence of the mCherry. The procedure for the isolation of the BMCs had to be modified as each construct led to the BMCs separating into slightly different fractions. Nonetheless it was possible to gain very clear images of fully intact BMCs, BMCs that had not quite closed, BMCS in various stages of folding and some large filaments (Figure 4.11).

From these experiments we can start to make some generalisations concerning the shell proteins. For PduA, the C-terminal region is more sensitive to modification than the N-terminus. It would seem likely that the C-terminal region plays a role in the shell protein-shell protein interaction. PduB cannot be modified at all, suggesting that it plays a major role within the facet of the overall structure. This is consistent with previos findings that highlighted the importance of PduB and B' in the formation of the BMC shell (Cheng et al. 2011). PduJ plays a role in preventing longer filaments forming, filaments that can form with PduA alone. It seems likely that PduJ is required to help in protein sheet formation, preventing the formation of PduA and possibly PduB into long filaments. PduN plays a key role in closing the BMC by providing the vertices for the structure. The spectacular image of long drawn out BMCs with the PduN-mCherry only go on to confirm this role (Figure 4.11). The effect of fusions on PduU are less obvious, especially as BMCs can form in the absence of PduU.

As well as the effects on the shape and formation of BMCs of tagging shell proteins, potential new regulatory mechanisms for shell proteins in the formation and length of PduV filaements were observed. Of particular interest was the finding that the tagging of PduU at either its N or C-terminus, or the absence of PduU from the operon resulted in the abolition of PduV filaments. Having been previously been shown to be non-essential in the formation of empty BMC shells (Parsons et al. 2010) this finding gives provides insight as to why PduU exists and the role it plays in the overall Pdu metabolome.

Chapter 5: The Characterisation of PduV

5.1. Introduction

Within eukaryotic cells there is a cytoskeleton of filamentous structures which play key roles in a diverse variety of cellular processes including maintenance of cell structure, intracellular transport of cargoes, endocytosis and chromosome segregation. This network is predominantly made up by the filaments of two proteins, actin and tubulin. Actin and tubulin filaments are formed by the polymerisation of globular actin or tubulin monomers to form the filament (Wegner 1976)(Summers & Kirschner 1979). A key characteristic of this process is the hydrolysis of the nucleotides ATP and GTP in the case of actin and tubulin respectively (Carlsson et al. 1977; Weisenberg, Deery & Dickinson 1976). More recently, homologues of both actin (MreB) and tubulin (FtsZ) have been identified within bacteria, with the hydrolysis of nucleotides again being required for their polymerisation to form filamentous structures (Bork, Sander & Valencia 1992; Erickson 1995; de Boer, Crossley & Rothfield 1992).

As has previously been shown, the BMC associated protein PduV is observed in linear, filamentous like structures within *E. coli* when co-expressed with the empty Pdu shell (Parsons et al. 2010). Currently it is not known whether PduV is able to polymerise to form filaments, or if it is attaching to existing filamentous structures within the cell. Interestingly sequence analysis of PduV has shown similarities with members of the Ras-like GTPase family of proteins, and preliminary experiments using purified PduV have suggested it may have a weak GTPase activity (Parsons et al. 2010). The fact that PduV is both observed in filamentous like structures, and is predicted to have a weak GTPase activity, suggests that it may also be a component of the bacterial cytoskeleton, in the same manner as MreB and FtsZ.

This investigation aims to further characterise PduV, its ability to exist in filamentous like structures and to determine if this is dependent upon its predicted GTPase activity. To do this, the process for purifying recombinant PduV from *E. coli* was optimised by co-expression with the empty Pdu shell, and the ability for PduV to polymerise into filaments *in vitro* was examined by fluorescence

microscopy. In addition, through the use of sequence alignments with other known GTPase proteins, several amino acids residues believed to be involved in the binding and hydrolysis of GTP were mutated by site directed mutagenesis. These mutants were then examined by fluorescence microscopy to investigate their ability to form filaments *in vivo* and attempts were made at measuring the GTPase activity of PduV and these mutants. Finally, in order to understand further PduV's existence in filamentous structures, thin sections of cells expressing PduV and empty microcompartments were examined by transmission electron microscopy.

5.2. Results

5.2.1. Purification of Recombinant PduV

An N-terminally His-tagged version of PduV was purified by affinity chromatography using a nickel column. This purified PduV could then be used to determine if filaments could be seen *in vitro*. In addition, as PduV is thought to be related to the small GTPase superfamily of proteins, activity assays could be carried out with purified protein to measure any potential GTPase activity associated with PduV.

Initially, a BL21(DE3) strain containing *pET14b-pduV* was grown overnight in a starter culture. 1L of LB media with chloramphenicol was inoculated with 1 mL of starter culture as outlined in section 2.2.2.2. The culture was then grown at 37°C on a shaking platform until an OD600 of 0.8 was reached .Protein expression was induced with IPTG and the growth temperature was dropped to 19°C. The cells were cultured overnight and harvested as described in Section 2.2.5. The cells were resuspended in binding buffer and sonicated, Section 2.2.6.1 and the sonicated lysate was centrifuged and the supernatant was applied to the nickel column, as described in Section 2.2.7.

The protein however was very difficult to purify due to the formation of precipitates during the purification process. When the supernatant was loaded into the top of the nickel column, or shortly after elution, the protein would either form precipitates or crash out of solution entirely. This indicated that PduV is largely insoluble outside of the cellular environment. After the purification was repeated in excess of 5 times with little success, it was decided that a strain expressing PduV-GFP would be cultured and the tagged protein purified. This was done to see if the addition of GFP could improve the solubility of the PduV, in a similar manner to Maltose Binding Protein and other tags, while also allowing the visualisation of any filamentous structures in the purified fraction by live cell imaging.

BL21(DE3) cells with *pET23b-pduV-GFP* were cultured and purified using the same method as previously described. Expression of the protein fusion caused the cells to become green. When the

green lysate was loaded onto the column, the location of PduV on the column could easily be seen, meaning that the majority of the protein eluted from the column could be collected in one fraction, leading to a higher yield of protein. In addition, the PduV-GFP fusion protein was easier to purify as the formation of precipitates did not occur with any of the purification repeats. This suggests that the addition of GFP is beneficial in increasing the solubility of PduV under the conditions used for the purification.

5.2.1.1. Optimisation of PduV Purification

There were 2 main aims for the use of purified PduV. The first was to determine if filaments that had been previously seen through live cell imaging, could be visualised outside of the cellular environment. In addition purified PduV-GFP could also be applied to GTPase assays to establish if PduV has the ability to bind and hydrolyse GTP.

It had already been shown that the addition of a GFP tag to PduV improved the solubility of the protein. The purification method was further optimised for these experiments by co-expressing mCherry-PduA-BJKNU with PduV-GFP using the following strain: BL21(DE3) *pLysS-mCherry-pduA-BJKNU pET23b-pduV-GFP*. This was necessary as PduV has only been visualised in a filamentous structure in the presence of Pdu BMCs, either from expression of the whole *pdu* operon, or by expression of recombinant *pdu*-encoded shell proteins containing the minimum set required for empty BMC formation (Parsons et al. 2010). Therefore by co-purifying PduV-GFP with the Pdu BMC shell it was more likely that filaments would be observed *in vitro.*

This strain was cultured and purified in an identical manner to the PduV-GFP purification protocol described above in Section 5.2.1. Samples were collected throughout the purification process and subjected to SDS PAGE analysis as shown in Figure 5.1 below, with PduV-GFP observed at 47 KDa. A large band can be seen in lane 6 of Figure 5.1 indicating that the final elution was relatively pure. However no distinguishable bands corresponding to shell proteins could be seen in the final elution.
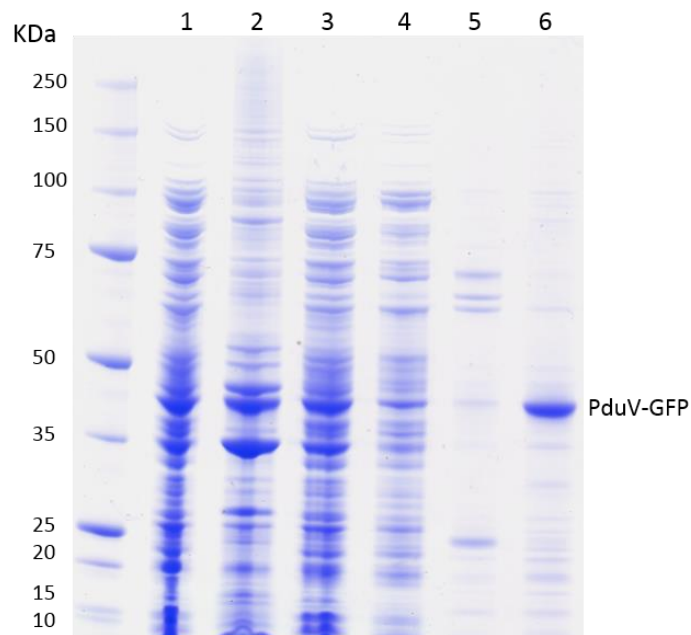
Figure 5.1. Optimising the expression of PduV. 5-20% SDS-PAGE gel showing the purification of PduV-GFP expressed in BL21-DE3 cells. Lane 1 shows the cell lysate after sonication, lane 2 the flow through after loading of the lysate onto the column, lane 3 the flow through after washing the column with binding buffer, lane 4 the flow through after washing the column with wash buffer 1, lane 5 the flow through after washing the column with wash buffer 2 and lane 6 the final elution of purified PduV-GFP from the column.

During the purification of PduV-GFP, in the presence of mCherry-PduA-BJKNU, it was noticed that a large amount of the fluorescent green colouration of the lysate was flowing through the column and into the initial flow-though. This was unusual as the column did not appear saturated with protein and did not occur when PduV-GFP was expressed and purified alone. To investigate why PduV-GFP was flowing through the column a sample of this fraction was quickly applied to a microscope slide and imaged by fluorescent microscopy, Figure 5.2.

Fluorescence imaging revealed that the initial column flow through contained linear structures consisting of PduV-GFP when co-expressed with mCherry-PduA-BJKNU, as can be seen in images B and C from Figure 5.2. The transmitted light image, shown in panel A, indicated that there was no contaminating material (dust, dirt etc.) on the slide that PduV-GFP could have adhered to, to cause the presence of linear structures.

The presence of filaments was observed in the flow-through fraction during a subsequent repetition of the purification of PduV-GFP in the presence of BMCs. In addition the flow through from each subsequent stage in the purification process was collected and imaged, however a filament-like arrangement of PduV-GFP was only seen in the initial flow-through after the cell lysate was loaded onto the column (data not shown). This would suggest that the filaments would also be present in the crude lysate, however when examined prior to application to the nickel column no filaments were observed.

5.2.2. Investigating the ability of PduV to Form Filaments *in vitro*

The filamentous structures observed in the flow-through during PduV-GFP purification gave some indication that PduV-GFP filaments may either be able to exist outside of the cellular environment, or even polymerise *in vitro*. However the conditions necessary for filamentous structures to occur *in vitro* are completely unknown. The fact that these structures were only seen in the initial flow through and not in subsequent washes of the column would indicate that either BMC shells were not present in high enough concentrations further along in the purification, or that PduV needs to be present in a certain concentration for filament formations to occur. It may also indicate that if PduV-GFP attaches to pre-formed filaments in the cell rather than self-assemble, the existing structures did not bind to the column when the cell lysate was loaded and therefore passed into the first flow-through. Therefore subsequent fractions did not contain cellular filaments for PduV-GFP to bind to so none were visualised by fluorescence microscopy.

Nevertheless it was clear that PduV-GFP filaments could be observed *in vitro* in specific conditions. To determine these conditions, a flow cell was created as described in Section 2.5.1.2. A flow cell allows PduV-GFP to be visualised by microscopy while solutions are pipetted onto the microscope slide. The effect can then be seen in real-time. The flow cell was used to add $MgCl_2$ to the sample, in order to see if the addition of Magnesium, which is needed for nucleotide hydrolysis had any effect. Interestingly, the addition of 1 µl of 1M MgCl2 caused the individual foci of PduV-GFP to

clump together into larger, non-linear aggregates. In this case, PduV-GFP was also co-purified with mCherry-Pdu-A-BJKNU and some mCherry foci were also present on the microscope slide. However due to the addition of extra liquid to the slide, it was very difficult to capture an image or timelapse of the protein clumping, therefore this could not be recorded. The addition of GTP was also considered, however as filaments had previously be observed in the sample containing only PduV-GFP it was believed there would be enough GTP within the cell extract to facilitate any filament formation. It would have been interesting however if time had permitted to repeat the experiment with the addition of GTP as well.
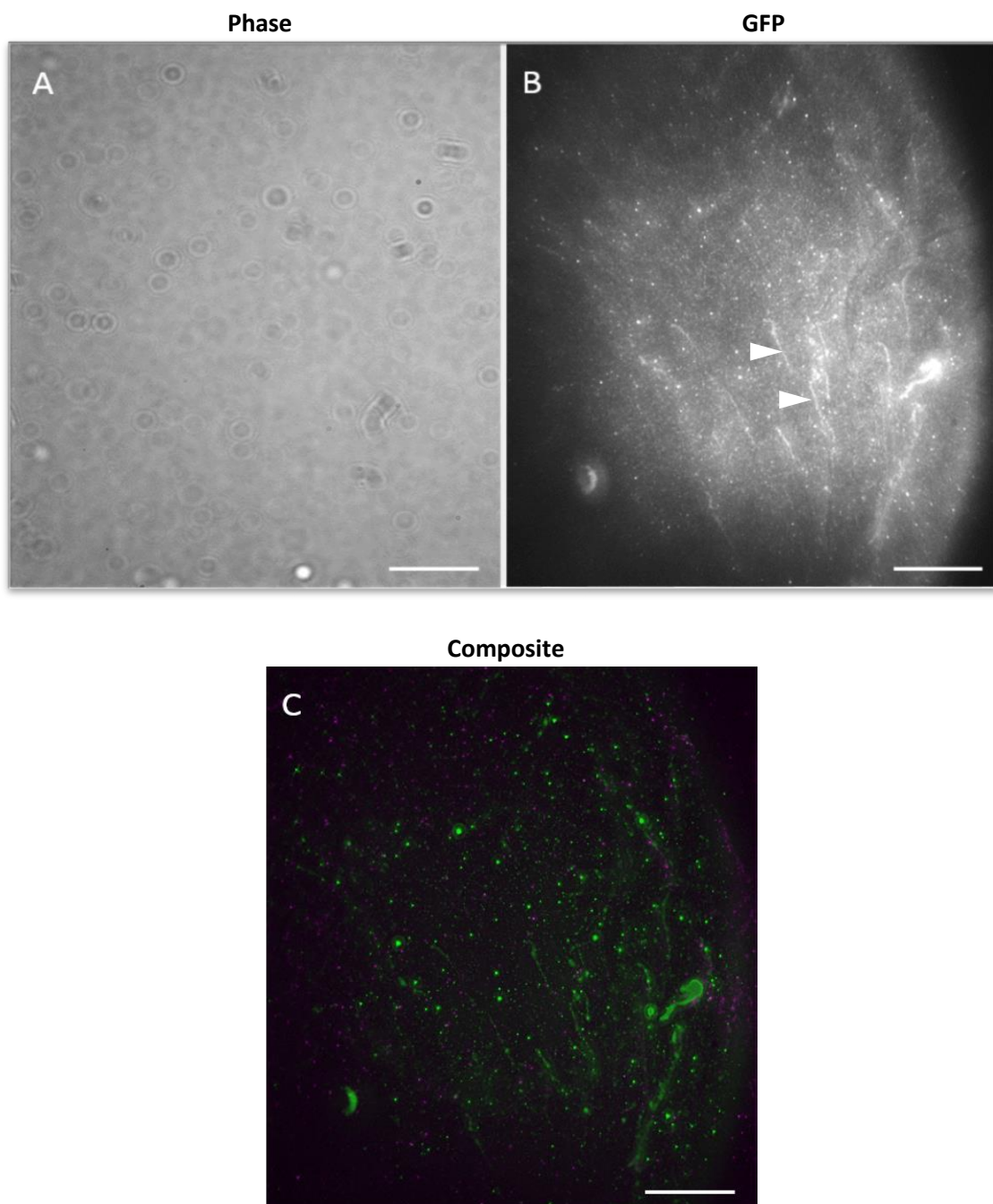
Figure 5.2. *In vitro* polymerisation of PduV-GFP. A sample of the initial flow through from loading cell lysate onto the column showing what appears to be filamentous structures of PduV-GFP. A) Phase contrast image image showing the absence of any filamentous structures observable by light microscopy, B) GFP signal showing filament like structures of PduV-GFP (white arrows) C) GFP and mCherry composite. The PduV-GFP and mCherry tagged BMC shell proteins did not appear ot interact, however the presence of BMC shells required for PduV filament formation *in vivo* in the flow through was confirmed. Scale Bar: 5 μm.

5.2.2.1. Exploring PduV Polymerisation by Sedimentation Assays

In order to explore the conditions required for PduV-associated filaments to be visualised *in vitro*, a series of sedimentation assays were carried out. It has long been known that ultracentrifugation at 100,000 rpm results in filamentous proteins being found in the pellet, and this strategy has recently been used to good effect in the case of the bacterial cytoskeletal protein MreB (Defeu Soufo et al. 2015). In these assays a constant amount of PduV-GFP was incubated with either mCherry-tagged BMCs which had been purified by the Yper method and subsequently added to the assay along with GTP, MgCl2 or a combination of these components. After incubation, the solutions were spun using an ultracentrifuge for 20 mins at 4 °C, 100,000 rpm. Samples of the supernatant and pellet fractions were then analysed by SDS PAGE; any PduV-GFP observed in the pelleted fraction would indicate that the protein had aggregated, possibly indicating the ability to assemble into filamentous structures. The incubation conditions and subsequent SDS Page analysis are shown in Figure 5.3.

Comparison of pellets and supernatants for each sample are shown in Figure 5.3. For the first two samples, the band for PduV-GFP is stronger in the supernatant than the pellet, indicating that the majority of the protein remained soluble and unaggregated in these conditions. This included the control sample with PduV-GFP in 20 mM Tris-HCl as well as with the addition of GTP in excess. When MgCl$_2$ was added, without Pdu BMC shells present, sample 3, PduV-GFP can be seen predominately in the pellet. This supports the previous observation that MgCl$_2$ promoted the aggregation of PduV.

Equal amounts of PduV-GFP can be seen in the pellet and supernatant of sample 4, containing PduV-GFP and Pdu BMC shells. This suggests that the addition of BMC shell protein to PduV-GFP also promotes aggregation, but to a lesser degree than the addition of MgCl$_2$. When MgCl$_2$ and GTP were added to PduV-GFP, the predominant band in the pellet corresponded to that of PduV-GFP, however there was still PduV-GFP in the supernatant, sample 5. There was an increase in PduV-GFP in the pellet compared to the supernatant in sample 6, containing BMC shells as well as MgCl$_2$ and in 7 and 8, containing BMCs in both with either GTP or GTP and MgCl$_2$ respectively, PduV-GFP was seen in both the pellet and supernatants in similar quantities.

Data therefore indicated that the presence of BMCs and MgCl$_2$ were likely to promote the aggregation of PduV-GFP, however the effect of GTP was unclear.
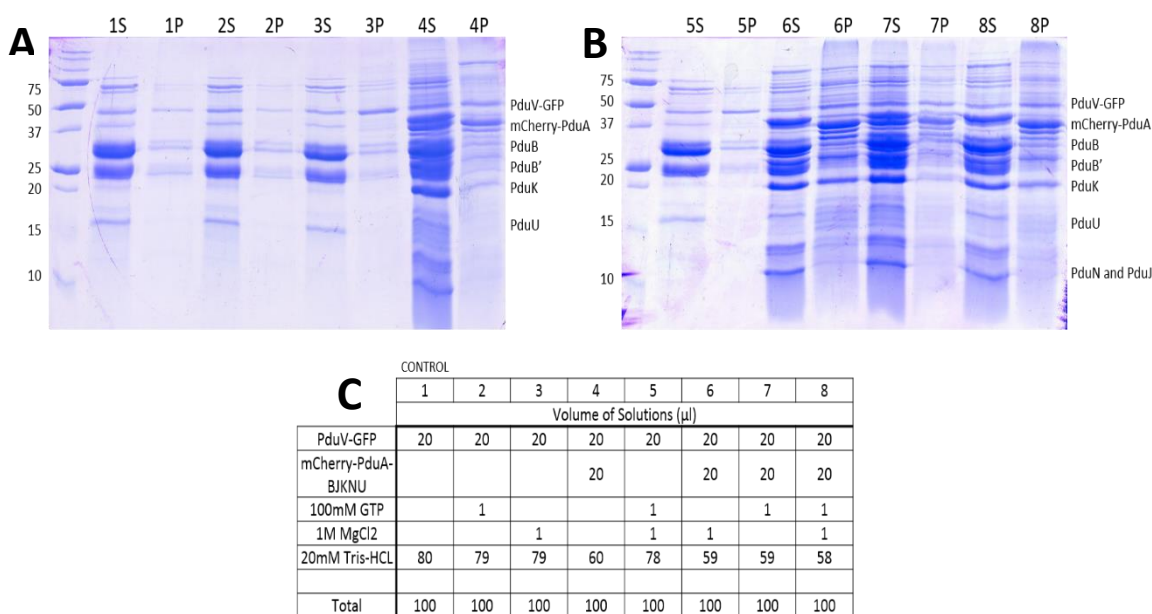
Figure 5.3. Exploring the conditions required for PduV to polymerise into filaments *in vitro.* A) and B) show 15% SDS-Page gels from sedimentation assays. Both the pellet and supernatant for each of the 8 assays were run on the gel. C) shows the condition for each of the 8 assays carried out.

5.2.2.2. Mutagenesis of Suspected GTPase Residues Within PduV

In order to further investigate the potential role of GTP in PduV polymerisation to form self-assembling filaments, or the role of GTP in facilitating attachment to pre-existing filaments in the

cell, several mutations of the predicted GTP binding site of PduV were engineered. The aim of these mutants was to prevent nucleotide hydrolysis by the prevention of nucleotide binding.

Initially, the amino acid sequence of PduV was aligned with that of other small GTPases found in bacteria such as EutP and ERA. This alignment revealed several residues that were conserved in all of these proteins, as shown in Figure 6.4. Further investigation using an NCBI conserved domain search revealed the presence of a P-loop, or Walker A motif, namely GxxxxGK(S/T). This is a conserved nucleotide phosphate-binding motif.

```
EUTP    -------MKRIAFVGSVGAGKTTLFNALQGNYTLARKTQAVEFNDKG------------D 41
PduV    -------MKRIMLIGPSQCGKTSLTQCMRGEALHYQKTQAIVWSPT-------------T 40
ERA     MSIDKSYCGFIAIVGRPNVGKSTLLNKLLGQKISITSRKAQTTRHRIVGIHTEGAYQAIY 60
               * ::*    **::*  : : *:    . :*

EUTP    IDTPGEYFNHPRWYHALI-----TTLQDVDMLIYVHG-------ANDPESRLPAG----- 84
PduV    IDTPGEYLENRCLYSALL-----ASACEADIIALVLN-------ADAPWSPFSPG----- 83
ERA     VDTPGLHMEEKRAINRLMNKAASSSIGDVELVIFVVEGTRWTPDDEMVLNKLREGKAPVI 120
        :*:** :::.        *:       ::  :.:::  *        :    . :   *

EUTP    --------------------------------------LLDIGVSKRQIAVISKTDMPDADVAA 110
PduV    --------------------------------------FTGP-MNRPVIGLVTKADLASPQRIS 108
ERA     LAVNKVDNVQEKADLLPHLQFLASQMNFLDIVPISAETGLNVDTIAAIVRKHLPEATHHF 180
                                              :.   *. : : .:...

EUTP    TRKLLLETG----------------------FEEPMFELNSHDPQSVQQLVDYLAS 144
PduV    LVESWLVQA----------------------GAQKVFFTSALENTGVDEMFIFLN- 141
ERA     PEDYITDRSQRFMASEIIREKLMRFLGAELPYSVTVEIERFVSNERGGYDINGLILVERE 240
          .     .                              *  .     .:: :.

EUTP    LTKQEEAGEKTHHSE---------------------------------------------- 159
PduV    ------AKESSCLTK---------------------------------------------- 150
ERA     GQKKMVIGNKGAKIKTIGIEARKDMQEMFEAPVHLELWVKVKSGWADDERALRSLGYVDD 300
                 :.    :

EUTP    -
PduV    -
ERA     L 301|
```

Figure 5.4. Identifying potential residues in PduV involved in GTP hydrolysis. Sequence alignment of PduV with two known small GTPases, EutP and ERA. Residues 8, 13, 14 and 43 identified as possible residues involved are highlighted.

The positions of these residues in PduV are: Glycine 8, Glycine 13 and Lysine 14. Threonine 43 was also thought to be involved in the GTPase activity of PduV, where it may be responsible for the release of GDP after GTP hydrolysis. Therefore these residues were subjected to overlap extension mutagenesis, involving the site-directed mutagenesis of each of these amino acids to Alanine.

Overlap extension mutagenesis involved the design of forward and reverse primers, listed in Table 2.3, for each mutation that included the individual base changes to cause the amino acid to change

from the original to alanine. Two PCR reactions were set up for each mutant, the first with the engineered forward primer and a T7 terminator primer and the second reaction with a PduV forward primer and the designed reverse primer. After running the PCR products on a 1% agarose gel to remove excess base pairs and check the band sizes, the gel extracted PCR products from the two reactions were combined using a PduV forward primer and T7 reverse primer. This is described in more detail in Section 2.3.1.2.

The final PCR product of each PduV variant was subcloned into a *pET3a* vector using restriction sites NdeI and SpeI. The *pduV* gene was then sequenced and subsequently subcloned to allow the encoded protein to be produced with a C-terminal Cerulean fluorescent protein. This was achieved by the digest of *pET3a-pduV-Cerulean* with NdeI and SpeI, replacing wild-type *pduV* with the mutant.

The ability of these PduV mutants to form filaments *in vivo* was then investigated by fluorescence microscopy. Cells expressing *pLysS-mCherry-pduA-BJKNU* and *pET3a-pduV-Cerulean*, including the four PduV mutants were each cultured in 25 mL of LB media with antibiotics at 37 °C until an OD_{600} of 0.6 was reached. The cells were then prepared for live cell imaging as described in Section 2.5.1. The images obtained are shown in Figure 5.5 below.

Figure 5.5 shows that only cells co-expressing mCherry-tagged BMC shells with wild-type PduV-Cerulean exhibited PduV filaments. The mCherry signal looked fairly similar in all of the strains, with the presence of many small, evenly distributed foci throughout the cell cytoplasm. In all of the mutant strains, PduV-Cerulean formed large foci located within the cytoplasm but also occasionally at the cell poles. It is clear that the mutation of each of the residues thought to be involved in GTP binding prevented either the formation of self-assembling filaments, or the attachment of PduV to pre-existing ones. However, the wild-type PduV-Cerulean strain, grown at the same time and in the same conditions as the mutants contained many elongated linear structures. This experiment was

repeated three times in the same growth conditions but on different days, and yielded the same results.

Interestingly, the absence of filaments did not seem to affect the distribution of mCherry foci within the cytoplasm, and foci of PduV-Cerulean was still seen to colocalise, observed by an overlap with signal for the mCherry-PduA-BJKNU shells resulting in white foci. This indicated that the potential inability for PduV to bind GTP had no effect on the ability of PduV to colocalise and interact with the Pdu BMC shell. Alternatively, the mutations may have affected the stability of the PduV protein, which whilst not affecting its distribution or colocalisation with BMC shells may have meant it was unable to from stable filaments. Attempts were made to measure the GTPase activity of wild-type PduV and these mutants to try and determine if the observatons were a result of diminished GTPase activity of PduV, however these preliminary GTPase activities were unsuccessful.

PduABJKNU PduV-Cerulean

Composite   Cerulean   mCherry   Phase
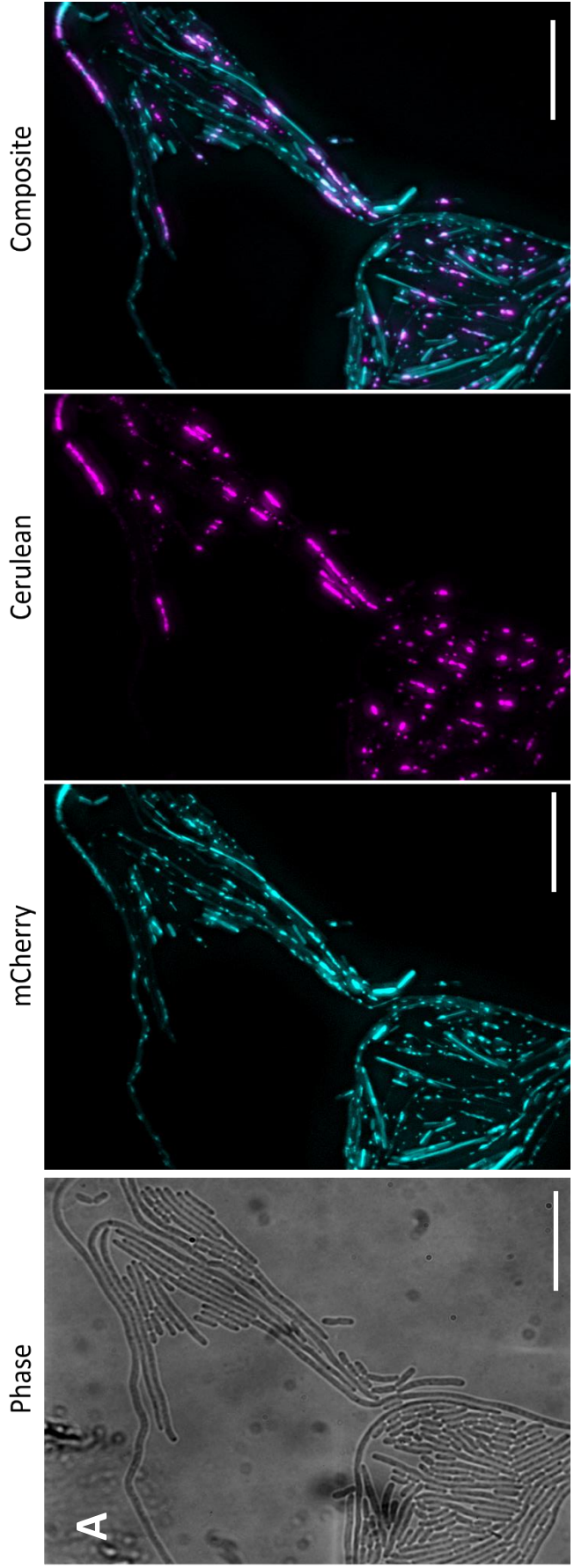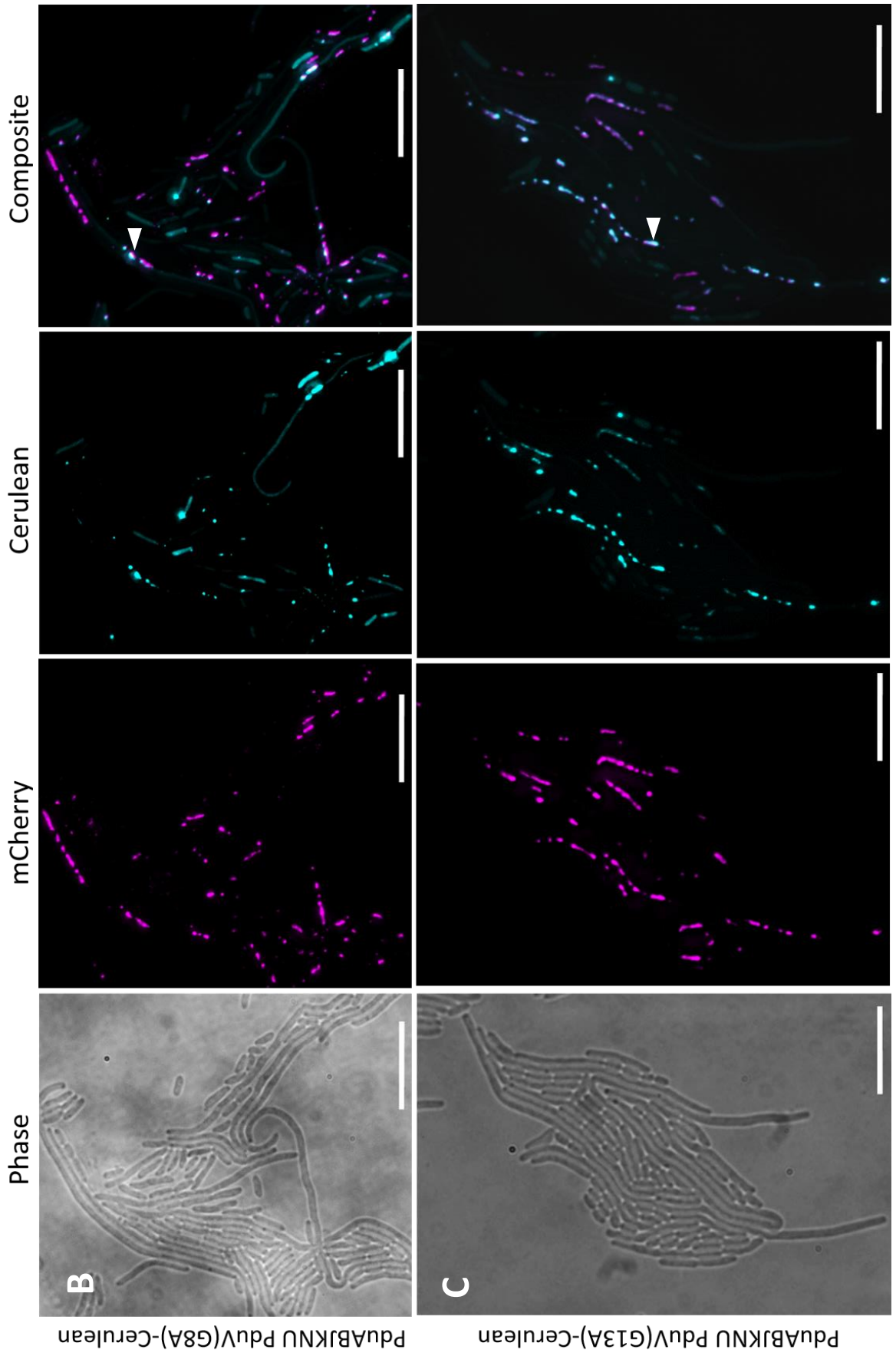
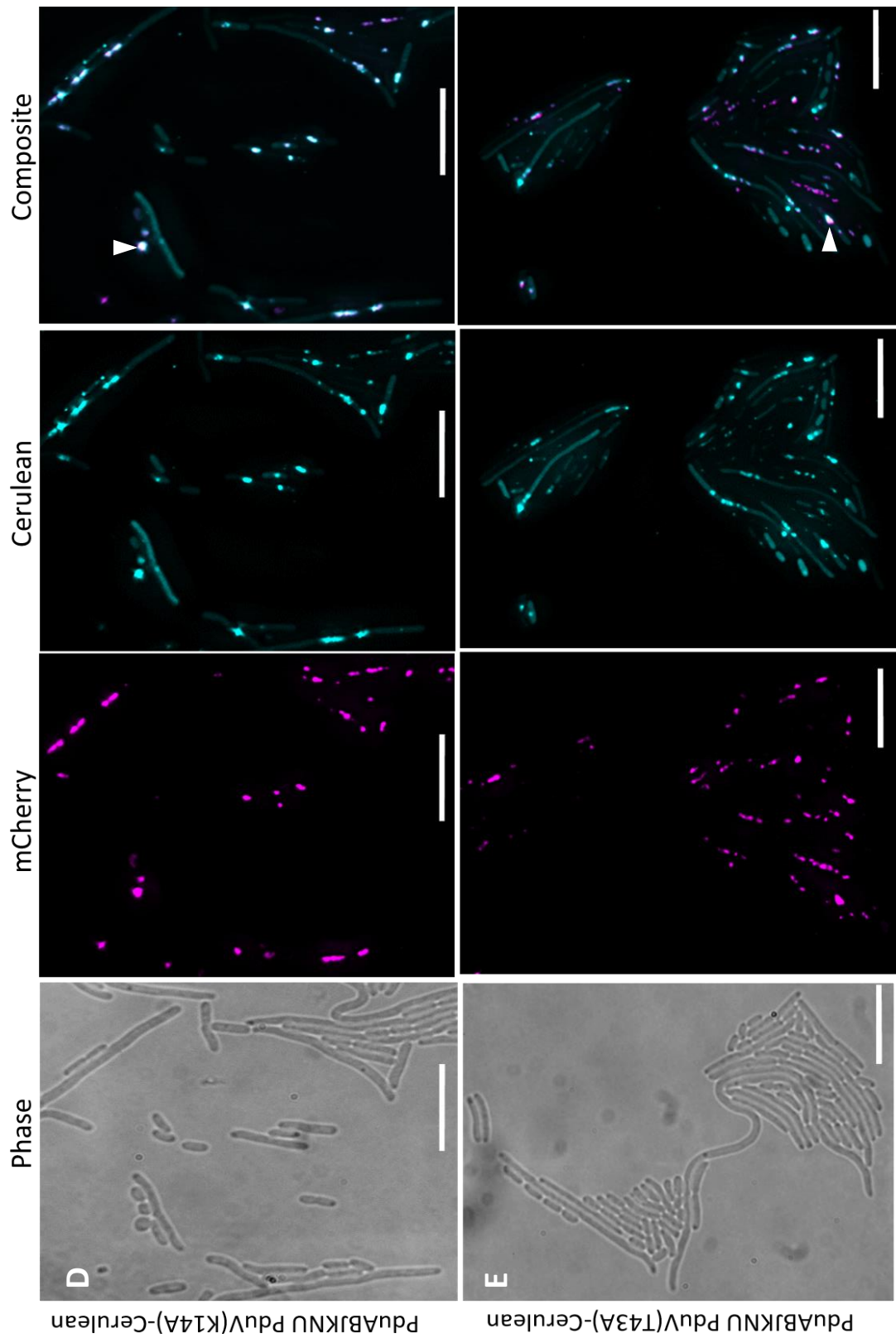**Figure 5.5.** Effect of mutating residues 8, 13, 14 and 43 on the ability of PduV to form filaments. Live cell images acquired show the Phase, mCherry, Cerulean and Composite signals. The *E. coli* strains visualised include mCherry-PduABJKNU co-expressed with A) PduV-Cerulean, B) PduV(G8A)-Cerulean C) PduV(G13A)-Cerulean, D) PduV(K14A)-Cerulean, E) PduV(T43A)-Cerulean. Although the expression of

mutated form of PduV abolished the formation of filament structures, PduV did appear to colocalise with BMC shells. This can be seen by the presence of white foci, highlighted by white arrows. Scale Bar: 5 μm

5.2.2. Exploring the Presence of PduV Filaments by TEM

To characterise the structure of PduV filaments by electron microscopy (EM), TEM thin sectioning of cells co-expressing mCherry-PduA-BJKNU and PduV-Cerulean was investigated. TEM images of this strain were compared to a strain grown on the same day, in the same conditions but only expressing the mCherry-tagged Pdu BMC shells. This was to determine if filaments were present and if they were likely to be due to PduV-Cerulean expression, or due to the overexpression of some shell proteins, such as PduA and PduJ, which are associated with filament-like structures.

5.2.1.1. Thin Section Analysis of Cells Expressing PduV

BL21 (DE3) cells co-expressing *pET23b-PduV-GFP* and *pLysS-mCherry-pduA-BJKNU* were cultured from a fresh transformation of BL21(DE3) competent cells with *pLysS-mCherry-pdu-ABJKNU* and *pET3a-pduV-cerulean*. Several colonies from the transformation plate were used to inoculate a 5 mL starter culture, which was in turn grown at 37 °C overnight. 50 mL of LB was then inoculated with 500 μl of starter culture and grown at 37 °C in a shaking incubator, as outlined in Section 2.2.2.2. Cells were grown to an OD_{600} of ~0.6 and harvested for TEM as outlined in Section 2.5.2.1.

Thin section images are shown in Figure 6.6. Images A and B demonstrate linear structures that were not observed in a control strain that only contained mCherry-tagged BMCs. These filamentous structures ranged from 45 nm to 52 nm in width when measured using imageJ (n=25). The filaments appeared to rarely be associated with BMCs and although they appeared to localise very near to BMC shells, the filaments were not seen to overlap or attach with the fully-formed BMC shells. These data provide evidence that firstly, TEM can be used to clearly visualise linear structures within the cell. It also shows that filaments are present when PduV-Cerulean is co-expressed with mCherry-tagged BMC shells but not when mCherry-tagged BMC shells are expressed alone.

However overexpression of PduA or PduJ has been associated with long, linear structures present in the cell cytoplasm. As it is not certain if the filaments visualised by TEM were a result of the
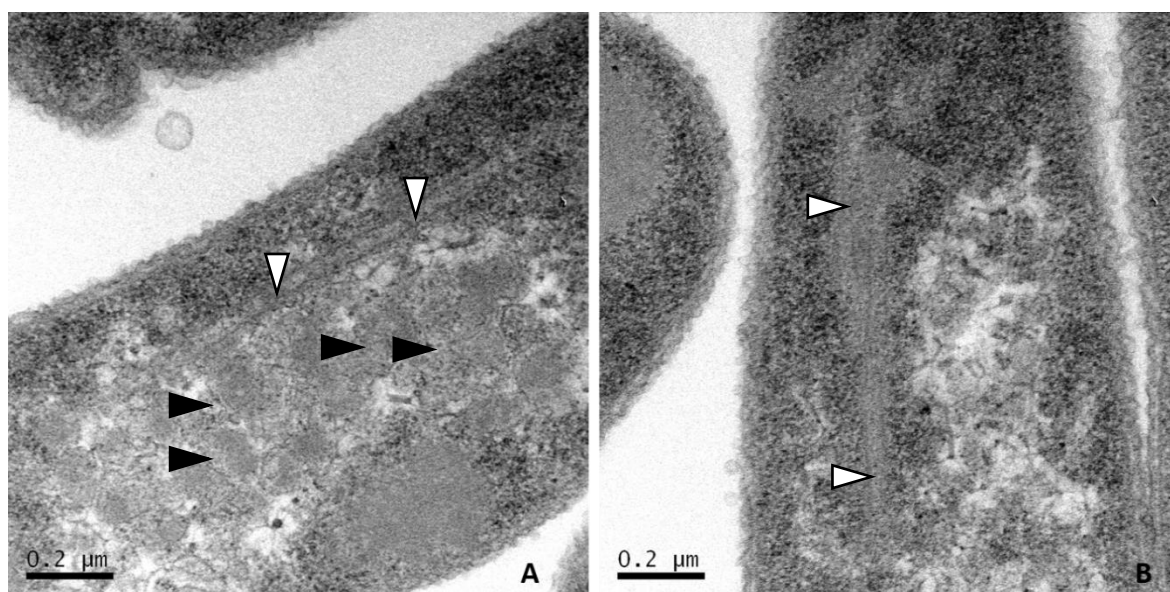
expression of PduV, immuno-gold labelling of PduV-GFP filaments was carried out to determine the localisation of PduV in the cell, using anti-GFP.

Figure 5.6. Investigating the presence of filamentous structures in cells. TEM analysis of whole cell thin sections and thin sections. A) and B) both show cells expressing PduV-GFP and mCherry-PduA-BJKNU, white arrows highlight filaments and black arrows highlight BMCs.

5.2.2.2. Immuno-gold TEM of Cells Expressing PduV

Cells co-expressing PduV-GFP and mCherry-PduA-BJKNU were grown and harvested as outlined in section 5.2.2.1. Cells were then prepared for immuno-gold labelling as described in Section 2.5.3, whereby 15 nm gold particles conjugated to secondary antibody were used to specifically target anti-GFP and therefore label the localisation of PduV-GFP in the cell. Several controls were used in this experiment, including a negative control lacking primary antibody and a negative control using a strain expressing BMCs alone. This was to ensure that there was no unspecific binding. Results showed that in these negative controls, the vast majority of cells did not have any gold particles; cells that did contain gold particles had between 1 and 4, indicating that we can be confident any gold particles seen when PduV-GFP was expressed was due to specific binding.

Figure 5.7 shows the results of immuno-gold labelling. Filaments were clearly visible, but due to the differed method of counterstaining compared with conventional microscopy, Pdu BMC shells were not as clearly visible. Gold particles can mostly be seen to associate with inclusion-like areas of the cytoplasm that have a high electron density. Some particles have localised to the outer edge of the filament structures, but only within the electron dense regions. The filaments appear to originate or protrude from these electron dense regions. However there was no clear pattern of gold particle distribution along these linear structures. Therefore evidence that the observed filaments are associated with PduV could not be convincingly provided by this immuno-gold labelling technique. However, the absence of filaments when PduV was not expressed would suggest that PduV had some involvement in the presence of the filaments, and may even suggest that the filaments were a result of PduV polymerisation rather than attachment to pre-existing filaments in the cell.
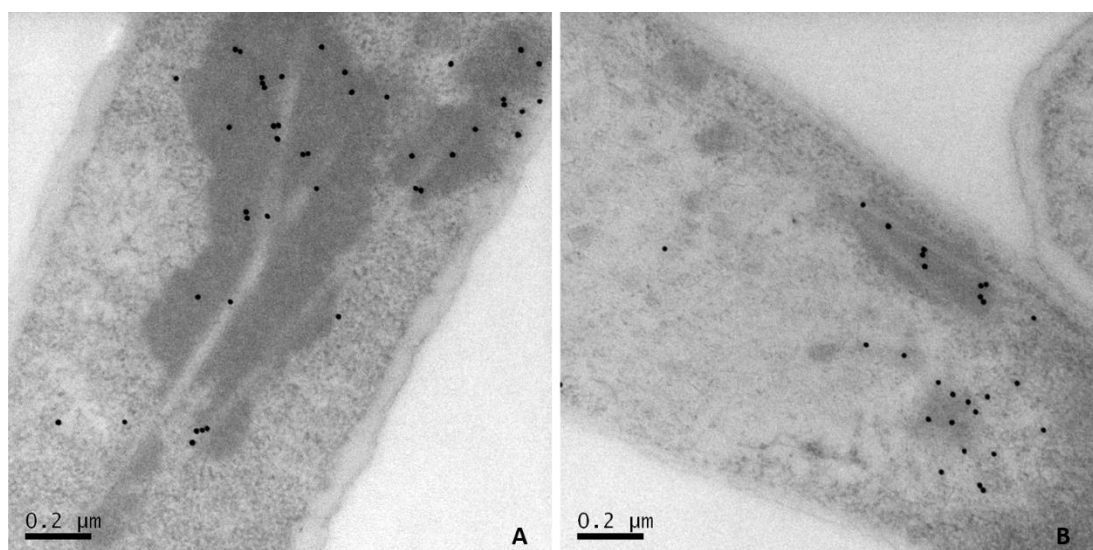
Figure 5.7. Investigating the presence of PduV-GFP in filamentous structures. TEM thin sections of whole cells prepared for immuno-gold labelling using 15 nm gold particles conjugated to an anti-Rabbit secondary antibody. The primary antibody used was anti-GFP. A) and B) both show cells expressing PduV-GFP and mCherry-PduA-BJKNU.

5.3. Summary

The aim of this chapter was to try to understand the role of PduV in the distribution of BMC's in the bacterial cell, and what the importance of its polymerisation into filament like structures was in this process. In order to investigate this both biochemical assays and microscopic techniques were

utilised. The starting point for these biochemical assays was to optimise the purification of PduV, to produce a high yield of pure, soluble PduV. Initial attempts to purify a His-tagged PduV using a nickel column were unsuccessful, with PduV forming precipitates, or becoming completely insoluble, indicating a high level of instability outside of the bacterial cell. In order to try and prevent this, a variant of PduV with a C-terminal GFP tag was expressed, which proved much more stable, with high yields of protein purified.

There were 2 main aims for this purified PduV, a) to see if it was possible to observe filamentous structure seen within the cell in an *in vitro* environment, and b) to examine the GTPase activity of PduV by GTP hydrolysis assays. Previous studies have shown that the presence of filamentous PduV structures within the cell are dependant on the presence of empty Pdu BMC shells, therefore, it was assumed that the same would apply in an *in vitro* environment. In order to explore this, PduV-GFP was co-purifed with PduABJKNU. During this purification it was noted that a large amount of PduV-GFP was not binding to the column, an observation not seen when PduV-GFP was purified alone. A sample of the unbound protein was examined by fluorescence microscopy, which revealed the presence of linear structures, similar to PduV filaments observed within the cell. This phenomenon was also observed in subsequent purifications. Each subsequent fraction during the purification process was also examined, however filamentous structures were only observed in the initial column flow-through. Whilst this provided the first signs that filamentous PduV structures could be formed *in vitro* the conditions required for this formation were not clear due to the fact that they were only observed in the initial flow-through from the column. Possible explanations for this are that empty BMC shells were not present in high enough concentrations in subsequent fractions of the purification, that there is a criticial concentration of PduV needed for filament formation that was only achieved in the initial flow through, or that there were other unknown factors playing a role in this. In order to further examine these conditions needed for filament formation *in vitro,* a series of sedimentation assays were carried out. It has long been known that filamentous proteins such as F-Actin can be pelleted by ultracentrifugation at 100,000 RPM. When

subjected to ultracentriguation at 100,000 RPM on its own, PduV remained in the supernatant, indicating it had not polymerised into filaments. However, when incubated with either empty BMC shells, $MgCl_2$ or a combination of both PduV-GFP was found in the pellet, suggesting that the presence of BMC shells and $MgCl_2$ caused PduV to aggregate, possibly into filamentous structures. The fact that the addition of $MgCl_2$ had such a dramatic effect was of interest, as Magnesium is required for nucleotide hydrolysis, which is essential for the polymerisation of other proteins such as Actin and Tubulin. This, coupled with the fact that PduV has previously been shown to have similarities to other small GTPase proteins, suggested that PduV polymerisation may have been dependant on the hydrolysis of GTP.

In order to investigate if GTP hydrolysis was required for the formation of PduV filaments, key amino acid residues for GTP hydrolysis within PduV were identified through alignment with other known GTPases. These residues were then mutated to Alanine residues and the effect on PduV filament formation was investigated *in vivo*. This was done through the use of fluorescence microscopy which revealed that the mutation of these residues abolished the presence of PduV filaments within the cell. In order to confirm that this was due to a reduction in GTP hydrolysis, it was hoped that the GTPase activity of each of these PduV variants could be measured through the use of GTPase assays. Whilst these attempts to quantify the GTPase activity of PduV were unsuccessful, fluorescence microscopy results did suggest that the ability of PduV to bind and hydrolyse GTP is needed for PduV filament formation.

Overall, the work described in this chapter has revealed evidence that the formation of filamentous structures by PduV is dependant on the ability of PduV to bind and hydrolyse GTP, whilst also confirming previous findings that it is also dependant on the presence of empty BMC shells. Furthermore, it has been shown that it is possible for PduV to form these filamentous structures in an *in vitro* environment, however the conditions for this formation remain unknown.

Chapter 6: Summary

The aim of the research in this thesis was to develop a further understanding of how Pdu bacterial microcompartment shells are formed, and how they are spatially arranged within the cell. Previous work had suggested that PduK within the Pdu BMC shell interacts with the small-GTPase like protein PduV which has been shown to form filament like structures (Parsons et al. 2010).

In order to observe this interaction *in vivo* a series of fluorescence microscopy experiments were planned. In generating the required plasmids it was found that PduK had to be present in the natural order of the *pdu* operon in order for intact BMC shells to form. Whilst it had previously been found that not all of the shell proteins are required for proper empty BMC with PduU and PduT being non-essential, the importance of gene location within the operon had not been obserbed. Subsequently, it has been shown that the location of PduJ within the *pdu* operon determines it's function, highlighting the importance of gene position (Chowdhury et al. 2016). It was also shown that tagging PduK with fluorescent protein at either the N or C-terminus prevented the correct formation of the BMC shell, which came as a surprise due to the fact BMCs have previously been visualised by tagging of another shell component, PduA (Parsons et al. 2010). This finding ultimiately meant that it was not possible to use a tagged variant of PduK to explore its interaction with PduV.

Previous work has shown that there in an unknown C-terminal extension on PduK, though it has been speculated to house an Fe-S Center (Crowley et al. 2010). It has been suggested that the C-terminal region may be associated with binding either internalized proteins or external facing proteins (possibly PduV?) or the uptake/control of external substrates. A series of truncations of PduK with different lengths of this C-terminal extension removed from the cell were generated and incorporated into the Pdu operon. It was observed that these truncated forms of PduK were not able to replace full length PduK, with improperly formed BMC shells generated. TEM analysis revealed structures suggesting that the BMC was unable to close properly. This came as a surprise as it had been thought that this C-terminal region would not play a role in the formation of the BMC

shell, as the N-terminal region of PduK contains a BMC-shell protein domain, thought to be involved in forming the structural hexameric tile that forms a key component of the facet of the overall BMC shell structure. Subsequently, work in this lab has shown that this C-Terminal extension is not required for PduK to interact with the P18 peptide used to target proteins to the interior of the BMC shell derived from the N-Terminus of PduP (Lawrence et al. 2014), further indicating that the C-terminal extension's role is that of maintaining the shape of the BMC shell than playing a role in the internalisation/transport of proteins. Further work is required to fully understand that function of PduK, and it's interaction with other Pdu proteins.

Having seen that the tagging of PduK with a fluorescent protein at both the N and C-terminus prevented the proper formation of BMC shells, it was decided that the effect of tagging other proteins in the BMC shell, PduA, PduB, PduJ, PduN and PduU with a fluorescent protein, mCherry would be investigated.

During the construction of plasmids needed to undertake this study, it was found that the vector used for the expression of BMCs containing these tagged variants of shell proteins had a dramatic effect on the expression of these BMC shells. When using *pET3a*, the main vector that would be used for expression studies, the BMC shells were not expressed correctly. However when using, *pLysS* a plasmid not usually used for expression studies, the expression of BMCs was much more successful. When examining this finding, it was found that using *pET3A* or *pLysS* resulted in successful protein synthesis, but BMC formation was more favoured in the presence of *pLysS*. The most reasonable explanation for this was that lysozyme also expressed from the *pLysS* plasmid, reducing T7 promoter activity, reduced stress within the *E. coli* cell, allowing more successful folding of the BMCs.

Once the conditions for successful production of BMC shells containing the tagged Pdu shell components were identified, it was possible to look at the effect of tagging these proteins with

mCherry. It was found that only the mCherry-PduA and mCherry-PduU constructs allowed proper BMC formation. All other combinations resulted in formation of aberrant structures, showing that the attachment of the comparatively bulky mCherry to the shell proteins generally results in mal-formation of the compartment, presumably through either improper folding or through steric hindrance in the "tiling" that takes place to make the shell. The most interesting observations of the effects of the mCherry-fusions on BMC formation came from the images of the isolated BMC fractions. Using these observations the following conclusions could be drawn: For PduA, the C-terminal region is more sensitive to modification than the N-terminus, PduB cannot be modified at all, suggesting that it plays a major role within the formation of the overall structure. Tagging of PduJ at the N-terminus gave mixed results, with intact BMC shells observed by fluorescence microscopy, whilst TEM showed forrmation of long strands of shell proteins. Tagging PduJ at the C-terminus again resulted in long strands of protein, indicating that tagging PduJ at either end of the protein prevents proper formation of BMC shells. The tagging of PduN at the N-terminus resulted in the formation of long, tubular BMC shells, whilst tagging at the C-terminus resulted in the formation of irregularly shaped BMC shells, providing further evidence for PduN playing a key role in closing the BMC by providing the vertices for the structure. The sensitivity of PduB, J and N to fluorescent tagging, and more so the impact this has on the formation of the BMC is consistent with prevous fidings which have shown that they are essential to proper BMC shell formation . The effect of fusions on PduU are less obvious, especially as BMCs can form in the absence of PduU (Parsons et al. 2010).

As well as the effect of tagging the Pdu shell proteins had on the formation of the BMC shell, the effect on PduV filaments within the cell was also investigated. Whilst it has previously been shown that tagging PduA at the N-terminus has no adverse effect on BMC shell formation, and subsequently no effect on PduV filaments, the effect of tagging other shell proteins was unknown. The tagging of PduA at the C-terminus, as well as PduN at the C-terminus had little effect on PduV filament length. Interestingly, tagging of PduN at the N-terminus resulted in much shorter PduV

filaments being observed in the cell, an interesting finding given that Pdu shells when expressed with this protein form longer elongated shells. Interstingly, the presence of N-terminally tagged PduJ resulted in a doubling of PduV filaments, despite the Pdu proteins forming long filamentous strands in the cell (an opposite effect to that observed with N-terminally tagged PduN) whilst C-terminal tagging abolished the presence of filaments completely. Interestingly, the tagging of PduU at either the N or C-terminus resulted in the abolishment of PduV filaments, despite intact BMC shells forming. This finding was also observed when PduV was expressed with BMC shells lacking PduU, indicating that PduU plays a regulatory role in the formation of PduV filaments. It had been hoped that the relationship between PduV and these shell proteins could be investigated further by looking for interactions using FLIM technqiues, however due to time constraints this was not possible.

The final portion of this thesis aimed to further characterise PduV, a member of the Pdu family, about which little was known. It had been observed in filamentous structures within the cell, however the way in which it formed these filaments, and the role these had in organising BMCs was unknown. Once a method had been developed to consistenly purify sufficient quantities of PduV attempts were made to replicate its ability to form filaments *in vitro*. Whilst filament-like structures were observed during certain steps of the purification process (namely after initial loading onto the Nickel column), the conditions required for this assembly remained unknown. A series of sedimentation assays gave further insight into these conditions, showing that PduV would pellet after ultracentrifugation when incubated with empty BMCs, $MgCl_2$ or a combination of both. The fact that $MgCl_2$ was able to cause this was of particular interest as Magneisum is required for nucleotide hydrolysis, and it had previously been speculated that PduV may have GTPase activity.

The finding that incubation with $MgCl_2$ resulted in PduV sedimentation (possibly through the formation of filaments) was investigated further by examining the GTPase activity of PduV. Upon sequence alignment with other known GTPases key residues within PduV were identified, and were

mutated by extension overlap mutagenesis. Fluorescence microscopy studies showed that the mutation of these filaments resulted in the abolishment of PduV filaments within the cell, suggesting that nucleotide hydrolysis was required for filament formation, similar to other filament forming proteins such as Actin and Tubulin. Attempts were made to quantify this activity, however attempts using 2 assays proved unsuccessful.

Overall, the work in this thesis has resulted in some interesting findings, posing further questions to be answered in order to gain an understanding of Pdu microcompartments. Having shown that PduK must be expressed in its natural order poses an interesting question into how the BMC shell is assembled, and whether other shell components are also so sensitive to the order in which they are expressed. Furthermore, the finding that truncating PduK to remove the uncharacterised C-terminal region results in aberrant formation of BMC shells is of great interest, as it had previously been thought that it was only the N-terminal domain of PduK that played a role in shell formation. Further work is needed to understand what role the C-terminal region plays in shell formation, and if it does have roles in binding to other internal and external proteins as previously thought. The exercise of tagging each shell protein at its N and C-terminus with the fluorescent protein mCherry revealed the interesting findings about each as outlined above, as well as revealing a potentially regulatory function for PduU in the formation of PduV filaments. In addition the fact that N-terminally tagging PduN resulted in the formation of long tubular BMC shells, which in turn resulted in shorter PduV filaments suggested a spatial regulatory mechanism for PduV filament length. Finally, mutagenesis studies provided further evidence for the fact that PduV function is dependant upon its ability to hydrolyse nucleotides, and further work should be done to quantify this activity.

In order to further develop the work presented in this thesis there are a number of different avenues to continue exploring. First and foremost, further work is required to understand how PduV filaments form and whether they do this alone, or through the interaction with other filaments such as MReB or FTsZ. This could be done through continuing to investigate the formation

of PduV filaments *in vitro* as well as undertaking fluorescence microscopy experiments with fluorescent tagged MReB/FTsZ. More work is also required to quantify the GTPase activity of PduV, which may require the optimisation of either the GTPase activity assay or the purification of PduV in order to eradicate the presence of other nucleotide hydrolysis proteins such as GroEL. The interaction between PduV and the shell proteins also requires further investigation as well as potential regulation of PduV filament formation and length. It may be best to do this with a combined biochemical and microscopic approach using immunoprecipitation assays and FRET/ FLIM FRET in order to provide sound evidence for these interractions. Finally, further work is required to understand the mechanism of Pdu shell formation. Having seen that shell formation required PduK to be expressed in the correct order within the *pdu* operon, similar work should be carried out to determine if the same is necessary for the other shell proteins. Continuing along work with PduK, further work is required to identify why the C terminal region is required for shell formation. The first port of call here would be to investigate if the absence of the C-terminal region affects the interaction of PduK with other shell proteins, again a combined biochemical and microscopic approach may be best for this in order to fully examine these potential losses of interaction.

References

Badger, M.R. & Bek, E.J., 2008. Multiple Rubisco forms in proteobacteria: their functional significance in relation to CO2 acquisition by the CBB cycle. *Journal of experimental botany*, 59(7), pp.1525–41. Available at: http://www.ncbi.nlm.nih.gov/pubmed/18245799 [Accessed July 9, 2014].

Badger, M.R. & Price, G.D., 2003. CO2 concentrating mechanisms in cyanobacteria: molecular components, their diversity and evolution. *Journal of Experimental Botany*, 54(383), pp.609–622. Available at: http://jxb.oxfordjournals.org/lookup/doi/10.1093/jxb/erg076 [Accessed July 18, 2014].

Bartolommei, G., Moncelli, M.R. & Tadini-Buoninsegni, F., 2013. A Method to Measure Hydrolytic Activity of Adenosinetriphosphatases (ATPases). *PLoS ONE*, 8(3).

Bazylinski, D.A. & Frankel, R.B., 2004. Magnetosome formation in prokaryotes. *Nature reviews. Microbiology*, 2, pp.217–230.

Beudeker, R.F., Cannon, G.C., Kuenen, J.G. & Shively, J.M., 1980. Relations between d-ribulose-1,5-bisphosphate carboxylase, carboxysomes and CO2 fixing capacity in the obligate chemolithotroph Thiobacillus neapolitanus grown under different limitations in the chemostat. *Archives of Microbiology*, 124, pp.185–189.

Bobik, T. a, 2006. Polyhedral organelles compartmenting bacterial metabolic processes. *Applied microbiology and biotechnology*, 70(5), pp.517–25. Available at: http://www.ncbi.nlm.nih.gov/pubmed/16525780 [Accessed July 10, 2014].

Bobik, T. a, Havemann, G.D., Busch, R.J., Williams, D.S. & Aldrich, H.C., 1999. The propanediol utilization (pdu) operon of Salmonella enterica serovar Typhimurium LT2 includes genes necessary for formation of polyhedral organelles involved in coenzyme B(12)-dependent 1, 2-propanediol degradation. *Journal of bacteriology*, 181(19), pp.5967–75. Available at: http://www.pubmedcentral.nih.gov/articlerender.fcgi?artid=103623&tool=pmcentrez&rendertype=abstract.

Bobik, T.A., Havemann, G.D., Busch, R.J., Williams, D.S. & Aldrich, H.C., 1999. The Propanediol Utilization (pdu) Operon of Salmonella enterica Serovar Typhimurium LT2 Includes Genes Necessary for Formation of Polyhedral Organelles Involved in Coenzyme B 12 -Dependent The Propanediol Utilization (pdu) Operon of Salmonella enteric. *Journal of Bacteriology*.

Bobik, T.A., Xu, Y., Jeter, R.M., Otto, K.E. & Roth, J.R., 1997. Propanediol utilization genes (pdu) of Salmonella typhimurium: Three genes for the propanediol dehydratase. *Journal of Bacteriology*, 179, pp.6633–6639.

de Boer, P., Crossley, R. & Rothfield, L., 1992. The essential bacterial cell-division protein FtsZ is a GTPase. *Nature*, 359, pp.254–256.

Bonacci, W., Teng, P.K., Afonso, B., Niederholtmeyer, H., Grob, P. & Silver, P.A., 2012. Modularity of a carbon- fixing protein organelle. *PNAS*, 109, pp.478–483.

Bork, P., Sander, C. & Valencia, A., 1992. An ATPase domain common to prokaryotic cell cycle proteins, sugar kinases, actin, and hsp70 heat shock proteins. *Proceedings of the National Academy of Sciences of the United States of America*, 89, pp.7290–4.

Bradbeer, C., 1965. The Clostridial Fermentations of Choline Ethanolamine. *Journal of bacteriological chemistry*, 240(12), pp.4669–4674.

Brinsmade, S.R., Paldon, T., Jorge, C. & Escalante-semerena, J.C., 2005. Minimal Functions and Physiological Conditions Required for Growth of Salmonella enterica on Ethanolamine in the Absence of the Metabolosome Minimal Functions and Physiological Conditions Required for Growth of Salmonella enterica on Ethanolamine in the A. *Journal of bacteriology*, 187(23), pp.8039–8046.

Cai, F., Sutter, M., Bernstein, S.L., Kinney, J.N. & Kerfeld, C. a, 2014. Engineering Bacterial Microcompartment Shells: Chimeric Shell Proteins and Chimeric Carboxysome Shells. *ACS synthetic biology*. Available at: http://www.ncbi.nlm.nih.gov/pubmed/25117559.

Cameron, J.C., Wilson, S.C., Bernstein, S.L. & Kerfeld, C. a, 2013. Biogenesis of a bacterial organelle: the carboxysome assembly pathway. *Cell*, 155(5), pp.1131–40. Available at: http://www.ncbi.nlm.nih.gov/pubmed/24267892 [Accessed December 8, 2014].

Cannon, G.C., Bradburne, C.E., Aldrich, H.C., Baker, S.H., Heinhorst, S. & Shively, J.M., 2001. Microcompartments in prokaryotes: carboxysomes and related polyhedra. *Applied and environmental microbiology*, 67, pp.5351–5361.

Cannon, G.C., Bradburne, C.E., Aldrich, H.C., Baker, S.H., Heinhorst, S. & Shively, J.M., 2001. MINIREVIEW Microcompartments in Prokaryotes : Carboxysomes and Related Polyhedra. , 67(12), pp.5351–5361.

Cannon, G.C. & Shively, J.M., 1983. Characterization of a homogenous preparation of carboxysomes from Thiobacillus neapolitanus. *Archives of Microbiology*, 134, pp.52–59.

Carlsson, L., Nyström, L.E., Sundkvist, I., Markey, F. & Lindberg, U., 1977. Actin polymerizability is influenced by profilin, a low molecular weight protein in non muscle cells. *Journal of Molecular Biology*, 115(3), pp.465–483.

Chang, G. & Chang, J., 1975. Evidence for the B12-dependent enzyme ethanolamine deaminase in Salmonella. *Nature*, 254, pp.150–151.

Chen, A.H., Robinson-Mosher, A., Savage, D.F., Silver, P.A. & Polka, J.K., 2013. The Bacterial Carbon-Fixing Organelle Is Formed by Shell Envelopment of Preassembled Cargo. *PLoS ONE*, 8.

Chen, P., Ailion, M., Bobik, T., Stormo, G., Roth, J. & Al, C.E.T., 1995. Five Promoters Integrate Control of the cob / pdu Regulon in Salmonella typhimurium. *Journal of bacteriology*, 177(19), pp.5401–5410.

Chen, P., Andersson, D.I. & Roth, J.R., 1994. The control region of the pdu/cob regulon in Salmonella typhimurium. *Journal of bacteriology*, 176(17), pp.5474–82. Available at: http://www.pubmedcentral.nih.gov/articlerender.fcgi?artid=196736&tool=pmcentrez&rend ertype=abstract.

Chen, P., Andersson, D.I. & Roth, J.R., 1994. The control region of the pdu/cob regulon in Salmonella typhimurium. *Journal of Bacteriology*, 176, pp.5474–5482.

Cheng, S. & Bobik, T.A., 2010. Characterization of the PduS cobalamin reductase of Salmonella enterica and its role in the Pdu microcompartment. *Journal of Bacteriology*, 192, pp.5071–5080.

Cheng, S., Fan, C., Sinha, S. & Bobik, T. a, 2012. The PduQ enzyme is an alcohol dehydrogenase used to recycle NAD+ internally within the Pdu microcompartment of Salmonella enterica. *PloS one*, 7(10), p.e47144. Available at: http://www.pubmedcentral.nih.gov/articlerender.fcgi?artid=3471927&tool=pmcentrez&ren dertype=abstract [Accessed January 14, 2015].

Cheng, S., Liu, Y., Crowley, C.S., Yeates, T.O. & Bobik, T. a, 2008. Bacterial microcompartments: their properties and paradoxes. *BioEssays : news and reviews in molecular, cellular and developmental biology*, 30(11–12), pp.1084–95. Available at: http://www.pubmedcentral.nih.gov/articlerender.fcgi?artid=3272490&tool=pmcentrez&ren dertype=abstract [Accessed March 11, 2012].

Cheng, S., Sinha, S., Fan, C., Liu, Y. & Bobik, T. a, 2011. Genetic analysis of the protein shell of the microcompartments involved in coenzyme B12-dependent 1,2-propanediol degradation by

Salmonella. *Journal of bacteriology*, 193(6), pp.1385–92. Available at: http://www.pubmedcentral.nih.gov/articlerender.fcgi?artid=3067621&tool=pmcentrez&rendertype=abstract [Accessed June 21, 2012].

Chowdhury, C., Chun, S., Sawaya, M.R., Yeates, T.O. & Bobik, T.A., 2016. The function of the PduJ microcompartment shell protein is determined by the genomic position of its encoding gene. *Molecular Microbiology*.

Chowdhury, C., Sinha, S., Chun, S., Yeates, T.O. & Bobik, T. a, 2014. Diverse bacterial microcompartment organelles. *Microbiology and molecular biology reviews : MMBR*, 78(3), pp.438–68. Available at: http://www.ncbi.nlm.nih.gov/pubmed/25184561 [Accessed January 23, 2015].

Crowley, C.S., Cascio, D., Sawaya, M.R., Kopstein, J.S., Bobik, T.A. & Yeates, T.O., 2010. Structural insight into the mechanisms of transport across the Salmonella enterica Pdu microcompartment shell. *Journal of Biological Chemistry*, 285, pp.37838–37846.

Crowley, C.S., Sawaya, M.R., Bobik, T. a & Yeates, T.O., 2008. Structure of the PduU shell protein from the Pdu microcompartment of Salmonella. *Structure (London, England : 1993)*, 16(9), pp.1324–32. Available at: http://www.ncbi.nlm.nih.gov/pubmed/18786396 [Accessed September 3, 2014].

Defeu Soufo, H.J., Reimold, C., Breddermann, H., Mannherz, H.G. & Graumann, P.L., 2015. Translation elongation factor EF-Tu modulates filament formation of actin-like MreB protein in vitro. *Journal of molecular biology*, 427(8), pp.1715–1727.

Erickson, H.P., 1995. FtsZ , a Prokaryotic Homolog of Tubulin? *Cell*, 80, pp.367–370.

Fan, C. & Bobik, T. a, 2011. The N-terminal region of the medium subunit (PduD) packages adenosylcobalamin-dependent diol dehydratase (PduCDE) into the Pdu microcompartment. *Journal of bacteriology*, 193(20), pp.5623–8.

Fan, C. & Bobik, T. a, 2008. The PduX enzyme of Salmonella enterica is an L-threonine kinase used for coenzyme B12 synthesis. *The Journal of biological chemistry*, 283(17), pp.11322–9. Available at: http://www.ncbi.nlm.nih.gov/pubmed/18308727 [Accessed January 14, 2015].

Fan, C., Cheng, S., Liu, Y., Escobar, C.M., Crowley, C.S., Jefferson, R.E., Yeates, T.O. & Bobik, T. a, 2010a. Short N-terminal sequences package proteins into bacterial microcompartments. *Proceedings of the National Academy of Sciences of the United States of America*, 107(16), pp.7509–14. Available at: http://www.pubmedcentral.nih.gov/articlerender.fcgi?artid=2867708&tool=pmcentrez&rendertype=abstract [Accessed March 2, 2012].

Fan, C., Cheng, S., Liu, Y., Escobar, C.M., Crowley, C.S., Jefferson, R.E., Yeates, T.O. & Bobik, T. a, 2010b. Short N-terminal sequences package proteins into bacterial microcompartments. *Proceedings of the National Academy of Sciences of the United States of America*, 107(16), pp.7509–14.

Fan, C., Cheng, S., Sinha, S. & Bobik, T.A., 2012. Interactions between the termini of lumen enzymes and shell proteins mediate enzyme encapsulation into bacterial microcompartments. *Proceedings of the National Academy of Sciences*, 109, pp.14995–15000.

Forouhar, F. et al., 2007. Functional insights from structural genomics. *J Struct Funct Genomics*, 8, pp.37–44.

Frank, S., Lawrence, A.D., Prentice, M.B. & Warren, M.J., 2013. Bacterial microcompartments moving into a synthetic biological world. *Journal of Biotechnology*, 163(2), pp.273–279.

Fukuzawa, H., Suzuki, E., Komukai, Y. & Miyachi, S., 1992. A gene homologous to chloroplast

carbonic anhydrase (icfA) is essential to photosynthetic carbon dioxide fixation by Synechococcus PCC7942. *Proceedings of the National Academy of Sciences of the United States of America*, 89, pp.4437–4441.

Harvey, P.C., Watson, M., Hulme, S., Jones, M.A., Lovell, M., Berchieri, J., Young, J., Bumstead, N. & Barrow, P., 2011. Salmonella enterica serovar typhimurium colonizing the lumen of the chicken intestine grows slowly and upregulates a unique set of virulence and metabolism genes. *Infection and Immunity*, 79, pp.4105–4121.

Havemann, G.D. & Bobik, T.A., 2003. Protein Content of Polyhedral Organelles Involved in Coenzyme B 12 -Dependent Degradation of 1 , 2-Propanediol in Salmonella enterica Serovar Typhimurium LT2 †. *Journal of Bacteriology*, 185(17), pp.5086–5095.

Havemann, G.D., Sampson, E.M. & Bobik, T.A., 2002. PduA Is a Shell Protein of Polyhedral Organelles Involved in Coenzyme B 12 -Dependent Degradation of 1 , 2-Propanediol in Salmonella enterica Serovar Typhimurium LT2. *Society*, 184(5), pp.1253–1261. Available at: http://www.pubmedcentral.nih.gov/articlerender.fcgi?artid=134856&tool=pmcentrez&rendertype=abstract.

Held, M., Quin, M.B. & Schmidt-Dannert, C., 2013. Eut bacterial microcompartments: Insights into their function, structure, and bioengineering applications. *Journal of Molecular Microbiology and Biotechnology*, 23(4–5), pp.308–320.

Hess, B. & Wurster, B., 1970. Transient time of the pyruvate kinase-lactate dehydrogenase system of rabbit muscle in vitro. *FEBS Letters*, 9(2), pp.73–77.

Hoa, S.N., Hunt, H.D., Horton, R.M., Pullen, J.K. & Peasea, L.R., 1989. Site-directed mutagenesis by overlap extension using the polymerase chain reaction. *Gene*, 77, pp.51–59.

Horswill, A.R. & Escalante-semerena, J.C., 1997. Propionate Catabolism in Salmonella typhimurium LT2 : Two Divergently Transcribed Units Comprise the prp Locus at 8 . 5 Centisomes , prpR Encodes a Member of the Sigma-54 Family of Activators , and the prpBCDE Genes Constitute an Operon. *Journal of bacteriology*, 179(3), pp.928–940.

Huseby, D.L. & Roth, J.R., 2013. Evidence that a metabolic microcompartment contains and recycles private cofactor pools. *Journal of bacteriology*, 195, pp.2864–79.

Iancu, C. V, Morris, D.M., Dou, Z., Heinhorst, S., Cannon, G.C. & Jensen, G.J., 2010. Organization, structure, and assembly of alpha-carboxysomes determined by electron cryotomography of intact cells. *Journal of molecular biology*, 396, pp.105–117.

Jeter, R.M., 1990. Cobalamin-dependent 1,2-propanediol utilization by Salmonella typhimurium. *Journal of general microbiology*, 136, pp.887–896.

Jeter, R.M., Olivera, B.M. & Roth, J.R., 1984. Salmonella typhimurium synthesizes cobalamin (vitamin B12) de novo under anaerobic growth conditions. *Journal of Bacteriology*, 159, pp.206–213.

Jorda, J., Liu, Y., Bobik, T. a & Yeates, T.O., 2015. Exploring Bacterial Organelle Interactomes: A Model of the Protein-Protein Interaction Network in the Pdu Microcompartment. *PLoS computational biology*, 11(2), p.e1004067. Available at: http://www.ncbi.nlm.nih.gov/pubmed/25646976 [Accessed February 4, 2015].

Jorda, J., Lopez, D., Wheatley, N.M. & Yeates, T.O., 2013. Using comparative genomics to uncover new kinds of protein-based metabolic organelles in bacteria. *Protein science : a publication of the Protein Society*, 22(2), pp.179–95. Available at: http://www.pubmedcentral.nih.gov/articlerender.fcgi?artid=3588914&tool=pmcentrez&rendertype=abstract [Accessed August 28, 2014].

Kaminski, C.F., Rees, E.J. & Schierle, G.S.K., 2014. A quantitative protocol for intensity-based live

cell FRET imaging. *Methods in Molecular Biology*, 1076, pp.445–454.

Kerfeld, C. a, Heinhorst, S. & Cannon, G.C., 2010. Bacterial microcompartments. *Annual review of microbiology*, 64, pp.391–408. Available at: http://www.ncbi.nlm.nih.gov/pubmed/20825353 [Accessed March 27, 2012].

Kerfeld, C. a, Sawaya, M.R., Tanaka, S., Nguyen, C. V, Phillips, M., Beeby, M. & Yeates, T.O., 2005. Protein structures forming the shell of primitive bacterial organelles. *Science (New York, N.Y.)*, 309(5736), pp.936–8. Available at: http://www.ncbi.nlm.nih.gov/pubmed/16081736.

Kinney, J.N., Axen, S.D. & Kerfeld, C.A., 2011. Comparative analysis of carboxysome shell proteins. In *Photosynthesis Research*. pp. 21–32.

Klein, M.G., Zwart, P., Bagby, S.C., Cai, F., Chisholm, S.W., Heinhorst, S., Cannon, G.C. & Kerfeld, C.A., 2009. Identification and Structural Analysis of a Novel Carboxysome Shell Protein with Implications for Metabolite Transport. *Journal of Molecular Biology*, 392, pp.319–333.

Kofoid, E., Rappleye, C., Stojiljkovic, I. & Roth, J., 1999. The 17-gene ethanolamine (eut) operon of Salmonella typhimurium encodes five homologues of carboxysome shell proteins. *Journal of bacteriology*, 181, pp.5317–29. Available at: http://www.pubmedcentral.nih.gov/articlerender.fcgi?artid=94038&tool=pmcentrez&rendertype=abstract.

Lawrence, A.D., Frank, S., Newnham, S., Lee, M.J., Brown, I.R., Xue, W., Rowe, M.L., Mulvihill, D.P., Prentice, M.B., Howard, M.J. & Warren, M.J., 2014. Solution Structure of a Bacterial Microcompartment Targeting Peptide and Its Application in the Construction of an Ethanol Bioreactor. *ACS synthetic biology*, 3(7), pp.454–465.

Leal, N. a, Havemann, G.D. & Bobik, T. a, 2003. PduP is a coenzyme-a-acylating propionaldehyde dehydrogenase associated with the polyhedral bodies involved in B12-dependent 1,2-propanediol degradation by Salmonella enterica serovar Typhimurium LT2. *Archives of microbiology*, 180(5), pp.353–61. Available at: http://www.ncbi.nlm.nih.gov/pubmed/14504694 [Accessed January 12, 2015].

Liu, Y., Leal, N. a, Sampson, E.M., Johnson, C.L. V, Havemann, G.D. & Bobik, T. a, 2007. PduL is an evolutionarily distinct phosphotransacylase involved in B12-dependent 1,2-propanediol degradation by Salmonella enterica serovar typhimurium LT2. *Journal of bacteriology*, 189(5), pp.1589–96. Available at: http://www.pubmedcentral.nih.gov/articlerender.fcgi?artid=1855771&tool=pmcentrez&rendertype=abstract [Accessed January 13, 2015].

Long, B.M., Rae, B.D., Badger, M.R. & Price, G.D., 2011. Over-expression of the beta-carboxysomal CcmM protein in Synechococcus PCC7942 reveals a tight co-regulation of carboxysomal carbonic anhydrase (CcaA) and M58 content. In *Photosynthesis Research*. pp. 33–45.

Mccullum, E.O., Williams, B. a R., Zhang, J. & Chaput, J.C., 2010. In Vitro Mutagenesis Protocols. *Methods in Molecular Biology*.

Mcgoldrick, H.M., Roessner, C.A., Raux, E., Lawrence, A.D., Mclean, K.J., Munro, A.W., Santabarbara, S., Rigby, S.E.J., Heathcote, P., Scott, A.I. & Warren, M.J., 2005. Identification and Characterization of a Novel Vitamin B 12 (Cobalamin) Biosynthetic Enzyme (CobZ) from Rhodobacter capsulatus , Containing Flavin , Heme , and Fe-S Cofactors *. , 280(2), pp.1086–1094.

Monnard, P., 2003. Liposome-entrapped polymerases as models for microscale/nanoscale bioreactors. *The Journal of membrane biology*, 191(2), pp.87–97. Available at: http://www.ncbi.nlm.nih.gov/pubmed/12533776 [Accessed October 2, 2014].

Murat, D., Quinlan, A., Vali, H. & Komeili, A., 2010. Comprehensive genetic dissection of the magnetosome gene island reveals the step-wise assembly of a prokaryotic organelle.

Proceedings of the National Academy of Sciences of the United States of America, 107, pp.5593–5598.

Niklowitz, W. & Drews, G., 1956. [Cytology of Cyanophycea. I. Research on the substructure of Phormidium uncinatum Gom]. *Archiv für Mikrobiologie*, 24(2), pp.134–46. Available at: http://www.ncbi.nlm.nih.gov/pubmed/13327991 [Accessed August 28, 2014].

Obradors, N., Badia, J., Baldoma, L. & Aguilar, J., 1988. Anaerobic metaoblism of the L-rhamnose fermentation product 1,2-propanediol in Salmonella typhimurium. *Journal of Bacteriology*, 170, pp.2159–2162.

Orus, M.I., Rodriguez, M.L., Martinez, F. & Marco, E., 1995. Biogenesis and Ultrastructure of Carboxysomes from Wild Type and Mutants of Synechococcus sp. Strain PCC 7942. *Plant physiology*, 107, pp.1159–1166.

Pang, A., Frank, S., Brown, I., Warren, M.J. & Pickersgill, R.W., 2014. Structural insights into higher order assembly and function of the bacterial microcompartment protein PduA. *The Journal of biological chemistry*, 289(32), pp.22377–84. Available at: http://www.pubmedcentral.nih.gov/articlerender.fcgi?artid=4139245&tool=pmcentrez&rendertype=abstract [Accessed January 29, 2015].

Pang, A., Liang, M., Prentice, M.B. & Pickersgill, R.W., 2012. Substrate channels revealed in the trimeric Lactobacillus reuteri bacterial microcompartment shell protein PduB. *Acta Crystallographica Section D: Biological Crystallography*, 68, pp.1642–1652.

Parsons, J.B., Dinesh, S.D., Deery, E., Leech, H.K., Brindley, A. a, Heldt, D., Frank, S., Smales, C.M., Lünsdorf, H., Rambach, A., Gass, M.H., Bleloch, A., McClean, K.J., Munro, A.W., Rigby, S.E.J., Warren, M.J. & Prentice, M.B., 2008. Biochemical and structural insights into bacterial organelle form and biogenesis. *The Journal of biological chemistry*, 283(21), pp.14366–75. Available at: http://www.ncbi.nlm.nih.gov/pubmed/18332146 [Accessed March 19, 2012].

Parsons, J.B., Frank, S., Bhella, D., Liang, M., Prentice, M.B., Mulvihill, D.P. & Warren, M.J., 2010. Synthesis of empty bacterial microcompartments, directed organelle protein incorporation, and evidence of filament-associated organelle movement. *Molecular cell*, 38(2), pp.305–15. Available at: http://www.ncbi.nlm.nih.gov/pubmed/20417607 [Accessed March 11, 2012].

Penrod, J.T., Mace, C.C. & Roth, J.R., 2004. A pH-sensitive function and phenotype: Evidence that EutH facilitates diffusion of uncharged ethanolamine in Salmonella enterica. *Journal of Bacteriology*, 186, pp.6885–6890.

Penrod, J.T. & Roth, J.R., 2006. Conserving a Volatile Metabolite : a Role for Carboxysome-Like Organelles in Salmonella enterica Conserving a Volatile Metabolite : a Role for Carboxysome-Like Organelles in Salmonella enterica. , 188(8).

Price-Carter, M., Tingey, J., Bobik, T.A. & Roth, J.R., 2001. The alternative electron acceptor tetrathionate supports B12-dependent anaerobic growth of Salmonella enterica serovar typhimurium on ethanolamine or 1,2-propanediol. *Journal of Bacteriology*, 183, pp.2463–2475.

Price, G.D. & Badger, M.R., 1989. Expression of Human Carbonic Anhydrase in the Cyanobacterium Synechococcus PCC7942 Creates a High Evidence for a Central Role for Carboxysomes in the CO2 Concentrating Mechanism. *plant physiologyl*, 91, pp.505–513.

Price, G.D., Badger, M.R., Woodger, F.J. & Long, B.M., 2008. Advances in understanding the cyanobacterial CO2-concentrating-mechanism (CCM): functional components, Ci transporters, diversity, genetic regulation and prospects for engineering into plants. *Journal of experimental botany*, 59(7), pp.1441–61. Available at: http://www.ncbi.nlm.nih.gov/pubmed/17578868 [Accessed September 3, 2014].

Rae, B.D., Long, B.M., Badger, M.R. & Price, G.D., 2013. Functions, compositions, and evolution of

the two types of carboxysomes: polyhedral microcompartments that facilitate CO2 fixation in cyanobacteria and some proteobacteria. *Microbiology and molecular biology reviews : MMBR*, 77(3), pp.357–79. Available at: http://www.pubmedcentral.nih.gov/articlerender.fcgi?artid=3811607&tool=pmcentrez&rendertype=abstract.

Reinhold, L., Kosloff, R. & Kaplan, A., 1991. A model for inorganic carbon fluxes and photosynthesis in cyanobacterial carboxysomes. *Canadian Journal of Botany*, 69(5), pp.984–988. Available at: http://www.nrcresearchpress.com/doi/abs/10.1139/b91-126.

Rizzo, M., Springer, G., Granada, B. & Piston, D., 2004. An improved cyan fluorescent protein varient useful for FRET. *Nature Biotechnology*, 4, pp.445–9.

Rodionov, D. a, Vitreschak, A.G., Mironov, A. a & Gelfand, M.S., 2003. Comparative genomics of the vitamin B12 metabolism and regulation in prokaryotes. *The Journal of biological chemistry*, 278(42), pp.41148–59. Available at: http://www.ncbi.nlm.nih.gov/pubmed/12869542 [Accessed November 10, 2014].

Rondon, M.R., Horswill, A.R. & Escalante-Semerena, J.C., 1995. DNA polymerase I function is required for the utilization of ethanolamine, 1,2-propanediol, and propionate by Salmonella typhimurium LT2. *Journal of Bacteriology*, 177, pp.7119–7124.

Rondon, M.R., Kazmierczak, R. & Escalante-semerena, J.C., 1995. Glutathione Is Required for Maximal Transcription of the Cobalamin and for the Catabolism of Ethanolamine , 1 , 2-Propanediol , and Propionate in Salmonella typhimurium LT2. *Journal of bacteriology*, 177(19), pp.5434–5439.

Roof, D.M. & Roth, J.R., 1992. Autogenous regulation of ethanolamine utilization by a transcriptional activator of the eut operon in Salmonella typhimurium. *Journal of Bacteriology*, 174, pp.6634–6643.

Roof, D.M. & Roth, J.R., 1988. Ethanolamine utilization in *Salmonella typhimurium*. *Journal of bacteriology*, 170(9), pp.3855–63. Available at: http://www.pubmedcentral.nih.gov/articlerender.fcgi?artid=207641&tool=pmcentrez&rendertype=abstract.

Roth, J.R., Lawrence, J.G. & Bobik, T.A., 1996. Cobalamin (coenzyme B12): synthesis and biological significance. *Annual review of microbiology*, 50, pp.137–181.

Sabet-Azad, R., Linares-Pastén, J. a, Torkelson, L., Sardari, R.R.R. & Hatti-Kaul, R., 2013. Coenzyme A-acylating propionaldehyde dehydrogenase (PduP) from Lactobacillus reuteri: kinetic characterization and molecular modeling. *Enzyme and microbial technology*, 53(4), pp.235–42. Available at: http://www.ncbi.nlm.nih.gov/pubmed/23931688 [Accessed January 12, 2015].

Sagermann, M., Ohtaki, A. & Nikolakakis, K., 2009. Crystal structure of the EutL shell protein of the ethanolamine ammonia lyase microcompartment. *Proceedings of the National Academy of Sciences of the United States of America*, 106, pp.8883–8887.

Salomons, F.A., Ida, J., Luttik, M.A.H., Ko, P., Dijken, J.P.V.A.N. & Pronk, J.T., 2000. The Saccharomyces cerevisiae ICL2 Gene Encodes a Mitochondrial 2-Methylisocitrate Lyase Involved in Propionyl-Coenzyme A Metabolism. , 182(24), pp.7007–7013.

Sampson, E.M. & Bobik, T. a, 2008. Microcompartments for B12-dependent 1,2-propanediol degradation provide protection from DNA and cellular damage by a reactive metabolic intermediate. *Journal of bacteriology*, 190(8), pp.2966–71. Available at: http://www.pubmedcentral.nih.gov/articlerender.fcgi?artid=2293232&tool=pmcentrez&rendertype=abstract [Accessed September 26, 2014].

Sargent, F., Davidson, F. a, Kelly, C.L., Binny, R., Christodoulides, N., Gibson, D., Johansson, E.,

Kozyrska, K., Lado, L.L., Maccallum, J., Montague, R., Ortmann, B., Owen, R., Coulthurst, S.J., Dupuy, L., Prescott, A.R. & Palmer, T., 2013. A synthetic system for expression of components of a bacterial microcompartment. *Microbiology (Reading, England)*, 159, pp.2427–36. Available at: http://www.pubmedcentral.nih.gov/articlerender.fcgi?artid=3836489&tool=pmcentrez&rendertype=abstract.

Sargent, F., Davidson, F.A., Kelly, C.L., Binny, R., Christodoulides, N., Gibson, D., Johansson, E., Kozyrska, K., Lado, L.L., MacCallum, J., Montague, R., Ortmann, B., Owen, R., Coulthurst, S.J., Dupuy, L., Prescott, A.R. & Palmer, T., 2013. A synthetic system for expression of components of a bacterial microcompartment. *Microbiology (United Kingdom)*, 159, pp.2427–2436.

Schulz, G.E., 2002. The structure of bacterial outer membrane proteins. *Biochimica et biophysica acta*, 1565, pp.308–317.

Shiveley, J., Ball, F. & Kline, B., 1973. Electron Microscopy of the Carboxysomes (Polyhedral Bodies) of Thiobacillus neapolitanus. *Science*, 116(3), pp.1405–1411.

Shively, A.J.M., Ball, F., Brown, D.H. & Saunders, R.E., 1973. Functional Organelles in Prokaryotes : Polyhedral Inclusions (Carboxysomes) of Thiobacillus neapolitanus. *Science*, 182(4112), pp.584–586.

Shively, J.M., Bradburne, C.E., Aldrich, H.C., Bobik, T.A., Mehlman, J.L., Jin, S. & Baker, S.H., 1998. Sequence homologs of the carboxysomal polypeptide CsoS1 of the thiobacilli are present in cyanobacteria and enteric bacteria that form carboxysomes - polyhedral bodies. *Canadian Journal of Botany*, 76, pp.906–916.

Sinha, S., Cheng, S., Fan, C. & Bobik, T. a, 2012. The PduM protein is a structural component of the microcompartments involved in coenzyme B(12)-dependent 1,2-propanediol degradation by Salmonella enterica. *Journal of bacteriology*, 194(8), pp.1912–8. Available at: http://www.pubmedcentral.nih.gov/articlerender.fcgi?artid=3318458&tool=pmcentrez&rendertype=abstract [Accessed January 12, 2015].

So, A.K., Espie, G.S., Williams, E.B., Shively, J.M., Heinhorst, S. & Cannon, G.C., 2004. A Novel Evolutionary Lineage of Carbonic Anhydrase (ε Class) Is a Component of the Carboxysome Shell. *Journal of bacteriology*, 186(3), pp.623–630.

Staib, L. & Fuchs, T.M., 2014. From food to cell: Nutrient exploitation strategies of enteropathogens. *Microbiology (United Kingdom)*, 160(PART 6), pp.1020–1039.

Steinbuchel, A., Aerts, K., Babel, W., Follner, C., Liebergesell, M., Madkour, M.H., Mayer, F., Pieper-Furst, U., Pries, A. & Valentin, H.E., 1995. Considerations on the structure and biochemistry of bacterial polyhydroxyalkanoic acid inclusions. *Canadian journal of microbiology*, 41 Suppl 1, pp.94–105.

Stojiljkovic, I., Bäumler, a J. & Heffron, F., 1995. Ethanolamine utilization in *Salmonella typhimurium*: nucleotide sequence , protein expression , and mutational analysis of the *cchA cchB eutE eutJ eutG eutH* gene cluster. *Journal of Bacteriology*, 177(5), pp.1357–1366.

Summers, K. & Kirschner, M.W., 1979. Characteristics of the polar assembly and disassembly of microtubules observed in vitro by darkfield light microscopy. *The Journal of Cell Biology*, 83, pp.205–17.

Tabita, F.R., 1999. Microbial ribulose 1 , 5-bisphosphate carboxylase / oxygenase : A different perspective. , pp.1–28.

Takenoya, M., Nikolakakis, K. & Sagermann, M., 2010. Crystallographic insights into the pore structures and mechanisms of the EutL and EutM shell proteins of the ethanolamine-utilizing microcompartment of Escherichia coli. *Journal of Bacteriology*, 192, pp.6056–6063.

Tanaka, S., Kerfeld, C.A., Sawaya, M.R., Cai, F., Heinhorst, S., Cannon, G.C., Yeates, T.O. & Sawaya, R., 2008. Atomic-Level Models of the Bacterial Carboxysome Shell. , 319(5866), pp.1083–1086.

Tanaka, S., Sawaya, M.R. & Yeates, T.O., 2010. Structure and mechanisms of a protein-based organelle in Escherichia coli. *Science (New York, N.Y.)*, 327, pp.81–84.

Toraya, T., Honda, S. & Fukui, S., 1979. Fermentation of 1,2-propanediol and 1,2-ethanediol by some genera of Enterobacteriaceae, involving coenzyme B12-dependent diol dehydratase. *Journal of Bacteriology*, 139, pp.39–47.

Tsai, Y., Sawaya, M.R., Cannon, G.C., Cai, F., Williams, E.B., Heinhorst, S., Kerfeld, C.A. & Yeates, T.O., 2007. Structural analysis of CsoS1A and the protein shell of the Halothiobacillus neapolitanus carboxysome. *PLoS Biology*, 5, pp.1345–1354.

Tsoy, O., Ravcheev, D. & Mushegian, A., 2009. Comparative genomics of ethanolamine utilization. *Journal of Bacteriology*, 191(23), pp.7157–7164.

Walker, G., Murphy, S. & Huennekens, F., 1969. Enzymatic conversion of vitamin B 12a to adenosyl-B 12: evidence for the existence of two separate reducing systems. *Archives of biochemistry and biophysics*, 134(1), pp.95–102.

Wegner, A., 1976. Head to tail polymerization of actin. *Journal of Molecular Biology*, 108(1), pp.139–50.

Weisenberg, R.C., Deery, W.J. & Dickinson, P.J., 1976. Tubulin-nucleotide interactions during the polymerization and depolymerization of microtubules. *Biochemistry*, 15, pp.4248–54.

Wheatley, N.M., Gidaniyan, S.D., Liu, Y., Cascio, D. & Yeates, T.O., 2013. Bacterial microcompartment shells of diverse functional types possess pentameric vertex proteins. *Protein science : a publication of the Protein Society*, 22(5), pp.660–5. Available at: http://www.pubmedcentral.nih.gov/articlerender.fcgi?artid=3649267&tool=pmcentrez&rendertype=abstract [Accessed September 22, 2014].

Yeates, T.O., Crowley, C.S. & Tanaka, S., 2010. Bacterial microcompartment organelles: protein shell structure and evolution. *Annual review of biophysics*, 39, pp.185–205. Available at: http://www.pubmedcentral.nih.gov/articlerender.fcgi?artid=3272493&tool=pmcentrez&rendertype=abstract [Accessed September 22, 2014].

Yeates, T.O., Kerfeld, C.A., Heinhorst, S., Cannon, G.C. & Shively, J.M., 2008. Protein-based organelles in bacteria: carboxysomes and related microcompartments. *Nature reviews. Microbiology*, 6, pp.681–691. Available at: http://image.sciencenet.cn/olddata/kexue.com.cn/upload/blog/file/2008/10/20081028212721145.pdf [Accessed January 26, 2015].

Yeates, T.O., Thompson, M.C. & Bobik, T. a, 2011. The protein shells of bacterial microcompartment organelles. *Current opinion in structural biology*, 21(2), pp.223–31. Available at: http://www.pubmedcentral.nih.gov/articlerender.fcgi?artid=3070793&tool=pmcentrez&rendertype=abstract [Accessed March 19, 2012].

Yeates, T.O., Tsai, Y., Tanaka, S., Sawaya, M.R. & Kerfeld, C. a, 2007. Self-assembly in the carboxysome: a viral capsid-like protein shell in bacterial cells. *Biochemical Society transactions*, 35(Pt 3), pp.508–11. Available at: http://www.ncbi.nlm.nih.gov/pubmed/17551640.